Design and Development of β-Sheet Polypeptides for Biomedical Applications

A thesis

submitted in partial fulfilment of the requirements

for the degree of

Doctor of Philosophy

Rahul Nisal

20143340

Indian Institute of Science Education and Research, Pune

Dr. Homi Bhabha Road, Pune,

Maharashtra 411008,

India

January 2023

Dedicated to

My Family

Declaration

I declare that this written submission represents my ideas in my own words, and where others' ideas have been included; I have adequately cited and referenced the original sources. I also declare that I have adhered to all principles of academic honesty and integrity and have not misrepresented or fabricated or falsified any idea/data/fact/source in my submission. I understand that violation of the above will be cause for disciplinary action by the Institute and can also evoke penal action from the sources that have not been properly cited or from whom proper permission has not been taken when needed.

Date:

30th Jan 2023

Rahul Nisal

Reg. No. 20143340

भारतीय विज्ञान शिक्षा एवं अनुसंधान संस्थान पुणे
INDIAN INSTITUTE OF SCIENCE EDUCATION AND RESEARCH PUNE
(An Autonomous Institution of Ministry of Human Resource Development, Govt. of India)
Dr. Homi Bhabha Road, Pune - 411 008.

Prof. Manickam Jayakannan
Department of Chemistry

CERTIFICATE

Certified that the work done in the thesis entitled "***Design and Development of β-Sheet Polypeptides for Biomedical Applications***" submitted by **Mr. Rahul Nisal** was carried out by the candidate under my supervision. The work presented here or any part of it has not been included in any other thesis submitted previously for the award of any degree or diploma from any other University or Institution.

Date: 30/01/2023
Pune, Maharashtra, India

Prof. M. Jayakannan
(Thesis Supervisor)

Acknowledgements

First of all, I would like to thanks to my thesis supervisor Prof. M. Jayakannan for his guidance, constant support, and encouragement throughout the course of my PhD. I am really thankful to him for having faith in me and taking me in to his group when I moved from another lab in fifth year of my PhD. During my PhD journey he was always approachable and his positive thinking, passion towards research always inspired me. He always took care of me, when my fellowship was not there, he supported me financially, I am very grateful to have him as my PhD supervisor. I feel very lucky to be mentored by him. Thanks a ton sir, it would have been an impossible task without you.

I would like to thank my Research Advisory Committee, Dr. H. N. Gopi sir, and Dr. Prakash P. Wadgaonkar sir. Their suggestions in RAC meeting always helped me to fix my project in better fashion. I would like to thank Prof. K. N. Ganesh (Former Director, IISER Pune) and Prof. Jayant B. Udgaonkar (Present Director, IISER Pune) for providing excellent research facilities of international standards. I would like to thank IISER Pune for supporting me financially by providing me fellowship for nearly one and half year. I would like to thank IIER Pune Dean's committee for understanding my problem and allowing me to change supervisor in fifth year of my PhD, especially thanks to Dr. Girish Ratnaparkhi sir, Dr. Bhas Bapat sir, Dr. Srabanti Chaudhari ma'am for all understanding and support.

Thanks to Shabana ma'am for always encouraging me and supporting me. I would like to thank Dr. S.K. Asha ma'am for allowing me to access her lab facilities without any hesitation.

I would like to express my heartfelt gratitude to entire IISER Pune administration and Chemistry Technical staff. Thanks to Mayuresh sir and Mahesh sir for all administrative related support. I would like to thank to all instrument operators without them my research would have not been possible. Thanks to Nitin Dalvi sir and Sandip Mishra sir for your help related to NMR based kinetics experiment and all urgent NMR sample analysis. Thanks to Sandip Kanade sir for all help related to urgent HRMS analysis. Thanks to Suresh Prajapat sir for helping me in MALDI-TOF analysis during Covid time. I would like to extend my thanks to Megha ma'am (for helping in AFM analysis) and Yatish sir (for helping in FE-SEM analysis). Thanks to Abhijit Biswas sir for helping me in FT-IR measurements. I would like to thank Ganesh Dimber sir for his help related to purchase.

I would like to thank my all my lab members for providing a good working environment. Special thanks to Parshuram, Shahid, Ruma and Uttareshwar for their support and exciting scientific discussions during tea breaks. Thanks to Akshaya and Rhujal for all the help that you have done. Thank you, Parshu, for all your support. Thank you, Shahid, for doing all cellular and mice related experiments for my thesis, without you it would have been an impossible to get such a nice data. Thank you Uttareshwar for your help in mice related experiments. I would like to thank Ruma for her help related to antimicrobial studies,

hemolysis experiments. Thanks, guys, for maintaining good lab environment. I would like to thank my senior lab members, Dr. Mehak and Dr. Dheeraj for their constant support.

I would like to thanks to my former lab members, Gregor, Aditi, and Debayan. Thanks to my batchmates, specially to Pavan, Mohan, Manisha, Sanjit, Ganesh. I would like to thank my friends, Yashaswi, Chitra, Nitin, Neha for always being with me in my ups and down. I would like to thanks Pradyut Roy for helping me in fluorescence measurements.

I would like to say thanks a lot to my wife, Shaila for all her sacrifices for my research. Thank you Shaila for always being with me, trusting me and keeping me mentally strong. I would like to thank my mother and father for all their support and encouragement throught my career. I would like to thanks to my uncle (“Kiran mama”) for all his support in my career.

I would like to say thanks to all those who I missed earlier and helped me in my PhD journey.

My PhD journey has been one of the most thrilling and hardest journeys of my life so far. It was a great experience; I learned a lot during these golden years.

Synopsis

Synthetic polypeptides are continued to be one of the most challenging area for synthetic chemist to mimic the properties of the natural biomolecules (i.e, proteins) to impart in artificial macromolecular systems for both fundamental understanding and technology development. It is rather surprising to notice that α-helical polypeptides are predominantly chosen by the researchers globally to develop new polymerization methodologies, catalyst developments or structure-property relationships, etc. The main reason for the selection of α-helical polypeptides has been associated with their excellent solubility in the organic solvents to carry out the polymerization in homogeneous phase, easy structural characterization and molecular weight determination and so on so forth. On the contrary, *β-Sheet* forming polypeptides are one of the least explored synthetic systems and this main restriction associated with the uncontrollable-precipitation of the polymer chains during their synthesis. The formation of β-sheet lamellae at the initial stage of the polymerization and strong inter-chain hydrogen bonding interactions were found to be responsible for this unwanted precipitation of chains. As a result, the resultant heterogenous polymerization was found to be "non-living" with dead propagation chains and they were also inefficient for the synthesis of block copolymer architectures. As a consequence, accomplishing complete control over the "livingness in *β-sheet polypeptides"* and expansion of the propagating polymer chains for building many unexplored block copolymer macromolecular architectures is still a distant dream for synthetic polymer chemist.

This unresolved problem is addressed in this thesis by carefully developing new "steric-hindrance assisted ring opening polymerization" strategy to yield high molecular weight *β-sheet polypeptides,* and expand the scope of the approach to open new avenue for the building inaccessible block copolymer macromolecular architectures. In this process, the propagating polypeptide chains were directed to undergo conformational transition from *β-sheet to α-helix* to produce freely soluble polymers and excellent "*living ROP polymerization*" characteristics was accomplished in building high molecular weight polypeptides. A *t*-butyl benzene steric unit as identified followed by several attempts as a conformational controller -cum- solubilizing handle to create in-situ secondary structural transition in the propagating chains to accomplish control in polymerization. The soluble and *living α-helical* propagating chains further opened new avenue for inaccessible block copolymer macromolecular architectures of poly(L-serine) and poly(L-cysteine). The thesis has been divided into four chapters and the details are given below:

1. Chapter 1 provides complete literature review on developments in NCA synthesis and their polymerization. Further attention was drawn to application of polypeptides, especially in antibacterial and drug delivery area. Finally, the synthetic challenges associated with β-sheet polypeptides and the aim of the thesis was described.
2. Chapter 2 describes the development of steric hindrance assisted ROP process to β-sheet polypeptides based on poly(L-serine) and poly(L-cysteine), detail analysis of the polymerization kinetics, and the secondary structures of the resultant polypeptides with appropriate mechanism.
3. Chapter 3 is dedicated to the development of β-sheet block copolymer architectures having hydrophobic poly(L-serine) at the core and hydrophilic poly(L-glutamate)s in the periphery.

The nano-assemblies were further encapsulated with anticancer drugs and studies their action *in vitro* cellular level. Near infra-red biomarker IR-780 loaded NP were employed to study the *in vivo* biodistribution in mice model.

4. Chapter 4 describes the development of ROP and polymerization induced self-assembly (PISA) together in the poly(L-serine) to make water dispersible and stable polypeptide emulsions and expand the scope of the process to in-situ encapsulation of large numbers of fluorescent dyes. This new classes of polypeptide nano-assemblies were further tested for their biocompatibility in cell lines.

The last chapter summarize the thesis work with future perspectives.

In chapter 2, steric-hindrance assisted ROP strategy is developed to precisely in-situ programmed the propagating polymer chains from *β-sheet to α-helical conformational* in the ring opening (ROP) process to accomplish homogeneous polymerization for high molecular weight polypeptides. The proof-of-concept was demonstrated successfully in two β-sheet forming polypeptides such as poly(L-serine) and poly(L-cysteine). New *t*-butylbenzene anchored N-carboxyl anhydride (NCA) monomers were designed by tailor-made approach and subjected to ring opening polymerization (ROP) using N-heterocyclic carbene as catalyst. The new SSCP process enabled the synthesis of poly(L-serine) and poly(L-cysteine) polypeptides having nearly 150 repeating units with narrow polydispersity of 1.2. Impressively, the newly produced *t*-butyl substituted polypeptides exhibited excellent solubility in common organic solvents such as chloroform and THF, and enabled their complete structural characterization and molecular weight determination. NMR and FT-IR spectroscopic methods were employed to study the real-time polymerization kinetics to establish the "living ROP process". Post-polymerization deprotection strategy enabled the *reversible conformational transition* from α-helix to *β-sheet and* restored the original *β-sheet-structures* in poly(L-serine)s.

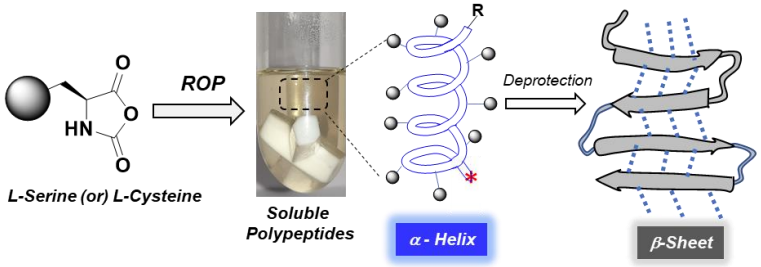

Steric-hindrance ROP Strategy for β-Sheet Polypeptides

In chapter 3, the scope of steric-hindrance assisted ROP strategy was expanded for preparation of block copolymers from polyserine macroinitiator. The polyserine-*b*-polyglutamate block copolymer was prepared by sequential ROP of serine and glutamate NCA monomers followed by deprotection. The α-helix to β-sheet conformational transition was observed upon

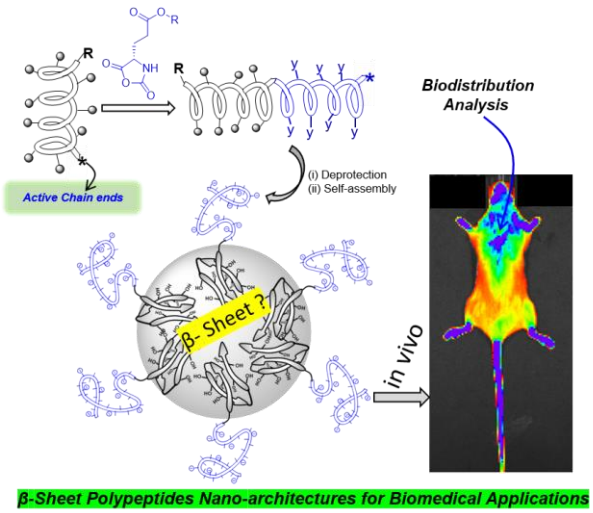

β-Sheet Polypeptides Nano-architectures for Biomedical Applications

deprotection of diblock copolymer. The deprotected serine-glutamate diblock copolymer was able to self-assemble in to small spherical nanoparticles of size ~ 30 nm with negative zeta potential (-50 mV). The size of nanoparticles was constant in pH range of 4 to 9, while their zetapotential became less negative with decreasing the pH. The diblock copolymer underwent helix to coil transition upon increasing pH above 5. The 15-fold enhancement in ThT fluorescence in presence of diblock copolymer corroborates the existence of β-sheet assemblies. The nontoxic and non-hemolytic nature of diblock copolymer set the foundation for further biological studies. The encapsulation of anticancer drug doxorubicin and near IR dye (IR-780) was carried out for *in vitro* and *in vivo* studies respectively. The *in vitro* cellular uptake studies using confocal microscopy reveals the successful uptake of DOX loaded nanoparticles by mammalian cells. The IVIS based *in vivo* biodistribution studies reveals the longer circulation time (compared to free dye) and *in vivo* stability of dye loaded polymer nanoparticles in mice model.

In chapter 4, the ring opening polymerization induced self-assembly (ROPISA) mediated polymerization of tert-butyl benzene functionalized serine NCA monomer was performed using MeO-PEG$_{5000}$-NH$_2$ at various M/I ratios and stable polypeptide emulsions in the form of opalescent solutions were obtained for M/I = 10 or 25 in the feed. The isolated amphiphilic di-block copolymers from these stable emulsions exhibited monomodal and narrow dispersed SEC profile with molecular weight in close agreement with desired molecular weight demonstrating the controlled polymerization process. The sizes of nano assemblies forming these polypeptide emulsions were around 20 to 30 nm and they displayed spherical nano particle morphology. The in-situ encapsulation of five different dyes such as curcumin, HPTS, Nile red, rhodamine B, and IR-780 in these nano assemblies were done by adding the dyes in the beginning of ROPISA mediated polymerization to obtain colorful polypeptide emulsions. The nontoxic and non-hemolytic nature of nascent polypeptide nanoparticles confirms their biocompatibility, additionally, their nontoxic nature retains after dye encapsulation. The confocal microscopy based *in vitro* cellular uptake studies on Nile red loaded nano particles shows the successful uptake in mammalian cells.

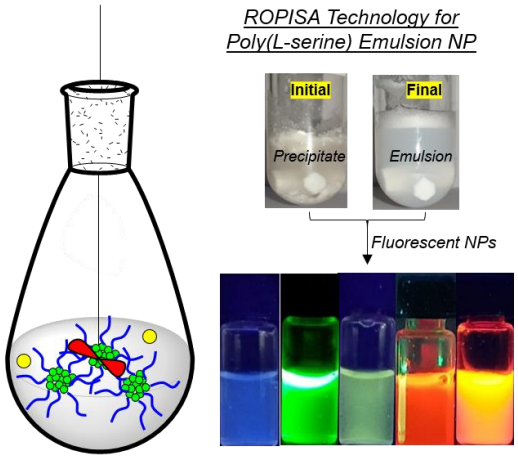

The new ROP process reported in this thesis opens up new platform for building high molecular weight β-sheet polypeptides by reversible conformation-transition strategy and also creates new avenue to explore diverse block copolymer architectures that have been distant dream so far. We strongly believe the "steric-hindrance assisted ring opening polymerization strategy" would open new avenue for large numbers of inaccessible β-sheet polypeptides and their higher order block copolymer architectures that are yet to be explored. The newly developed β-sheet polypeptides and their block copolymers are expected to make significant contribution for long-term impact in material and biomedical filed.

Table of Contents

Chapter 1

Introduction

1.1. Introduction to Polypeptides

Proteins are vital biomolecules having supreme importance in our life. Proteins are made up of building blocks called as amino acids and in proteins, these amino acids linked together by amide bond (or peptide bond) to form a protein or peptides (if chain length is small).[1] Nature makes these protein molecules with the help of complex cellular ribosomal machinery and it involves two major processes known as transcription and translation.

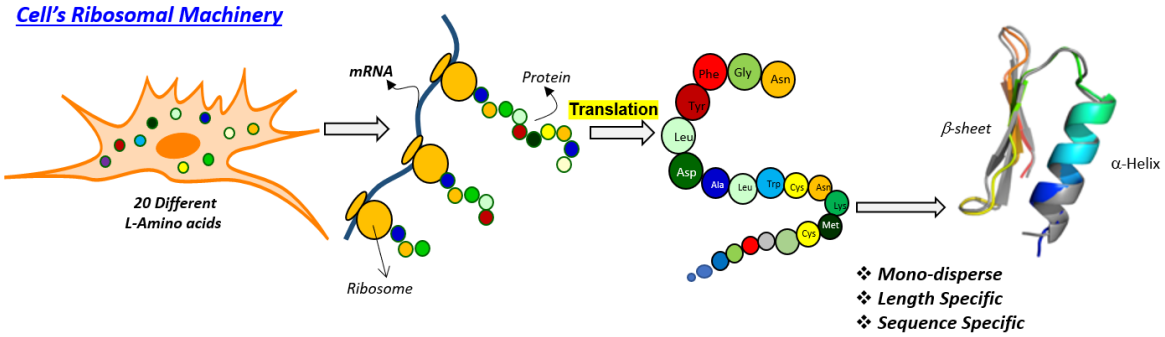

Figure 1.1. *Illustration of protein biosynthesis by cellular machinery.*

In the process of transcription, a portion of DNA which encodes protein which is also called as gene is converted in to a template molecule known as messenger RNA (mRNA) with the help of enzyme RNA polymerases in the nucleus of cell. The synthesized mRNA is then exported from nucleus to cytoplasm of cell where translation occurs.[2] In translation, the ribosome reads nucleotide sequence of mRNA and determines the amino acid sequence of desired protein (See Figure 1.1). The ribosome recognizes nucleotide sequence of mRNA in the form of triplets, i.e. three consecutive nucleotides in mRNA which are also known as codons and each codon corresponds to particular amino acid. The ribosome utilizes transfer RNA (tRNA) to bring the correct amino acid to ribosome for the process of translation. The tRNA binds to codon within the mRNA and brings the specific amino acid. The tRNA molecule has complementary triplet (known as anticodon) for its binding to codon on mRNA. When first amino acid is brought by tRNA then second tRNA binds to next codon and brings the second amino acid, subsequently the peptidyl transferase enzyme in ribosome catalyzes the formation of amide bond between these two amino acids. When the first dipeptide is formed then ribosome moves over mRNA and releases first tRNA and third tRNA comes in along with amino acid and binds to third codon and the process repeats till the desired sequence is obtained. Finally, the formed protein is released and it starts adopting secondary structure and starts performing its activity. This ribosomal machinery is so unique that it makes variety of proteins from 20 different natural amino

acids in one pot fashion and the resultant proteins are always monodisperse, length specific and sequence specific. These synthesized proteins plays vital roles in our body such as, providing structural and mechanical support to cells, tissues, and organs, catalysis of various biochemical reactions, and regulation of cell signaling, cell adhesion, and immune responses.[1] This versatility in their functions comes from their ability to form higher-order secondary structures such as α-helices and β-sheets, which engrossed the scientists for synthesizing proteins or protein mimicking molecules that can adopt these higher-ordered secondary structures.

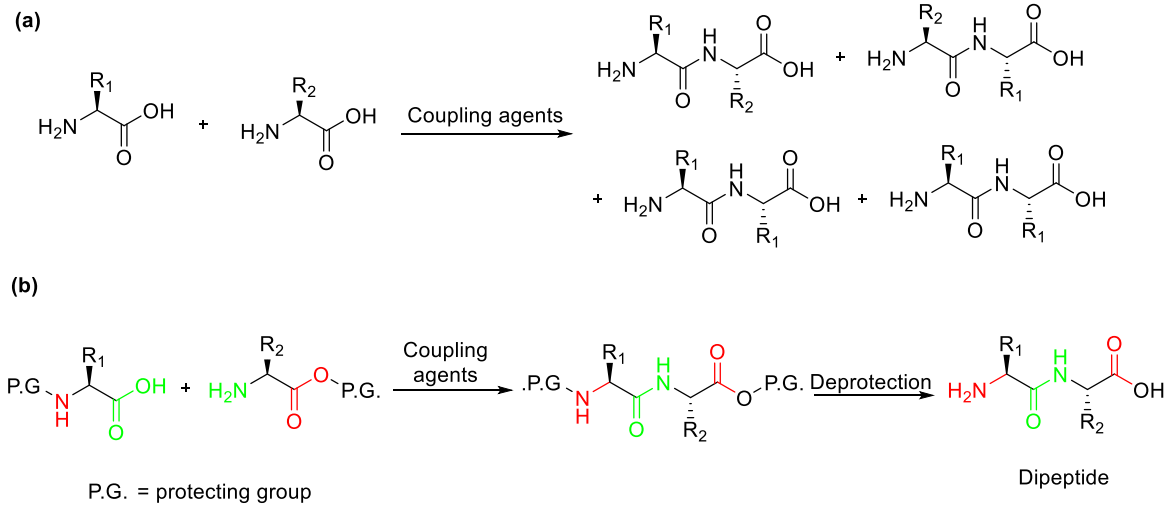

Scheme 1.1. *(a) Scheme illustrating solution phase coupling of two unprotected amino acids, (b) Scheme illustrating solution phase coupling of two appropriately protected amino acids.*

If we try to mimic the ribosomal machinery and try to make proteins from 20 amino acids in one pot manner then it would give a heterogeneous mixture of so many peptides and it would be impractical to purify it. If we try to simplify the process and try to couple only two amino acids in one pot then still it would give four kinds of dipeptides and their separation would be impractical (see scheme 1.1a). To avoid this, protection and deprotection strategy is employed for synthesis of peptides or proteins and it is shown for simple dipeptide in Scheme 1.1b, wherein carboxylic acid of one amino acid is protected and amino group of other amino acid is protected and the coupling reaction is carried out to afford single desired dipeptide in protected form which is then deprotected at the end to get desired dipeptide. Using this approach, amino acids can be coupled in solution phase by adding them sequentially but each coupling involves protection and deprotection and importantly it involves purification at each protection, deprotection and coupling step, hence it is very laborious and rarely practiced. The peptide synthesis was revolutionized by

pioneering contribution from Robert Bruce Merrifield and for which he was awarded with Nobel prize in 1984.[3-5] The Merrifield's peptide synthesis method is also known as solid phase peptide synthesis (SPPS), which involves the sequential coupling of protected amino acids on solid resin support but in this case all reactions are carried out on resin support hence the product peptide always remains attached to resin support while impurities, excess reagents can be easily washed out. The synthesis occurs from C-terminus end to N-terminus of peptide and the steps involved in SPPS are shown in Figure 1.2.

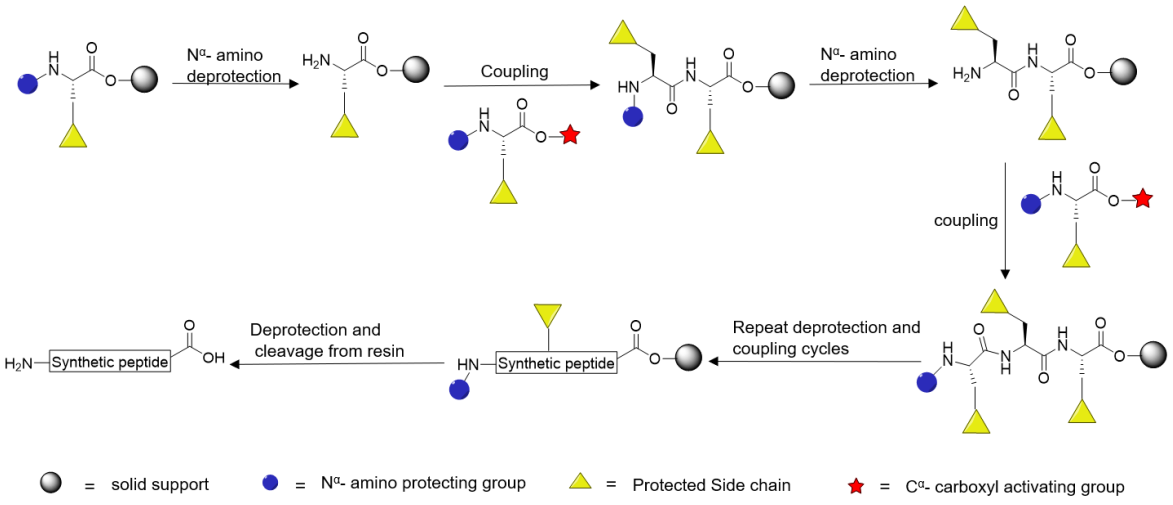

Figure 1.2. *Schematic representation of Solid phase peptide synthesis (SPPS)*

The synthesis starts with attachment of carboxylic acid end of amino (α-NH_2) protected amino acid (N-protected amino acid) to the solid support (resin), then amine group is deprotected and it is coupled to next N-protected amino acid to get N-terminus protected dipeptide on resin. Then the cycle of deprotection, coupling is repeated till the desired sequence of peptide is obtained. At the end, the peptide is cleaved from resin and all side chain functionalities are also deprotected in one step called as "global deprotection step" to get desired peptide. The peptide obtained from SPPS method is also monodisperse, length specific and sequence specific but it is limited to small scale and short peptides (~50 residues). To overcome the limitation of production of short peptides by SPPS, the peptide ligation chemistries were developed which regioselectivity connects the short peptides produced by SPPS to form longer peptides and the total synthesis of proteins is carried out.[6, 7] In past two decades, there has been tremendous development in the area of peptide ligation and chemical synthesis of proteins and it has been shown that proteins up to 200 unit can be

chemically synthesized.[8, 9] This is very exciting but the scale at which these chemistries are done is very low and these proteins are synthesized in very small amounts (< 5 mg) and the overall yields of synthesis are extremely low (< 10%). For most practical purposes these methods are not useful hence another method for making protein mimicking material is desirable and the polymerization approach is developed.

1.2. Polypeptide Synthesis by NCA Route

The synthetic peptide-based polymers are known as polypeptides and they are typically synthesized by ring-opening polymerization (ROP) of cyclic N-carboxy-anhydride (NCA) moiety with the help of nucleophile or base as an initiator (see scheme 1.2).[10, 11] The ROP of NCA is the most efficient and practical method for synthesis of polypeptides as it utilizes simple reagents and very high molecular weight polypeptides can be produced in excellent yields (> 90%) and in more quantity (in grams) without compromising the chirality of amino acids. Although polypeptides synthesized by NCA ROP lacks sequence specificity, the cost effectiveness and synthesis in bulk quantities makes this method more powerful and practical.

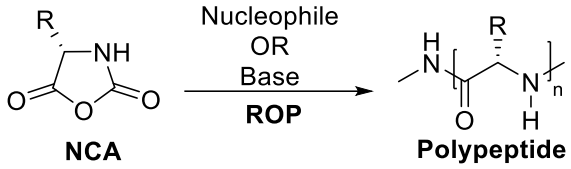

Scheme 1.2. *Schematic representation of polymerization of NCA*

It all began in 1906 when Herman Leuch accidently synthesized the NCA molecule and later for many years NCA was known as Leuch's anhydride.[12] Even though NCA was first synthesized in 1906, the work on ROP of NCA for preparation of polypeptides actually started from 1921, when the things just came to normal after World War I and importantly after the acceptance of Staudinger's concept on macromolecules by community.[12] Later, several research groups across the globe have put enormous efforts to develop the polypeptide field and it has taken polypeptides to very different level that we see today. Furthermore, the polypeptide research was boosted dramatically in last two decades after discovery of organometallic catalysis by Deming in late 1990's for NCA ROP to prepare very high molecular weight polypeptides and their block copolymers with living characteristics.[13, 14] Till now, there has been more than 200 NCAs are reported with wide variety of functionalities for several applications.[15] In last five years or so there has been

growing interest in developing new catalysts, initiators to carry out NCA ROP at extremely high speed, also several developments were happened in NCA synthesis itself and these advancements will be summarized below.

The NCA molecule is synthesized from amino acid by two methods as shown in scheme 1.3.[16] The first method is two-step process that it involves the treatment of amino acids with alkoxy chloroformates to afford N-carbamoyl amino acid intermediate and it is subsequently reacted with any of the halogenating agents such as PCl_3, PCl_5, PBr_3, $SOCl_2$, etc to get NCAs. This was the original method developed by Leuch hence it is also known as Leuch's method. In the second method, the amino acid is cyclized in one step to NCA with the help of phosgene or other stable phosgene equivalents (like diphosgene or triphosgene) and the process is called as Fuchs-Farthing method. Among these two methods, owing to its simplicity and ease of isolation of NCA, the Fuchs-Farthing method is the most commonly practiced procedure for preparation of NCA. Although, the Fuchs-Farthing method seems to be quite simple for preparation of NCA, it generates HCl as by-product and it has to be removed efficiently to get pure NCA since the HCl can terminate the growing polypeptide chain and also the chloride ion can open the NCA at elevated temperature leading to unwanted side reactions and the control over polymerization is lost.

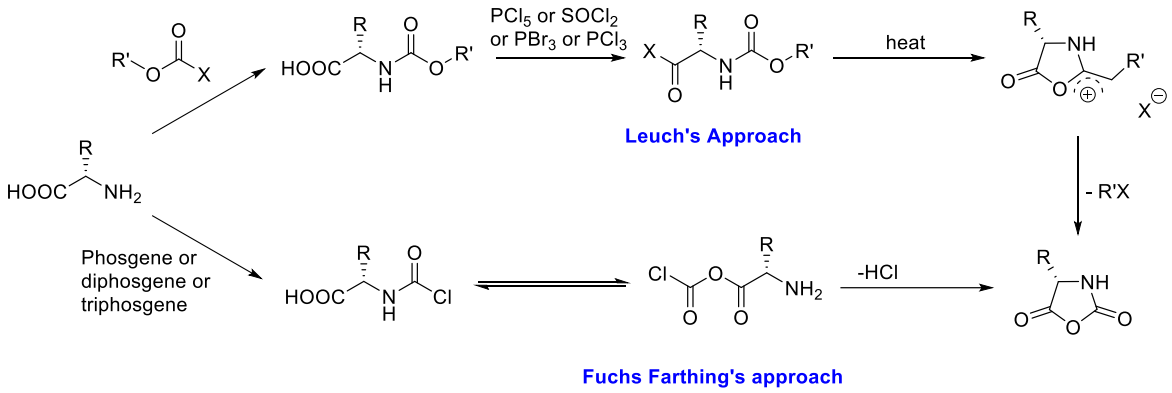

Scheme 1.3. *Schematic representation of synthesis of NCA*

To overcome this issue, there has been several advancements towards making ultra-pure NCAs devoid of HCl impurities. The most common practice to purify NCA after isolation is to recrystallize NCA at least three times. Due to moisture sensitivity of NCA, these recrystallizations have to be carried out under inert conditions such as inside glove box and using dry solvents, also the special glass apparatus has been designed to carry out recrystallization of NCA under vacuum.[17] The repetitive recrystallizations involve yield loss

and it is time consuming, also the liquid NCAs cannot purified by recrystallization. Additionally, the HCl quenchers such as α-pinene or limonene have been tried but their lipophilicity can complicate the isolation of NCA.[11] The other methods such as rapid aqueous work up at low temperature and slight basic pH (maintained by 0.05% $NaHCO_3$) followed by extensive drying,[18] flash chromatography under inert conditions[19] and filtration over celite bed[20] were attempted to purify the NCA. The filtration over celite bed was found to efficient in purifying the NCAs at large scales (>100 g) just by filtering the NCA solution in dichloromethane over celite bed and subsequent single recrystallization afforded NCAs with chloride content as low as 115 ppm.

Due to moisture sensitivity associated with NCA and toxic nature of phosgene, also to avoid dealing with by products like HCl, Endo and co-workers have come up with the in-situ NCA generation strategy during polymerization.[21, 22] Their process involves the synthesis of N-aryl carbamates of amino acid by treatment with nontoxic bis-aryl carbonates. These N-aryl carbamates of amino acids are stable under ambient conditions and can acts as precursor for NCA monomer via thermal intramolecular cyclization during polypeptide synthesis. These greener approach without using toxic phosgene have gain lot of interest in recent years. Additionally, another set of analogues which are Sulphur variant of NCAs known as N-thiocarboxyanhydride (NTAs) have been developed for polypeptide synthesis.[23] NTAs are highly stable towards moisture or heat and hence bench stable for long period and their polymerization can be carried out under ambient conditions. However, almost all NTAs reported till date are achiral in nature due to involvement of racemization during their synthesis and hence, polymerization of these racemic NTAs leads to racemic polypeptides which does not have privilege to adopt secondary structures that restricts them to be used in many applications. Recently, Flow chemistry was employed for synthesis of NCA and wide variety of NCAs with several acid sensitive groups like silyl, tert-butyl ether, acetonide, trityl, Boc, etc. were synthesized.[24] The flow chemistry method involves the rapid mixing of aqueous solution of sodium salt of amino acid containing N-methyl morpholine with triphosgene solution in acetonitrile in a “V” shaped mixer to afford NCAs in less than one second and it is followed by flash dilution with ethyl acetate for isolation of NCA. The process is carried out in specially designed microfluidic device and the isolated NCA after

evaporation of ethyl acetate needs extra purification by recrystallization only in few cases otherwise most NCAs obtain are highly pure and can be directly used.

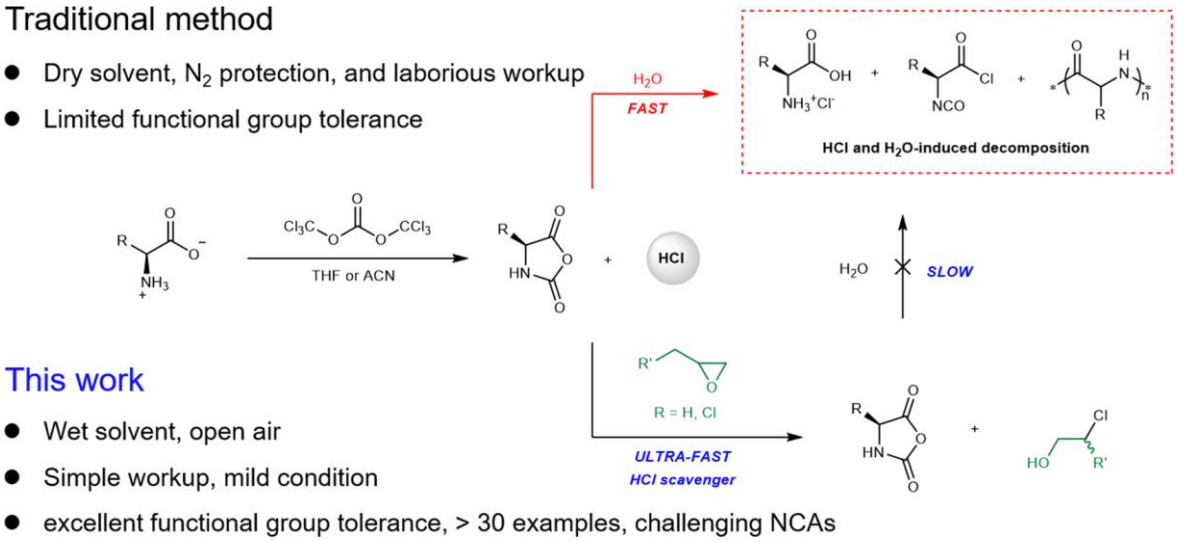

Figure 1.3. *Schematic representation of synthesis of NCA by using propylene oxide as HCl quencher. (adapted from Tian, ZY et al. Nat Commun.* **2021**, *12*, 5810).

Another notable recent development in synthesis of NCA is the development of moisture tolerant protocol for synthesis of NCA by using propylene oxide or epichlorohydrin as HCl quencher.[25] In their report, Hua Lu and co-workers have shown that, the HCl is the main culprit responsible of NCA degradation by water and if it is eliminated effectively, then NCAs can be synthesized by using Fuch-Farthing method without the use of anhydrous conditions (see Figure 1.3). The method involves treatment of amino acid in THF with triphosgene at room temperature in presence of propylene oxide or epichlorohydrin. Due to the heat evolved in the reaction, it can be carried out without external heating and the NCAs can be isolated by simple work up followed by crystallization under ambient conditions without need of anhydrous solvents. For liquid NCAs, the purification can be done using flash chromatography in open air without using anhydrous solvents. Remarkably, the NCAs of unprotected functional amino acids such as L-glutamic acid, L-serine, L-cysteine, were synthesized for the first time using this approach. L-Glutamic acid NCA was successfully polymerized to get polyglutamic acid directly without involvement of any protection-deprotection step and also, cysteine NCA was polymerized to make hyperbranched architectures. This report is the praiseworthy contribution in the field of polypeptide and it has almost eliminated all the hurdles in NCA synthesis.

The advancements in ring opening polymerization of NCA monomers involves the development of new initiators for polypeptide synthesis or it involves the development in catalysts for NCA polymerization. The ring opening polymerization (ROP) of NCA is traditionally initiated by nucleophiles or bases such as primary amines, alkoxides, tertiary amines, etc.[10, 26] There is no universal initiator or optimal polymerization conditions to make high molecular weight polypeptides from any NCA monomer, it all depends on properties such as solubility and reactivity of individual NCA monomer and resulting polymers, as well as it is significantly dependent on side reactions involved during polymerization. The ROP of NCA mostly follows two general pathways which are called as normal amine mechanism (NAM) and activated monomer mechanism (AMM) (see Scheme 1.4a and 1.4b).[26]

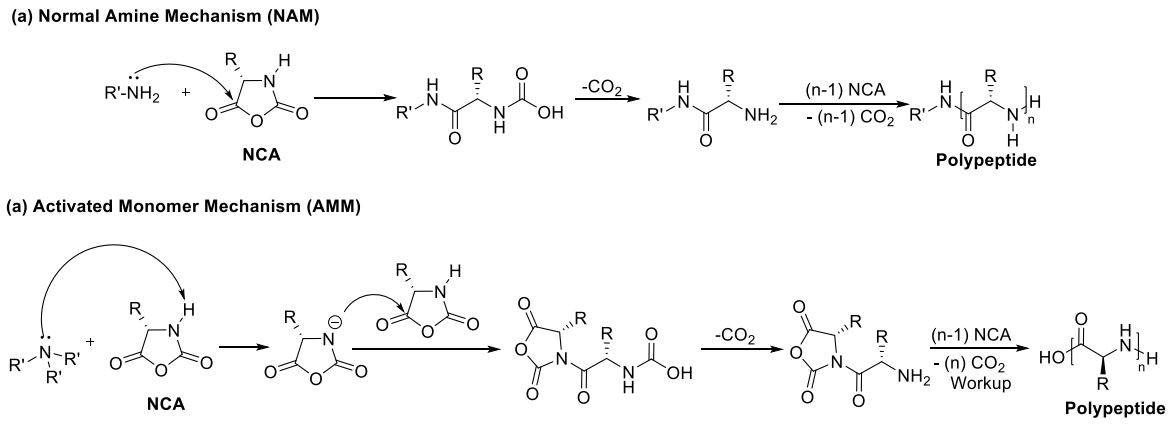

Scheme 1.4. *Schematic representation of (a) Normal amine mechanism for NCA ROP, (b) Activated monomer mechanism for NCA ROP*

The NAM involves the attack of nucleophile on anhydride carbonyl of NCA, that results in opening of highly strained ring of NCA to form unstable carbamic acid intermediate which undergoes decarboxylation (loss of CO_2) to generate species with terminal amine functionality, which attacks the next NCA monomer and the process repeats to get polypeptide (See Scheme 1.4a). In case of NAM, rate of initiation is usually higher than rate of propagation and hence polymer should grow linearly if side reactions are absent and that results in great control over polymerization process and polypeptides with desired molecular weight can be produced (degree of polymerization matches to M/I in the feed). On the other hand, AMM involves the deprotonation of NCA to generate NCA anion that acts as nucleophile and opens the other NCA monomer and polymerization proceeds further (see Scheme 1.4b). In case of AMM, polymerization is usually uncontrolled due to slow initiation and faster propagation that results in polypeptides with higher molecular weights

than expected (high degree of polymerization than M/I in the feed) and with higher dispersity (Đ). In conventional polymerizations, these two mechanisms can operate simultaneously and compete with each other and it all depends on extent of nucleophilicity or basicity of initiator. If initiator is more basic, such as in case of alkoxides or tertiary amines then it predominantly follows AMM and results in poor control in polymerization process. On the other hand, if initiator is more nucleophilic such as in case or primary amines, NAM is followed predominantly and hence they are highly preferred initiators for NCA ROP. Although, primary amines are better nucleophiles and follows NAM pathway, but still, they are basic in nature and hence can follow AMM pathway as well to some extent, as a side reaction, and it results in loss of control in polymerization especially for preparation of high molecular weight polymers since it requires very low concentration of initiator. In addition to this, conventional NCA ROP by primary amines suffers side reactions such as chain termination due to reaction with DMF solvent considering these limitations of conventional ROP of NCA, not many architectures like block copolymers and high molecular weight polymers were not prepared until the discovery of organometallic initiators.[13, 14]

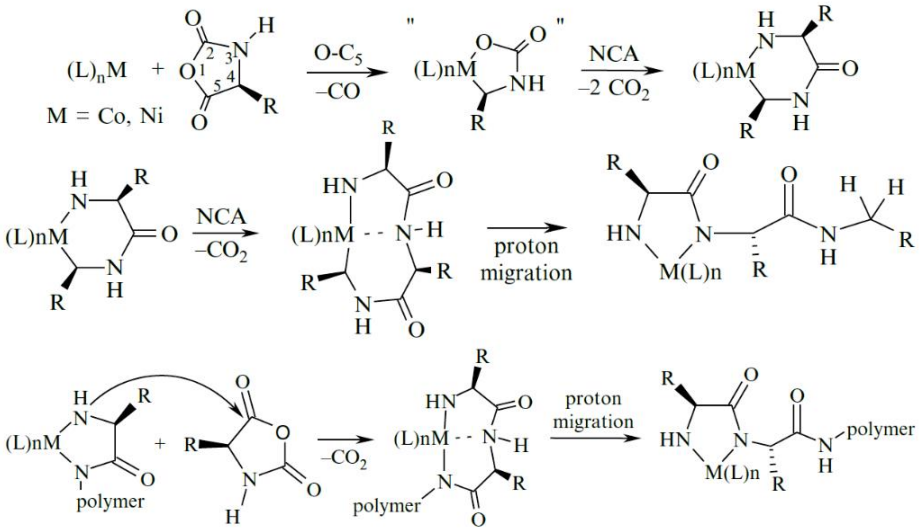

Scheme 1.5. *Schematic representation of mechanism of NCA ROP by transition metal initiators*

In late 1990s, Deming reported the zerovalent Ni or Co based organometallic initiators for living ROP of NCA and the high molecular weight polypeptides and block copolypeptides were synthesized for the first time. [13, 14] The zerovalent Ni [in the form of bpyNi(COD)] or zerovalent Co [in the form of $(PMe_3)_4Co$] undergoes oxidative addition across anhydride bond of NCA to form metallacyclic complex that reacts with second NCA molecule to form 6-membered amido-alkyl metallacycle which upon further reaction with

next NCA monomer, undergoes ring contraction by decarboxylation followed by proton migration to form 5-membered amido-alkyl metallacycle (see Scheme 1.5). These 5-membered amido-alkyl metallacycle are active polymerization intermediates and the chain propagation occurs after their reaction with upcoming NCA monomers to yield polypeptides of tailorable molecular weights ($500 < M_n < 500{,}000$) and extremely low dispersities ($Đ < 1.2$). In this method, metal migrates along the growing polypeptide chain, while being held by chelation with active chain end (in the form of 5 membered amido-alkyl metallacycle) and this chelation is key to give living polymerization characteristics. One major drawback of this method is that it is not applicable to NCAs bearing secondary amine, e.g. proline NCA since it lacks N-H moiety. Recently, this was overcome by Kramer and co-workers by using the Ni-amidoamidate complex as initiator for ROP of proline NCA.[27] In this method, chain end functionalization of C-terminus is not possible which is overcome by development of allyloxycarbonylaminoamides as a general precursor to amido-amidate Nickelacycle and to produce polypeptides with chain end functionality at C-terminus.[28] Although this method is excellent method for synthesis of polypeptides, it requires very stringent inert conditions and has to be performed in glove-box.

After development of the transition metal catalysis, the polypeptide literature was flooded with several reports on controlled ROP of NCA.[11, 29] The controlled ROP of NCA was shown by using amine hydrochloride salts by Schaalad.[30] The amine hydrochloride salt is less nucleophilic but cannot acts as base hence AMM is impossible with it. Also, the control in polymerization is achieved through equilibrium between dormant amine salt and active amine to yield polypeptides with very low dispersities ($Đ = 1.03$). The polymerization with amine hydrochloride is extremely slow and can take three days, also incomplete polymerization may occur due to slow reactivity. To improve the kinetics, combination of tertiary amine and primary amine hydrochloride salt was tried for controlled ROP of NCA and the polymerization was found to be accelerated and controlled as long as the ratio of primary amine hydrochloride and tertiary amine is maintained below 0.9 (upon decreasing further, it leads to uncontrolled polymerization due to AMM by more tertiary amine).[31] In the same context, controlled NCA ROP was attempted using amine tetrafluoroborate salt that allowed synthesis of polypeptides up to 800 units with narrow dispersity ($Đ < 1.2$).[32] In the same manner, the controlled NCA ROP was reported using frustrated Lewis pair consisting of aromatic amine and bulky borane Lewis acids.[33] The another Lewis acid, zinc acetate, was found to control the ROP of NCA and well defined polypeptides were produced.[34]

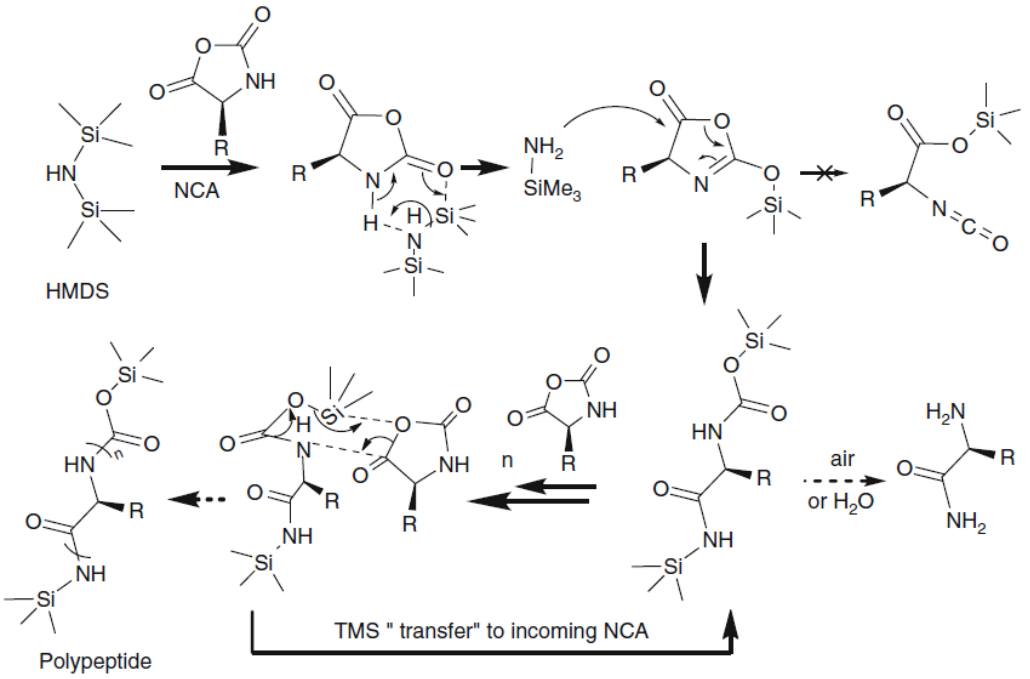

Scheme 1.6. *Mechanism for NCA ROP initiated by silazane derivatives. (adapted from Cheng, Jianjun et al. Top Curr Chem.* ***2012****, 310, 1-26*).

Another notable example of controlled NCA polymerization is the use of silazane derivatives developed by Cheng and co-workers. Hexamethyldisilazane (HMDS) was employed for ROP of NCA and the controlled polymerization was observed with living features.[35] Later, primary amine silazane derivatives were employed for living NCA ROP.[36] The mechanism involves the formation of TMS-carbamate as an intermediate and TMS group migrates along growing polypeptide chain in the form of TMS carbamate and this turned out to be key to give living features to polymerization (see Scheme 1.6). Along the same lines, the phenylterimethylsilyl sulfide (PhS-$SiMe_3$)[37] was developed by Lu and co-workers as an initiator for controlled ROP of NCA and polymerization mechanism was similar as that for HMDS but yielded polypeptide with C-terminal thioester functionality that can be used in chemoselective native chemical ligation post polymerization.[38] Later on, to improve the kinetics of silyl group based NCA polymerization, the trimethylstannyl phenyl sulfide (PhS-$SnMe_3$)[39] was developed by same group and the polymerization was controlled and rapid compared to that initiated by PhS-$SiMe_3$ or HMDS. The PhS-$SnMe_3$ initiated polymerization was also followed same mechanism as that for PhS-$SiMe_3$ or HMDS

but it involved trimethytin (Me_3Sn)-carbamate intermediate instead of TMS (Me_3Si)-carbamate and that lead to faster propagation as "Sn" is softer than "Si".

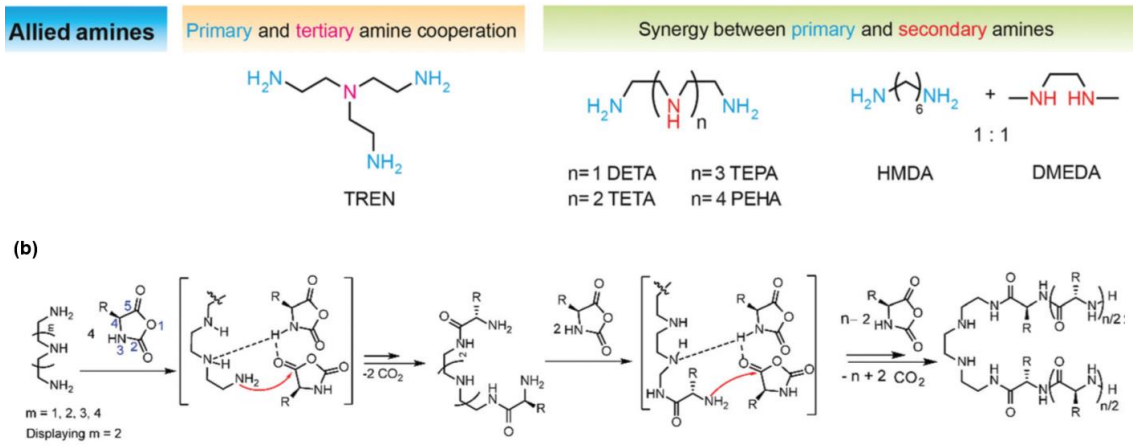

Figure 1.4. *(a) Structures of allied amines, (b) Mechanism for NCA ROP initiated by allied amines (adapted from Rasines Mazo, Alicia et al. Chem. Soc. Rev.,* ***2020****, 49, 4737-4834*).

The Hadjichristidis and co-workers reported an interesting initiator comprising of tertiary amine and primary amine together in one molecule, called as TREN (triethylaminetriamine).[40] TREN facilitated NCA ROP at high speed compared to primary amines without losing control over polymerization though it has tertiary amine. The tertiary amine present in TREN is weakly basic and cannot abstract the NCA proton hence it cannot undergo AMM but the tertiary amine can activate the terminal amino group of growing chain for attack on NCA, hence makes the faster propagation leading to superior kinetics. In the similar connection, secondary amine and primary amine together in one molecule (DETA, TETA, TEPA, PEHA, see Figure 1.4a for structures) were developed by same group and they also follow same mechanism of activation of terminal amino group for attack on NCA (see Figure 1.4b).[41] The authors coined this phenomenon as accelerated amine mechanism by monomer activation (AAMMA) and these amines were named as allied amines.

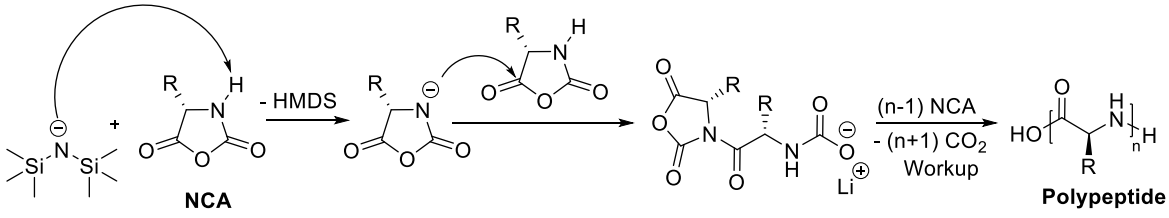

Scheme 1.7. *Mechanism for NCA ROP initiated by LiHMDS.*

Recently, Runhui Liu and co-workers reported the first ever polymerization of NCA under anhydrous conditions using lithium hexamethyldisilazide (LiHMDS) as an initiator to yield very high molecular weight polypeptides with narrow dispersities.[42] The

polymerization proceeds via AMM (see Scheme 1.7 for mechanism) but still produces polypeptides with narrow dispersities, but the polypeptides with higher molecular weight than expected were obtained in most cases. The polymerization involves lithium carbamate as intermediate and lithium migrates along growing polypeptide chain in the form of lithium carbamate that is responsible for faster kinetics. The polymerization was so fast that, it was completed within 2 h for M/I = 500 in the feed. The LiHMDS initiated polymerization of NCA was one of the fastest polymerization methods among all methods reported for synthesis of linear polypeptides by NCA ROP till that time and superfast kinetics allowed the polymerization to proceed under ambient conditions (in open air) without hydrolysis of NCA monomer. Besides, the same group reported further acceleration in polymerization by using potassium hexamethyldisilazide (KHMDS) and sodium hexamethyldisilazide (NaHMDS) and this time the polymerization was even faster and followed similar mechanism via potassium or sodium carbamate intermediate.[43] The rate of polymerization by these initiators followed the order, KHMDS > NaHMDS > LiHMDS which suggests that the larger the size of cation migrating over growing polypeptide chain in the form of carbamate salt, faster the polymerization kinetics. Keeping this in mind, same group reported further acceleration in polymerization kinetics with the use of tetraalkyl ammonium carboxylate as an initiator.[44] The tetraalkyl ammonium carboxylates works via NAM kind of mechanism as carboxylate anion attacks NCA and the bulky tetraalkyl ammonium cation migrates over growing polypeptide chain in the form of tetraalkyl ammonium carbamate (see Scheme 1.8). The polymerization with tetraalkyl ammonium carboxylates was ultrafast and it was completed within 5 min for M/I = 100 in the feed. These superfast polymerizations were found to have rate constants ($k_{obs} = k_p \times [I]$) of 51.67 h^{-1}, 6.42 h^{-1}, 2.79 h^{-1}, 1.69 h^{-1} for tetraalkyl ammonium acetate, KHMDS, NAHMDS and LiHMDS respectively versus 0.07 h^{-1} for hexyl amine-initiated polymerization for glutamate NCA at M/I = 100. This indicates the polymerization initiated by tetraalkyl ammonium carboxylate is nearly 750 times faster than that initiated by hexyl amine. The ultrafast polymerization kinetics in case of tetraalkyl ammonium carboxylate allowed polymerization in presence of water and importantly, the multiblock copolymer with 15 blocks was prepared by sequential addition of monomers.

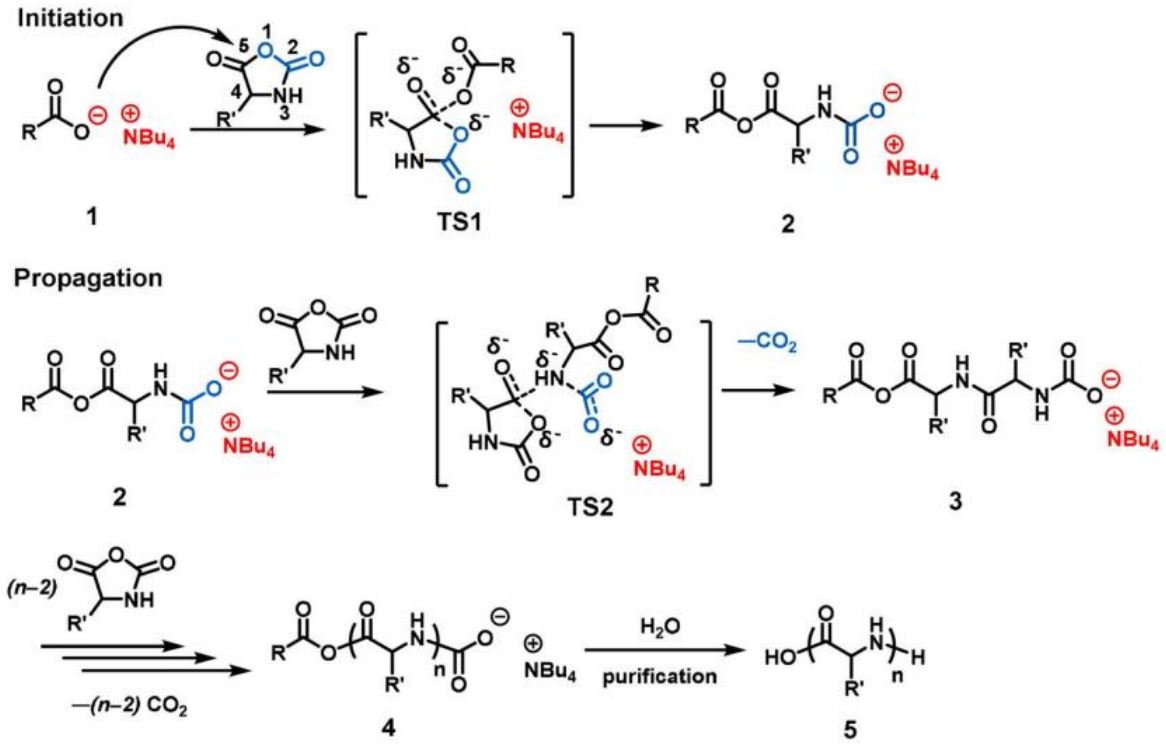

Scheme 1.8. *Mechanism for NCA ROP initiated by tetraalkyl ammonium carboxylates. (adapted from Y. Wu, et. al, Angew. Chem. Int. Ed.* ***2021****, 60, 26063.*).

In addition to these novel initiators described above, several catalysts were developed to control and accelerate the ROP of NCA. Among them, notable examples are the organocatalysts which will be discussed in this section. N-Heterocyclic carbenes (NHCs) were known to be excellent catalysts for ROP of several lactone monomers for synthesis of linear or cyclic polyesters.[45-47] For synthesis of polypeptides, NHCs were employed for the first time by Lu and co-workers to accelerate the ROP of NCA initiated by HMDS.[48] The NHCs are highly moisture sensitive and they have to be handled strictly under inert conditions. Daniel Taton and co-workers shown that, the bicarbonate salts of NHCs [NHC(H)(HCO_3)] are highly air stable compounds and can act as precursors for NHC since they release free NHCs in-situ with formal loss of water and CO_2.[49] Recently, Kim and co-workers employed these NHC-bicarbonate salts for ROP of NCA and the linear or cyclic polypeptide architectures were synthesized.[50] When the NHC-bicarbonates were employed along with primary amines as an initiator then linear polypeptides were obtained and in absence of amine initiators, NHC alone was found to be initiate ROP of NCA to yield cyclic polypeptides. The in-situ generated NHCs were found to dramatically accelerate the ROP of NCA and polymerizations were completed in less than 20 min in DMF as solvent and polymerization was found to be living in nature. On the other hand, under similar conditions,

without any catalysts, the polymerization takes nearly 20 h for completion.[51] The NHCs are strong σ-donors and they have excellent Bronsted base properties hence they can form hydrogen bonding interaction with amine initiator or amine terminus of growing polypeptide chain thereby accelerating the polymerization (see Scheme 1.9). Alike NHC, guanidines are also strong bases and they also have been employed for ROP of NCA.[52, 53] In the beginning, the tetramethyl guanidine was employed for alcohol-initiated ROP of NCA of N-alkyl amino acids to generate polypeptoids[53] and very recently, Zhibo Li and co-workers shown that, tetramethyl guanidine can accelerate of ROP of amino acid NCA initiated by alcohol, or primary amine or even carboxylic acids to make polypeptides at accelerated rate in controlled manner with mechanism similar to that for NHC.[52]

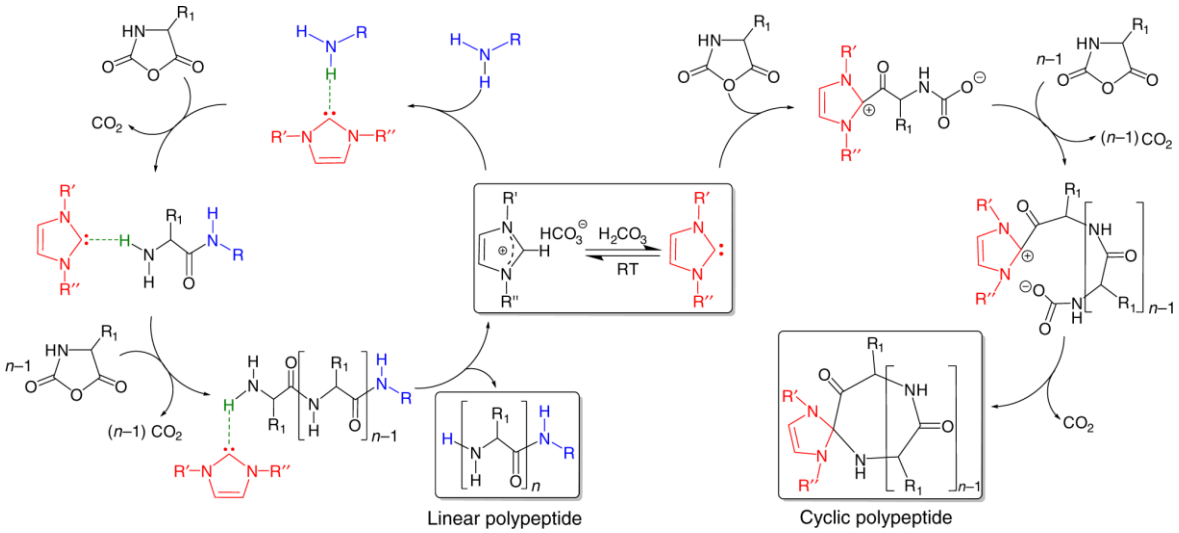

Scheme 1.9. *Mechanism for NCA ROP catalyzed by NHC bicarbonate salt. (adapted from Zhang, Y., et. al, Commun. Chem.* ***2018,*** *1, 40.)*

For any ring opening polymerization, faster initiation than propagation is the key to get polymers of desired molecular weight hence ROP of NCA is usually initiated by strong nucleophiles like primary amines. The alcohols are less nucleophilic than amine and as a result initiation will be slower than propagation because in case of NCA ROP, the propagating species is more nucleophilic (primary amine). To have control over NCA ROP initiated by alcohols, catalysts were developed in last few years. Among them, H-bond acceptor moiety, such as guanidine is utilized for alcohol initiated NCA ROP due to its strong basicity and it is already discussed above.[53] All other catalysts developed for alcohol initiated NCA ROP are H-bond donors and activates NCA carbonyl by H-bonding interaction. In this category, the N,N-bis[3,5-bis(trifluoromethyl)phenyl]-thiourea

(schreiner's thiourea)[54, 55] and fluorinated alcohols like 1,3-bis(2-hydroxyhexafluoroisopropyl) benzene (1,3-bis HFAB)[56] were reported by Hadjichristidis and co-workers for ROP of NCA initiated by amino alcohols. The rapid polymerization kinetics was observed for both catalysts and polypeptides with degree of polymerization up to 1290 were synthesized in control manner with very narrow dispersities.

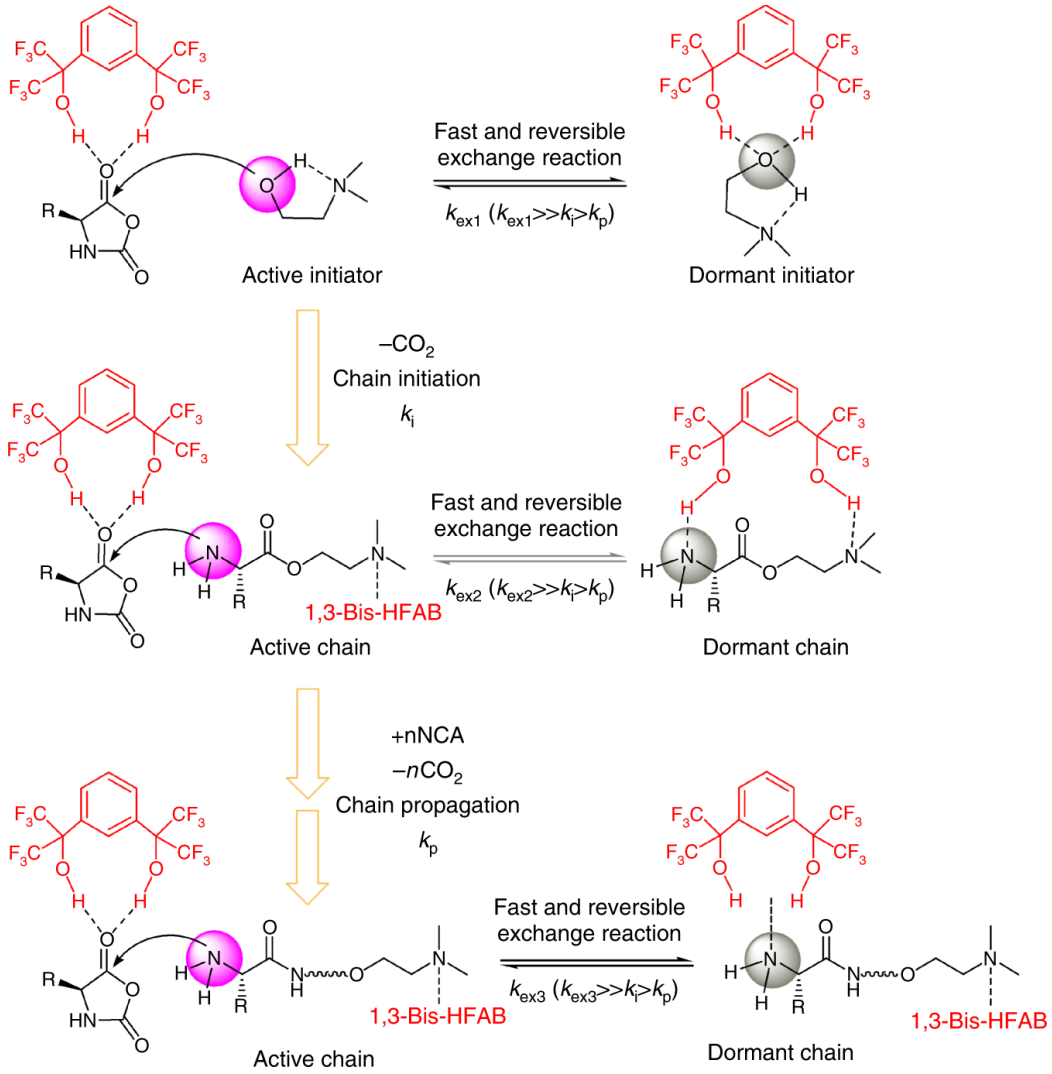

Scheme 1.10. *Mechanism for alcohol initiated NCA ROP catalyzed by fluorinated alcohol. (adapted from Zhao, W., et. al., Nat Commun,* ***2019****, 10, 3590).*

The choice of amino alcohol as an initiator is very interesting and tertiary amine functionality present in them is necessary to activate the alcohol for attack on NCA but one should not forget that it can also carry out unwanted side reactions via AMM pathway and here comes the role of thiourea or fluorinated alcohols, they perform three important roles in this polymerization (see Scheme 1.10 for mechanism). Firstly, they silence the tertiary

amine by H-bonding interactions and does not allow AMM. Secondly, they activate the electrophilic carbonyl of NCA by H-bonding interactions and make it more electrophilic for attack by alcohol (during initiation) or growing amine chain (during propagation) that makes huge role in acceleration of polymerization. Lastly, it reversibly deactivates the terminal amine group of growing polymer chain that gives the excellent control over polymerization. Pahovnik and co-workers reported the methane sulphonic acid as a catalyst for alcohol-initiated ROP of NCA. The methane sulphonic acid catalyzes the attack of alcohol on NCA to form amino acid ester with amine functionality completely dormant for propagation, this allows the complete initiation that can be monitored spectroscopically and when initiation is completed then base (DIPEA) is added to neutralize the dormant amine and start the propagation.[57] The polymerization was controlled and hybrid block copolymers like PCL-*b*-polypeptide or polycarbonate-*b*-polypeptides were synthesized in one pot using sequential ring opening of caprolactone (or cyclic carbonate) followed by NCA.[58]

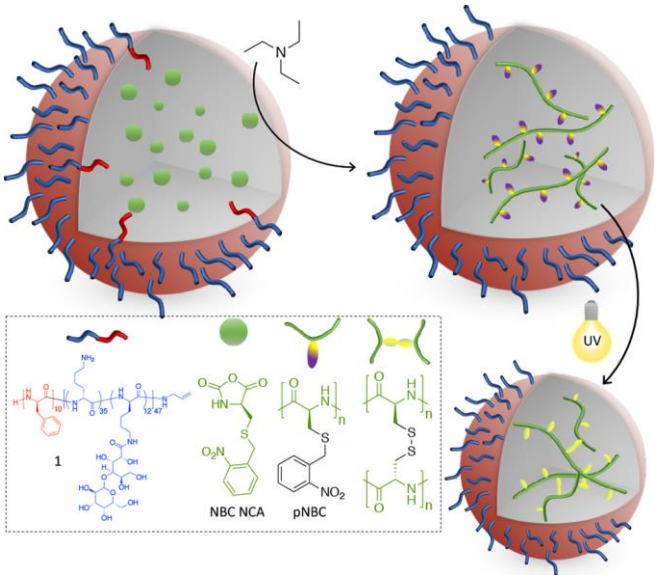

Figure 1.5. *Schematic representation for miniemulsion polymerization of S-(2-nitrobenzyl)-L-cysteine NCA and subsequent UV-cross-linking (adapted from Jacobs, J. et al. J. Am. Chem. Soc.* ***2019****, 141, 32, 12522–12526*).

In addition to all these developments in catalysts or initiators for controlled ROP of NCA, another way to control NCA ROP is simply by optimizing polymerization conditions. The most common way of minimizing side reactions in any synthesis is to reduce the temperature of reaction. Andreas Heise and co-workers have shown that, by reducing the temperature, side reactions in NCA ROP can be avoided and hence control over polymerization can be achieved.[59] The NCA ROP involves the loss of a CO_2 molecule per

consumption of one NCA molecule and hence if generated CO_2 is removed in time, then polymerization kinetics would enhance according to Le Chatelier′s principle. This concept was used by Andreas Heise and co-workers and they have shown that, the controlled NCA ROP and enhanced kinetics could be achieved by performing polymerization under high vacuum.[60] In the same note, Karen Wooley and co-workers demonstrated the acceleration and control in rate of NCA polymerization when it is performed under constant nitrogen flow and also the rate of polymerization was directly proportional to flow rate of nitrogen.[51]

The traditional emulsion polymerization conditions were employed by Jacobs et. al. for NCA ROP to prepare polypeptide nanoparticles (see Figure 1.5).[61] The S-(2-nitrobenzyl)-L-cysteine NCA was polymerized using typical miniemulsion polymerization conditions in dicloromethane-water mixture (1: 5, v/v). The glycosylated polypeptide diblock copolymer developed by same group was used as surfactant to stabilize the droplets/micelles containing encapsulated NCA monomer and these droplets or micelles were acted as microreactors. The polymerization was initiated using triethyl amine to follow AMM pathway for polymerization to yield polypeptide latex in short period of time. Finally, the latex was crosslinked by UV irradiation to yield stable emulsion comprising polypeptide nanoparticles of diameter around 200 nm. Recently, the scope of NCA ROP is expanded to polymerization induced self-assembly (PISA). The ROPISA of NCA monomer is shown in THF,[62] DMSO,[63] or water[64, 65] as solvent and polypeptide nanoparticles were produced. The aspects of PISA and ROPISA of NCA monomers is discussed in detail in Chapter 4.

1.3. Applications of Polypeptides

These synthetic advancements in the field of polypeptides, opens up avenues for wide variety of polypeptide architectures and any kind of polypeptide material can be now made easily as per requirement. Importantly, NCA monomers with wide range of functional group handles can be easily made (nearly 200 NCA monomers are known, and it will be expanded further as per requitements)[15] and that remarkably improves the scope of polypeptide applications in comparison to natural proteins which are limited to 20 natural amino acids. The biocompatible and biodegradable nature of polypeptides and their protein mimicking ability to form various secondary structures makes them a strong candidate in plethora of applications such as material applications,[66] gene delivery,[67-72] tissue engineering,[73-78] biosensors,[79-82] antifouling,[83-85] bioadhesive,[86-88] antimicrobial,[89-106] drug delivery,[107-128] etc. Among them, the antibacterial application and drug delivery applications

are discussed in brief (see Figure 1.6a). For most of the biomedical applications,[29] amphiphilic polypeptides are explored and most of them are block copolymers with polyethylene glycol (PEG). The PEG serves the hydrophilic block and polypeptide component is hydrophobic block and the hybrid PEG-polypeptide block copolymer can be easily synthesized by ring opening polymerization of NCA monomers using amine terminated PEG as macroinitiator (see Figure 1.6b).

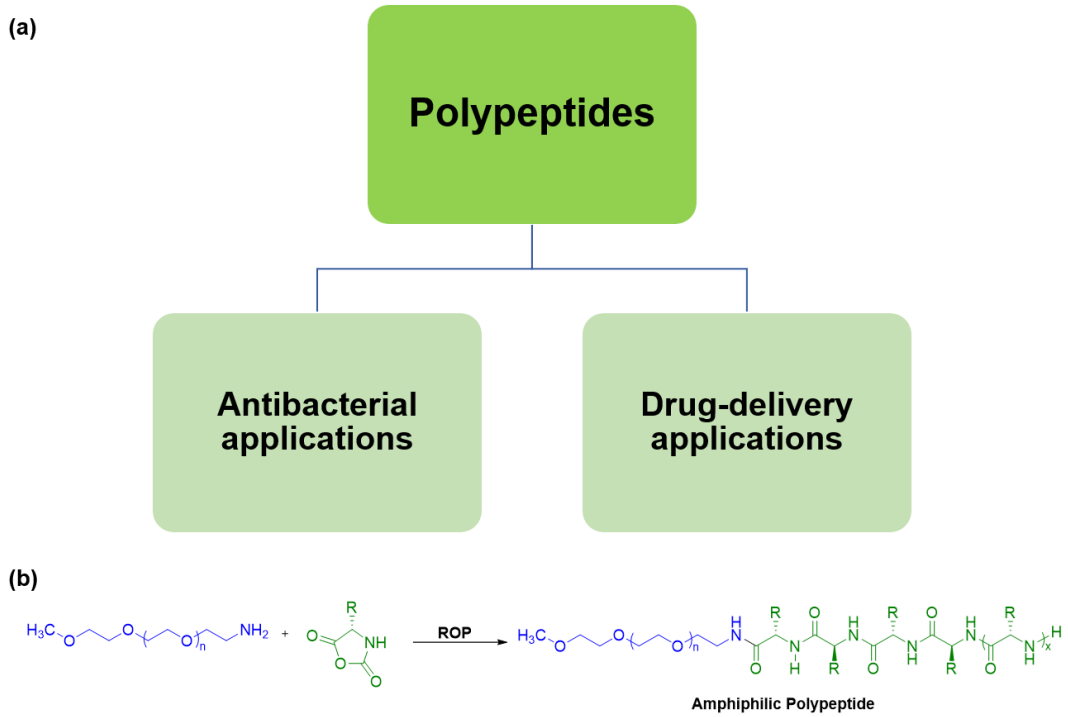

Figure 1.6. *(a) Scheme representing application of polypeptides in antibacterial and drug delivery field. (b) Scheme for synthesis of simplest amphiphilic polypeptide.*

Antimicrobial Applications: Amphiphilic polypeptides comprising of hydrophobic and cationic amino residues interact with the negatively charged phospholipids of bacterial membrane through electrostatic interactions. This event results in bacterial membrane disruption and then it leads to killing of bacteria (See Figure 1.7a). This mode of action is a preferred alternative over very specific targeted action of antibiotics, which is susceptible for antibacterial resistance. Over past two decades or so, the various linear architectures,[89-91] star shaped polypeptides,[92-95] cyclic polypeptides,[96] hyperbranched,[97] and grafted polypeptides[98-100] with various secondary structures are employed as antibacterial agents. The lysine or arginine are most preferable cationic building block while alanine, leucine, phenyl alanine or valine are most studied hydrophobic residues for these antibacterial

polypeptides and both block-copolymer and random copolymer architectures have been employed for antimicrobial applications.

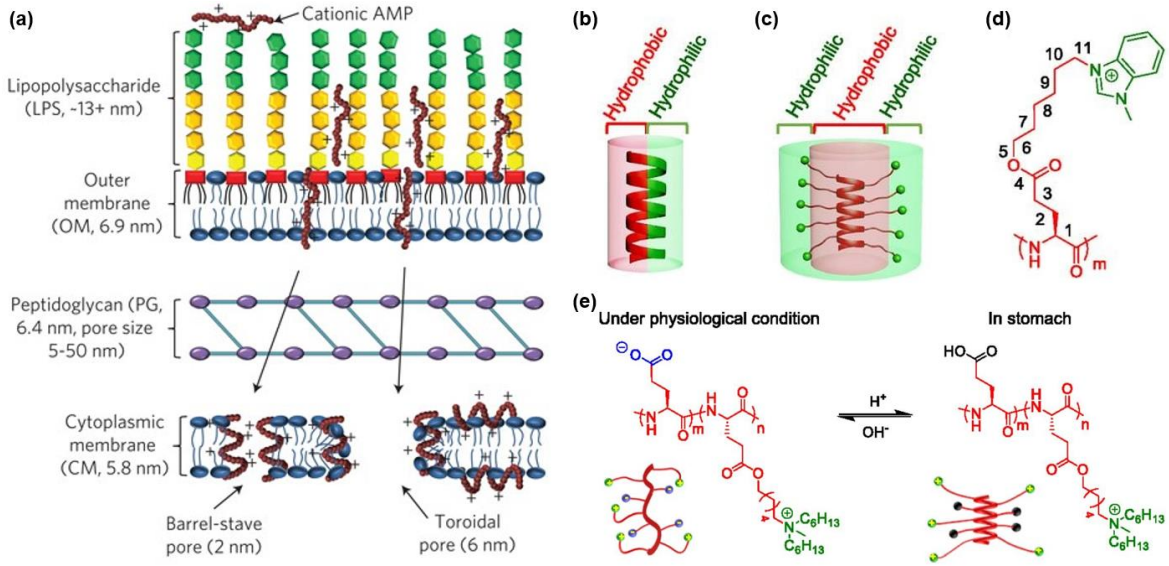

Figure 1.7. *(a) General mechanism of action of cationic antimicrobial peptides or polypeptides for bacterial membrane disruption. (adapted from Lam, S. J. et. al., Nat. Microbiol.* ***2016,*** *1, 16162). (b) Facial amphiphilic antimicrobial polypeptide (c) Radial amphiphilic (RA) antimicrobial polypeptide (d) Structure of RA polypeptide. (adapted from Xiong, M. et.al., Proc. Natl. Acad. Sci. U. S. A.* ***2015,*** *112, 13155. (e) pH-Responsive RA antimicrobial polypeptide effective against H. pylori (adapted from Xiong, M. et.al., Proc. Natl. Acad. Sci. U. S. A.* **2017,** *114*, 12675)

The secondary structures of polypeptides found to modulate the antibacterial activity and it was found that in most cases polypeptide bearing ordered secondary structures such as α-helices were better antimicrobial agents compared to polypeptide with no ordered conformation (random coils).[129] The α-helical polypeptide bearing cationic group are not usually stable moiety, Cheng and co-workers have shown that the cationic group separated from α-helical backbone by 11 σ bonds tend to form stable helices and they were called as radially amphiphilic polypeptides, on the other hand for shorter spacers, the helix is destabilized and it adopts random coil conformation (see Figure 1.7b, 1.7c and 1.7d).[91] The radially amphiphilic polypeptides were better antimicrobial agents compared to their random coil analogue. The stimuli responsive zwitterionic radially amphiphiles were designed which contains both cationic and negatively charged residues and they were found to exists in random coil conformation and exhibited poor antibacterial activity.[101, 102] But, upon removal of negative charge by stimuli (enzyme[101] or pH[102]), they became cationic and

adopted α-helical conformation and also their antibacterial activity increased drastically (see Figure 1.7e for pH responsive RA). In addition to secondary structures, the polypeptide architecture played important role in governing their antibacterial activity and it was found that, the star shaped polypeptides were better antibacterial agents (40 times higher minimum bactericidal concentration, MBC) compared to linear polypeptide of same composition.[94, 95] Apart from solution phase activity of polypeptide antibacterial agents, they were explored in other forms such as antibacterial hydrogel,[103, 104] antibacterial cryogel[105] and antibacterial material surfaces.[100, 106] The studies published in the past few years demonstrates the great interest in applying NCA ROP for the synthesis of polypeptides as antimicrobial agents having broad activity with reduced emergence of bacterial resistance and hence as antibiotic replacements.

Drug-delivery applications: The most common application of polypeptides is the delivery of therapeutics.[107] Due to synthetic advances in polypeptides, several amphiphilic architectures such as linear polymers, brush polymers, and star polymers can be easily synthesized and they can self-assembled in to various nano architectures like vesicles, micelles, gels, etc.[130] Although complex nano-architectures can be made using NCA ROP, the widely used morphologies for drug delivery applications are the micelles or vesicles synthesized via self-assembly of linear amphiphilic polypeptide block copolymers.[16, 29, 131] The polypeptides adopting various secondary structures exhibit different self-assembly behaviour with encapsulated and/or conjugated drug molecule that results in distinct role in their performance as nano carrier.[129] A notable example for role of polypeptide secondary structure in drug delivery application is the report from Kataoka and co-workers wherein they shown that, cis-platin loaded polymeric micelle composed of bundled α-helices formed by PEG-*b*-poly(L-glutamate) or PEG-*b*-poly(D-glutamate) exhibit higher micelle yield, displayed prolong release profile and prolong circulation in plasma compared to cisplatin loaded micelle composed of racemic PEG-*b*-poly(DL-glutamate).[108] However, in some cases ordered secondary structures adopted by polypeptide hampers the co-assembly or drug encapsulation in polypeptide based nano carriers due to their strong self-assembly and one such example was reported by Semple and co-workers.[109] In which they demonstrated that the micelle formed by racemic PEG-*b*-poly(DL-glutamate) exhibit better loading of irinotecan compared to that formed by helical PEG-*b*-poly(L-glutamate). In addition to secondary structure of polypeptides, the functionalities present on side chain of amino acid plays crucial role in drug encapsulation in polypeptide based nano carriers and it has been

demonstrated in outstanding report by Zhiyuan Zhong and co-workers wherein they have shown the ultra-high loading (63 wt%) of anticancer drug doxorubicin in PEG-*b*-polytyrosine due to enhanced π-π stacking between aromatic tyrosine residues and drug molecule (see Figure 1.8a).[110]

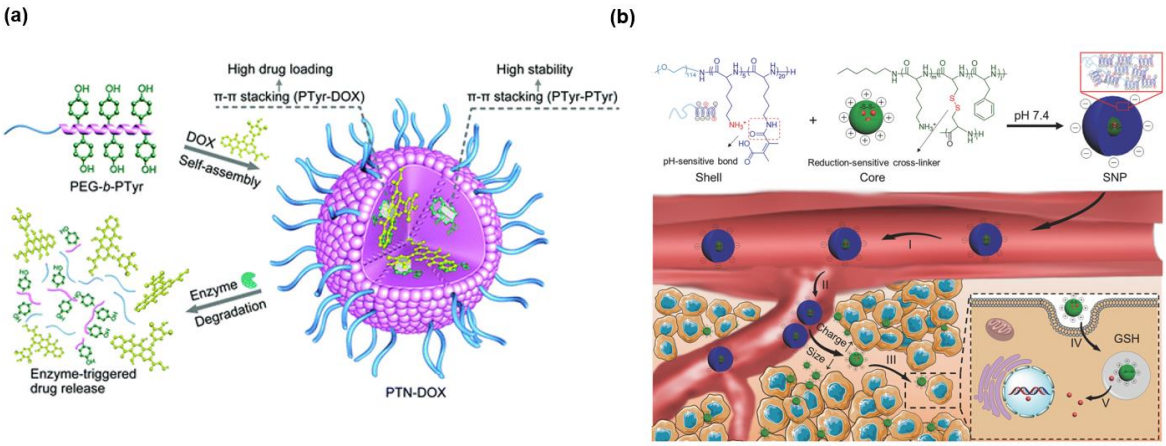

Figure 1.8. *(a) Illustration of poly(ethylene glycol)-b-poly(L-tyrosine) block copolymer nanoparticles for ultra-high loading of DOX and its enzymatic release. (adapted from Gu, X., et. al., Biomater. Sci.* ***2018,*** *6, 1526-1534). (b) Sequential responsive polypeptide nano particles for deep penetratin in to solid tumor (adapted from Chen, J., et. al., Adv. Funct. Mater.* ***2017,*** *29, 1701170).*

There has been growing interest in targeted chemotherapy and several polypeptide nanocarriers with targeting ligand are synthesized. The notable examples for targeted ligands are folic acid,[111, 112] hyaluronic acid,[113, 114] glycoamino acids,[115] cyclic-RGD peptide,[116] etc. Furthermore, there has been increased attention towards development of stimuli responsive polypeptide nanocarriers. The widely used stimuli are pH,[117-119] reduction,[120-122] ROS,[123, 124] enzyme,[110, 123, 125] UV light,[126, 127] etc. The stimuli responsive system allows the on-demand release of cargoes at desired locations. The Chen, J., et. al. demonstrated the sequential pH and reduction responsive polypeptide nanoparticles for deep penetration in to solid tumours (see Figure 1.8b).[132] Due to the advancements in polypeptide synthesis and polypeptide based nano-carriers, in past two decades many polypeptide-based drug delivery systems are in clinical trials with notable example of PEG-*b*-poly(aspartic acid) micelle containing paclitaxel, underwent phase III clinical trials.[128] These advancements in drug delivery applications of polypeptides hints the possible clinical use of polypeptide-based nanomaterials in upcoming future.

1.4. Role of α-Helix on NCA ROP

The synthetic polypeptides are most versatile protein mimicking materials which have ability to adopt various secondary structures like α-helices or β-sheets. These secondary structures play a major role in governing the properties of polypeptides and importantly plays a major role during polymerization. During NCA polymerization, the growing polypeptide chain can adopt secondary structures like α-helix or β-sheet and that decides the fate of polymerization. In the initial stage of NCA polymerization before 10-12 mers are produced, the growing polypeptide chain usually exists in random coil or β-sheet conformation and at this stage of nearly 10-12 units, it can switch its conformation to α-helix and continue to grow as helical chain till the end of polymerization or it can remain in β-sheet conformation and further grow in the form of β-sheets. At this crucial stage of NCA polymerization, if growing polypeptide chain adopts α-helical conformation then polymerization occurs homogeneously and polypeptides with high molecular weight can be produced (see Figure 1.09). On the other hand, if growing polypeptide chain remains in β-sheet conformation then it usually starts precipitating during polymerization and this induced heterogeneity in polymerization leads to production of low molecular weight polymers (see Figure 1.09).

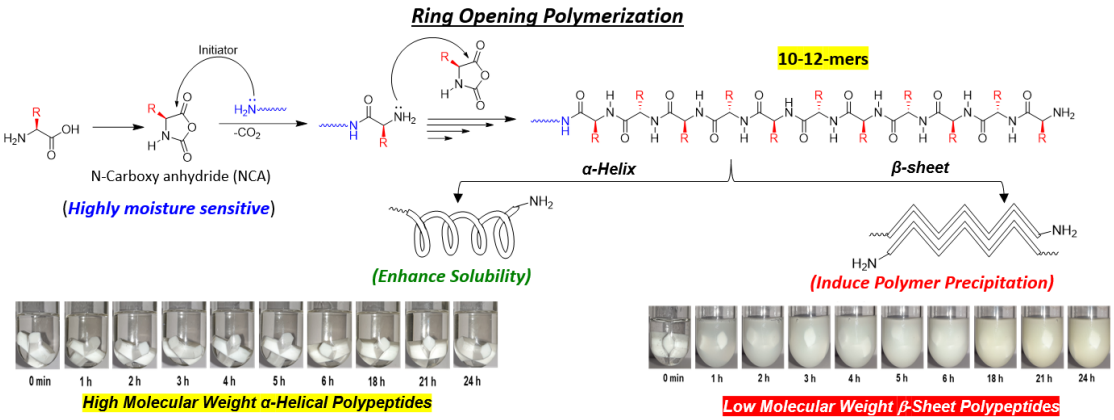

Figure 1.09. *Secondary structures involved during NCA ROP and effect of solvent on secondary structures.*

The secondary structures adopted by growing polypeptide chain is heavily dependent on polymerization solvent or amino acid used to make NCA. The chlorinated solvents having low dielectric constant such as dichloromethane or $CHCl_3$ ($\varepsilon = 4.8$) were found to stabilize α-helical structures on the other hand solvents with high dielectric solvent like THF ($\varepsilon = 7.5$) and DMF ($\varepsilon = 36.7$) were found to destabilize the α-helix motifs. The polypeptide derived from amino acids like valine, isoleucine, glycine, serine, threonine, tyrosine, and cysteine have propensity to form β-sheet structures and their polypeptides are highly insoluble.[12] On the other hand, the polypeptides composed of leucine, β-esters of aspartic acid, γ-esters of glutamic acid, N-substituted lysine, histidine, and methionine tend to adopt α-helical conformation and their polypeptides are soluble in polymerization solvents.[12] The homogeneous polymerization and living polymerization characteristics allow the synthesis of block copolymer architectures (see Figure 1.10).

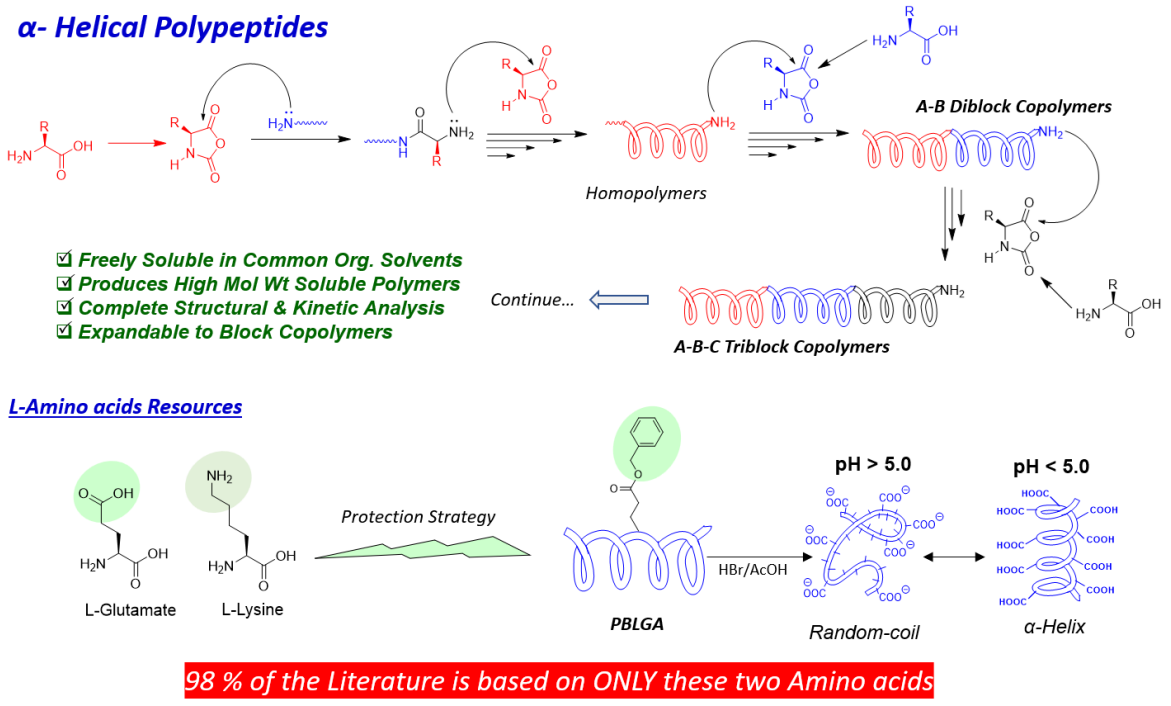

Figure 1.10. *Figure representing the advantages of α-helical polypeptides for synthesis of block copolymers and also demonstrating the pH dependent secondary structure transition in polyglutamate.*

As a result of this, most of the polypeptide literature (~98 %) is focused on amino acids having propensity to form α-helical polypeptides while the β-sheet polypeptides are rarely explored and that will be discussed in detail in section 1.5 of this chapter. Among the amino acids having propensity to form α-helical polypeptides, L-glutamic acid and L-lysine are highly explored in the polypeptide field and majority of polypeptide literature including

catalyst development, applications, etc. is focused on these two amino acids. Additionally, polypeptides synthesized from these two amino acids are charged polypeptides (after deprotection of side chain protecting group) and have tendency to undergo pH dependent secondary structure transition (see Figure 1.10 for pH dependent secondary structure transition in polyglutamate) and hence they are highly explored in biomedical applications as well.

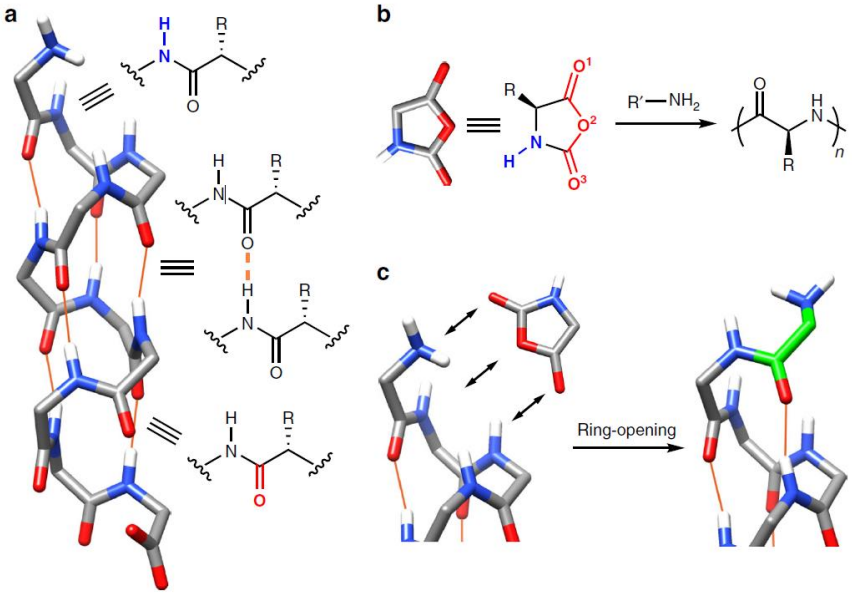

Figure 1.11. *Schematic depiction of the catalytic strength of an α-helix. (a) Probable interaction sites at the N-terminus of α-helical polypeptide. H-bonds involved in helix formation are shown with orange lines and the side chains are not shown for simplicity. (b) H-bond acceptors in NCA molecule are shown in red while the H-bond donors are shown in blue. (c) Anticipated interaction of NCA molecule with the N-termini of α-helix and its propagation by ring opening. The newly chain extended residue is decorated in green. (adapted from Song, Z et al. Nat. Commun.* ***2019,*** *10, 5470*).

In addition to homogeneous polymerization features, the α-helical polypeptides possess some remarkable properties such as self-catalysis for their own propagation and co-operativity in polymerization resulting in tremendous acceleration in polymerization rates. As mentioned above, for amino acids having propensity to form helices, the growing polypeptide chain undergoes conformational transition from random coil or β-sheet to α-helix in the beginning of NCA polymerization in helecogenic solvents (helix promoting solvents such as dichloromethane, $CHCl_3$). This conformational transition is responsible for two stage kinetics for these polypeptides since it was found that, the polypeptide chain in α-helical conformation grows extremely fast compared to that in random coil or β-sheet conformation. This auto acceleration of self-propagation is due to the interaction of

incoming NCA and terminus of growing polypeptide chain (see Figure 1.11).[133] It was demonstrated by Cheng and co-workers that the four free N-H groups (not involved in intramolecular H-bonding of helix) at the N-terminus of growing polypeptide chain have reduced rotational freedom as evident from their alignment in the direction of macrodipole of helix. The incoming NCA has three H-bond acceptors and hence can bind reversibly to those four N-H present at the terminus that enables the NCA ring opening at accelerated rates thereby increasing the polymerization kinetics. Furthermore, same group reported that the crown ether (18-crown-6) can change the binding geometry between NCA and N-terminus of growing polypeptide chain that promotes the molecular interactions and lowers the energy barrier for ring opening of NCA and ultimately leading to ultrafast polymerization kinetics.[134] The hexyl amine-initiated polymerization of glutamate NCA ([NCA] = 0.4 M) catalyzed by crown ether was completed within 2 minutes for M/I = 100 and it was found to tolerate presence of water in the polymerization solvent.

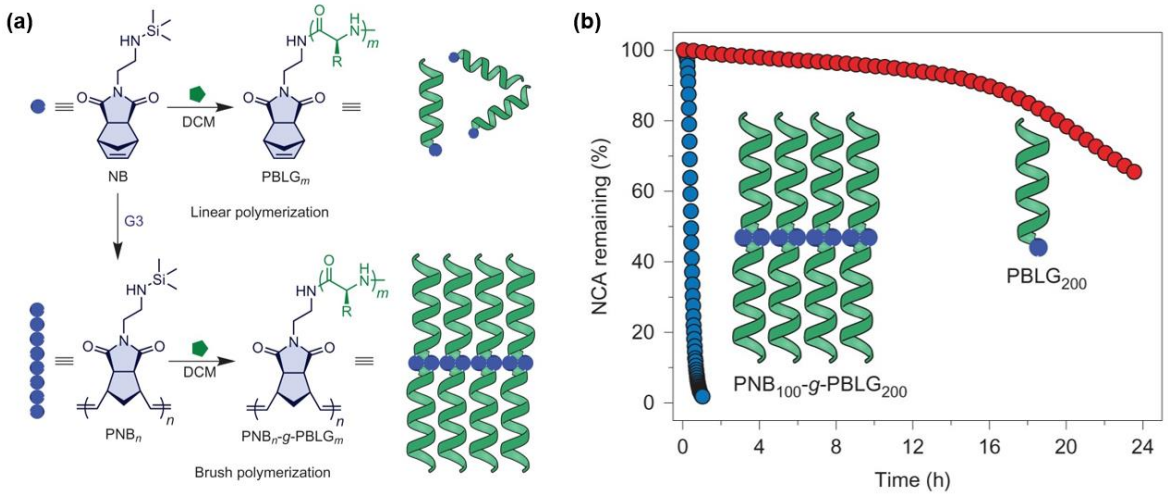

Figure 1.12. *The acceleration of polymerization rate by helix co-operativity. (a) Schematic representation of the linear polymerization (using linear NB initiator) and brush polymerization (using PNB macroinitiators). (b) The amount of NCA remaining with time for linear polymerization (using NB, shown in red) and that for brush polymerization (using PNB100 macroinitiator, shown in blue). (adapted from Baumgartner, R., et.al, Nat. Chem.* ***2017,*** *9, 614-622*).

In addition to the autocatalytic behaviour, the α-helical polypeptide possesses a co-operative behaviour and this was observed for the first time by Cheng and co-workers. The co-operative behaviour was observed in case of grafting-from polymerization of NCA having helical propensity using poly(norbornene) functionalized with TMS amine as macroinitiators to obtain brush polymeric architectures (see Figure 1.12).[135] The huge difference in polymerization rate was observed in case of brush system (initiated by

polynorbornene based TMS amine macroinitiator) and a linear system (norbornene based TMS amine initiator) under identical conditions (same M/I per chain, same concentration of monomer, etc.). the difference in polymerization rate was so huge that, in particular case the 30% monomer consumption was observed in 24 h for linear system while for brush system complete consumption of monomer was observed within 1 h. The polymerization of brush system was about 1000 times faster than that of linear system under identical experimental conditions. Using this technique, brush copolymer with very high molecular weight (up to $M_n = 4.3 \times 10^7$ Da) and extremely narrow dispersity ($Đ < 1.1$) was obtained. The reason behind this dramatic acceleration was the interaction between parallelly growing helices along polynorbornene backbone. The polypeptide helix acts as macrodipole and the cooperative interaction between parallelly aligned macrodipoles in close proximity results in substantial acceleration in polymerization kinetics. In the same context, it was shown that the aliphatic diamine initiators [$H_2N(CH_2)_nNH_2$] with linker length from n = 2 to 12 exhibit faster polymerization kinetics compared to monoamine initiator (hexyl amine).[136] The polymerization of glutamate NCA (with helical propensity) initiated using 1,6-diaminohexane was completed within 40 min while only 10% conversion was observed for hexyl amine-initiated polymerization of glutamate under similar conditions. The acceleration in kinetics were more pronounced for shorter carbon spacers ($n \leq 6$)) while the effect was diluted for initiator with longer spacers (n = 10 to 12). These diamines upon polymerization of NCA having helical propensity generates the polypeptide double helix motif, which they called as hinged polypeptides and the similar macrodipole interactions as observed in brush system accelerates the polymerization kinetics. Furthermore, the helix co-operativity (or proximity-induced rate acceleration) observed in NCA ROP was expanded to star shaped initiators like PAMAM dendrimers and polypeptide with highest molecular weight ever was produced ($M_n = 8.7 \times 10^7$ Da), with extremely narrow dispersity ($Đ < 1.05$) within few hours.[137] The resultant star shaped polypeptides were found to self-assemble into unimolecular micelles upon post polymerization deprotection. In all these cases, proximity-induced rate acceleration in NCA ROP was observed only when polymerization was performed in helecogenic solvents such as dichloromethane or $CHCl_3$ and importantly for optically pure amino acid NCAs having tendency to give helical polypeptides and the effect would be not possible for racemic amino acid NCAs as they cannot adopt any secondary structures.

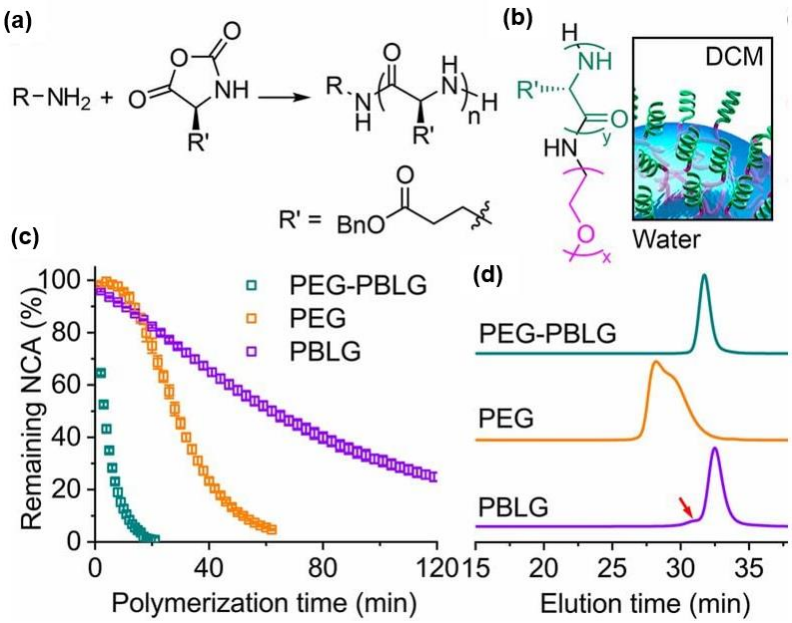

Figure 1.13. *SIMPLE (*segregation-induced monomer purification*) polymerization strategy. (a) Scheme for polymerization of BLG-NCA. Anticipated interfacial anchoring behaviour of PEG-b-PBLG macroinitiators (c) % of BLG NCA remaining in a w/o emulsion in the presence of PEG-b-PBLG, PEG-NH_2, PBLG macroinitiators and (d) Normalized SEC traces of resultant polymers. (adapted from Song, Z. et al. Proc. Natl. Acad. Sci. U. S. A.,* ***2019****, 116, 10658*).

Moreover, the proximity induced rate acceleration was translated to emulsion polymerization of NCA in dichloromethane-water (or $CHCl_3$-water) by Cheng and co-workers.[138] The helical PEG-*b*-polybenzylglutamate (PEG-*b*-PBLG) was synthesized and it was envisioned that this amphiphilic di-block copolymer would self-assemble in biphasic system (dichloromethane-water) in such a manner that, PEG chains will be in water layer in the form of interfacial anchors and the PBLG chains would fold in to α-helical arrays protruding into dichloromethane layer as the macroinitiators to yield water-in-oil (w/o) emulsion (see Figure 1.13). This self-assembled structure is nothing but supramolecular arrangement of polypeptide helices in close proximity and hence is susceptible to proximity induced rate acceleration in NCA ROP. Indeed, the PEG-*b*-PBLG generated the stable w/o emulsion in dichloromethane-water system and upon addition of glutamate NCA, the chain extension happened at extremely high speed with complete consumption of monomer in 20 minutes for M/I = 100 in the feed and the resultant polymer was found to possess extremely narrow dispersity (< 1.1), indicating the polymerization driven by proximity-induced rate acceleration. The aqueous phase was additionally used for the in-situ removal of impurities associated with crude NCA through segregation and allowed the remarkably fast and controlled polymerization of unpurified NCAs. While, the unpurified NCAs were failed to

polymerize in 12 h in an anhydrous condition, that confirms the disadvantageous inhibitory effect of traces of impurities for NCA ROP. Authors called this strategy as “segregation-induced monomer purification and initiator localization promoted rate enhancement (SIMPLE)”. This “SIMPLE” strategy can be a major breakthrough in the field of NCA ROP, since, this strategy not only evades the anhydrous conditions during NCA polymerization but also avoids the tedious NCA purification process.

1.5. Role of β-Sheet on NCA ROP

Although there has been an immeasurable amount of study on NCA ROP methodologies for α-helical polypeptides, there has been a scarcity in the studies on the synthesis of insoluble β-sheet forming polypeptides because of complications associated with their preparation via NCA ROP.

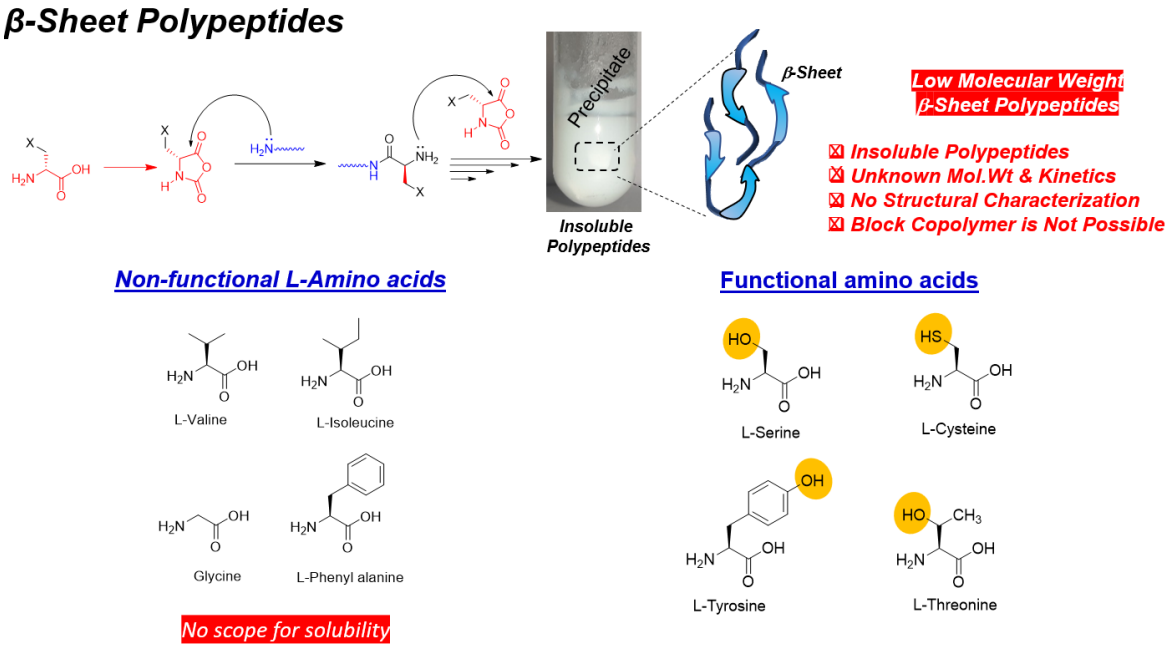

Figure 1.14. *Challenges associated with synthesis of β-sheet polypeptides and amino acids having propensity to form β-sheet polypeptides are shown.*

These complications arise from the precipitation of oligopeptides at the beginning of polymerization in the form of β-sheet lamellae (See Figure 1.14). Even though chain growth can still happen from the surface of these β-sheet lamellae, these chains tend to folds back to form interchain antiparallel sheets that finally deactivates the still "living" (growing) chain ends due to steric hindrance.[12, 139] This physical death of the growing polymer chain restricts molecular weight building in β-sheet forming polypeptides. Besides limiting the molecular

weight of polypeptide, it also restricts the synthesis of higher-order structures such as block copolymers from these precipitated β-sheet chains. Hence, it is challenging to make high molecular weight β-sheet forming polypeptides; besides that, it is almost impossible to produce block copolymers from these insoluble β-sheet polypeptides. Additionally, due to the insolubility of these polypeptides, it is practically impossible to determine their molecular weight distribution by GPC analysis. Polypeptides derived from amino acids such as glycine, phenyl alanine, tyrosine and amino acids containing branching or presence of heteroatom (O or S) in place of β-carbon such as isoleucine, valine, serine, and cysteine have very high propensities for the formation of β-sheet secondary structures (See Figure 1.14),[12] which makes them insoluble in common organic solvents; as a result, they suffer from limited access to high molecular weights polymers and higher-order structures.

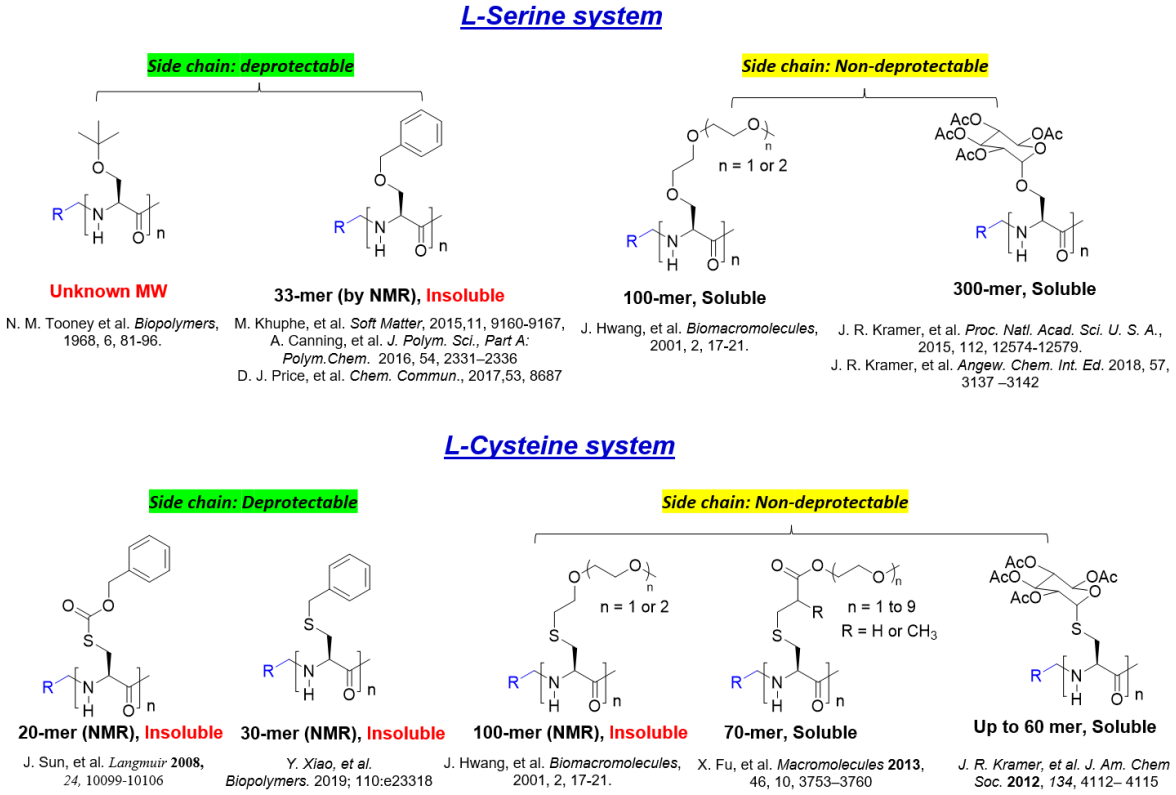

Figure 1.15*. Commonly employed masking groups for* L*-serine and* L*-cysteine for polypeptide synthesis.*

Among these amino acids, non-functional amino acids such as isoleucine, valine, glycine, phenyl alanine cannot be modified and hence their properties cannot be changed. On the other hand, in case of amino acids such as L-serine, L-cysteine, L-threonine and L-tyrosine there is scope to improve solubility of resultant polypeptide by attaching various masking groups to amino acid side chains. L-tyrosine and L-threonine are very least explored

and very few examples are reported. The side chain hydroxy or thiol functionality of L-serine or L-cysteine has to be protected before NCA synthesis otherwise these functionalities will have adverse effects on NCA polymerization (see Figure 1.15 for commonly employed protecting groups for L-serine or L-cysteine). Commonly, hydroxy group of L-serine is protected as benzyl ether,[60, 140-142] *tert*-butyl ether[143] or acetate[144-147] and thiol group of L-cysteine is typically protected as benzyl thioether,[148] 2-nitrobenzyl thioether,[120, 149-151] benzyl thiocarbamate,[152-154] tert-butyl disulfide,[155] S-alkylsulfonyl,[156, 157] etc. In case of most of these removable (deprotectable) protecting groups as masking groups for serine or cysteine, low molecular weight insoluble polymers were obtained. While in some cases low molecular weight soluble polymers were synthesized from L-serine and L-cysteine using amine terminated PEG as macroinitiator[144-147, 153] (see Figure 1.16) for various applications such as in glucose responsive insulin delivery,[144, 145, 147] in cancer therapeutics,[146, 158, 159] etc. However, the high molecular weight polymers were not reported from any of these conventional protecting groups due to the insolubility of polymers.

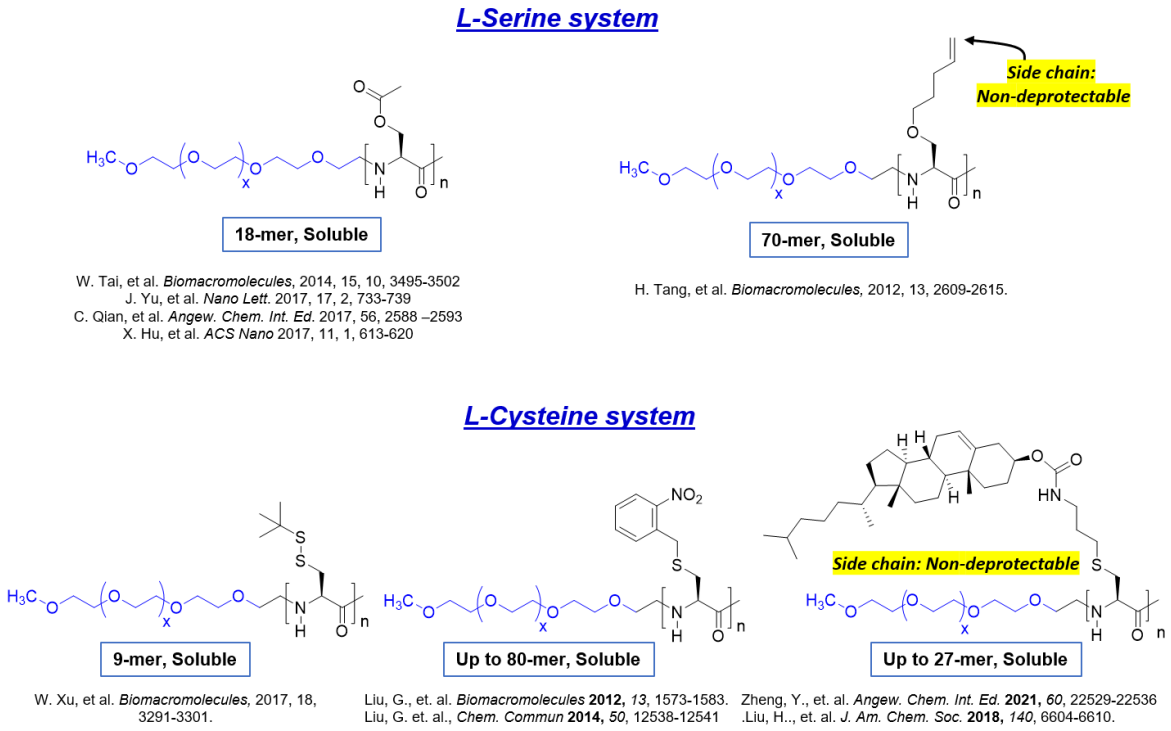

Figure 1.16*. Notable examples of PEG-diblock copolymers with serine and cysteine.*

Nevertheless, there have been some efforts towards the synthesis of high molecular weight polymers from L-serine and L-cysteine. The simplest way to impart solubility to these kinds of insoluble β-sheet polypeptides is to make a di-block copolymer with a polyethylene glycol unit (see some notable examples in Figure 1.16). It has been shown to work in few

cases, and polymers with the β-sheet forming unit having a degree of polymerization (DP) up to ~ 80 have been reported.[120, 160, 161] Furthermore, there has been a report on overcoming these insolubility issues using their racemic NCA instead of optically pure (L or D) form.[162] Even though polypeptides derived from this racemic NCA are highly soluble in common organic solvents, they suffer from the major drawback of not forming any secondary structures. Aside from the use of racemic NCA, there have been efforts on putting β-sheet weakening units at hetero atoms in serine and cysteine to improve the solubility of corresponding polypeptides by disruption of β-sheet structures (see Figure 1.15 for few examples). In the case of serine, β-sheet weakening units were incorporated in the form of glycidyl ethers,[163, 164] oligo ethylene glycol ethers,[165] and phosphate ester.[166] Similarly, in the case of cysteine, β-sheet disrupting units were introduced in the form of glycidyl thioethers,[167] oligo ethylene glycol thioethers,[168] bulky menthyl thioether,[169] *t*-butoxycarbonylmethyl thioether.[170] Although the incorporation of these β-sheet weakening units makes corresponding polymer soluble and high molecular weight polymers with narrow dispersities (Đ) were reported, these newly introduced units are not cleavable without disrupting peptide backbone to get back corresponding high molecular weight polyserine or polycysteines. Additionally, the synthesis of amino acids and especially NCAs with some these units is highly challenging, requiring an anhydrous column chromatographic purification in most of these cases, limiting access to these kinds of polypeptides. Despite these few recent successes, new efficacious approaches for the synthesis of soluble, high molecular weight β-sheet forming polypeptides with narrow dispersities (Đ) are urgently needed, especially with respect to their ability to undergo deprotection under the mild condition to obtain high molecular weight native polyserines or cysteines.

1.6. Aim of Thesis

With the aforementioned detailed polypeptide literature review, it is very clear that the uncontrolled polymer precipitation in β-sheet polypeptide is still unresolved problem in the literature. As a consequence, accomplishing complete control over the "livingness in β-sheet polypeptides" and expansion of the propagating polymer chains for building many unexplored block copolymer macromolecular architectures is still a distant dream for synthetic polymer chemist. We took this a challenge and try to solve this problem in my thesis. Our aim is to develop the "*steric hinderance assisted ROP strategy"* for synthesis of high molecular weight β-sheet polypeptides, and expand the scope of this approach for the

building inaccessible block copolymer macromolecular architectures (see Figure 1.17). Furthermore, to study the self-assembly of these novel β-sheet containing block copolymers and explored them for *in vitro* and *in vivo* studies related to hemolysis, cellular toxicity, pharmacokinetics, etc. Lastly to expand the scope of newly developed NCA monomers to aqueous ROPISA strategy for in-situ encapsulation of cargoes.

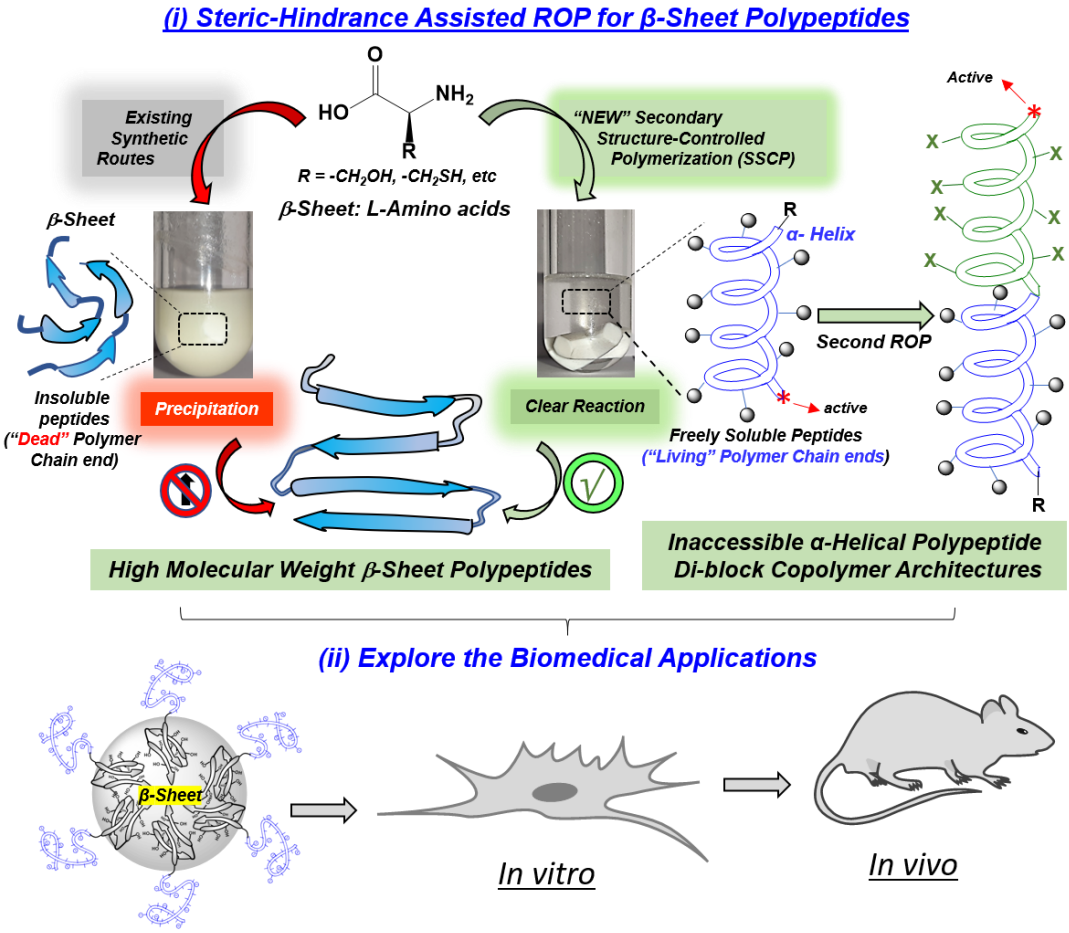

F***igure 1.17.*** *Design of steric hindrance assisted NCA ROP and its expansion to prepare block copolymer architectures for biomedical applications.*

My thesis work has been divided into three chapters and an insight into these have been briefly here. In the **Chapter 2**, the new "*steric hinderance assisted ROP strategy"* for synthesis of high molecular weight β-sheet polypeptides is developed. In this process, the propagating polypeptide chains were directed to undergo conformational transition from *β-sheet to α-helix* to produce freely soluble polymers and excellent "*living ROP polymerization*" characteristics was accomplished in building high molecular weight polypeptides. A *t*-butyl benzene steric unit was identified as a conformational controller—

cum—solubilizing handle to create in-situ secondary structural transition in the propagating chains to accomplish control in polymerization. The soluble and *living α-helical* propagating chains further deprotected to yield high molecular weight β-sheet polypeptides. In **Chapter 3**, the scope of "*steric hinderance ROP strategy"* was expanded for synthesis of block-copolymer architectures. A novel block copolymer, Poly(serine)-*b*-poly(glutamate) was synthesized by utilizing polyserine bearing *t*-butyl benzene steric unit as macroinitiator for ROP of glutamate NCA and subsequent post polymerization deprotection. The block copolymer Poly(serine)-*b*-poly(glutamate) adopted β-sheet conformation in water and found to enhance ThT fluorescence by 15 times. A detailed DLS analysis, zeta-potential measurements and secondary structure analysis by CD was carried out at various pH. The di-block copolymer was found to encapsulate doxorubicin drug and *in vitro* cytotoxicity as well as cellular uptake was studied. Further, encapsulation of IR-780 dye in block copolymer enabled us to perform *in vivo* biodistribution studies by IVIS. In **Chapter 4**, the ring opening polymerization induced self-assembly (ROPISA) strategy was employed for polymerization of *t*-butyl benzene steric unit functionalized NCA monomer using amine terminated PEG as a hydrophilic macroinitiator to obtain polypeptide di-block copolymer nano assemblies. Five different dyes were encapsulated in-situ by adding them in the beginning of ROPISA mediated polymerization to afford dye loaded polypeptide nanoparticle's emulsions in various colors. The nascent polypeptide nanoparticles were nontoxic and non-hemolytic in nature, while dye loaded polypeptide nanoparticles were also nontoxic to mammalian cells. As a proof of concept, the cellular uptake of Nile red loaded nanoparticles was shown using confocal microscopy.

Finally, the summary of entire work and directions towards the future research is provided in the last section of the Thesis.

Chapter 2

Development of Steric-Hindrance Assisted Ring Opening Polymerization Strategy for β-Sheet Polypeptides

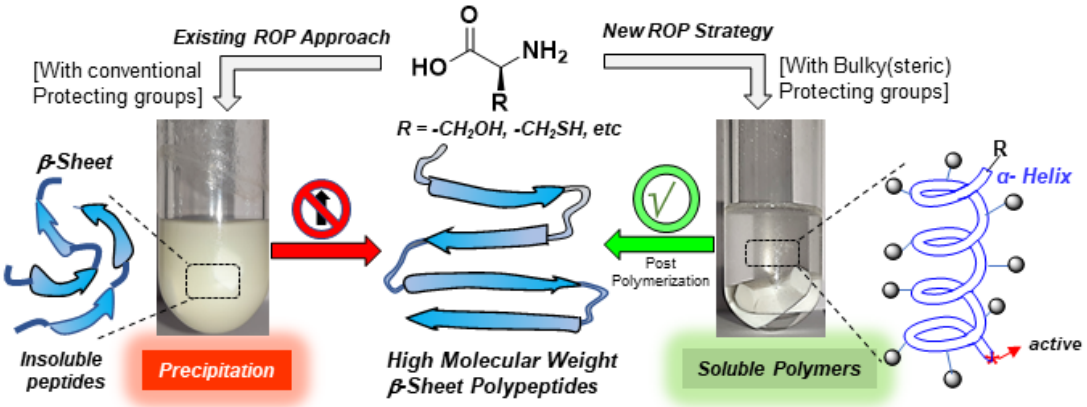

Abstract

β-Sheet forming polypeptides are one of the least explored synthetic systems due to their uncontrolled precipitation in the ring opening polymerization (ROP) synthetic methodology. Here, a new *t*-butylbenzene functionalization approach is introduced to overcome this limitation by sterically controlling the propagating polymer chains and homogeneous polymerization with good control over chain growth was accomplished. New Bulky N-carboxyanhydride (NCA) monomers were designed having *t*-butylbenzene pendant by multi-step organic synthesis and N-heterocyclic carbene was explored as a catalyst to make high molecular weight and narrow polydisperse soluble polypeptides. This ROP process was successfully demonstrated for two β-sheet forming polypeptides such as poly(L-serine) and poly(L-cysteine). These new *t*-butylbenzene functionalized polypeptides were found to be readily soluble in tetrahydrofuran and chloroform, etc, and they were produced in high molecular weights having M_n = 32 kDa with dispersity $Đ \leq 1.3$. ROP kinetics were studied by real-time FT-IR and ^{1}H-NMR to determine the actual content of the secondary structures in the propagating chains. These studies established that α-helical conformational front in the propagation chain was speeding up the polymerization kinetics with good degree of control in the ROP process. Reversible-conformational transitions in the post polymerization deprotection was found to restore the β-sheet secondary structures in poly(L-serine)s. The newly developed *t*-butylbenzene substituted steric-hindrance approach is valuable in yielding soluble polymers and this approach could be useful for exploring new polypeptide architectures for long-term impact.

2.1. Introduction

Synthetic polypeptides are protein-like polymers having precise control over α-helical and β-sheet conformations for wide range of applications in materials science[66] and biomedical fields.[16, 29, 131, 171] Polypeptides are synthesized by ring-opening polymerization (ROP) of N-carboxyanhydride (NCA) monomers of L-amino acids by nucleophile or base initiator[10, 15, 25, 27, 51] and in this process secondary structures of the propagating polypeptide chains are rationalized as being a foremost deciding factor in determining the kinetics and building high molecular weight polymers.[172] α-Helical polypeptides render excellent solubility in the polymerization medium to speed up the ROP process[133, 135-138] and exhibit "livingness" to make extended block copolymer architectures.[173]

α-Helical polypeptides such as poly(L-lysine) and poly(L-glutamate), etc. were reported using Ni- and Co- organometallic catalyst,[13, 14] Schreiner's thiourea,[55] *N*-heterocyclic carbenes (NHCs),[50] fluorinated alcohol,[56] crown-ethers,[134] LiHMDS,[42] tetraalkylammonium carboxylates,[44] and also methodologies like polymerization induced self-assembly,[64, 65] emulsion polymerization,[61, 138] and so on so forth. On the contrary, β-sheet polypeptides were known to undergo uncontrollable-precipitation in polymerization medium which further restricted the polymer chain growth and hampered the molecular weight build-up.[12] The formation of β-sheet lamellae at the initial stage of the polymerization and strong inter-chain hydrogen bonding interactions were found to be responsible for the precipitation process. The heterogenous polymerization was found to be non-controllable with inactive propagation chains; thus, they were found inefficient for the synthesis of block copolymers.[139] As a result, β-sheet forming polypeptides such as poly(L-serine)s and poly(L-cysteine)s were predominately produced as insoluble low molecular weight polymers.[60, 141, 142, 155, 156, 159, 174, 175] This limitation was partially overcome by incorporating solubilizing units like glycidyl ether,[163, 164, 167] oligo ethylene glycol ether,[165, 168, 176] phosphate ester[166, 177] or PEGlated initiators[145-147, 155, 160, 178] to improve the homogeneity of polymerization medium to attain higher degree of control in the molecular weight build-up. The substituted β-sheet polypeptides were reported as synthetic mucin chimeras to adhere on the HEK 293T mammalian cell surfaces,[163] glucose-mediated insulin delivery and anticancer drug delivery, etc.[145-147, 155] During the investigation of this work, Deming and co-workers have published *t*-butylacetyl-substitution approach to make soluble poly-L-cysteine derivatives and subsequently converted into fluorescent poly(dehydroalanine)s.[170] These efforts have emphasized the importance of control over the molecular weight and secondary structures

in β-sheet polypeptides. Nevertheless, the uncontrolled polymer precipitation in β-sheet polypeptide synthesis in the ROP process is one of most challenging synthetic problem yet to be resolved. Henceforth, new synthetic approaches are important to be developed to have complete control over the propagation of β-sheet polypeptide chains in building high molecular polymers to explore their potential for applications in biomedical and material science.

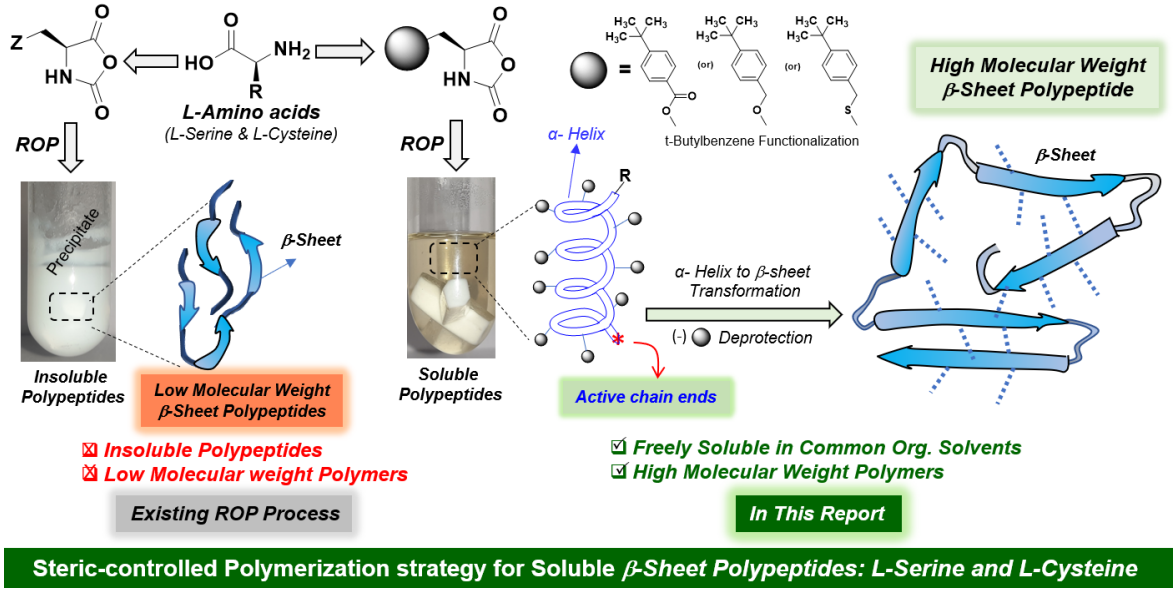

Figure 2.1. *Development of t-butylbenzene steric-hindrance assisted strategy for β-sheet polypeptides.*

Here, we report the design and development of novel *t*-butylbenzene functionalization approach for readily soluble and high molecular weight *β-sheet polypeptides.* In this process, the propagating polypeptide chains were initially found to adopt β-sheet conformation at oligomeric stage that upon further chain extension adopted *α-helix* conformation to produce freely soluble polymers for the building of high molecular weight polypeptides. The strategy is highly robust to reverse the conformational transition from α-helix to *β-sheet polypeptides* in the post-polymerization step. This new *t*-butylbenzene functionalization approach is shown in Figure 2.1. A bulky-steric unit was cleverly identified as conformational controller -cum- solubilizing handle to create in-situ structural transition in the propagating chains to accomplish complete solubility in polymerization medium. For this purpose, *t*-butylbenzene unit was anchored in the L-serine and L-cysteine and new classes of bulky NCA-monomers were tailor-made by multi-step organic synthesis. Impressively, the newly produced *t*-butylbenzene substituted

polypeptides exhibited excellent solubility in common organic solvents such as chloroform and tetrahydrofuran, and enabled their complete structural characterization and molecular weight determination. NMR and FT-IR spectroscopic methods were employed to study the real-time polymerization kinetics and the actual content of β-sheet and α-helix conformations to establish the mechanism of the ROP process. N-Heterocyclic carbene (NHC) was employed as catalyst to attain complete control over ROP process. The in-situ generated α-helix conformation was found to be excellent choice to speed up the polymerization kinetics and produce molecular weights with narrow dispersity (Đ).

2.2. Experimental Methods

2.2.1. Materials: $LiAlH_4$, phosphorus tribromide (PBr_3), α-pinene, sodium hydride (60 % dispersion in mineral oil), benzyl bromide, polyethylene glycol monomethyl ether (MW = 5000), and anhydrous solvents such as chloroform and dimethylformamide (DMF) were purchased from aldrich Chemicals and used without further purification. L-Serine, L-cysteine, triphosgene, 4-*tert*-butyl benzoic acid, di-*t*-butyl dicarbonate (Boc_2O), trifluoroacetic acid (TFA) were purchased from avra Synthesis and directly used without further purification. Thionyl chloride was distilled before use.

2.2.2. Methods: The progress of reactions was monitored by thin-layer chromatography (TLC) using 0.25 mm Merck precoated (60 F254) silica gel plates. For visualization of TLC spots, UV light of wavelength 254 nm (for UV active compounds) was used. TLC spots were visualized for non-UV active compounds using ninhydrin or phosphomolybdic acid (PMA) staining solutions. ^{1}H and ^{13}C NMR spectra were recorded on 400 MHz Bruker or Jeol spectrometers. Chemical shifts are reported as parts per million (δ) relative to tetramethylsilane (TMS) as internal standard and coupling constants (*J* values) in Hertz (Hz). Multiplicities are indicated as follows: s (singlet), d (doublet), t (triplet), dd (doublet of doublet), bs (broad singlet), and m (multiplet). High-resolution mass spectra (HRMS) were recorded on HRMS-ESI-Q-Time of Flight LC/MS (Synapt G2, Waters). MALDI-TOF mass spectrometry of polymers was performed on 4800 Plus MALDI TOF/TOF instrument from AB Sciex. The polymer solution (2 mg/mL in $CHCl_3$ – TFA mixture (6: 1, v/v)) and dithranol matrix solution (20 mg/ mL solution in THF) were mixed in 1:1 proportion, and 1−2 μL aliquot of this mixture was used directly for the MALDI-TOF MS analysis.Attenuated total reflectance-fourier transform infrared spectroscopy (ATR-FTIR)

spectra were recorded on Bruker alpha-E. Size exclusion chromatography (SEC) was performed on a system equipped with an isocratic pump (Viscotek VE 1122 pump), a differential refractometer (DRI) detector (viscotek VE 3580 RI). For SEC with THF as an eluent, separations were performed using serially connected size exclusion columns (two T6000M, General Mixed Organic 8 × 300 mm, from Viscotek) at 25 °C and at a flow rate of 1.0 mL/min and molecular weights were determined from the calibration curve generated from narrow polystyrene standards. In case of SEC with $CHCl_3$ as an eluent, separations were performed using serially connected size exclusion columns (two PLgel 10 µm MIXED-B, 7.5 × 300 mm, from Agilent) at 25 °C at a flow rate of 1.0 mL/min and absolute molecular weights were determined using RI, RALS, LALS signals (Viscotek 270 dual detector with a 670 nm light source) processed by Omnisec software and calibration was done with single polystyrene standard (PolyCAL^{TM} PS-99K, Mw=99209 from Viscotek). Five different polymer concentrations of each polymer (polyserine-1, polyserine-2 and polycysteine-3) were prepared and SEC analysis was carried out to determine the accurate Refractive index increment (*dn/dc*) values of polymers in $CHCl_3$ at 25°C. Differential refractive index data were obtained for each solution and plotted versus concentration using the Omnisec software to get *dn/dc* and it was found to be 0.0841 ml/g, 0.0744 mL/g and 0.1055 mL/g for polyserine-1, polyserine-2 and polycysteine-3, respectively. Thermal analysis of the polymers was carried out on TA Q20 differential scanning calorimeter (Indium standards were used for calibration of the instrument, and the analysis was carried out under nitrogen atmosphere at 10 °C/min cooling or heating rate). The thermal stability of polymer was determined using PerkinElmer thermal analyzer STA 6000 model at a heating rate of 10 °C/min in a nitrogen atmosphere. Circular dichroism (CD) analysis of the polymer samples was performed on a JASCO J-815 CD spectrometer at 25 °C.

2.2.3. Synthetic procedures

Synthesis of O-(4-*tert*-Butylbenzoyl)-L-serine hydrochloride (1): To a suspension of 4-*tert*-butyl benzoic acid (30 g, 168.3 mmol) in toluene (40 mL), a catalytic amount of DMF (0.5 mL) and freshly distilled thionyl chloride (30.5 mL, 420.8 mmol) were added at 0 °C under nitrogen via addition funnel. The reaction mixture was stirred under the inert atmosphere at 80 °C for 12 h, during which it became a clear solution. Subsequently, the solvent and excess thionyl chloride were removed by distillation to afford crude 4-*tert*-butylbenzoyl chloride as a yellow oil. The crude 4-*tert*-butylbenzoyl chloride was used directly without further purification for arylation of L-serine by employing reported

procedure.[179] Trifluoroacetic acid (50 mL) was taken in a round bottom flask and cooled to 0 °C on an ice bath. Subsequently, L-serine (10 g, 95.2 mmol) was added to it in small portions under vigorous stirring (partially dissolves). The reaction mixture was stirred for 15 min at 0 °C and further at 25 °C for 5 min. Freshly prepared 4-*tert*-butylbenzoyl chloride (168.3 mmol) was added to it in a single portion, and the mixture was stirred at 25 °C for 12 h. Eventually, the reaction mixture solution was cooled to 0 °C on an ice bath, and Et_2O (150 mL) was added under vigorous stirring. The resulting white suspension was further stirred at 0 °C for 15 min and then filtered to get the crude product. The crude solid product was washed with diethyl ether (100 mL) and acetone (100 mL) and then dried in a vacuum to give pure O-(4-*tert*-butylbenzoyl)-L-serine hydrochloride (**1**) as white solid. Yield: 17.5 g (61 %). ^{1}H NMR (400 MHz, DMSO-d_6) δ 8.88 (s, 3H, $^+$N**H**$_3$), 7.99 (d, *J* = 8.5 Hz, 2H, Ar-**H**), 7.55 (d, *J* = 8.5 Hz, 2H, Ar-**H**), 4.68 (d, *J* = 3.5 Hz, 2H, CHC**H**$_2$), 4.44 (t, *J* = 3.2 Hz, 1H, C**H**CH$_2$), 1.30 (s, 9H, C(C**H**$_3$)$_3$). ^{13}C NMR (101 MHz, DMSO-d_6) δ 168.4, 165.2, 156.9, 129.7, 126.2, 125.5, 62.3, 51.4, 35.0, 30.8. ATR-FTIR (cm^{-1}): 3414 (br), 2967, 2904, 2869, 1723, 1609, 1503, 1462, 1410, 1366, 1258, 1190, 1113, 1099, 1017, 975, 923, 854, 773, 705. HRMS (ESI) [M+H]$^+$ calculated for $C_{14}H_{20}NO_4$, 266.1392; found, 266.1396.

(4-(*tert*-Butyl)phenyl)methanol (2): To a suspension of $LiAlH_4$ (7.03 g, 185.2 mmol) in dry THF (300 mL), a solution of 4-(*tert*-butyl)benzoic acid (30 g, 168.3 mmol) in dry THF (70 mL) was added dropwise at 0 °C under a nitrogen atmosphere. The suspension was stirred at 0 °C for 6 h and then stirred at 25 °C for overnight. Subsequently, the mixture was cooled to 0 °C on an ice bath, and the reaction was quenched slowly by sequentially adding water (5 mL), followed by 2 N aqueous NaOH (20 mL) and again water (30 mL). The resulting mixture was allowed to stir at 0 °C for 10 min, then filtered. The white solid residue was washed with THF (2 × 200 mL). Filtrate and washings were combined and concentrated on a rotary evaporator to get oil. The oil was then dissolved in ethyl acetate (150 mL) and extracted with aqueous saturated $NaHCO_3$ (60 mL), water (60 mL) and brine (60 mL). The organic layer was dried over Na_2SO_4, concentrated on a rotary evaporator to get a pure desired product (4-(*tert*-butyl)phenyl)methanol (**2**) as a pale-yellow oil. Yield: 26.9 g (97 %). ^{1}H NMR (400 MHz, $CDCl_3$) δ 7.40 (d, *J* = 8.4 Hz, 2H, Ar-**H**), 7.31 (d, *J* = 8.6 Hz, 2H, Ar-**H**), 4.66 (s, 2H, Ar-C**H**$_2$O), 1.71 (s, 1H, O**H**), 1.33 (s, 9H, C(C**H**$_3$)$_3$). ^{13}C NMR (101 MHz, $CDCl_3$) δ 150.9, 138.1, 127.0, 125.6, 65.3, 34.7, 31.5. ATR-FTIR (cm^{-1}): 3330, 2961, 2867, 1615, 1513, 1462, 1410, 1394, 1363, 1268, 1240, 1215, 1107, 1041, 1011, 849, 833,

818, 670, 608. HRMS (ESI) $[M+Na]^+$ calculated for $C_{11}H_{16}NaO$, 187.1099; found, 187.1098.

1-(Bromomethyl)-4-(*tert*-butyl)benzene (3): To a solution of (4-(*tert*-butyl)phenyl)methanol (**2**) (26.4 g, 160.9 mmol) in anhydrous dichloromethane (200 mL) was added phosphorus tribromide (18.3 mL, 52.3 g, 193.2 mmol) at 0 °C under a nitrogen atmosphere. The reaction mixture was stirred at 0 °C for 4 h and then at 25 °C for overnight. Subsequently, the reaction mixture was cooled to 0 °C on ice and quenched by slowly adding water (40 mL). After stirring the mixture for 10 min at 0 °C, it was further diluted with water (100 mL), and the layers were separated. The aqueous layer was extracted once with ethyl acetate (200 mL). The organic layers were combined and further extracted with aqueous saturated $NaHCO_3$ (100 mL), water (100 mL), and brine (100 mL) and then dried over anhydrous Na_2SO_4, filtered, and concentrated under reduced pressure to get pure desired product 1-(bromomethyl)-4-(*tert*-butyl)benzene (**3**) as a pale-yellow oil. Yield: 33.3 g (91 %). ^{1}H NMR (400 MHz, $CDCl_3$) δ 7.38 (d, *J* = 8.4 Hz, 2H, Ar-**H**), 7.34 (d, *J* = 8.5 Hz, 2H, Ar-**H**), 4.50 (s, 2H, Ar-C**H**$_2$Br), 1.32 (s, 9H, C(C**H**$_3$)$_3$). ^{13}C NMR (101 MHz, $CDCl_3$) δ 151.7, 134.9, 128.9, 125.9, 34.8, 33.8, 31.4. ATR-FTIR (cm^{-1}): 2962, 1611, 1514, 1463, 1439, 1410, 1394, 1364, 1268, 1230, 1203, 1107, 811, 664, 605.

N-(*tert*-Butoxycarbonyl)-O-(4-(*tert*-butyl)benzyl)-L-serine (4): According to the procedure of Boal *et al*.,[180] sodium hydride (3.02 g of a 60% dispersion in mineral oil, 1.99 g, 82.84 mmol) was suspended in anhydrous DMF (25 mL) and cooled to 0 °C in a flask fitted with a dropping funnel. Eventually, a solution of (*tert*-butoxycarbonyl)-L-serine (6.8 g, 33.14 mmol) in anhydrous DMF (50 mL), was added dropwise to the suspension of sodium hydride for 30 minutes using a dropping funnel. Subsequently, 1-(bromomethyl)-4-(*tert*-butyl)benzene (**3**) (7.53 g, 33.14 mmol) was added, and the flask contents were warmed to 25 °C, and stirring was continued for another 3 h. The reaction was quenched by the addition of water (15 mL). The solvents were then removed by vacuum distillation (temperature was not exceeded 60 °C), and the residue was dissolved in water (50 mL), which was extracted with diethyl ether (2 × 50 mL). The resulting aqueous phase's pH was adjusted to 2–2.5 with 2 N HCl, and it was immediately extracted with ethyl acetate (3 × 50 mL). The combined organic extracts were dried over anhydrous Na_2SO_4, filtered, and concentrated under reduced pressure to get the crude product as a brown oil. The crude product was then dissolved in diethyl ether (100 mL), and cyclohexylamine (3 mL) was

added to the solution. A white precipitate of the cyclohexyl ammonium salt of the product was formed and isolated by filtration. The residue was washed once with diethyl ether (50 mL). Subsequently, the residue was dissolved in dichloromethane (100 mL) and extracted with 1 N HCl (2 × 50 mL) and brine (50 mL). The resulting organic layer was dried over anhydrous Na_2SO_4, filtered, and concentrated under reduced pressure to get pure desired product N-(*tert*-butoxycarbonyl)-O-(4-(*tert*-butyl)benzyl)-L-serine (**4**) as pale-brown sticky oil. Yield: 6.1 g (52 %). ^{1}H NMR (400 MHz, $CDCl_3$) δ 7.36 (d, *J* = 8.4 Hz, 2H, Ar-**H**), 7.23 (d, *J* = 8.3 Hz, 2H, Ar-**H**), 5.42 (d, *J* = 8.2 Hz, 1H, N**H**), 4.61 – 4.37 (m, 3H, ArC**H**$_2$O and C**H**CH$_2$), 3.93 (dd, *J* = 2.3, 9.0 Hz, 1H, OC**H**(H)CH), 3.71 (dd, *J* = 3.5, 9.4 Hz, 1H, OCH(**H**)CH), 1.45 (s, 9H, OC(C**H**$_3$)$_3$), 1.31 (s, 9H, ArC(C**H**$_3$)$_3$). ^{13}C NMR (101 MHz, $CDCl_3$) δ 175.3, 155.9, 151.1, 134.4, 127.7, 125.5, 80.5, 73.4, 69.7, 53.9, 34.7, 31.5, 28.4. ATR-FTIR (cm^{-1}): 2963(br), 2868, 1714, 1513, 1457, 1366, 1268, 1161, 1108, 936, 817. HRMS (ESI) $[M+Na]^+$ calculated for $C_{19}H_{29}NNaO_5$, 374.1943; found, 374.1944

O-(4-(*tert*-Butyl)benzyl)-L-serine hydrochloride (5): To a solution of N-(*tert*-butoxycarbonyl)-O-(4-(*tert*-butyl)benzyl)-L-serine (**4**) (5.6 g, 15.84 mmol) in 1,4-dioxane (20 mL) was added 4 M HCl in dioxane (19.8 mL). The reaction mixture was stirred at room for 5 h. Subsequently, the solvent was removed by rotary evaporation to get a pale-yellow solid. The solid material was triturated with diethyl ether (3 × 50 mL) to get the pure product O-(4-(*tert*-butyl)benzyl)-L-serine hydrochloride **(5)** as a white solid. Yield: 3.7 g (82 %). ^{1}H NMR (400 MHz, CD_3OD) δ 7.40 (d, *J* = 8.4 Hz, 2H, Ar-**H**), 7.29 (d, *J* = 8.5 Hz, 2H, Ar-**H**), 4.65 – 4.53 (m, 2H, ArC**H**$_2$O), 4.19 (dd, *J* = 3.3, 4.7 Hz, 1H, C**H**CH$_2$), 3.92 (dd, *J* = 4.7, 10.4 Hz, 1H, OC**H**(H)CH), 3.84 (dd, *J* = 3.3, 10.4 Hz, 1H, OCH(**H**)CH), 1.31 (s, 9H, C(C**H**$_3$)$_3$). ^{13}C NMR (101 MHz, CD_3OD) δ 169.8, 152.2, 135.5, 129.0, 126.4, 74.3, 68.0, 54.3, 35.4, 31.8. ATR-FTIR (cm^{-1}): 3242(br), 2960, 2870, 1756, 1598, 1523, 1486, 1360, 1269, 1219, 1132, 1108, 1084, 775. HRMS (ESI) $[M+H]^+$ calculated for $C_{14}H_{22}NO_3$, 252.1600; found, 252.1605.

S-(4-(*tert*-Butyl)benzyl)-L-cysteine (6): According to the procedure of Milani *et al.*,[181] to a solution of L-cysteine hydrochloride hydrate (3.4 g, 19.4 mmol) in aqueous 2 M sodium hydroxide solution (23.2 mL) and ethanol (46 mL) was added 1-(bromomethyl)-4-(*tert*-butyl)benzene (**9**) (4 g, 17.6 mmol) in a single portion. The reaction mixture was vigorously stirred at 25 °C for 30 min. Subsequently, the reaction mixture was neutralized to pH 7 using 6 N hydrochloric acid to precipitate the desired product. The precipitate was filtered and

washed successively with water, ethanol, and ether to give crude product. The crude product was resuspended in water (150 mL) and stirred at 60 °C for 15 min. The mixture was filtered under a vacuum, and the residue was washed once with water (100 mL). Finally, the residue was dried using azeotropic distillation over toluene to obtain the pure product S-(4-(*tert*-butyl)benzyl)-L-cysteine (**6**) as a white powder. Yield: 3.7 g (79 %). ^{1}H NMR (400 MHz, CD_3OD) δ 7.35 (d, *J* = 8.4 Hz, 2H, Ar-**H**), 7.29 (d, *J* = 8.4 Hz, 2H, Ar-**H**), 3.79 (d, *J* = 2.7 Hz, 2H, ArC**H**$_2$S), 3.76 (dd, *J* = 4.0, 8.4 Hz, 1H, SCH_2C**H**), 3.06 (dd, *J* = 4.0, 14.7 Hz, 1H, SC**H**(H)CH), 2.88 (dd, *J* = 8.4, 14.7 Hz, 1H, SCH(**H**)CH), 1.30 (s, 9H, C(C**H**$_3$)$_3$). ^{13}C NMR (101 MHz, CD_3OD) δ 172.4, 151.3, 136.1, 129.9, 126.4, 54.7, 36.5, 35.3, 33.3, 31.8. ATR-FTIR (cm^{-1}): 2961(br), 1618, 1590, 1512, 1393, 1346, 1299, 1134, 1109, 826. HRMS (ESI) $[M+H]^+$ calculated for $C_{14}H_{22}NO_2S$, 268.1371; found, 268.1374.

O-Benzoyl-L-Serine hydrochloride (7): The product was obtained as a white solid from L-serine (10 g, 95.16mmol) and benzoyl chloride (19.7 mL, 23.78 g, 169.19 mmol) by employing the similar procedure as that for O-(4-*tert*-butylbenzoyl)-L-serine hydrochloride (**1**). Yield: 14.1 g (60 %). ^{1}H NMR (400 MHz, DMSO-d_6) δ 8.90 (s, 3H, $^{+}$N**H**$_3$), 8.07 (d, *J* = 7.4 Hz, 2H, Ar-**H**), 7.68 (t, *J* = 7.4 Hz, 1H, Ar-**H**), 7.54 (t, *J* = 7.7 Hz, 2H, Ar-**H**), 4.70 (d, *J* = 3.4 Hz, 2H, CHC**H**$_2$), 4.46 (t, *J* = 3.3 Hz, 1H, C**H**CH_2). ^{13}C NMR (101 MHz, DMSO-d_6) δ 168.4, 165.2, 133.8, 129.7, 128.9, 128.7, 62.5, 51.4. ATR-FTIR (cm^{-1}): 3085 (br), 2985, 2924, 1724, 1582, 1490, 1462, 1449, 1415, 1351, 1314, 1285, 1264, 1250, 1226, 1095, 1070, 998, 883, 709. HRMS (ESI) $[M+H]^+$ calculated for $C_{10}H_{12}NO_4$, 210.0766; found, 210.0775.

N-(*tert*-Butoxycarbonyl)-O-benzyl-L-serine (8): The product was obtained as a colourless oil from (*tert*-butoxycarbonyl)-L-serine (6.8 g, 33.14 mmol) and benzyl bromide (3.94 mL, 5.7 g, 33.14 mmol) by employing the same procedure as that for N-(*tert*-butoxycarbonyl)-O-(4-(*tert*-butyl)benzyl)-L-serine (**4**). Yield: 5.89 g (60 %)**.** ^{1}H NMR (400 MHz, $CDCl_3$) δ 8.53 (bs, 1H, COO**H**), 7.34 – 7.24 (m, 5H, Ar-**H**), 5.44 (d, *J* = 8.4 Hz, 1H, N**H**), 4.60 – 4.41 (m, 3H, ArC**H**$_2$O and C**H**CH_2), 3.92 (dd, *J* = 2.7, 9.3 Hz, 1H, OC**H**(H)CH), 3.71 (dd, *J* = 3.4, 9.4 Hz, 1H, OCH(**H**)CH), 1.45 (s, 9H, OC(C**H**$_3$)$_3$). ^{13}C NMR (101 MHz, $CDCl_3$) δ 175.5, 155.9, 137.4, 128.6, 128.0, 127.8, 80.5, 73.5, 69.8, 54.0, 28.4. ATR-FTIR (cm^{-1}): 2600 – 3300 (br), 1680, 1604, 1509, 1233, 1192, 1018, 831, 738. HRMS (ESI) $[M+Na]^+$ calculated for $C_{15}H_{21}NNaO_5$, 318.1317; found, 318.1317.

O-Benzyl-L-serine hydrochloride (9): The product was obtained as a white solid from N-(*tert*-butoxycarbonyl)-O-benzyl-L-serine (**8**) (5.8 g, 19.79 mmol) and 4 M HCl in dioxane

(24.7 mL) by employing the same procedure as that for O-(4-(*tert*-butyl)benzyl)-L-serine hydrochloride (**5**). Yield: 3.8 g (83 %)**.** ^{1}H NMR (400 MHz, DMSO-d6) δ 13.86 (s, 1H, COO**H**), 8.60 (s, 3H, $^{+}$N**H**$_3$), 7.60 – 7.10 (m, 5H, Ar-**H**), 4.64 – 4.48 (m, 2H, ArC**H**$_2$O), 4.21 – 4.13 (m, 1H, C**H**CH$_2$), 3.94 – 3.81 (m, 2H, CHC**H**$_2$). ^{13}C NMR (101 MHz, DMSO-d6) δ 169.0, 137.6, 128.3, 127.7, 127.6, 72.4, 67.6, 66.4, 52.4. ATR-FTIR (cm^{-1}): 3407, 2973, 2870, 1728, 1585, 1502, 1356, 1225, 1152, 1103, 1071, 836, 745, 695. HRMS (ESI) [M+H]$^{+}$ calculated for $C_{10}H_{14}NO_3$, 196.0974; found, 196.0973.

S-Benzyl-L-cysteine (10): The product was obtained as a white solid from L-cysteine hydrochloride hydrate (5.65 g, 32.16) and benzyl bromide (3.47 mL, 5 g, 29.23 mmol) by employing the same procedure as that for S-(4-(*tert*-butyl)benzyl)-L-cysteine) (**6**). Yield: 5.5 g (88 %)**.** ^{1}H NMR (400 MHz, $CDCl_3$ – TFA) δ 7.44 – 7.27 (m, 7H, Ar-**H** and N**H**$_2$), 4.05 (bs, 1H, C**H**CH$_2$), 3.79 (s, 2H, ArC**H**$_2$S), 3.15 (dd, *J* = 4.1, 15.3 Hz, 1H, SC**H**(H)CH), 3.01 (dd, *J* = 8.9, 15.2 Hz, 1H, SCH(**H**)CH). ^{13}C NMR (101 MHz, $CDCl_3$ – TFA) δ 171.7, 136.4, 129.5, 128.9, 128.5, 53.1, 36.6, 31.0. ATR-FTIR (cm^{-1}): 3591(br), 3145, 2944, 1657, 1582, 1555, 1491, 1409, 1391, 1341, 1278, 1226, 1070, 922, 766, 693. HRMS (ESI) [M+H]$^{+}$ calculated for $C_{10}H_{14}NO_2S$, 212.0745; found, 212.0747.

1,3-Bis(2,4,6-trimethylphenyl)imidazolium bicarbonate (NHC catalyst): To a solution of 1,3-Bis(2,4,6-trimethylphenyl) imidazolium chloride (0.5 g, 1.47 mmol) in anhydrous methanol (5 mL) was added dry potassium bicarbonate (0.18 g, 1.76 mmol), and the resulting mixture was stirred under a nitrogen atmosphere for 48 h at 25 °C. Subsequently, the reaction mixture was filtered, and the filtrate was evaporated under a vacuum to get crude product. The crude product was washed with acetone and dried under vacuum to get pure 1,3-bis(2,4,6-trimethylphenyl) imidazolium bicarbonate as a white solid. Yield: 0.41 g (76 %). ^{1}H NMR (400 MHz, CD_3OD) δ 8.05 (s, 2H, C**H**=C**H**), 7.20 (s, 4H, *m*-C**H**Mes), 2.39 (s, 6H, *p*-C**H**$_3$Mes), 2.18 (s, 12H, *o*-C**H**$_3$Mes). ^{13}C NMR (101 MHz CD_3OD) δ 161.4, 142.9, 135.7, 132.3, 130.9, 126.5, 126.3, 21.2, 17.4. HRMS (ESI) [M]$^{+}$ calculated for $C_{21}H_{25}N_2$, 305.2018; found, 305.2018.

Synthesis of MeO-PEG$_{5000}$-NH$_2$: It was synthesized by employing the reported procedure.[21] To a solution of PEG monomethyl ether (MeO-PEG$_{5000}$-OH, Mn = 5000, 4 g, 0.8 mmol) in anhydrous dichloromethane (32 mL) was added triethylamine (0.33 mL, 0.24 g, 2.4 mmol). Subsequently, the mixture was cooled to 0 °C and methane sulfonyl chloride (0.12 mL, 0.18 g, 1.6 mmol) was added dropwise over 5 min with stirring. Upon addition of

all the reagent, the mixture was stirred at the same temperature for additional 15 min, then kept stirring at 25 °C for 24 h. Eventually, the mixture was concentrated by rotary evaporation and precipitated into cold diethyl ether to get the PEG mesylate (MeO-PEG_{5000}-OMs) as white solid. The obtained PEG mesylate was dissolved in aqueous ammonia (25%, 100 mL) and was left to stir for 5 days in a sealed flask. Then, the mixture was extracted with dichloromethane (3 × 100 mL), the organic fractions were combined, dried over anhydrous Na_2SO_4, filtered, and it was concentrated on rotary evaporator to ~ 5 mL and the product was precipitated by adding di-ethyl ether. Mixture was kept at -20 °C for overnight and then filtered to get MeO-PEG_{5000}-NH_2 as a white solid. Yield: 2.88 g, 72 %**.** ^{1}H NMR (400 MHz, $CDCl_3$) δ 3.85 – 3.44 (m, 545H, OC**H**$_2$C**H**$_2$O), 3.38 (s, 3H, C**H**$_3$OCH_2CH_2), 2.87 (t, *J* = 5.2 Hz, 2H, OCH_2C**H**$_2$$NH_2$). ^{13}C NMR (400 MHz, $CDCl_3$) δ 72.0, 70.7, 59.1, 41.8.

Serine-ester NCA Monomer-M1: O-(4-t*ert*-butylbenzoyl)-L-serine hydrochloride (**1**) (8 g, 26.51 mmol) was dried under a high vacuum for 2 hours in a flame-dried round bottom flask before suspending in a freshly dried THF (60 mL). The suspension was heated to 50 °C, and under vigorous stirring, the solution of triphosgene (3.93 g, 13.26 mmol) in freshly dried THF (20 mL) was added via cannula. The mixture was stirred at 50 °C for 3 h, during which the mixture became a completely clear solution, indicating the completion of the reaction. Subsequently, the mixture was poured into dry hexane (320 mL) under an inert atmosphere with a cannula's help. The mixture was kept at -20 °C for overnight to ensure complete precipitation. The mixture was filtered, washed with dry hexane (100 mL), and the residue was dried under a high vacuum for 1 h to get crude NCA. The crude NCA was dissolved in THF (40 mL) and crystallized by layering with dry hexane (200 mL). The mixture was allowed to stand for overnight at -20 °C, filtered, washed with dry hexane (100 mL), and dried under a high vacuum for 1 h to yield pure crystalline NCA. The repurification process was repeated at least twice to get highly pure serine-ester NCA monomer-**M1** as a white crystalline solid. Yield: 5.2 g (67 %). ^{1}H NMR (400 MHz, DMSO-d_6) δ 9.28 (s, 1H, N**H**), 7.83 (d, *J* = 8.7 Hz, 2H, Ar-**H**), 7.58 (d, *J* = 8.7 Hz, 2H, Ar-**H**), 4.95 – 4.83 (m, 1H, C**H**CH_2), 4.60 (dd, *J* = 3.0, 11.9 Hz, 1H, OC**H**(H)CH), 4.47 (dd, *J* = 3.7, 11.9 Hz, 1H, OCH(**H**)CH), 1.29 (s, 9H, C(C**H**$_3$)$_3$). ^{13}C NMR (101 MHz, DMSO-d6) δ 169.4, 164.9, 157.0, 152.0, 129.0, 126.0, 125.8, 62.2, 57.1, 34.9, 30.7. ATR-FTIR (cm^{-1}): 3315, 2964, 2871, 1860, 1786, 1723, 1609, 1461, 1410, 1364, 1300, 1269, 1190, 1116, 1036, 1016, 992, 919, 856, 774, 758, 707. HRMS (ESI) $[M+Na]^+$ calculated for $C_{15}H_{17}NNaO_5$, 314.1004; found, 314.1001.

Serine-ether NCA Monomer-M2: According to the procedure of Canning *et al.*,[31] O-(4-*tert*-butylbenzyl)-L-serine hydrochloride (**5**) (3.6 g, 12.51 mmol) was dried under high vacuum for 2 h in a flame-dried round bottom flask before suspending in a freshly dried ethyl acetate (20 mL). Subsequently, the α-pinene (5.96 mL, 5.11 g, 37.53 mmol) was added, and the suspension was refluxed (80 °C) for 5 minutes. Eventually, the solution of triphosgene (2.41 g, 8.13 mmol) in freshly dried ethyl acetate (8 mL) was added via cannula, and the mixture was refluxed for 3 h. In the end, it was a slightly turbid solution which, upon cooling to 25 °C, was filtered under an inert atmosphere via cannula. The resulting clear solution was concentrated to about ~ 8 mL under reduced pressure. Afterward, the dry hexane (100 mL) was added to it under an inert atmosphere, and the mixture was kept at -20 °C for overnight. The crude yellow viscous oily product was settled at the bottom, and it was isolated by decanting the supernatant and followed by drying under a high vacuum for 1 h. The crude NCA was dissolved in ethyl acetate (5 mL), and then dry hexane (100 mL) was added to it, and the mixture was kept at -20 °C for overnight. Again, the viscous oily product was isolated by decantation of supernatant. This repurification process was repeated at least one more time to get pure serine-ether NCA monomer-**M2** as a yellow viscous oil. Yield: 2.3 g (66 %). ^{1}H NMR (400 MHz, $CDCl_3$) δ 7.38 (d, *J* = 8.4 Hz, 2H, Ar-**H**), 7.22 (d, *J* = 8.4 Hz, 2H, Ar-**H**), 6.15 (s, 1H, N**H**), 4.59 – 4.48 (m, 2H, ArC**H**$_2$O), 4.43 (dd, *J* = 3.2, 5.4 Hz, 1H, C**H**CH$_2$), 3.77 (dd, *J* = 3.2, 10.1 Hz, 1H, OC**H**(H)CH), 3.73 (dd, *J* = 5.4, 10.1 Hz, 1H, OCH(**H**)CH), 1.32 (s, 9H, C(C**H**$_3$)$_3$). ^{13}C NMR (101 MHz, $CDCl_3$) δ 167.1, 152.6, 151.5, 133.6, 127.9, 125.7, 73.7, 67.9, 58.5, 34.7, 31.4. ATR-FTIR (cm^{-1}): 3279, 2960, 2868, 1857, 1783, 1672, 1628, 1516, 1462, 1363, 1300, 1269, 1108, 1019, 918, 819. HRMS (ESI) [M+Na] + calculated for $C_{15}H_{19}NNaO_4$, 300.1212; found, 300.1206.

Cysteine NCA Monomer-M3: The product was obtained as a white crystalline solid from S-(4-(*tert*-butyl)benzyl)-L-cysteine (**6**) (3.5 g, 13.09 mmol) and triphosgene (1.9 g, 6.54 mmol) by employing the same procedure as that for serine-ester NCA monomer-**M1**. The amount of THF and hexane used was double than that used in the synthesis of serine-ester NCA monomer-**M1**. Additionally, the purification of crude NCA was carried out by crystallization from ethyl acetate – Hexane (1: 4) instead of THF – Hexane. Yield: 2.3 g (59 %). ^{1}H NMR (400 MHz, $CDCl_3$) δ 7.37 (d, *J* = 8.3 Hz, 2H, Ar-**H**), 7.24 (d, *J* = 8.3 Hz, 2H, Ar-**H**), 6.15 (s, 1H, N**H**), 4.33 (dd, *J* = 3.6, 7.5 Hz, 1H, C**H**CH$_2$), 3.75 (s, 2H, ArC**H**$_2$S), 2.97 (dd, *J* = 3.6, 14.5 Hz, 1H, SC**H**(H)CH), 2.77 (dd, *J* = 7.5, 14.5 Hz, 1H, SCH(**H**)CH), 1.31 (s, 9H, C(C**H**$_3$)$_3$). ^{13}C NMR (101 MHz, $CDCl_3$) δ 168.2, 151.8, 151.1, 134.1, 128.7, 126.0,

57.8, 36.8, 34.7, 32.9, 31.4. ATR-FTIR (cm^{-1}): 3312, 2961, 2868, 1858, 1777, 1515, 1463, 1396, 1362, 1288, 1179, 1108, 1084, 930, 839, 776, 755. HRMS (ESI) $[M+Na]^+$ calculated for $C_{15}H_{19}NaO_3S$, 316.0983; found, 316.0979.

Serine-ester NCA Monomer-M4: The product was obtained as a white solid from O-Benzoyl-L-serine hydrochloride (**7**) (8 g, 32.6 mmol) and triphosgene (4.8 g, 16.3 mmol) by employing the same procedure as that for serine-ester NCA monomer-**M1**. Please note that the THF and hexane amount was twice than that used in the synthesis of serine-ester NCA monomer-**M1**. Yield: 6.1 g (80 %). ^{1}H NMR (400 MHz, DMSO-d_6) δ 9.30 (s, 1H, N**H**), 7.91 (d, *J* = 7.3 Hz, 2H, Ar-**H**), 7.69 (t, *J* = 7.4 Hz, 1H, Ar-**H**), 7.56 (t, *J* = 7.7 Hz, 2H, Ar-**H**), 4.92 (t, *J* = 3.1 Hz, 1H, C**H**CH_2), 4.62 (dd, *J* = 3.0, 11.9 Hz, 1H, OC**H**(H)CH), 4.49 (dd, *J* = 3.9, 11.9 Hz, 1H, OCH(**H**)CH). ^{13}C NMR (101 MHz, DMSO-d_6) δ 169.4, 165.1, 152.0, 133.9, 129.2, 129.0, 128.8, 62.5, 57.1. ATR-FTIR (cm^{-1}): 3298, 2932, 2852, 1857, 1777, 1709, 1601, 1601, 1452, 1380, 1283, 1179, 1115, 1073, 1029, 1000, 976, 936, 757, 740, 709. HRMS (ESI) $[M+Na]^+$ calculated for $C_{11}H_9NNaO_5$, 258.0378; found, 258.0380.

Serine-ether NCA Monomer-M5: The product was obtained as a white crystalline solid from O-Benzyl-L-serine hydrochloride (**9**) (3.6 g, 15.54 mmol) and triphosgene (3 g, 10.10 mmol) by employing the same procedure as that for serine-ether NCA Monomer-**M2**. Please note that, as the obtained NCA was solid instead of liquid and it was isolated by filtration instead of decantation of supernatant. Yield: 2.1 g (62 %)**.** ^{1}H NMR (400 MHz, $CDCl_3$) δ 7.34 – 7.17 (m, 5H, Ar-**H**), 6.52 (s, 1H, N**H**), 4.54 – 4.42 (m, 2H, ArC**H**$_2$O), 4.34 (t, *J* = 3.9 Hz, 1H, C**H**CH_2), 3.73 – 3.63 (m, 2H, CHC**H**$_2$). ^{13}C NMR (101 MHz, DMSO-d6) δ 167.8, 152.7, 136.7, 128.8, 128.4, 128.0, 73.8, 67.8, 58.5. ATR-FTIR (cm^{-1}): 3278, 2867, 1856, 1772, 1525, 1496, 1363, 1297, 1217, 1097, 1022, 914, 737, 696, 630. HRMS (ESI) [M+Na] + calculated for $C_{11}H_{11}NNaO_4$, 244.0586; found, 244.0585.

S-Benzyl-L-cysteine NCA Monomer-M6: The product was obtained as a white crystalline solid from S-Benzyl-L-cysteine (**10**) (4 g, 18.93 mmol) and triphosgene (2.81 g, 9.47 mmol) by employing the same procedure as that for serine-ester NCA monomer-**M1** The amount of THF and hexane used was double than that used in the synthesis of serine-ester NCA monomer-**M1**. Yield: 2.4 g (53 %)**.** ^{1}H NMR (400 MHz, $CDCl_3$) δ 7.40 – 7.27 (m, 5H, Ar-**H**), 6.15 (s, 1H, N**H**), 4.28 (ddd, *J* = 0.7, 3.7, 7.5 Hz, 1H, C**H**CH_2), 3.77 (s, 2H, ArC**H**$_2$S), 2.96 (dd, *J* = 3.6, 14.5 Hz, 1H, SC**H**(H)CH)), 2.77 (dd, *J* = 7.5, 14.5 Hz, 1H, SCH(**H**)CH). ^{13}C NMR (101 MHz, $CDCl_3$) δ 168.1, 151.9, 137.2, 129.1, 129.0, 127.9, 57.7, 37.1, 32.9.

ATR-FTIR (cm^{-1}): 3305, 1861, 1792, 1250, 1123, 1078, 938, 928, 895, 774, 754, 713. HRMS (ESI) $[M+Na]^+$ calculated for $C_{11}H_{11}NNaO_3S$, 260.0357; found, 260.0353.

Synthesis of polypeptides: Detailed polymerization procedure is explained for the synthesis of ***polyserine-1*** by octadecyl amine-initiated polymerization of serine-ester NCA monomer-**M1** in $CHCl_3$ - DMF (85: 15, v/v) with M/I = 100 using NHC catalyst. To a solution of serine-ester NCA monomer-**M1** (0.58 g, 2.00 mmol) in a mixture of anhydrous DMF - chloroform (1:7 v/v, 8 mL) was added a 20 mM solution of octadecyl amine (1 mL, 0.02 mmol, for M/I =100) in anhydrous chloroform under nitrogen atmosphere. Subsequently, the 8 mM solution of 1,3-Bis(2,4,6-trimethylphenyl) imidazolium bicarbonate (1 mL, 8 µmol) in a mixture of anhydrous DMF – chloroform (1:1, v/v) was added, and the reaction mixture was stirred under nitrogen atmosphere at 25 °C. After 24 h of stirring, chloroform was removed under reduced pressure, and the polymer was precipitated by adding methanol (40 mL). The suspension was transferred into a centrifuge tube and centrifuged at 6000 rpm for 10 min. After discarding the supernatant, the pellet was triturated with methanol and finally dried under high vacuum to obtain polyserine-**1** as a white solid. Yield: 336 mg (67 %). ^{1}H NMR (400 MHz, $CDCl_3$ – TFA (0.7 mL, 6:1, v/v) δ 8.31 (d, *J* = 6.7 Hz, 96H, N**H**CO), 7.72 (d, *J* = 8.4 Hz, 210H, Ar-**H**), 7.30 (d, *J* = 8.5 Hz, 230H, Ar-**H**), 5.09 (bs, 99H, COC**H**NH), 4.89 – 4.43 (m, 203H, COCHC**H**$_2$), 1.50 – 1.00 (m, 982H, C(C**H**$_3$)$_3$ and (C**H**$_2$)$_{16}$CH$_3$), 0.88 (t, *J* = 6.9 Hz, 3H, C**H**$_3$(CH$_2$)$_{16}$). ^{13}C NMR (101 MHz, $CDCl_3$ – TFA (0.7 mL, 6:1, v/v) δ 170.6, 168.9, 159.2, 129.9, 126.0, 125.0, 64.5, 53.8, 35.3, 30.7, and 30.0. ATR-FTIR (cm^{-1}): 3277, 2963, 2905, 2870, 1721, 1660, 1610, 1553, 1464, 1409, 1365, 1313, 1266, 1190, 1128, 1117, 1098, 1018, 853, 773, 756, 705, and 620.

Synthesis of polyserine-2: Similar to the general polymerization procedure is employed using serine-ether NCA monomer-**M2** (0.56 g, 2.00 mmol) in a mixture of anhydrous DMF - chloroform (1:7 v/v, 8 mL), 20 mM solution of octadecyl amine (1 mL, 0.02 mmol) in anhydrous chloroform, and 8 mM solution of 1,3-Bis(2,4,6-trimethylphenyl) imidazolium bicarbonate (1 mL, 8 µmol) in a mixture of anhydrous DMF – chloroform (1:1, v/v). Yield: 266 mg, 56 %. ^{1}H NMR (400 MHz, $CDCl_3$ – TFA (0.7 mL, 6:1, v/v) δ 8.03 (bs, 88H, N**H**CO), 7.30 (d, *J* = 8.3 Hz, 175H, Ar-**H**), 7.11 (d, *J* = 8.2 Hz, 180H, Ar-**H**), 4.98 – 4.69 (m, 88H, COC**H**NH), 4.56 – 4.36 (m, 179H, ArC**H**$_2$O), 3.92 – 3.61 (m, 181H, COCHC**H**$_2$), 1.48 – 1.06 (m, 886H, C(C**H**$_3$)$_3$ and (C**H**$_2$)$_{16}$CH$_3$), 0.89 (t, *J* = 6.8 Hz, 3H, C**H**$_3$(CH$_2$)$_{16}$). ^{13}C NMR (101 MHz, $CDCl_3$ – TFA (0.7 mL, 6:1, v/v) δ 171.5, 152.1, 132.6, 128.2, 125.8, 74.0,

68.6, 53.6, 34.7, 31.2, 29.9. ATR-FTIR (cm^{-1}): 3278, 2961, 2866, 1657, 1547, 1515, 1470, 1394, 1361, 1312, 1293, 1267, 1217, 1108, 1096, 1018, 852, 835, 816, 754, 673.

Synthesis of polycysteine-3: Similar to the general polymerization procedure is employed using cysteine NCA-monomer-**M3** (0.59 g, 2.00 mmol) in a mixture of anhydrous DMF - chloroform (1:7 v/v, 8 mL), 20 mM solution of octadecyl amine (1 mL, 0.02 mmol) in anhydrous chloroform, and 8 mM solution of 1,3-Bis(2,4,6-trimethylphenyl) imidazolium bicarbonate (1 mL, 8 µmol) in a mixture of anhydrous DMF – chloroform (1:1, v/v)**.** Yield: 441 mg, 88 % ^{1}H NMR (400 MHz, $CDCl_3$ – TFA (0.7 mL, 6:1, v/v) δ 7.73 (d, *J* = 6.7 Hz, 87H, N**H**CO), 7.28 (d, *J* = 8.3 Hz, 228H, Ar-**H**), 7.14 (d, *J* = 8.3 Hz, 199H, Ar-**H**), 4.71 – 4.54 (m, 91H, COC**H**NH), 3.61 (s, 189H, ArC$\mathbf{H_2}$S), 2.97 – 2.67 (m, 185H, COCHC$\mathbf{H_2}$), 1.52 – 1.05 (m, 934H, C(C$\mathbf{H_3}$)$_3$ and (C$\mathbf{H_2}$)$_{16}$CH$_3$), 0.88 (t, *J* = 6.8 Hz, 1H, C$\mathbf{H_3}$(CH$_2$)$_{16}$). ^{13}C NMR (101 MHz, $CDCl_3$ – TFA (0.7 mL, 6:1, v/v) δ 172.1, 151.1, 133.9, 128.7, 126.0, 53.8, 36.4, 34.7, 32.9, 31.3, 30.0. ATR-FTIR (cm^{-1}): 3278, 2961, 2867, 1657, 1544, 1525, 1464, 1416, 1363, 1269, 1107, 1019, 835, 755.

Synthesis of polyserine-4: Similar to general polymerization procedure is employed using serine-ester NCA Monomer-**M4** (0.47 g, 2.00 mmol) in a mixture of anhydrous DMF - chloroform (1:7 v/v, 8 mL), 20 mM solution of octadecyl amine (1 mL, 0.02 mmol) in anhydrous chloroform, and 8 mM solution of 1,3-Bis(2,4,6-trimethylphenyl) imidazolium bicarbonate (1 mL, 8 µmol) in a mixture of anhydrous DMF – chloroform (1:1, v/v). Yield: 220 mg, 57% ^{1}H NMR (400 MHz, $CDCl_3$ – TFA (0.7 mL, 6:1, v/v) δ 8.37 – 8.20 (m, 54H, N**H**CO), 7.92 – 7.74 (m, 112H, Ar-**H**), 7.64 – 7.45 (m, 59H, Ar-**H**), 7.45 – 7.28 (m, 93H, Ar-**H**), 5.03 (bs, 48H, COC**H**NH), 4.87 – 4.45 (m, 109H, COCHC$\mathbf{H_2}$), 1.45 – 1.14 (m, 26H, (C$\mathbf{H_2}$)$_{16}$CH$_3$), 0.88 (t, *J* = 6.5 Hz, 3H, C$\mathbf{H_3}$(CH$_2$)$_{16}$). ^{13}C NMR (101 MHz, $CDCl_3$ – TFA (0.7 mL, 6:1, v/v) δ 170.6, 168.8, 135.0, 129.9, 129.0, 127.9, 64.4, 53.9, 30.0. ATR-FTIR (cm^{-1}): 3289, 1726, 1635, 1514, 1450, 1367, 1316, 1267, 1221, 1176, 1116, 1069, 1025, 720, 708.

Synthesis of polyserine-5: Similar to general polymerization procedure is employed using Serine-ether NCA-(**M5**) (0.44 g, 2.00 mmol) in a mixture of anhydrous DMF - chloroform (1:7 v/v, 8 mL), 20 mM solution of octadecyl amine (1 mL, 0.02 mmol) in anhydrous chloroform, and 8 mM solution of 1,3-Bis(2,4,6-trimethylphenyl) imidazolium bicarbonate (1 mL, 8 µmol) in a mixture of anhydrous DMF – chloroform (1:1, v/v). Yield: 135 mg, 38 %. ^{1}H NMR (400 MHz, $CDCl_3$ – TFA (0.7 mL, 6:1, v/v) δ 7.92 (d, *J* = 7.0 Hz, 31H, N**H**CO),

7.37 – 7.11 (m, 188H, Ar-**H**), 4.85 – 4.66 (m, 34H, COC**H**NH), 4.57 – 4.37 (m, 71H), 3.86 – 3.53 (m, 69H, ArC**H**$_2$O), 1.44 – 1.04 (m, 32H, (C**H**$_2$)$_{16}$CH$_3$), 0.89 (t, *J* = 6.7 Hz, 3H, C**H**$_3$(CH$_2$)$_{16}$). ^{13}C NMR (101 MHz, CDCl$_3$ – TFA (0.7 mL, 6:1, v/v) δ 171.4, 135.9, 128.8, 128.7, 128.2, 74.0, 68.5, 53.6, 29.9. ATR-FTIR (cm^{-1}): 3274, 2868, 1717, 1629, 1522, 1445, 1361, 1261, 1219, 1105, 1025, 772, 737, 698, 607.

Synthesis of polycysteine-6: Similar to general polymerization procedure is employed using cysteine NCA monomer-**M6** (0.48 g, 2.00 mmol) in a mixture of anhydrous DMF - chloroform (1:7 v/v, 8 mL), 20 mM solution of octadecyl amine (1 mL, 0.02 mmol) in anhydrous chloroform, and 8 mM solution of 1,3-Bis(2,4,6-trimethylphenyl) imidazolium bicarbonate (1 mL, 8 µmol) in a mixture of anhydrous DMF – chloroform (1:1, v/v). Yield: 189 mg, 48 % ^{1}H NMR (400 MHz, CDCl$_3$ – TFA (0.7 mL, 6:1, v/v) δ 7.57 (d, *J* = 6.9 Hz, 46H, N**H**CO), 7.36 – 7.16 (m, 282H, Ar-**H**), 4.61 – 4.38 (m, 51H, COC**H**NH), 3.65 (s, 105H, ArC**H**$_2$S), 2.88 – 2.66 (m, 102H, COCHC**H**$_2$), 1.51 – 1.19 (m, 32H, (C**H**$_2$)$_{16}$CH$_3$), 0.88 (t, *J* = 6.9 Hz, 3H, C**H**$_3$(CH$_2$)$_{16}$). ^{13}C NMR (101 MHz, CDCl$_3$ – TFA (0.7 mL, 6:1, v/v) δ 172.0, 137.1, 129.03, 128.98, 127.9, 53.7, 36.6, 32.6, 29.9. ATR-FTIR (cm^{-1}): 3266, 3057, 2910, 2847, 1691, 1626, 1516, 1494, 1450, 1412, 1222, 1067, 1025, 771, 697.

By following similar procedure, octadecyl amine-initiated polymerization of NCA monomers were carried in different solvents such as DMF, THF, CHCl$_3$, or CHCl$_3$ - DMF mixture were carried out.

Synthesis of MeO-PEG$_{5000}$-NH$_2$ initiated di-*block*-copolymers: Detail procedure is described for the synthesis of PEG-*b*-polyserine-2 using monomer serine-ether monomer **M2.** A mixture of serine-ether NCA monomer-**M2** (0.28 g, 1.00 mmol) and MeO-PEG$_{5000}$-NH$_2$ (50 mg, 0.01 mmol) in an anhydrous DMF - chloroform (1:15 v/v, 4 mL) was stirred under nitrogen atmosphere for 15 min. Subsequently, the 4 mM solution of 1,3-Bis(2,4,6-trimethylphenyl) imidazolium bicarbonate (1 mL, 4 µmol) in a mixture of anhydrous DMF – chloroform (1:1, v/v) was added, and the reaction mixture was stirred under nitrogen atmosphere at 25 °C. After 24 h of stirring, chloroform was removed under reduced pressure, and the polymer was precipitated by adding water (40 mL). The suspension was transferred into a centrifuge tube and centrifuged at 6000 rpm for 10 min. After discarding the supernatant, the pellet was triturated with water and finally dried by lyophilization to obtain PEG-*b*-polyserine-2 as a white solid. Yield: 198 mg, 70 %. ^{1}H NMR (400 MHz, CDCl$_3$ – TFA (0.7 mL, 6:1, v/v) δ 8.00 (bs, 1H, N**H**CO), 7.28 (d, *J* = 7.66 Hz, 2H, Ar-**H**), 7.09 (d, *J*

= 8.05 Hz, 2H, Ar-**H**), 4.80 (bs, 1H, COC**H**NH), 4.52 – 4.32 (m, 2H, ArOC**H**$_2$), 3.92 – 3.52 (m, 8H, COCHC**H**$_2$, (OC**H**$_2$C**H**$_2$O)$_n$C**H**$_3$), 1.47 – 1.02 (m, 12H, C(C**H**$_3$)$_3$).

Similar procedure was employed using serine ether monomer **M5** to obtain PEG-*b*-polyserine5 as a white solid. Yield: 214 mg, 94 % ^{1}H NMR (400 MHz, $CDCl_3$ – TFA (0.7 mL, 6:1, v/v) δ 7.96 (bs, 1H, N**H**CO), 7.45 – 7.04 (m, 5H, Ar-**H**), 4.77 (bs, 1H, COC**H**NH), 4.58 – 4.34 (m, 2H, ArOC**H**$_2$), 4.06 – 3.41 (m, 9H, COCHC**H**$_2$, (OC**H**$_2$C**H**$_2$O)$_n$C**H**$_3$).

Deprotection of polyserine-2: To a solution of polyserine-2 (100 mg) in TFA (1.5 mL) at 0 °C was added HBr in acetic acid (33 wt%, 0.65 mL). The reaction mixture was stirred at 0 °C for 30 min, then contents were warmed to 25 °C, and stirring was continued for 18 h. Subsequently, diethyl ether (30 mL) was added to precipitate the polymer. The suspension was transferred into a centrifuge tube and centrifuged at 6000 rpm for 10 min. After discarding the supernatant, the pellet was triturated with diethyl ether and finally dried under a high vacuum to obtain polyserine-2D as a pale-yellow solid. Yield: 35 mg (94 %). ^{1}H NMR (400 MHz, TFA-d) δ 5.12 – 4.91 (m, 90H, C**H**CH_2), 4.60 – 4.06 (m, 162H, C**H**CH_2), 1.35 – 1.26 (m, 34H, (C**H**$_2$)$_{16}CH_3$), 0.86 (t, *J* = 6.3 Hz, 3H, C**H**$_3$(CH_2)$_{16}$).

Similar procedure was employed to deprotect PEG-*b*-polyserine-2 (100 mg) using HBr in acetic acid (33 wt%, 0.65 mL) to obtained PEG-*b*-polyserine-2D as a pale-yellow solid. Yield: 40 mg (83%). ^{1}H NMR (400 MHz, TFA-d) δ 5.23 – 5.08 (m, 104H, C**H**CH_2), 4.60 – 4.29 (m, 211H, C**H**CH_2), 4.10 (s, 548H, (OC**H**$_2$C**H**$_2$O)$_n$C**H**$_3$).

2.2.4. Procedure for monitoring the polymerization of serine-ether NCA monomer-M2 in chloroform by FT-IR

To a solution of serine-ether NCA monomer-**M2** (0.28 g, 1.00 mmol) in anhydrous chloroform (10 mL) was added a 20 mM solution of octadecyl amine (1 mL, 0.02 mmol) in anhydrous chloroform under nitrogen atmosphere. Subsequently, the 8 mM solution of 1,3-Bis(2,4,6-trimethylphenyl) imidazolium bicarbonate (1 mL, 8 μmol) in anhydrous chloroform was added, and the reaction mixture was stirred under nitrogen atmosphere at 25 °C. The aliquots (0.1 mL) were taken at different intervals and small portion of it was spotted on Zn-Se crystal of ATR-FTIR spectrometer, subsequently the spectrum was recorded after evaporation of solvent from spotted sample (usually it takes ~ 10 seconds for evaporation).

Similar procedure was employed for FT-IR based monitoring of polymerization of other NCA monomers such as cysteine NCA monomer-**M3** in $CHCl_3$, THF and $CHCl_3$+DMF (85: 15, v/v) and serine-ester NCA monomer-**M1** in THF and $CHCl_3$+DMF (85: 15, v/v) by using corresponding solvents.

2.2.5. Procedure for monitoring the polymerization of serine-ether NCA monomer-M2 in chloroform-D by ^{1}H NMR and SEC

To a solution of serine-ether NCA monomer-**M2** (0.28 g, 1.00 mmol) in anhydrous chloroform-D (10 mL) was added a 20 mM solution of octadecyl amine (1 mL, 0.02 mmol) in anhydrous chloroform-D under nitrogen atmosphere. Subsequently, the 8 mM solution of 1,3-Bis(2,4,6-trimethylphenyl) imidazolium bicarbonate (1 mL, 8 µmol) in anhydrous chloroform-D was added, and the reaction mixture was stirred under nitrogen atmosphere at 25 °C. The aliquots (0.1 mL) taken at different intervals were quenched by adding 0.1 mL TFA and submitted to ^{1}H NMR after diluting with more chloroform-D (0.5 mL). Also, another 0.1 mL aliquot of the reaction mixture at different time intervals was diluted to 1 mL using 0.9 mL of THF (or $CHCl_3$, in case of SEC in $CHCl_3$) and directly injected in to SEC column for SEC analysis using THF (or $CHCl_3$) as eluent. Similar procedure was employed for monitoring polymerization of cysteine NCA monomer-**3** by ^{1}H NMR using cysteine NCA monomer-**M3** (0.28 g, 1.00 mmol).

2.3. Results and Discussion

2.3.1. Synthesis of Bulky Monomers and Polypeptides

L-Serine and L-cysteine based new NCA monomers **M1**, **M2** and **M3** were tailor-made by multi-step organic synthesis using 4-*t*-butyl benzoic acid and 4-*t*-butyl benzyl bromide as bulky pendant groups as shown in Scheme 2.1. Alternatively, benzoyl chloride and benzyl bromide were employed to synthesize non-bulky NCA monomers **M4**, **M5** and **M6** as shown in Scheme 2.2. These NCA monomers were synthesized in 60-80 % yield (NMR data is given in appendix) and their solubility in N,N-dimethyl formamide (DMF), tetrahydrofuran (THF), and chloroform ($CHCl_3$) were found to be significantly different with respect to their chemical structure (see Table 2.1). 1,3-Bis(2,4,6-trimethylphenyl) imidazolium hydrogen carbonate (IMes.HCO_3) was chosen as a catalyst to in-situ generate N-heterocyclic carbenes (NHC) to activate the ROP .[50]

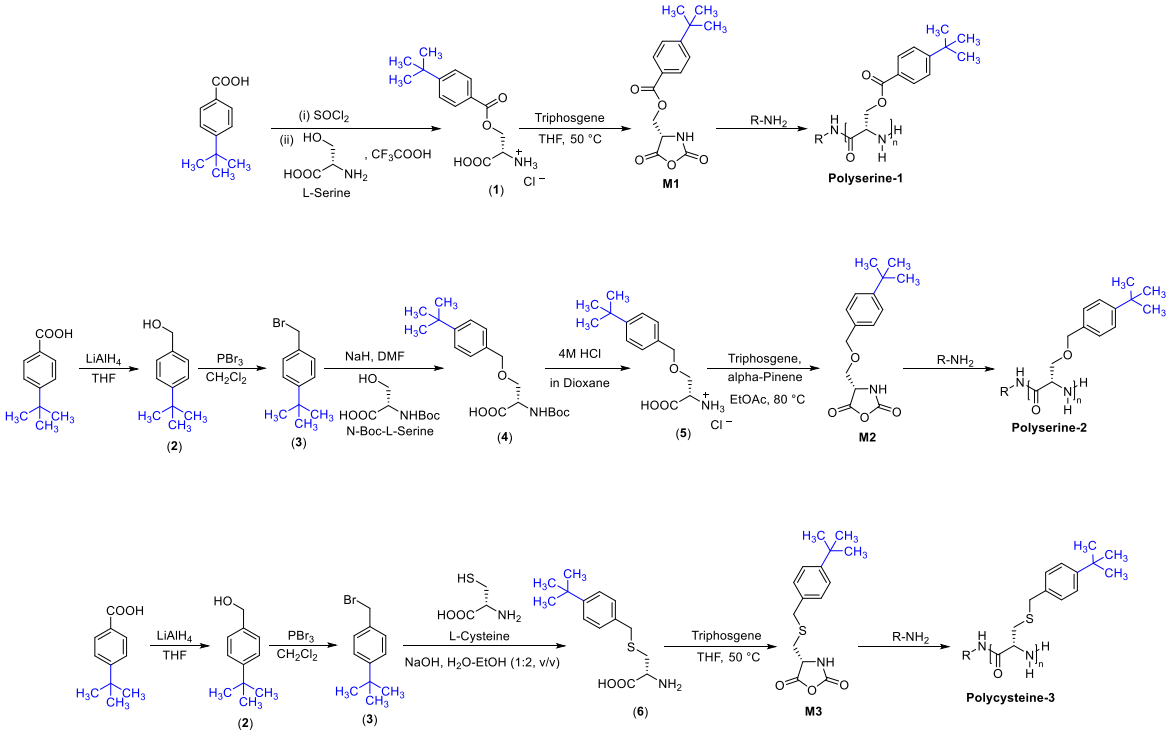

Scheme 2.1. *Synthesis and polymerization of monomers **M1**, **M2** and **M3***

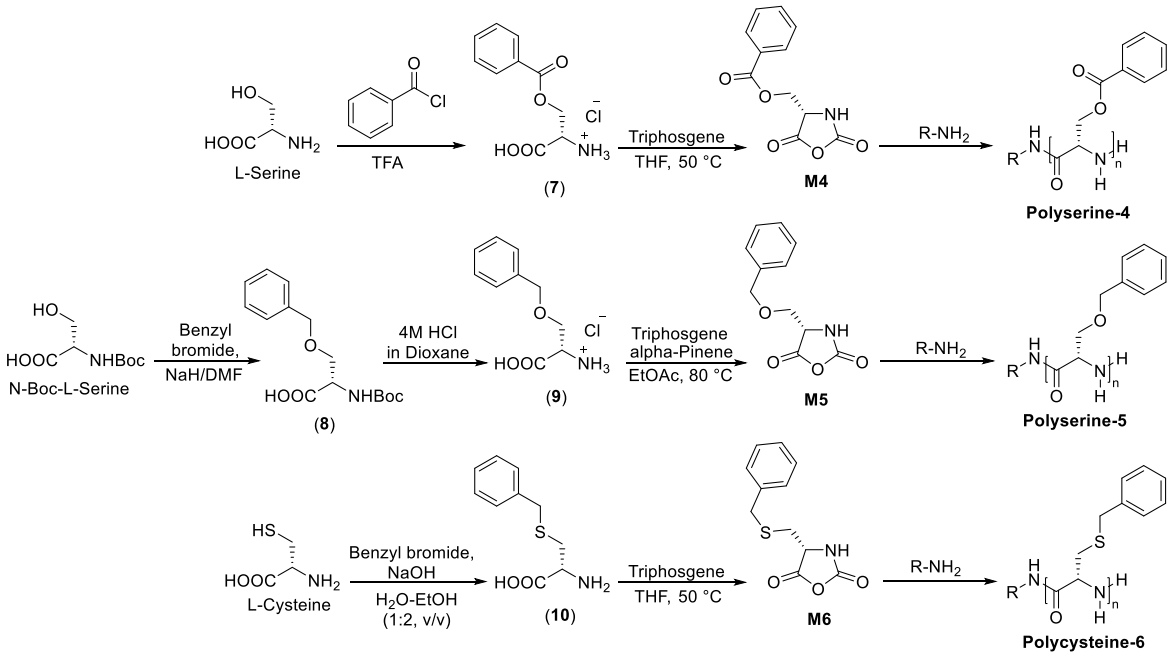

Scheme 2.2. *Synthesis and polymerization of monomers* ***M4****,* ***M5*** *and* ***M6***

Table 2.1. *Solubility of NCA monomers and corresponding polymers in common organic solvents*

Monomer	Solubility in DMF	Solubility in THF	Solubility in $CHCl_3$
Serine-ester NCA monomer (M1)	Freely Soluble	Freely Soluble	~ 0.5 %
Serine-ether NCA monomer (M2)	Freely Soluble	Freely Soluble	Freely Soluble
Cysteine NCA monomer (M3)	Freely Soluble	Freely Soluble	~ 2.5 %
Serine-ester NCA monomer (M4)	Freely Soluble	~ 4.3 %	Insoluble
Serine-ether NCA monomer (M5)	Freely Soluble	Freely Soluble	Freely Soluble
Cysteine NCA monomer (M6)	Freely Soluble	Freely Soluble	~ 2 %
Polyserine-1	Insoluble	Freely Soluble	Freely Soluble
Polyserine-2	Insoluble	Freely Soluble	Freely Soluble
Polycysteine-3	Insoluble	Freely Soluble	Freely Soluble
Polyserine-4	Insoluble	Insoluble	Insoluble
Polyserine-5	Insoluble	Insoluble	Insoluble
Polycysteine-6	Insoluble	Insoluble	Insoluble

Note: The term “freely soluble” refers to solubility of monomer at the minimum concentration of 50 mg/mL (5%, w/v) in a corresponding solvent.

The ROP process was first optimized for serine-ester NCA monomer-**M1** using octadecyl amine as an initiator in three different solvents DMF, THF, and $CHCl_3$ and the details are reported in the Table 2.2. The concentration of the monomer was maintained as 0.2 M, the monomer to initiator ratio (M/I) was fixed as 100 in feed, and the polymerization was carried out at 25°C for 24 h under nitrogen atmosphere. Subsequently, the % conversion was determined by subjecting polymerization reaction mixture to FT-IR spectroscopy at the end of 24 h and these values are given in Table 2.2.

Table 2.2. *Monomer, polymerization solvent, and ^{1}H-NMR, SEC molar mass and percentage conversion are given.*

Entry	Monomer	Polymerization Solvent (s)	Catalyst[e]	n (NMR)[f]	M_n NMR (g/mol)[g]	SEC in THF		SEC in $CHCl_3$		Conversion (%)[j]
						M_n (g/mol)[h]	Đ[h]	M_n (g/mol)[i]	Đ[i]	
1	M1	DMF	Yes	45	11100	8300	1.6	12700	1.4	50
2	M1	DMF	No	20	4900	5700	2.9	8100	1.3	30
3	M1	THF	Yes	69	17100	9600	1.4	19200	1.3	57
4	M1	THF	No	45	11100	5800	1.8	14800	1.2	38
5	M1	$CHCl_3$	Yes	59	14600	11800	1.5	19300	1.3	> 99
6	M1	$CHCl_3$	No	26	6400	6800	1.2	9400	1.2	ND
7	M1	$CHCl_3$[a]	Yes	21	5500	ND	ND	7600	1.6	10
8	M1	THF+$CHCl_3$[b]	Yes	89	22000	9800	1.3	27000	1.3	> 99
9	M1	$CHCl_3$+DMF[c]	Yes	99	24500	9100	1.2	24200	1.1	> 99
10	M1	$CHCl_3$+DMF[c]	No	67	16600	9000	1.3	18100	1.1	70
11	M1	DMSO	Yes	38	9400	ND	ND	9400	1.1	44
12	M1	NMP	Yes	49	12100	ND	ND	16000	2.0	> 99
13	M1	Dioxane	Yes	51	12600	ND	ND	14800	1.3	60
14	M1	Acetonitrile	Yes	21	5200	ND	ND	8400	1.6	26
15	M2	THF	Yes	47	11000	8200	1.4	19100	1.3	40
16	M2	$CHCl_3$	Yes	87	20300	9500	1.1	28200	1.2	> 99
17	M2	$CHCl_3$+DMF[c]	Yes	88	20500	8600	1.1	31300	1.1	> 99
18	M3	THF	Yes	62	15500	12800	1.2	20200	1.5	70
19	M3	$CHCl_3$	Yes	46	11500	9400	1.6	15600	1.5	> 99
20	M3	$CHCl_3$[d]	Yes	77	19200	14100	1.2	35700	1.1	> 99
21	M3	$CHCl_3$+DMF[c]	Yes	91	22700	13200	1.2	38000	1.1	> 99

The concentration of the monomer [M] was maintained as 0.2 M, N,N-dimesytlene substituted carbene was generated as catalyst in-situ and n-octadecylamine was used as initiator. The monomer/Initiator ratio was maintained as 100 in the feed. [a] [M] was 16.7 µM, [b] THF+$CHCl_3$ is 50:50 v/v, [c] $CHCl_3$+DMF is 85:15 v/v, [d] [M3] was 0.083 M, [e] N,N-dimesytlene substituted carbene was generated in-situ, [f] Degree of polymerization (n) was determined from ^{1}H-NMR. [g] NMR-number average molar mass (M_n = n × repeating unit mass). [h] molar mass and dispersity (Đ) were determined by size exclusion chromatography in THF at 25 °C with respect to polystyrene standards. [i] molar mass and dispersity (Đ) were determined by size exclusion chromatography in $CHCl_3$ at 25 °C using triple detector (RI, RALS and LALS) setup. [j] Determined using FT-IR spectroscopy from integration of NCA anhydride peak at ~1780 cm^{-1} at the beginning and end of reaction.

The monomer **M1** exhibited different trend in the polymerization reaction depending upon the solubility of the resultant polypeptide in the solvent (see Table 2.1 for solubility of polypeptides and Figure 2.2 for snapshots of polymerization vials at various time intervals of polymerization). The polymerization in DMF occurred from clear to turbid and the polymer became insoluble in DMF in less than 10 minutes (see vials in Figure 2.2a for snapshots at different time period) which led to only ~50% consumption of monomer in 24 h. Due to the excellent solubility of the polyserine-1 chains, the polymerization proceeded homogenously and solution was clear without any traces of precipitate in THF (see vials in Figure 2.2b). Unfortunately, only ~60 % monomer conversion was noticed even after 24 h of polymerization. The monomer **M1** was partially soluble in $CHCl_3$; thus, the polymerization began as heterogenous and gradually turned into clear solution followed by the excellent solubility of the propagating polymer chains in $CHCl_3$ (see vials in Figure 2.2c). In this case, complete conversion was noticed at the end of the polymerization (> 99 % conversion). This is a very good example for polymer solubility driven ring opening process in which the solubility of the growing polypeptide chains drove the polymerization to proceed in homogeneous manner. In order to carry out the polymerization in $CHCl_3$ in homogeneous manner from the beginning, the concentration of the monomer was decreased ([**M1**] = 16.7 μM); however, the low concentration of the monomer in the dilution polymerization led only 10 % monomer conversion even after 48 h (see Table 2.2 for data). Mixture of solvents were also established for **M1** polymerization and it was found that minimum 50% v/v THF+$CHCl_3$ or 15% + 85 % v/v DMF+$CHCl_3$ were required to solubilize **M1** under polymerization conditions ([**M1**] = 0.2 M). Increasing the amount of DMF was found to precipitate the polymer chains which is attributed to the hydrogen bonding interaction between the polypeptide chains and DMF solvent molecules. It was also observed that dielectric constant (ε) of the solvents played a major role in the stabilization of α-helical polypeptide conformation in the polymerization medium.[133, 135-138] Chlorinated solvents having low dielectric constant such as dichloromethane or $CHCl_3$ (ε = 4.8) were found to be better choice for stabilizing the α-helical structures compared to that of high dielectric solvent like THF (ε = 7.5) and DMF (ε = 36.7). Hence, we believe that more β-sheet structures were formed via strong inter-chain hydrogen bonding interaction in DMF that resulted in the polymer precipitation. The solubility of the polyserine-1 in common organic solvents such as THF and $CHCl_3$ was attributed to the unique ability of *t*-butylbenzene side chain towards the steric-hindrance in the polymer chain. The

polymerization of **M1** was also attempted in other polar solvents such as DMSO, dioxane, N-Methyl-2-pyrrolidone (NMP) and acetonitrile; however, the uncontrolled polymer precipitation was noticed in these solvents (see data in Table 2.2).

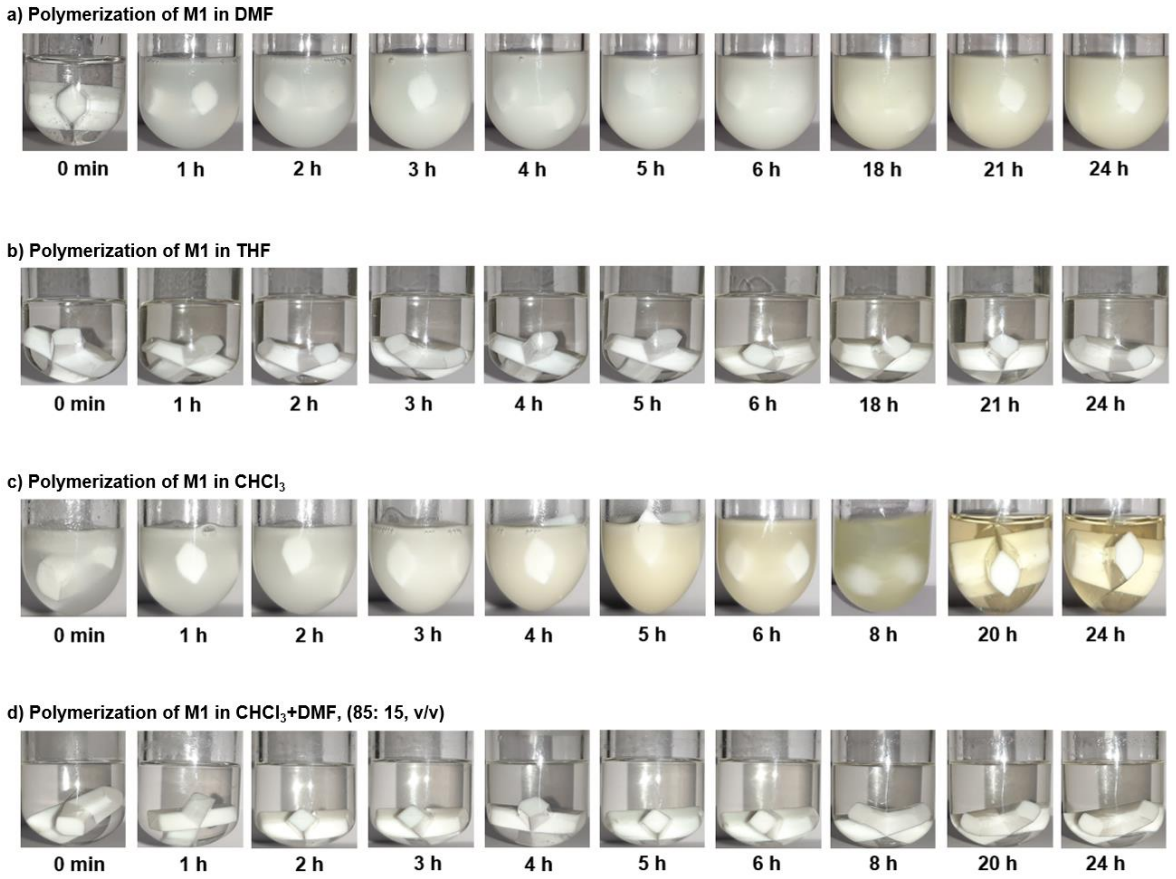

Figure 2.2: *Snapshots of polymerization reaction mixture of serine-ester NCA monomer-**M1** in different solvents such as (a) in DMF, (b) in THF, (c) in $CHCl_3$, (d) in* $CHCl_3$+DMF *(85: 15, v/v).*

The degree of polymerization (n) of the polypeptide was determined using ^{1}H-NMR by comparing the integration of the initiator proton-C**H**$_3$ (0.88 ppm, proton-a) to that of the polypeptide proton (for example C**H**, proton-b at 5.09 ppm) as shown in Figure 2.3a. The number average molecular weight (M_n) was estimated by NMR and the values are summarized in the Table 2.2 (see entry 1 to 14). In-situ generated NHC catalyst was found to be an excellent choice to accelerate the polymerization to give high % conversion and yield high molecular weight polymers compared to those produced in the absence of catalyst (see Entry 2, 4, 6, and 10 in Table 2.2 for data corresponding to polymerization reactions without NHC catalyst). The NHC catalyst was found to be the best in solvent mixtures such as THF+$CHCl_3$ (50:50 v/v) and $CHCl_3$+DMF (85:15 v/v) where a complete consumption of

monomer was observed and high molecular weight polymers were produced. The polymerization in $CHCl_3$+DMF solvent mixture with NHC catalyst was found to be the ideal condition to yield the chain length of nearly n = 99 for M/I = 100 in the feed (Entry 9 in Table 2.2).

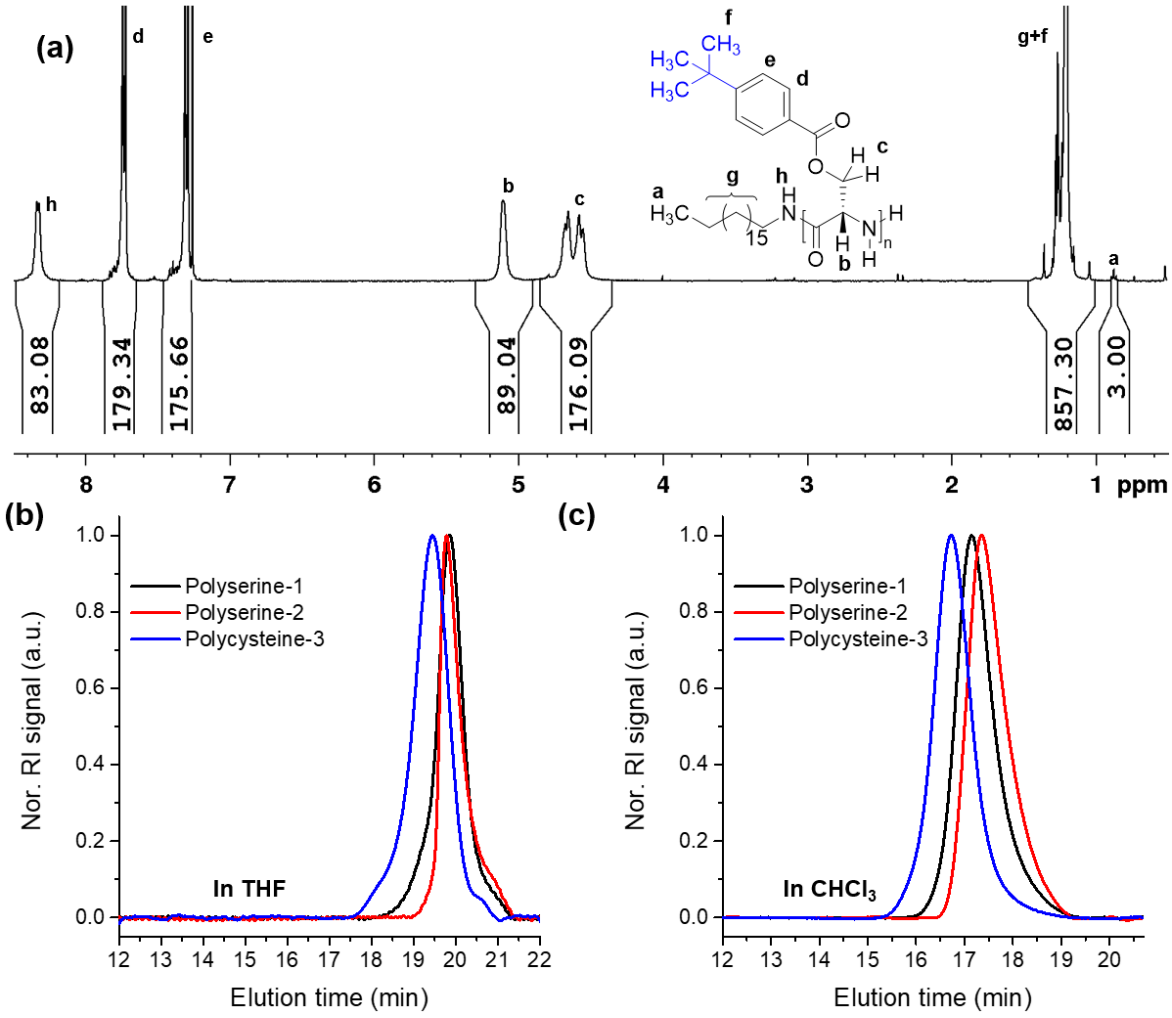

Figure 2.3. *(a) ^{1}H-NMR spectrum of polyserine-1 in $CDCl_3$+CF_3COOH and the peaks are assigned via alphabets with respect to the chemical structure. (b) Size exclusion chromatogram of the t-butylbenzene substituted polypeptides in THF at 25℃ (c) Size exclusion chromatogram of the t-butylbenzene substituted polypeptides in $CHCl_3$ at 25℃.*

The solubility of the new polypeptides facilitated the molecular weight determination by size exclusion chromatography (SEC) in THF and $CHCl_3$. Representative SEC plot of polymer is given in Figure 2.3b (with THF as eluent) and Figure 2.3c (with $CHCl_3$ as eluent) and their molecular weight data is summarized in the Table 2.2 (see Appendix for SEC traces corresponding to each entry). The molecular weight and dispersity

(Đ) were determined in THF based on polystyrene standards using differential refractive index (DRI) detector signals. The M_n of the polymers determined by SEC was found in good correlation with ^{1}H-NMR for ≤ 10,000 g/mol; however, for high molecular weight samples, obtained molecular weights were less than that expected. The molecular weight of the polypeptides was obtained as $M_n = 12\times10^3$ g/mol with the dispersity (Đ) of 1.2 to 1.5. SEC plots in THF exhibited tailing-trend which was attributed to the existence of small aggregates of the initially formed β-sheet segments during the re-dissolving of the polymers in sample preparation. The molecular weight determination of polymers was also carried out in $CHCl_3$ as an eluent using triple detector setup using RALS and LALS light scattering detector along with RI detector. RI signals for the polymers are shown in Figure 2.3c and the molecular weights are summarized in Table 2.2 (SEC chromatograms for RALS and LALS signals are shown in Appendix). There is no tailing observed in $CHCl_3$ SEC plots confirming the uniform molecular weight distribution. The absolute molecular weights thus obtained were in quite good agreement with molecular weights determined from ^{1}H NMR analysis in Table 2.2. SEC analysis in $CHCl_3$ established the formation of high molecular weight (M_n) polypeptides in the range of 7.6×10^3 to 27×10^3 g/mol with the narrow dispersity (Đ) of 1.1 to 1.4. Furthermore, in order to study the structural diversity of the initiator in the ROP; 1-hexyl amine and 2-(4-methoxyphenoxy)-ethane-1-amine (MPEA) were employed for the polymerization of serine ester monomer-**M1** and the data are summarized in Table 2.3 and Figures 2.4). The detailed investigation was evident that the newly designed *t*-butylbenzene substituted bulky NCA monomers were robust to structural variation in both initiators resulting in soluble and high molecular weight polypeptides.

Table 2.3. *Table contains the polymerization conditions, degree of polymerization (n) and M_n determined by ^{1}H-NMR and SEC molecular weights and percent conversion,*

Entry	Monomer	Solvent(s)	n (NMR)[b]	M_n NMR (g/mol)[c]	SEC in THF		SEC in $CHCl_3$		Conversion (%)[f]
					M_n (g/mol)[d]	Đ[d]	M_n (g/mol)[e]	Đ[e]	
22	Hexyl amine	$CHCl_3$+DMF[a]	80	19800	10200	1.2	21100	1.2	> 99
23	MPEA	$CHCl_3$+DMF[a]	95	23500	10500	1.4	26000	1.1	> 99

[M] was maintained as 0.2 M, N,N-dimesytlene substituted carbene was generated in-situ. The monomer/Initiator ratio was maintained as 100 in the feed. [a] $CHCl_3$+DMF is 85:15 v/v, [b] Degree of polymerization (n) was determined from ^{1}H-NMR. [c] NMR-number average molar mass (M_n = n × repeating unit mass). [d] molar mass and dispersity (Đ) were determined by size exclusion chromatography in THF at 25 ºC with respect to polystyrene standards. [e] molar mass and dispersity (Đ) were determined by size exclusion chromatography in $CHCl_3$ at 25 ºC using triple detector (RI, RALS and LALS) setup. [f] Determined using FT-IR spectroscopy from integration of NCA anhydride peak at ~1780 cm^{-1} at the beginning and end of reaction.

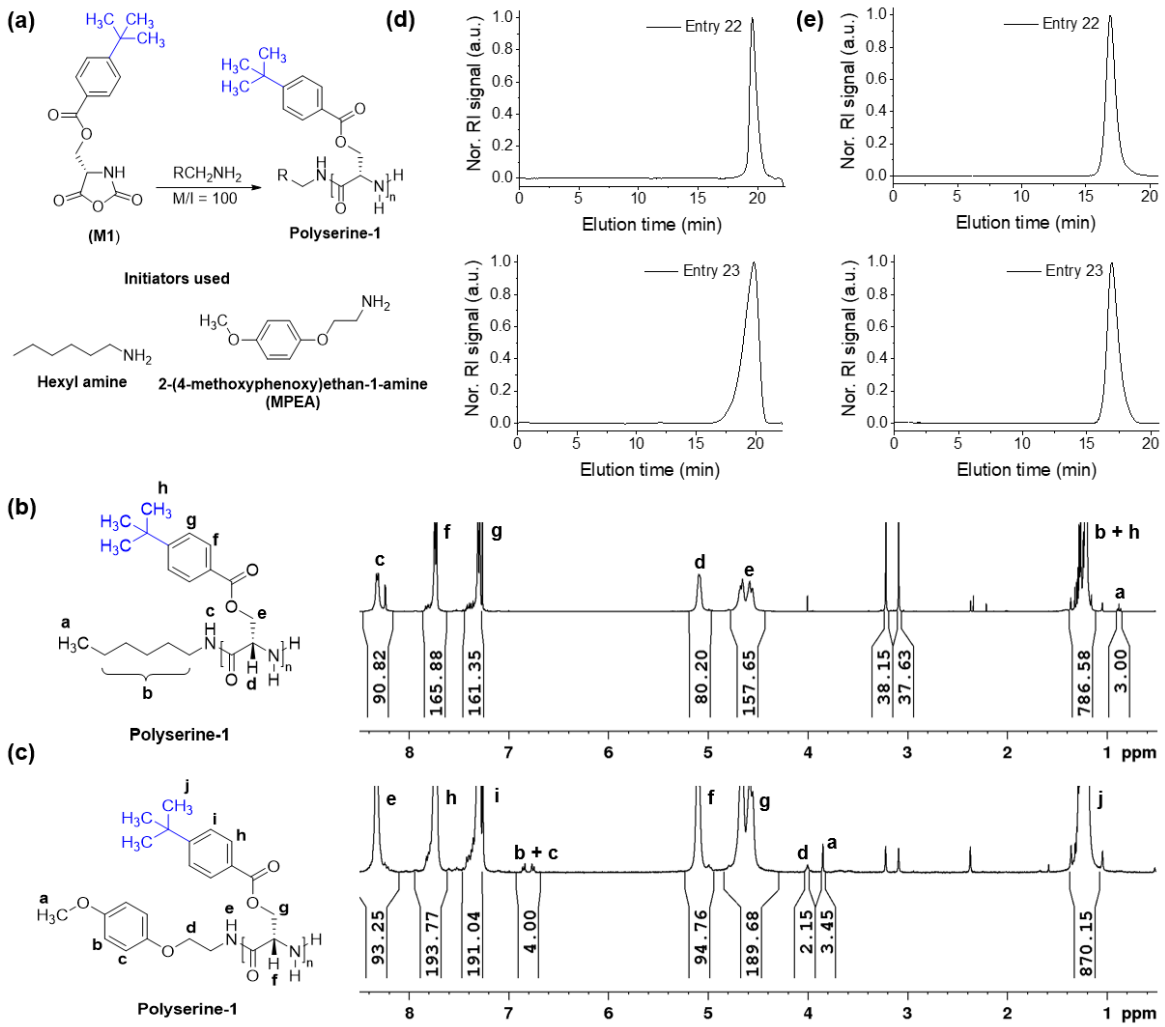

Figure 2.4: *(a) Scheme for polymerization of serine-ester NCA monomer-**M1** in* $CHCl_3$+DMF *(85: 15, v/v) using various initiators, (b)* ^{1}*H-NMR of polyserine-1 obtained by polymerization of **M1** by hexyl amine as an initiator, (c)* ^{1}*H-NMR of polyserine-1 obtained by polymerization of **M1** by 2-(4-methoxyphenoxy)ethan-1-amine (MPEA) as an initiator. (d) SEC traces of polyserine-1 obtained by polymerization of **M1** by different initiators using THF as eluent at 25 ℃, (e) SEC traces of polyserine-1 obtained by polymerization of **M1** by different initiators using* $CHCl_3$ *as eluent at 25 ℃.*

Serine-ether NCA monomer-**M2** was polymerized in $CHCl_3$, THF and $CHCl_3$+DMF and the details are given in Table 2.2 (entry 15 to 17, see Figure 2.5a for photographs). Polymerization was incomplete in THF while complete conversion of monomer was observed in case of polymerization in $CHCl_3$ or $CHCl_3$+DMF. The resultant polyserine-2 was found to be freely soluble and their degree of polymerization was obtained close to 90 units for M/I=100 in $CHCl_3$ or $CHCl_3$+DMF (Figure 2.5b for ^{1}H-NMR and Figure 2.3b, 2.3c

for representative SEC chromatograms in THF and $CHCl_3$ respectively, (see Appendix for other SEC plots).

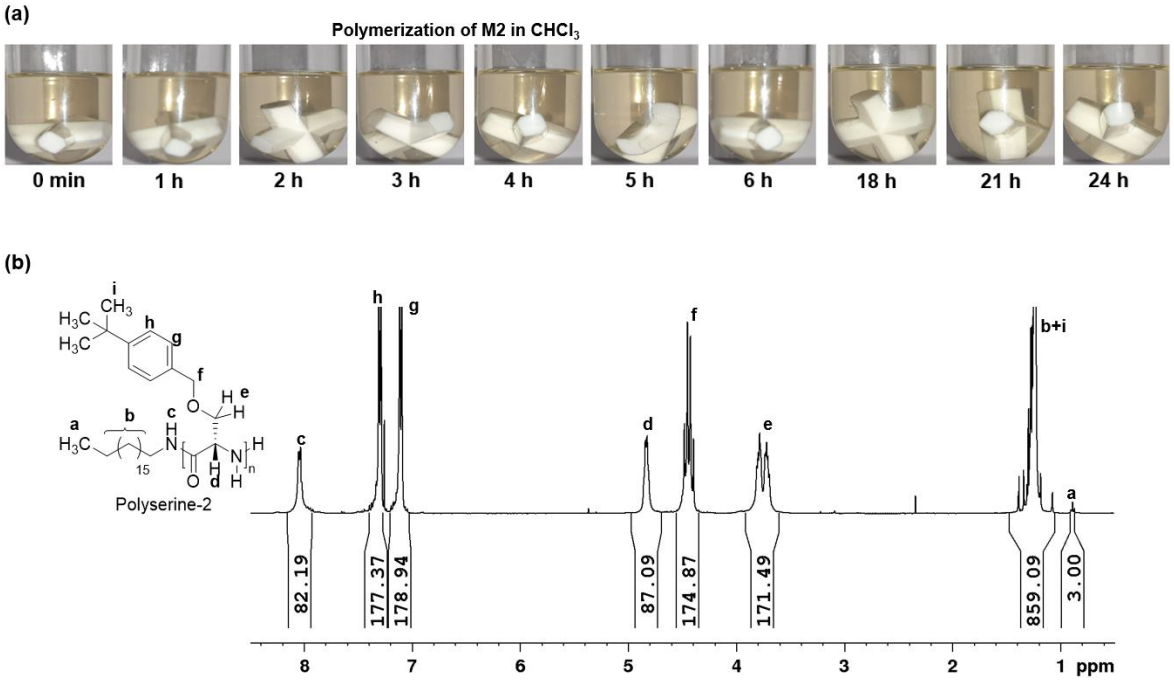

***Figure 2.5**: (a) Snapshots of polymerization reaction mixture of serine-ether NCA monomer-**M2** in $CHCl_3$, (b) ^{1}H NMR of polyserine-2 in $CDCl_3$+Trifluoroacetic acid (6:1, v/v).*

The monomer **M2** was liquid in nature and it is freely soluble in $CHCl_3$; however, the solid NCA monomer **M3** was partially soluble in $CHCl_3$ at high concentration (0.2 M) and completely soluble at low concentrations (0.086 M). To make uniform comparisons in Table 2.2, the monomer concentrations were fixed at 0.2 M for all the cases corresponding to entry 18 to 21 in Table 2.2 (except for entry 20). In this process, the monomer **M3** underwent polymerization from turbid (due to monomer's partial solubility) to clear solution due to complete solubility of the polymer. Additionally, the polymerization was attempted at dilute conditions ([**M3**] = 0.086 M) at which monomer **M3** was completely soluble in $CHCl_3$ and the polymerization proceeded homogeneously throughout the course (entry 20 in Table 2.2). The complete consumption of monomer **M3** was observed for polymerization in $CHCl_3$ or $CHCl_3$+DMF while, only ~70% conversion was observed in case of polymerization in THF. The resultant polycysteine-3 was found to be freely soluble and produced in high molecular weights with low dispersity (Đ) as shown in Table 2.2 (entry 18 to 21) (^{1}H-NMR in Figure 2.6 and representative SEC traces in Figures 2.3b and 2.3c, while other SEC traces are in Appendix). End group analysis by MALDI-TOF-MS for polycysteine-3 confirmed the presence of peaks well-separated by 249 amu with respect to

the repeating unit mass and followed the expected formula of $RNH+P_n+Na^+$. The mass peaks for P_9, P_{15} and P_{22} are assigned in given in Appendix. Similarly, the MALDI-TOF MS spectra for polyserine-1 and polyserine-2 also confirmed the expected polymer structure in Appendix. To study the effect of temperature on polymerization of the bulky NCA monomer, the polymerization of monomer **M3** was carried out at different temperatures such as 4 °C, 25 °C and 40°C in $CHCl_3$+DMF and the data is given in Figure 2.7. In all the cases, reaction mixture was homogeneous and polymer having good molecular weights with narrow dispersity (Đ) were obtained. Only the obvious effect of temperature on polymerization kinetics was seen as the complete consumption of monomer requiring 18 h, 6 h and 4 h for polymerization at 4°C, 25°C and 40°C respectively.

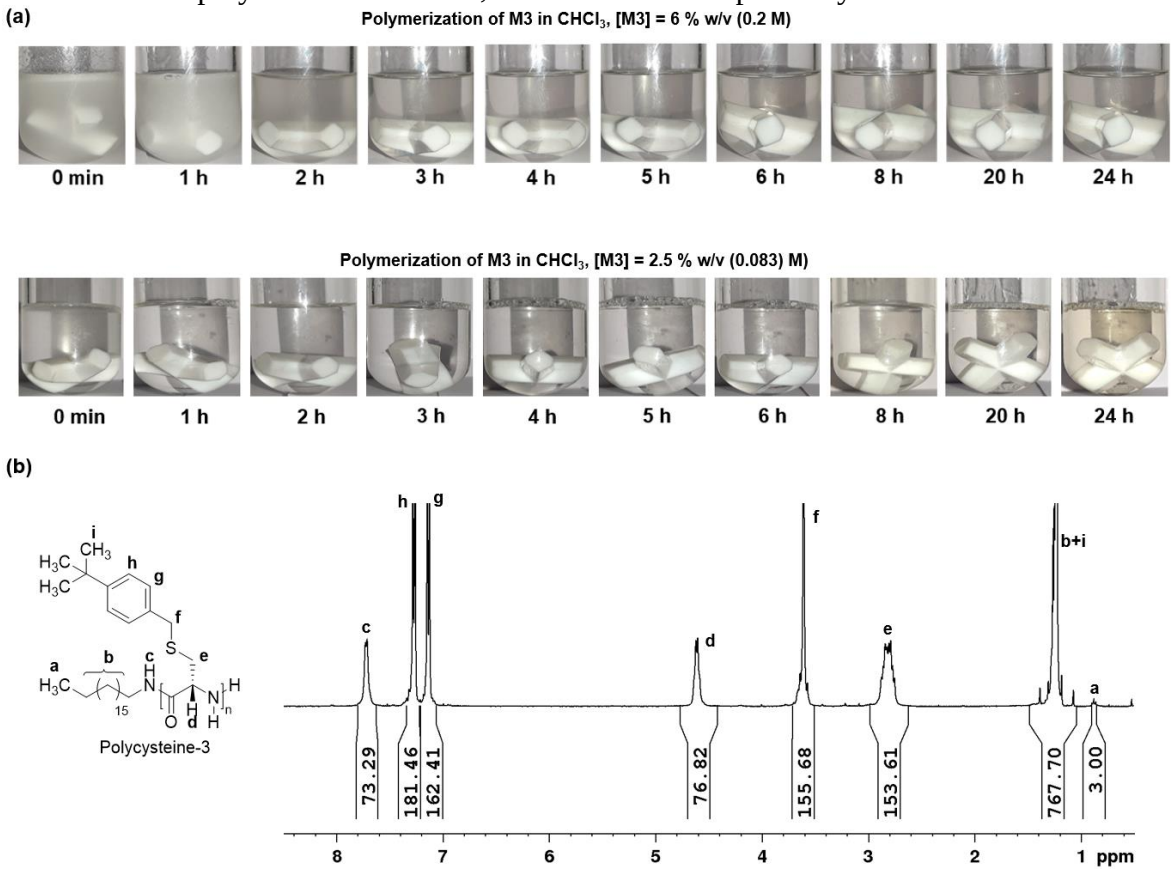

***Figure 2.6**: (a) Snapshots of polymerization reaction mixture of cysteine NCA monomer-**M3** in $CHCl_3$, (b) ^1H NMR of polycysteine-3 in $CDCl_3$+Trifluoroacetic acid (6:1, v/v).*

(a)

Temperature (°C)	n (NMR)[a]	M_n NMR (g/mol)[b]	M_n SEC (g/mol)[c]	Đ SEC (g/mol)[c]	Conversion (%)[d]
4	90	22400	36700	1.2	> 99
25	91	22700	38000	1.1	> 99
40	89	22200	36200	1.2	> 99

Polymerization was carried out in $CHCl_3$+DMF (85:15, v/v) using octadecyl amine as an initiator (M/I = 100) and in-situ generated N,N-dimesitylene substituted carbene as a catalyst at different temperatures. [a] Degree of polymerization (n) was determined from ^{1}H-NMR. [b] NMR-number average molar mass (M_n = n × repeating unit mass). [c] molar mass and dispersity (Đ) were determined by size exclusion chromatography in $CHCl_3$ at 25 °C using triple detector (RI, RALS and LALS) setup. [d] Determined using FT-IR spectroscopy from integration of NCA anhydride peak at ~1780 cm^{-1} at the beginning and end of reaction.

(b)

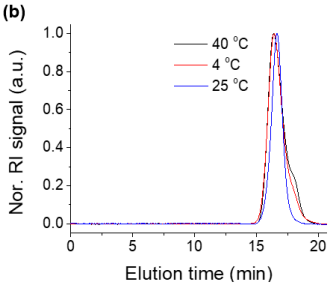

Figure 2.7: *(a) Table contain the polymerization conditions, degree of polymerization (n) and M_n determined by ^{1}H-NMR and SEC molecular weights and percent conversion, (b) SEC traces of polycysteine-3 obtained by polymerization of **M1** by polymerizations at various temperature using $CHCl_3$ as eluent at 25 ℃.*

As anticipated, the L-serine and L-cysteine monomers without *t*-butylbenzene unit substitution (monomers **M4**, **M5** and **M6**) produced insoluble polypeptides irrespective of the polymerization solvents. The polymer precipitation was noticed within first 5 minutes of the polymerization and the reaction mixtures were turbid throughout the course of polymerization (see Figure 2.8 for photographs). These polypeptides were found to be insoluble in $CHCl_3$, THF (or DMF) and hence SEC analysis was not possible. They were subjected to ^{1}H NMR analysis (in $CDCl_3$ + CF_3COOH, otherwise it if not possible) and the spectra are given in Figure 2.9. The degree of polymerization was found to be around 40-50 for all cases irrespective of monomer or polymerization solvent. The degree of polymerization and molecular weight thus obtained are summarized in Table 2.4. These results clearly emphasize the fact that, serine or cysteine NCA monomers with conventional protecting groups (Benzyl, Bn or benzoyl, Bz) are not polymerizable effectively to obtain high molecular weight polymers, also the resultant low molecular weight polymers are insoluble in common organic solvents which makes them impractical for any applications. The above experimental evidence clearly supports the idea of employing the bulky *t*-butylbenzene unit to overcome the solubility issues in L-serine and L-cysteine for building of high molecular weight polypeptides.

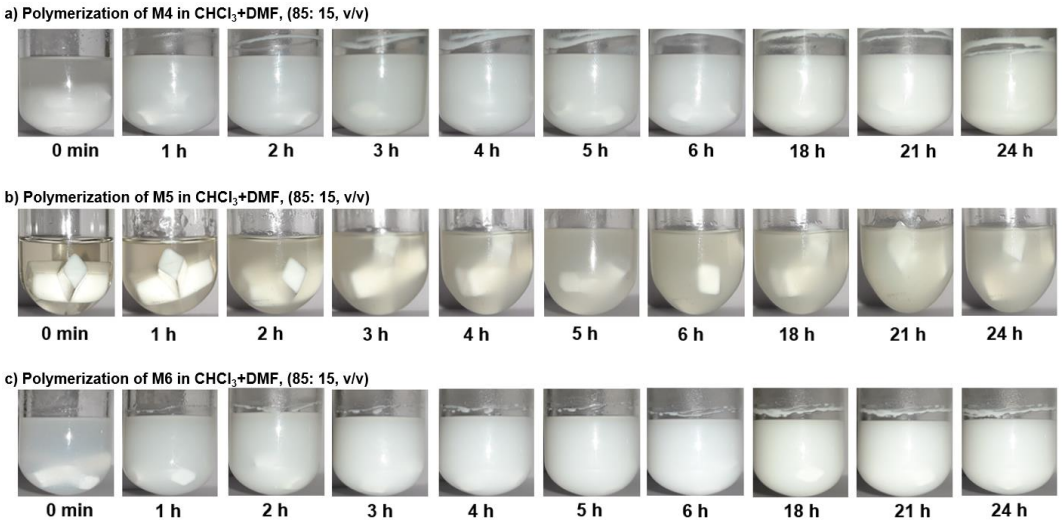

Figure 2.8: *(a) Snapshots of polymerization reaction mixture of serine-ester NCA monomer-**M4** in* $CHCl_3$+DMF *(85: 15, v/v), (b) Snapshots of polymerization reaction mixture of serine-ether NCA monomer-**M5** in* $CHCl_3$+DMF *(85: 15, v/v), (c) Snapshots of polymerization reaction mixture of cysteine NCA monomer-**M6** in* $CHCl_3$+DMF *(85: 15, v/v).*

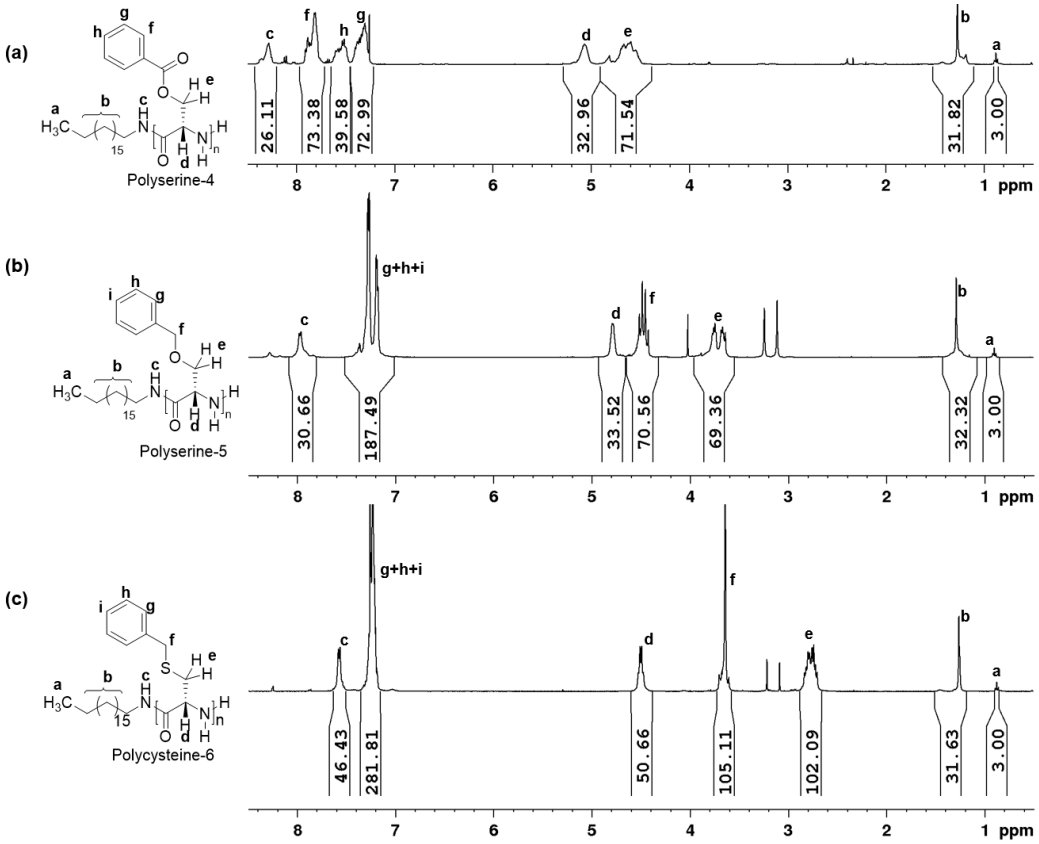

Figure 2.9: *^{1}H NMR spectra of polyserine-4, polyserine-5 and polycysteine-6 in $CDCl_3$+Trifluoroacetic acid (6:1, v/v).*

Table 2.4: *Polymerization of monomers **M4**, **M5**, **M6** in several solvents. Table contain the polymerization conditions, degree of polymerization (n) and M_n determined by ^{1}H-NMR*

Entry	Monomer	Solvent(s)	n (NMR)[b]	M_n NMR (g/mol)[c]	M_n SEC (g/mol)[d]	M_w SEC (g/mol)[d]	Đ[d]	Conversion (%)
1	M4	DMF	42	8000	ND	ND	ND	57
2	M4	THF	33	6300	ND	ND	ND	39
3	M4	$CHCl_3$	49	9400	ND	ND	ND	Can not be determined
4	M4	$CHCl_3$+DMF[a]	48	9200	ND	ND	ND	47
5	M5	$CHCl_3$+DMF[a]	34	6000	ND	ND	ND	60
6	M6	$CHCl_3$+DMF[a]	51	9900	ND	ND	ND	65

[M] was maintained as 0.2 M, N,N-dimesytlene substituted carbene was generated in-situ and n-octadecylamine was used as initiator. The monomer/Initiator ratio was maintained as 100 in the feed. [a] $CHCl_3$+DMF is 85:15 v/v, [b] Degree of polymerization (n) was determined from ^{1}H-NMR. [c] NMR-number average molar mass (M_n = n × repeating unit mass). [d] Polymers are not soluble in THF, DMF or $CHCl_3$, hence their molar mass and dispersity (Đ) are not determinable.

Thermogravimetric analysis (TGA) of the polymers (Figure 2.10a) revealed that these newly synthesized polypeptides were thermally stable up to 250 °C. DSC thermograms of these polymers in Figure 2.10b showed only glass transition temperature with respect to amorphous polymers. The glass transition temperature (T_g) for the polymers is given in Figure 2.10c and it was found that polymers with tert-butyl benzene functionality exhibited higher glass transition temperature compared to that without bulky tert-butyl benzene substitution.

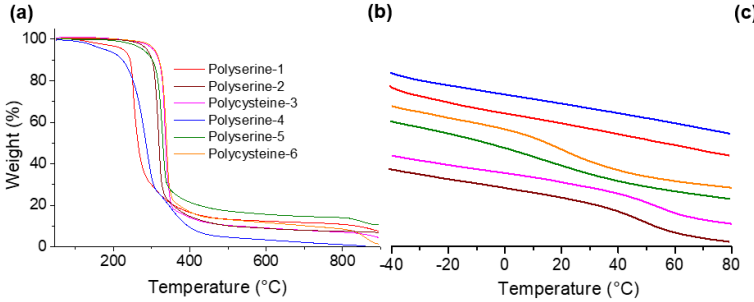

No.	Polymer	T_g °C
1	Polyserine-1	-
2	Polyserine-2	51
3	Polycysteine-3	54
4	Polyserine-4	-
5	Polyserine-5	12
6	Polycysteine-6	21

Figure 2.10: *Thermal analysis of polymers. (a) TGA analysis of polypeptides, (b) DSC thermograms of polypeptides at 10 °C/min in the heating cycle (colour codes are same as those for TGA curves), (c) Table showing glass transition temperatures of polypeptides.*

2.3.2. Real-time FT-IR Kinetic Analysis

To study the kinetics of the newly designed bulky NCA monomers and trace the secondary structural details of resultant soluble polypeptides, the polymerization reactions were subjected to real-time ATR-FTIR and ^{1}H-NMR analysis. Aliquots of the homogeneous mixtures of the polymerization of NCA monomers **M1**, **M2** and **M3** in $CHCl_3$, THF and $CHCl_3$+DMF were monitored at regular intervals by FT-IR. The FT-IR spectra of serine-ether NCA monomer-**M2** polymerizations in $CHCl_3$ are shown in Figure 2.11a, Figures 2.12a and 2.12b contains FT-IR spectra at different time intervals for polymerization in $CHCl_3$+DMF and THF respectively. The carbonyl peaks in the monomer at 1857 cm^{-1} for HC-**C=O** stretching frequency and at 1780 cm^{-1} for HN-**C=O** were monitored to study the progress of the polymerization.[51] The gradual decrease in the intensities of carbonyl peaks with increasing reaction time confirmed the depletion of monomer concentration in the ROP. The peaks corresponding to new polypeptide bonds emerged in the region of 1700 to 1500 cm^{-1} and an isosbestic point was clearly visible with respect to the conversion of monomer to polypeptide chains. The ratio of the area of the peaks at 1780 cm^{-1} at time (t=0, initial) to a particular time interval "t" estimates the actual amount of NCA remaining in the polymerization medium. The % of NCA remaining was plotted against reaction time "t" in Figure 2.13a. The plots revealed the occurrence of ROP in controlled manner and the entire monomer **M2** was consumed completely at the end of the polymerization in $CHCl_3$. The polymerization reaction in $CHCl_3$ and $CHCl_3$+DMF mixture was almost identical and nearly complete. However, it was very slow in THF and only 70 % of monomer was found to be consumed at the end of the polymerization even after 72 h.

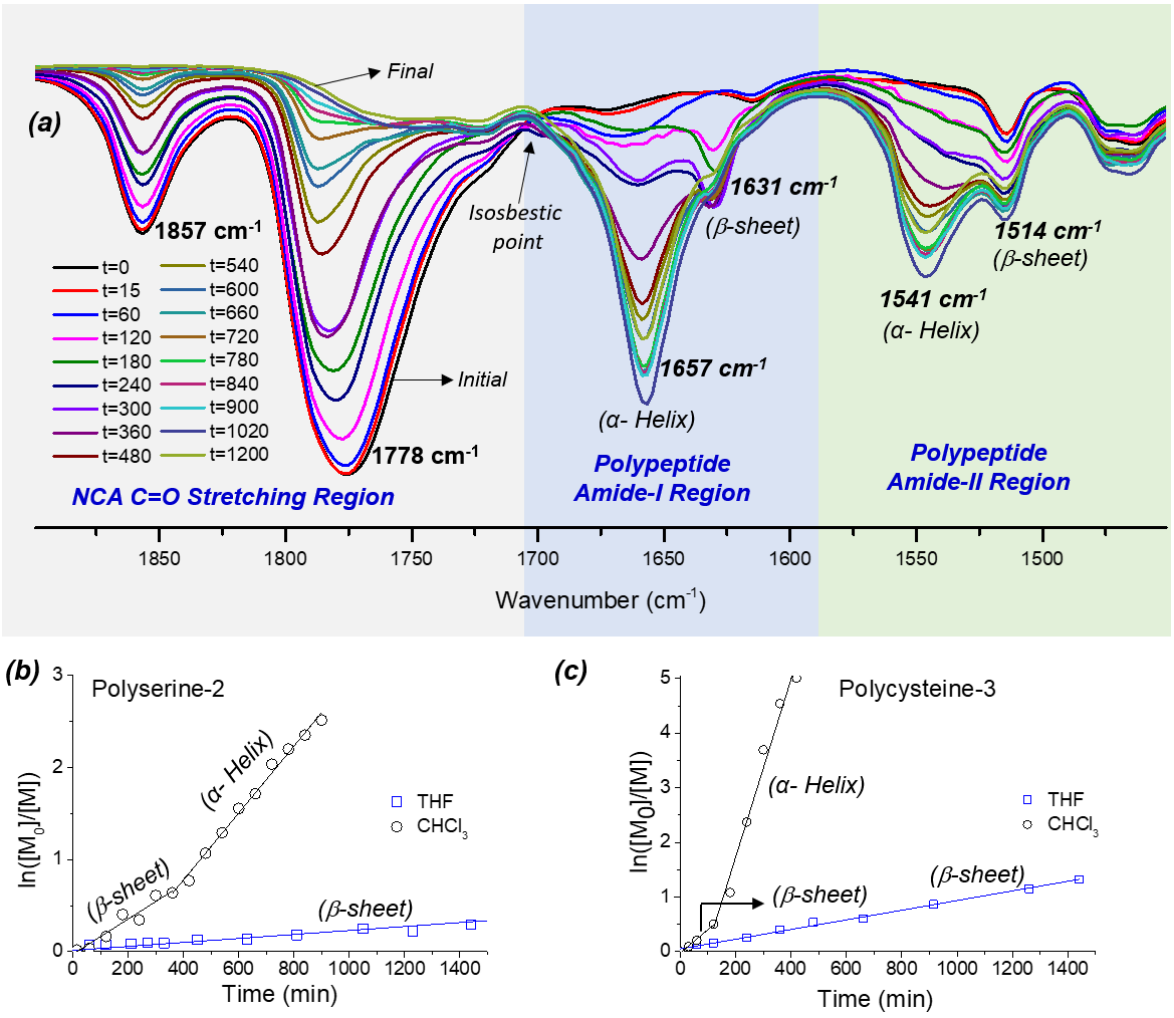

Figure 2.11. (a) *FT-IR spectra of the aliquots of polymerization of serine-ether NCA monomer-**M2** in $CHCl_3$. (b) Plots of ln($[M_0]/[M]$ vs time for polymerization of serine ether NCA monomer-**M2** in $CHCl_3$ and THF. (c) Plots of ln($[M_0]/[M]$ vs time for polymerization of cysteine NCA monomer-**M3** in $CHCl_3$ and THF. The polymerization reactions were carried out using IMes.HCO_3 catalyst and octadecyl amine initiator for M/I = 50.*

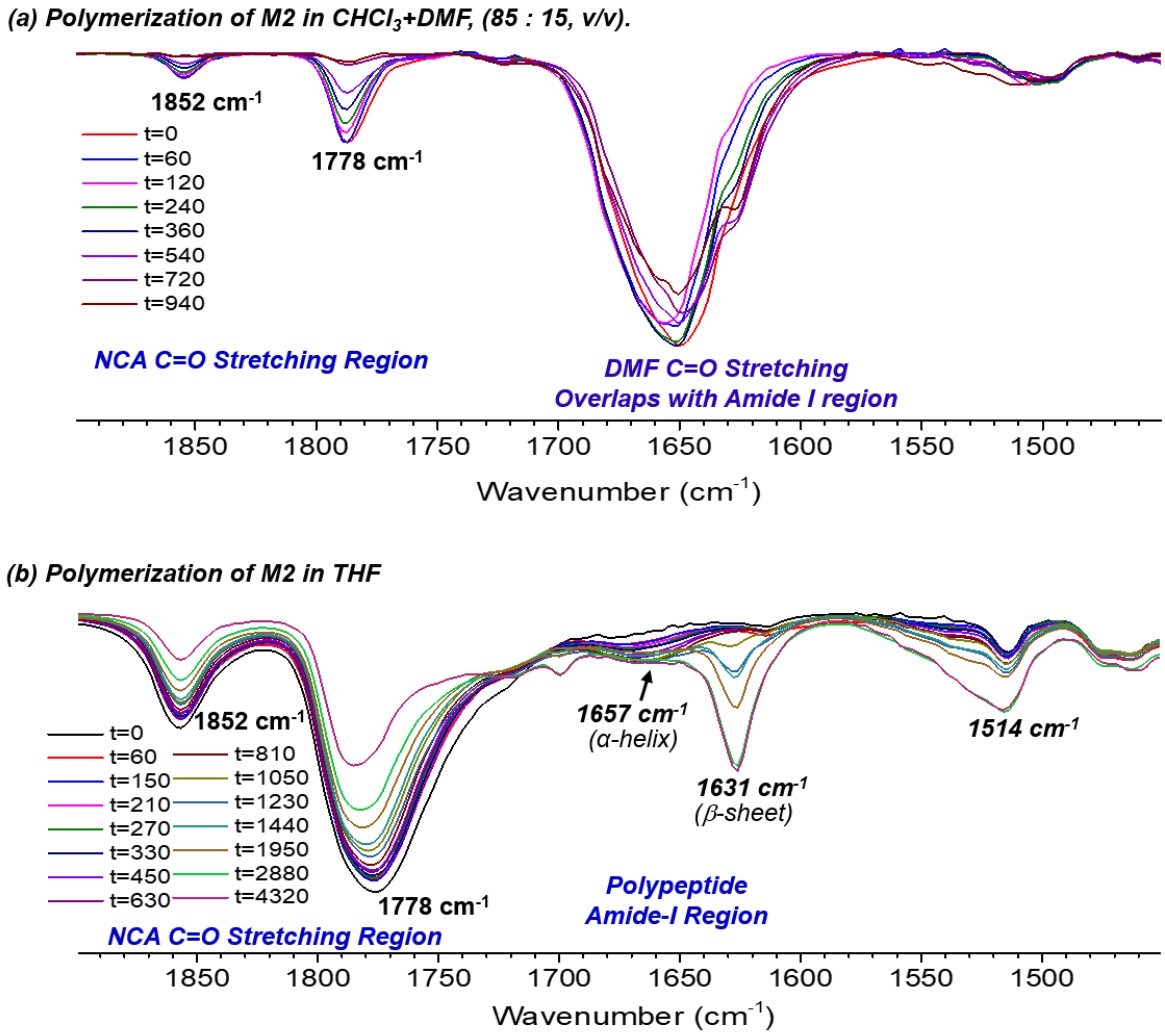

Figure 2.12: *FT-IR Spectra of the aliquots of polymerization kinetics of serine-ether NCA monomer-**M2** in (a)* $CHCl_3$+DMF *(85: 15, v/v) and* (b) *THF.*

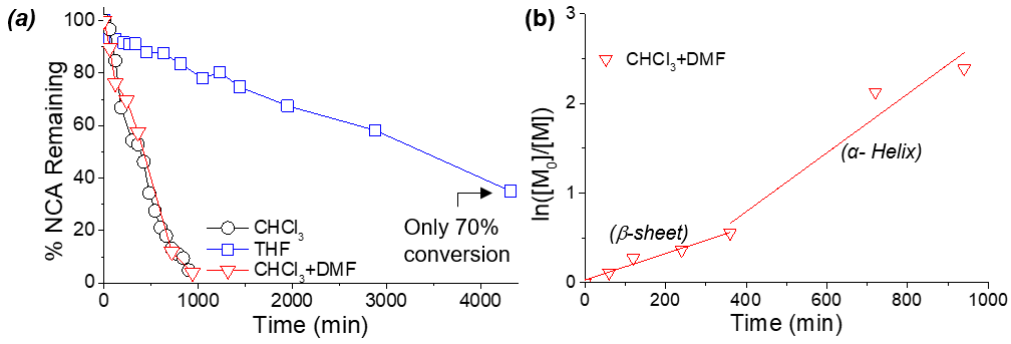

Figure 2.13: *(a) Plots of % NCA remaining versus time for polymerization of serine-ether NCA monomer-**M2** in* $CHCl_3$*, THF and* $CHCl_3$*+DMF mixture, (b) Plot of* $ln([M_0]/[M]$ *vs time for polymerization of serine-ether NCA monomer-**M2** in* $CHCl_3$*+DMF mixture.*

The secondary structures of polypeptide chains are known to be main driving force to build high molecular weight polymers in α-helical polypeptides such as poly(L-lysine) and poly(L-glutamate)s, etc.[133] It was also observed that dielectric constant (ε) of the solvents played a major role in the stabilization of α-helical polypeptide conformation in the polymerization medium.[133, 135-138] Chlorinated solvents having low dielectric constant such as dichloromethane or $CHCl_3$ (ε = 4.8) were found to be a better choice for stabilizing the α-helical structures compared to that of high dielectric solvent like THF (ε = 7.5) and DMF (ε = 36.7).[133, 135-138] The *t*-butylbenzene substitution in the L-serine and L-cysteine in the present investigation enabled the homogeneous polymerization in $CHCl_3$, THF and $CHCl_3$+DMF solvent mixture; thus, provide opportunity to study the factors that govern the secondary structures of the growing polypeptide chains. The peaks in the FT-IR spectra corresponding to amide-I and amide-II region in Figure 2.11a were analyzed in detail. In the amide-I region (1580-1700 cm^{-1}), two new peaks appeared for C=O stretching frequencies at 1657 cm^{-1} and 1630 cm^{-1} with respect to α-helix and β-sheet secondary structures, respectively.[172] The peak intensities at 1630 cm^{-1} initially increased gradually with the progress of polymerization indicating the formation of β-sheet oligomers. Subsequently, the intensity of the β-sheet peak suppressed or became invariant, and a new peak at 1657 cm^{-1} belonging to α-helix conformation emerged. The intensity of the α-helix peak increased with the propagation of the polypeptide chains. In the amide-II region (1450-1600 cm^{-1} in Figure 2.11a), the C-N stretching frequencies with respect to α-helix (at 1541 cm^{-1}) and β-sheets (at 1514 cm^{-1}) structures also exhibited similar trend. Similarly, the FT-IR spectra of the polymerization of monomer-**M2** in $CHCl_3$+DMF and THF (Figure 2.12a and 2.12b respectively) was also analyzed. The polymerization in THF was found to proceed predominantly via β-sheet conformation (peak at 1631 cm^{-1}) with negligible amount of α-helix (peak at 1657 cm^{-1}). This observation suggests that the propagating polypeptide chains adopted different conformations depending on their polymerization solvent. The low dielectric solvent $CHCl_3$ facilitated the in-situ transformation of β-sheets oligomers into long chain α-helical conformation in the propagating chains. This process seems to be less influenced by the $CHCl_3$+DMF (85:15, v/v) solvent mixture. Therefore, low dielectric constant solvents (like $CHCl_3$) enhanced the kinetics of the ROP by promoting α-helical conformation in the propagating polymer chains and ensured the complete monomer consumption to make desired high molecular weight polypeptides.[133] On the other hand, high dielectric solvent like THF allowed the propagating chains to continuously adopt β-

sheet conformation that account for the slow kinetics. In $CHCl_3$+DMF solvent mixture (85:15, v/v), the amount of the low dielectric constant is predominant and thus follows the kinetics and secondary structures similar to that of the $CHCl_3$.

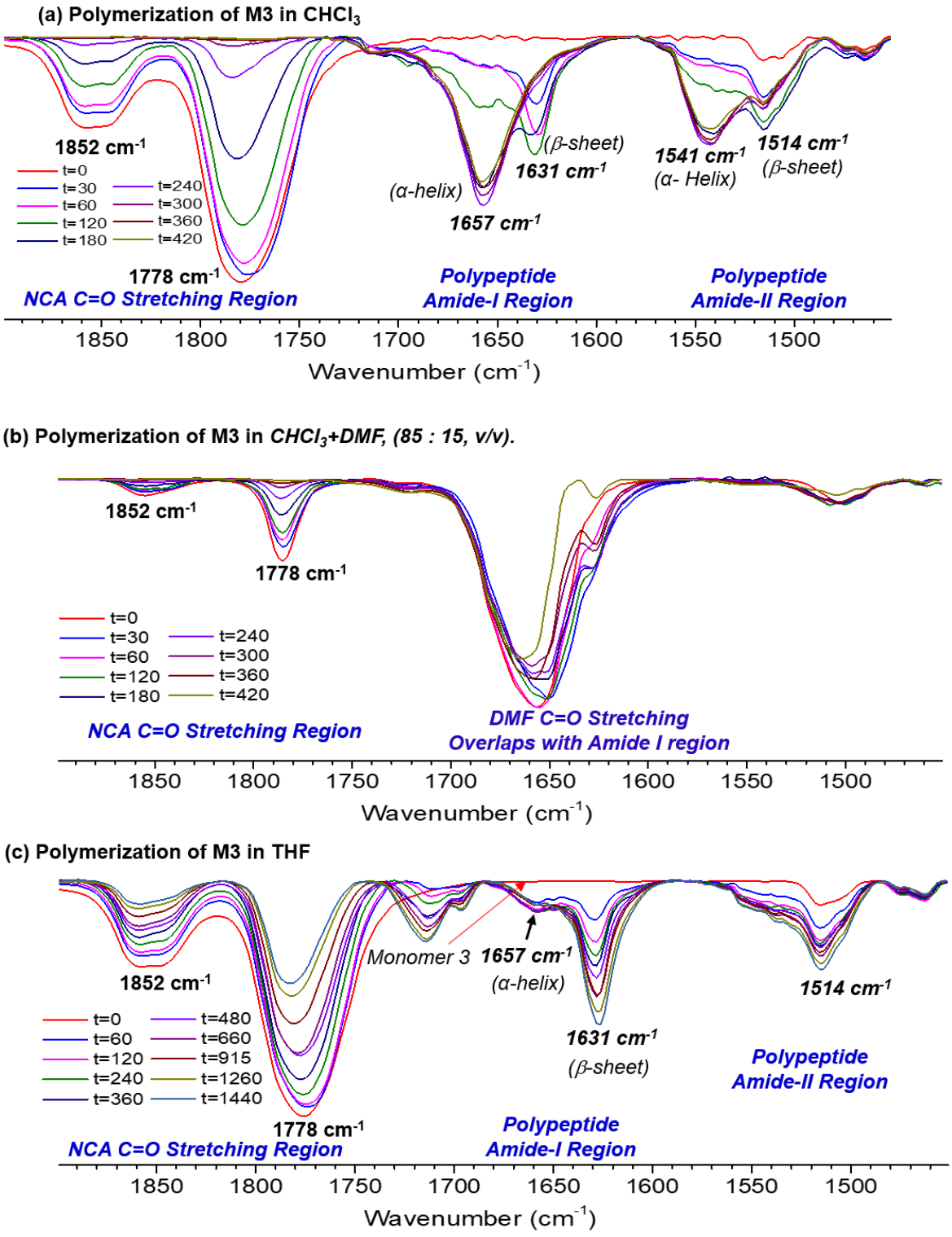

Figure 2.14: *FT-IR Spectra of the aliquots of polymerization kinetics of cysteine NCA monomer-**M3** in (a) $CHCl_3$, (b) $CHCl_3$+DMF (85:15) and (c) THF.*

Similarly, the ROP kinetics of serine ester NCA monomer-**M1** and cysteine NCA monomer-**M3** were also studied in all three solvents by FT-IR and the data is given in Figures 2.14 to 2.17. Figures 2.14a, 2.14b and 2.14c are corresponding to the FT-IR analysis of polycysteine-3 in $CHCl_3$, $CHCl_3$+DMF and THF solvent, respectively. Figures 2.15 represents kinetic plot for polycysteine-3. The polymerization of cysteine NCA monomer-**M3** followed similar trend as shown in Figure 2.13a; however, the process was found to be more rapid compared to serine monomer **M2**. The polymerization was completed in 4 h in $CHCl_3$ for cysteine NCA monomer-**M3** (Figure 2.15a) compared to that of 12 h required by the serine-ether NCA monomer-**2** (Figure 2.13a). The analysis of amide I and amide II regions for polymerization of cysteine monomer **M3** revealed similar trend to monomer **M2** where, secondary structure transition from β-sheet to α-helix was observed in $CHCl_3$ on the other hand only β-sheet structures were observed for polymerization in THF.

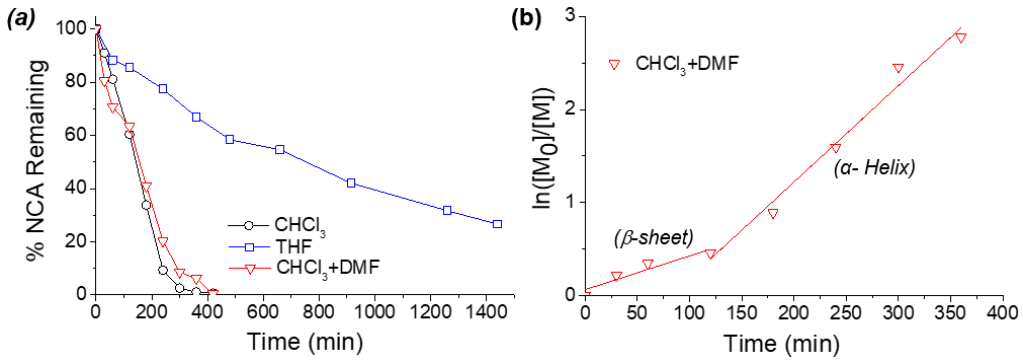

Figure 2.15: *(a) Plots of % NCA remaining versus time for polymerization of cysteine NCA monomer-**M3** in $CHCl_3$, THF and $CHCl_3$+DMF mixture. (b) Plot of ln($[M_0]/[M]$) vs time for polymerization of cysteine NCA monomer-**M3** in $CHCl_3$+DMF mixture.*

Figures 2.16a and 2.16b are corresponding to FT-IR analysis of polyserine-1 in $CHCl_3$+DMF and THF solvent, respectively (FT-IR analysis for polyserine-1 is not possible in $CHCl_3$ due to insolubility of the monomer **M1** in $CHCl_3$). Figure 2.17 represents kinetics plots for polyserine-1 and reveals the slow kinetics of monomer **M1**. The polymerization of monomer **M1** is slowest among all tested monomers and it took 24 h for completion of polymerization in $CHCl_3$+DMF solvent while polymerization in THF was only 50% complete. The analysis of amide I and amide II regions for polymerization of serine ester monomer **M1** revealed similar trend to monomer **M2** (or monomer **M3)** where, only β-sheet structures were observed for polymerization in THF. The slow kinetics for polymerization in THF resulted in poor conversion. In case of polymerization in $CHCl_3$+DMF, amide I

region could not be analyzed as DMF peak overlaps with amide I peak hence restricts the secondary structure analysis.

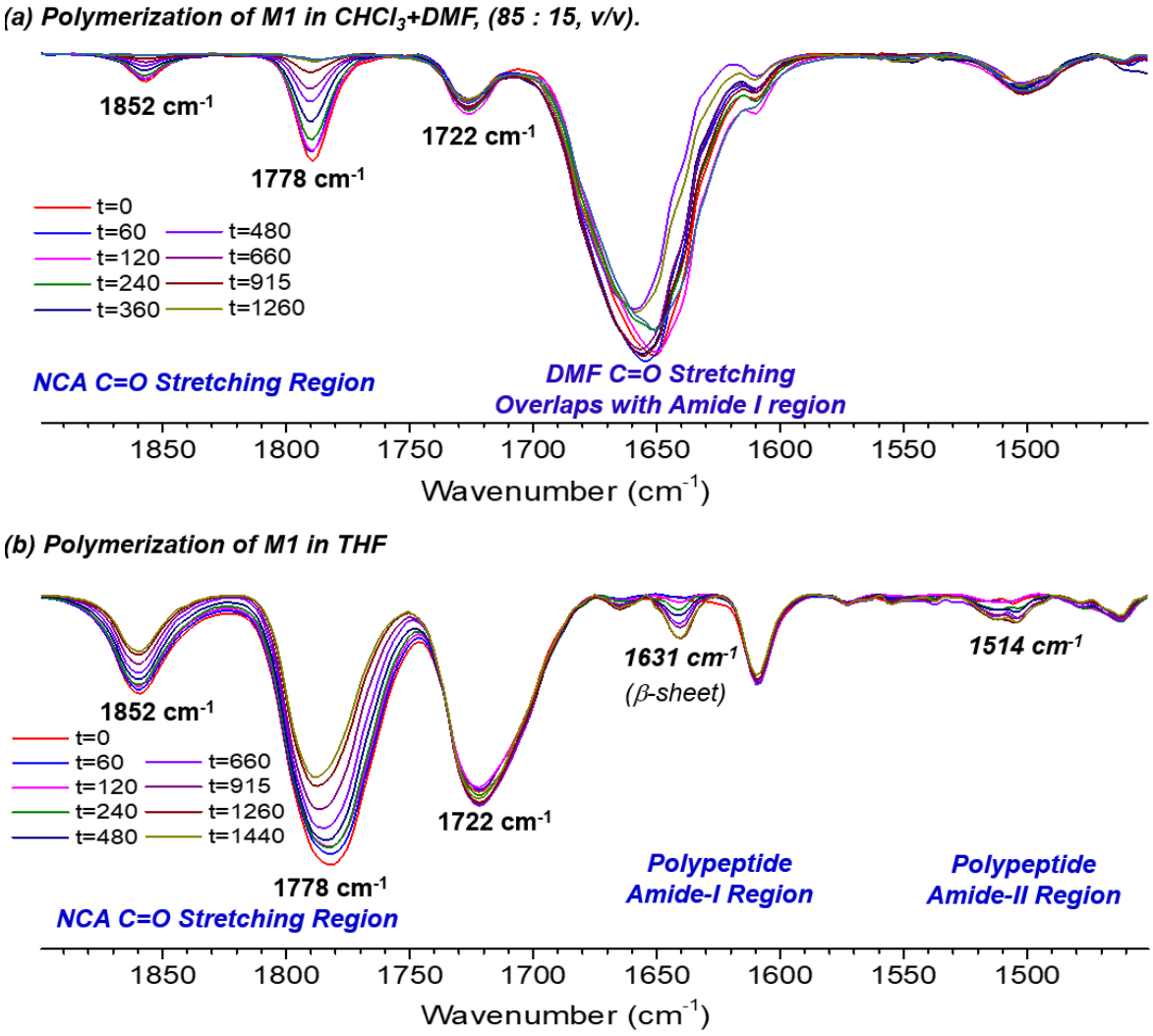

Figure 2.16: (a) *FT-IR Spectra of the aliquots of polymerization kinetics of serine-ester NCA monomer-**M1** in* $CHCl_3$+DMF *(85: 15, v/v),* (b) *FT-IR Spectra of the aliquots of polymerization kinetics of serine-ester NCA monomer-**M1** in THF.*

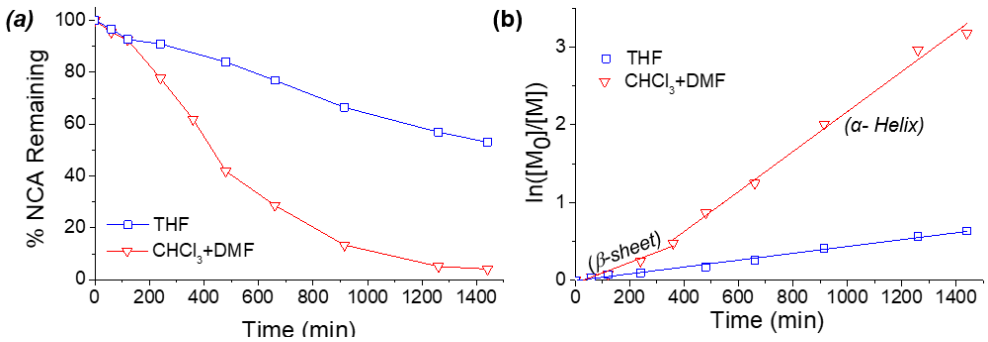

Figure 2.17: *(a) Plots of % NCA remaining versus time for polymerization of serine-ester NCA monomer-**M1** in THF and* $CHCl_3$*+DMF mixture, (b) Plot of* $ln([M_0]/[M]$ *vs time for polymerization of serine-ester NCA monomer-**M1** in THF and* $CHCl_3$*+DMF mixture.*

To determine the rate constant, plots of $\ln([M]_0/[M])$ versus time were generated from unreacted NCA at different time points and plotted in Figure 2.11b and Figure 2.11c for monomers **M2** and **M3**, respectively (other data in Figure 2.13b and Figure 2.15b for monomers **M2** and **M3** respectively). In THF, the $\ln([M]_0/[M])$ was found to linearly increase with time confirming the typical first order kinetics of the ROP.[51] On the other hand in $CHCl_3$ (See Figure 2.11b and 2.11c) (and also in $CHCl_3$+DMF, see Figure 2.13b and 2.15b), a typical two-stage kinetic was observed. The two-stage kinetics is a typical characteristic of polypeptides having tendency for secondary structure transition during the ROP process. Cheng and co-workers, and Hadjichristidis and co-workers have independently reported a two stage kinetics for poly-L-glutamates for the transformation of initially formed β-sheet oligomers to α-helical secondary structure transitions in the chain propogation.[55, 56, 133] As supported by the FT-IR kinetic analysis, see Figure 2.11a (also Figure 2.14a), the *t*-butylbenzene substituted poly-L-serine and poly-L-cysteine systems in the present investigation were also found to be following the β-sheet oligomers to α-helical secondary structure transitions. Therefore, the plot of $\ln([M]_0/[M])$ versus time in Figure 2.11b for polymerization of serine-monomer **M2** in $CHCl_3$ was fitted as two linear plots with respect to the initial β-sheet oligomers having rate constant $k_{obs} = 1.9 \times 10^{-3}$ min^{-1} (up to 400 min) and the second fit having rate constant $k_{obs} = 3.6 \times 10^{-3}$ min^{-1} for the growth of α-helical chains. A similar trend was also observed for the polymerization of cysteine monomer **M3** in Figure 2.11c with two step process. It is interesting to note that the polymerization of cysteine monomer **M3** was found to be much faster compared to serine monomer **M2**. These rate constants were determined from the slopes of plots and tabulated in Table 2.5. The comparison of the rate constants for cysteine and serine monomers revealed that the cysteine was 5 to 6 times faster in undergoing ROP process. The rate constants in THF were estimated to be 10 times lower than that of $CHCl_3$ (or $CHCl_3$+DMF mixture) which was further supported by the incomplete consumption of monomers in THF. It is important to note that the polymerization solution was clear and homogeneous throughout the reaction; thus, there is no question of precipitation or heterogeneity to account for the larger variation in the rate constants in $CHCl_3$ and THF.

Table 2.5 *Rate constants (k_{obs}) for polymerization of monomers **M1**, **M2** and **M3** in different solvents*

Polymerization Solvent	Polyserine-2 K_{obs} (min^{-1})	Polycysteine-3 K_{obs} (min^{-1})	Polyserine-1 K_{obs} (min^{-1})
$CHCl_3$ (FT-IR)	1.9×10^{-3} (6 h, 47 %)[a] 3.6×10^{-3} (15h, 95 %)[b]	4.2×10^{-3} (2 h, 40 %)[a] 16.3×10^{-3} (5h, 98 %)[b]	-
$CHCl_3$ (NMR)	2.4×10^{-3} (4 h, 46 %)[a] 6.8×10^{-3} (10h, 92 %)[b]	8.8×10^{-3} (1.5 h, 54 %)[a] 16.9×10^{-3} (5h, 97 %)[b]	-
DMF+ $CHCl_3$	1.5×10^{-3} (6 h, 43 %)[a] 3.3×10^{-3} (15h, 96 %)[b]	3.6×10^{-3} (2 h, 37 %)[a] 10.4×10^{-3} (6h, 94 %)[b]	1.3×10^{-3} (6 h, 38 %)[a] 2.6×10^{-3} (24h, 94 %)[b]
THF	0.2×10^{-3} (72 h, 65 %)[a]	0.9×10^{-3} (24 h, 73 %)[a]	0.4×10^{-3} (24 h, 47 %)[a]

[a]The values in the brackets are corresponding to the time at the end of first linear fit corresponding to β-sheet structures and % conversion of the monomer at that time.
[b]The values in the brackets are corresponding to the time at the end of second linear fit corresponding to α-helical structures and % conversion of the monomer at that time.

The role of catalyst on the rate of polymerization was investigated on polymerization of cysteine monomer-**M3** in $CHCl_3$ due to its fast kinetics. We found that the polymerization without catalyst was slow and required nearly 8.5 h for complete consumption of monomer. On the other hand, the complete consumption of monomer was achieved in 4 h in presence of catalyst (Figure 2.18 compares the data for polymerization of **M3** in $CHCl_3$ in presence and absence of catalyst). This result suggests that the polymerization with catalyst is much faster than that without the catalyst.

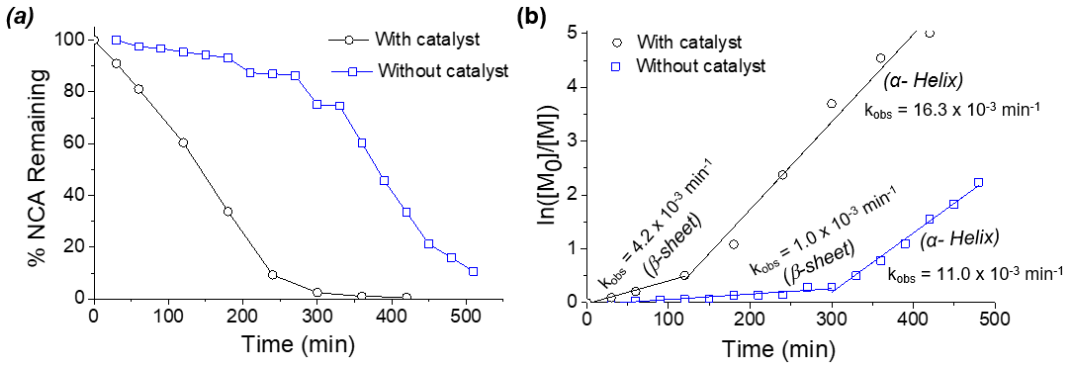

Figure 2.18: *(a) Plots of % NCA remaining versus time for polymerization of cysteine NCA monomer-**M3** in $CHCl_3$ with and without NHC catalyst, (b) Plot of ln($[M_0]/[M]$ vs time for polymerization of cysteine NCA monomer-**M3** in in $CHCl_3$ with and without NHC catalyst.*

2.3.3. Real-time ^{1}H-NMR Kinetic Analysis

^{1}H-NMR spectroscopy was employed to study the polymerization kinetics due to the excellent solubility of both the monomers and polypeptides in $CDCl_3$. The polymerization was carried out in $CDCl_3$ using NHC catalyst and the aliquots were retrieved at various time interval and quenched using trifluoracetic acid, and subjected to ^{1}H-NMR analysis.

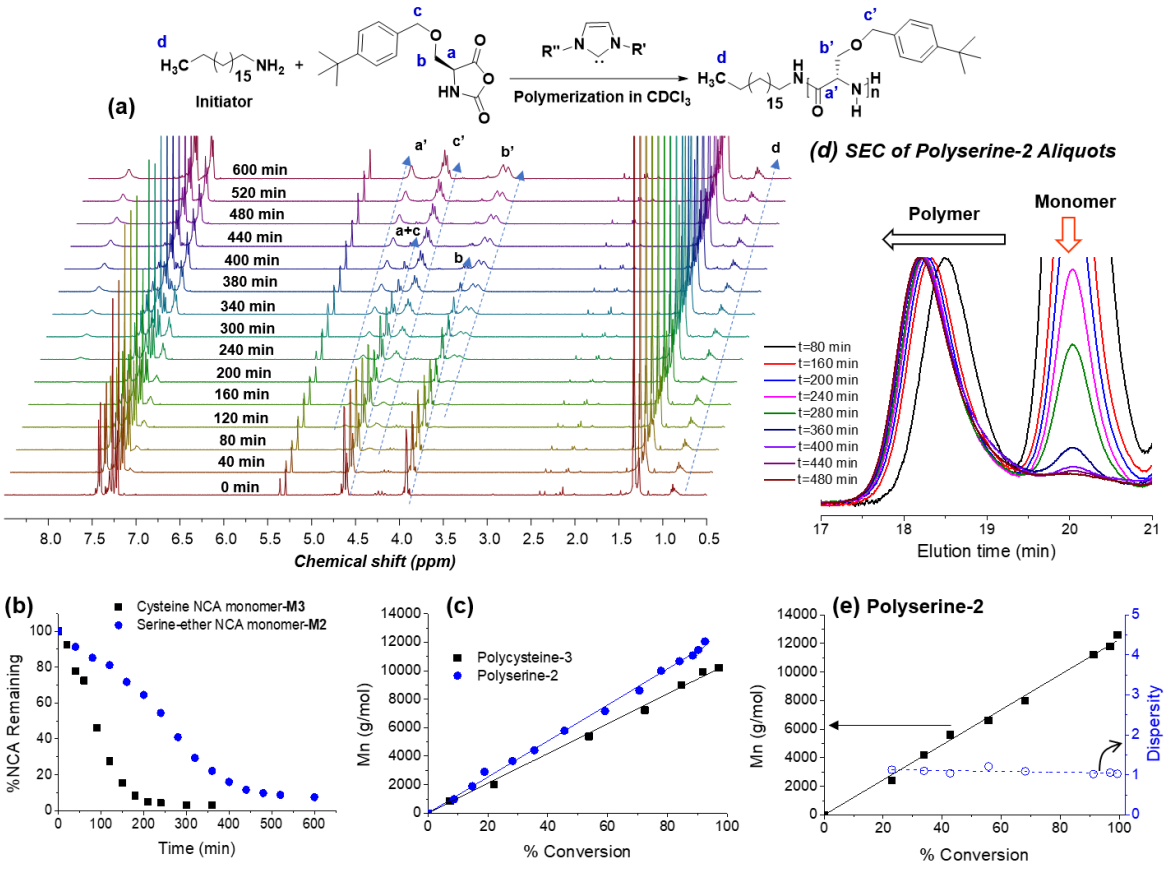

Figure 2.19. *^{1}H-NMR spectra of aliquots for the polymerization of serine-ether NCA monomer-**M2** in $CDCl_3$. Peaks in the NMR spectra were assigned for different protons in the chemical structure of NCA monomer and polyserine-2 by alphabets. (b) Plots of % NCA remaining versus reaction time for serine and cysteine NCA monomers **M2** and **M3** for the polymerization in $CDCl_3$. (c) Plot of M_n versus monomer % conversion for the serine and cysteine-NCA monomers. (d) SEC traces of aliquots of polymerization reaction of monomer **M2** in $CDCl_3$ at different time intervals. (e) Plot of M_n and dispersity ($Đ$) for polymerization reaction aliquots at various % conversion of the monomer.*

^{1}H-NMR spectra for the polymerization of serine-ether NCA monomer-**M2** are shown in Figure 2.19a. The protons in NCA monomer such as chiral-C**H**CH$_2$O (proton a) along with ArC**H**$_2$O (proton-c) at 4.62 ppm and chiral-CHC**H**$_2$O (proton-b) at 3.94 ppm, were significantly influenced by ROP and they were shifted to 4.82 ppm (chiral-C**H**CH$_2$O,

proton a'), 4.43 ppm (ArC**H**$_2$O, proton-c'), and 3.75 ppm (chiral-CHC**H**$_2$O, proton-b'), respectively. It is very clear from the NMR stack plots in Figure 2.19a that the intensities of the NCA monomer peaks gradually decreased with increase in reaction time, and disappeared completely at the end. The intensities of initiator -C**H**$_3$ (peak-d) was compared with that of NCA monomer (peak-b) to quantify the amount of the unreacted NCA monomer at a given time point. The new peaks for the polypeptide chains gradually appeared with progress of polymerization. The comparison of peak-b' in the polymer with the initiator (peak-e) estimated the degree of polymerization (n) and number average molecular weight (M_n). Similarly, cysteine NCA monomer-**M3** was polymerized in $CDCl_3$ and their ^{1}H-NMR signals in Figure 2.20 were compared for real-time kinetics. Four protons in the NCA monomer **M3** corresponding to the N-H (protons-a, 6.99 ppm), chiral-C**H**CH$_2$S (proton-b, 4.47 ppm), chiral-CHC**H**$_2$S (proton-c, 2.95 ppm), and ArC**H**$_2$S (proton-d, 3.77 ppm) were found to be completely different from its corresponding polypeptide. Upon polymerization, these peaks were shifted to N-H (protons a', 7.72 ppm), chiral-C**H**CH$_2$S (proton-b', 4.63 ppm), chiral-CHC**H**$_2$S (proton-c', 2.82 ppm), and ArC**H**$_2$S (proton-d', 3.62 ppm), respectively. The plots of % NCA remaining versus the time in Figure 2.19b clearly elucidates that the polymerization reaction was much faster in cysteine NCA monomer-**M3** (≤ 4h) compared to serine-ether NCA monomer-**M2** (≤ 10 h). FT-IR data in Figure 2.15a and NMR data in Figure 2.19b are matching very well which confirmed the reproducibility of the kinetic data. The linear plot of ln([M]$_0$/[M]) versus time in Figures 2.20b and 2.20c are also indicative of two stage kinetics and gave the rate constant for serine-ether NCA monomer-**M2** as k_{obs}= 2.4×10^{-3} min^{-1} and 6.8×10^{-3} min^{-1}, while for cysteine NCA monomer-**M3** as k_{obs} = 8.8×10^{-3} min^{-1} and 16.9×10^{-3} min^{-1} which are almost identical to that of the values obtained by FT-IR in Figure 2.11b and Figure 2.11c (also see Table 2.5). ^{1}H-NMR spectra further enabled the quantitative determination of the degree of polymerization (n) for a particular monomer % conversion. This would further lead to plot the actual M_n versus % conversion to infer the controlled ROP process. The plots in Figure 2.19c revealed that the polymerization reactions followed the linear trend in M_n versus % conversion confirming their controlled ROP kinetics for producing desired molecular weight.

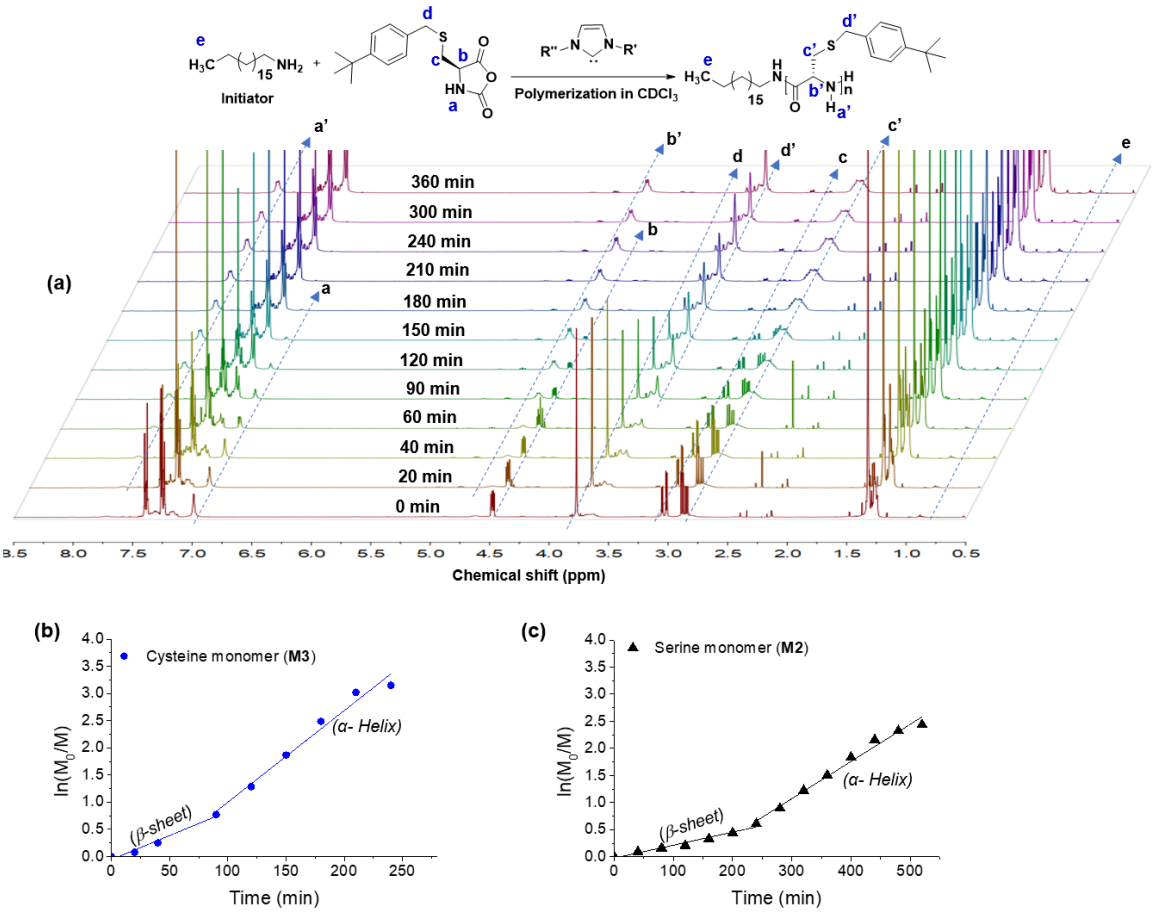

Figure 2.20: *(a) ^{1}H NMR spectra of aliquots for the polymerization of cysteine NCA monomer-**M3** in $CDCl_3$. Peaks in the NMR spectra were assigned for different protons in the chemical structure of NCA monomer and polycysteine-3 by alphabets, (b) Plots of $ln([M_0]/[M]$ vs time for polymerization of cysteine NCA monomer-**M3** in $CDCl_3$, (c) Plots of $ln([M_0]/[M]$ vs time for polymerization of serine-ether NCA monomer-**M2** in $CDCl_3$.*

The polymerization aliquots were subjected to SEC analysis with chloroform as eluent as shown in Figure 2.19d. SEC plots in Figure 2.19d exhibited mono-modal distribution for the polymers and the retention time decreased with increase in the formation of higher molecular weight chains. Interestingly, the intensities of peak corresponding to the monomer was also gradually decreased with the progress of polymerization, and completely vanished at the end of reaction. The polymers were obtained in very narrow dispersity (Đ) in the range of 1.02 to 1.13. The plot of absolute molecular weight-M_n (from SEC in $CHCl_3$ as eluent) versus % conversion showed a linear trend (see Figure 2.19e). SEC kinetics was also carried out in THF as eluent and the data is given in Figure 2.21. The plot of Mn vs % conversion from SEC in THF (see Figure 2.21b) exhibited good linear fit only up to only 85

% conversion which and this limitation is attributed to the fact that SEC plots were merged at the higher % conversion samples.

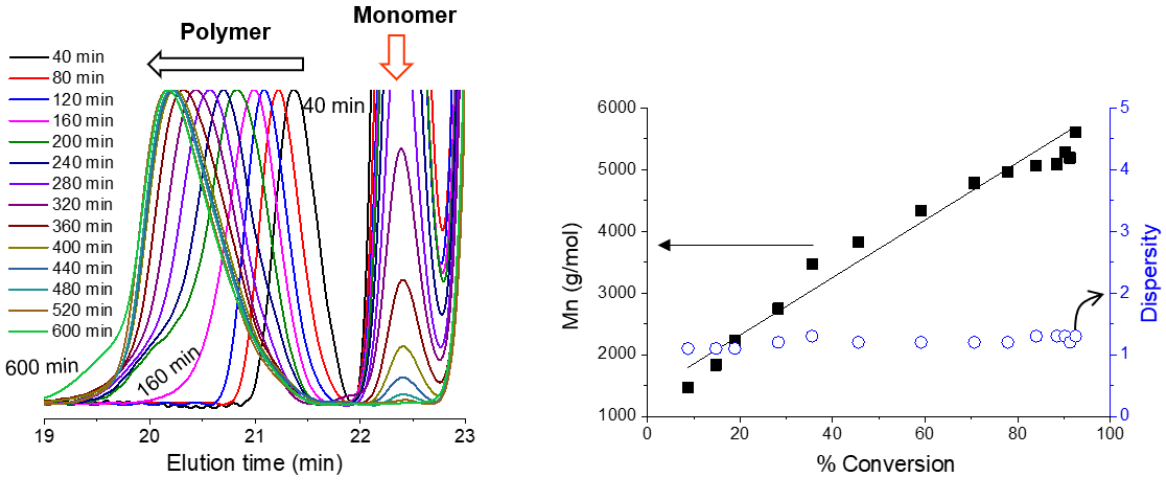

Figure 2.21: *(a) SEC traces (THF as eluent) of aliquots of polymerization reaction of monomer **M2** in $CDCl_3$ at different time intervals. (b) Plot of M_n (from SEC in THF) and dispersity (Đ) for polymerization reaction aliquots at various % conversion of the monomer.*

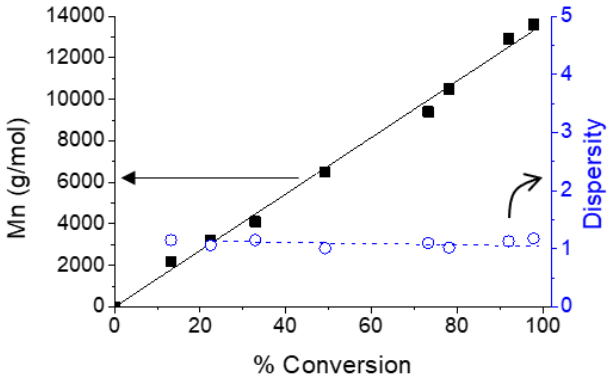

Figure 2.22: *Plot of M_n (from SEC in $CHCl_3$) and dispersity (Đ) for polymerization reaction aliquots at various % conversion (from FT-IR) of the monomer **M2**.*

This study confirmed that the *t*-butylbenzene bulky substitution in the NCA monomer facilitated the solubility as well as retain the ROP process controlled. The plot of M_n (from SEC) vs % conversion (from FT-IR) was also found to be linear and shown in Figure 2.22. The controlled ROP was further tested by carrying out polymerization of cysteine NCA monomer-**M3** and serine-ester NCA monomer-**M1** by varying M/I in the feed from 25 to 150 in $CHCl_3$+DMF using NHC catalyst. The data in Figure 2.23 showed very good agreement for experimental values with theoretical molecular weights having narrow

dispersity (Đ) of 1.1 to 1.4. Based on the above FT-IR and NMR real-time polymerization kinetic analysis it may be summarized that the developed synthetic route indeed assisted the propagating chains to grow in controlled manner following the controlled ROP characteristics.

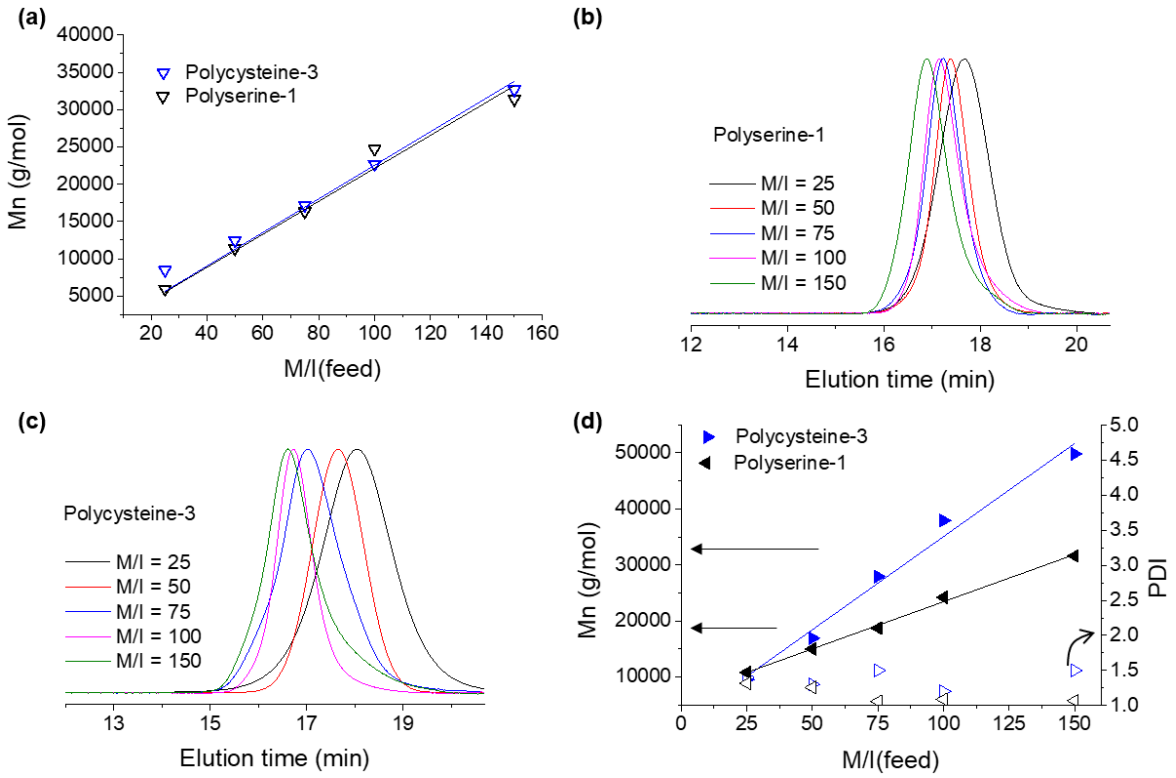

Figure 2.23: *(a) Plot of Mn (from ^{1}H NMR) vs M/I feed for ROP of monomer **M1** and **M3.** **(b)** SEC traces ($CHCl_3$ as an eluent) for polyserine-1 obtained from ROP at various M/I feed. (c) SEC traces ($CHCl_3$ as an eluent) for polycysteine-3 obtained from ROP at various M/I feed. (d) Plot of Mn (from SEC in $CHCl_3$, represented by solid symbol) and PDI (represented by hollow symbol) vs M/I feed for ROP of monomer **M1** and **M3.***

To quantify the amount of β-sheet and α-helix conformations in the propagating polymer chains, the peak areas at 1657 cm^{-1} and 1631 cm^{-1} in FT-IR in Figure 2.11a were estimated by integration. The amount of secondary structures in the propagating polymer chains for the synthesis of polyserine-2 in $CHCl_3$ polymerization medium is plotted and shown in Figure 2.24a. These plots represent the % mole fraction of the of β-sheet and α-helix conformations for a given % conversion of the monomer **M2**. The degree of polymerization determined from ^{1}H-NMR kinetic experiments were also plotted and showed in the x-axis in Figure 2.24a (blue colour). This would directly allow correlation of both the degree of polymerization and % conversion of the monomer to the extent of β-sheet or α-

helix secondary structures in the polypeptides. At the initial stage (up to 30-40 % of monomer consumption and n= 15-20 mers), the polymerization proceeded with the co-existence of both β-sheet and α-helix conformation together in the propagating chains. Subsequent attack of the NCA monomers on the propagating front facilitated the formation of α-helical structure and this in-situ secondary structure transformation account for the fast kinetics of the ROP and consumption of > 99 % NCA monomer.

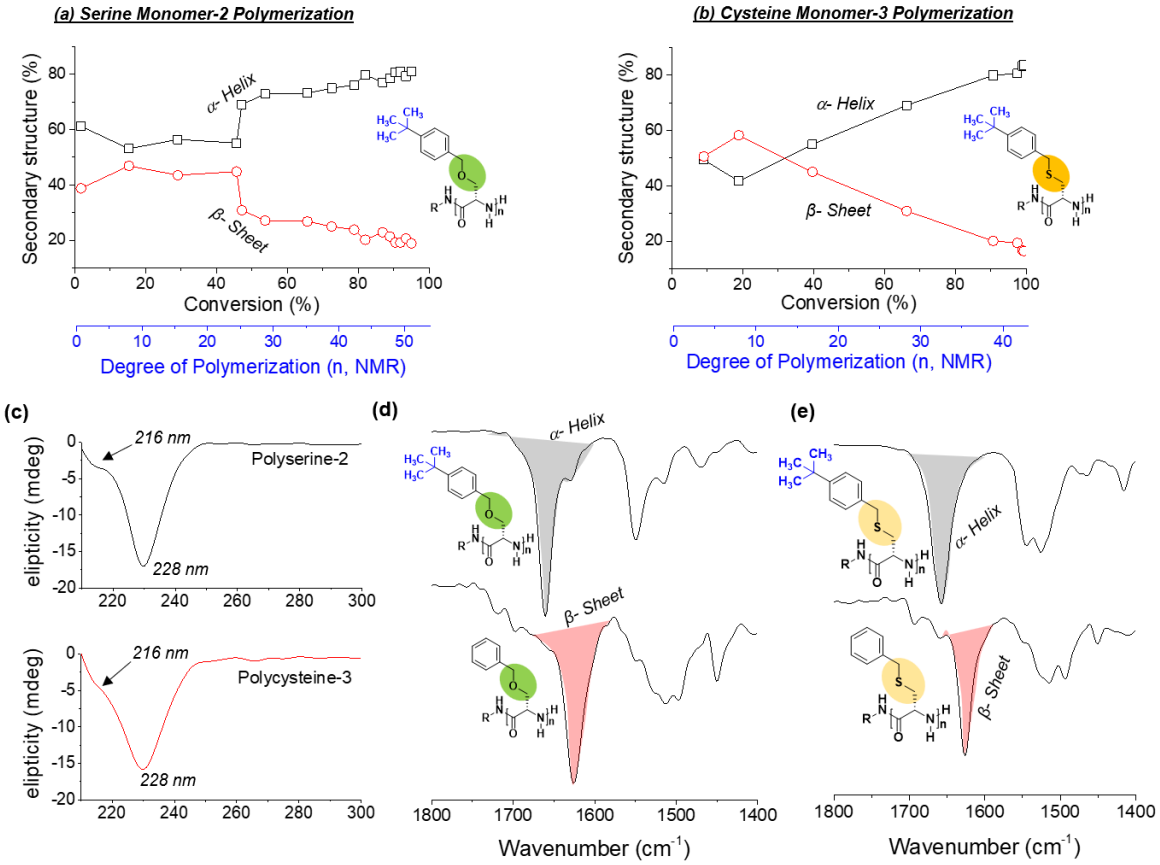

Figure 2.24. *(a) The percentage of β-sheet and α-helix secondary structures estimated from each aliquot in Figure 2.11a by comparing the peak integrals of 1631 and 1657 in amide-I region for the polymerization of monomer-**M2** in $CHCl_3$. Degree of polymerization was determined by ^{1}H-NMR analysis from Figure 2.19a with respect to the % conversion of the monomers. (b) The percentage of β-sheet and α-helix secondary structures estimated from each aliquot in Figure 2.14a by comparing the peak integrals of 1631 and 1657 in amide-I region for the polymerization of monomer-**M3** in $CHCl_3$. Degree of polymerization was determined by ^{1}H-NMR analysis from Figure 2.20a with respect to the % conversion of the monomers. (c) CD spectra of polyserine-2 and polycysteine-3 in THF. (d) FT-IR spectra of polyserine-2 and polyserine-5. (e) FT-IR spectra of polycysteine-3 and polycysteine-6.*

Polycysteine-3 polymerization FT-IR data in Figure 2.14a was also analyzed and the amount of secondary structures were estimated and plotted in Figure 2.24b. Polycysteine-3 has also exhibited similar in-situ conformation transformation as similar to polyserine-2 in Figure 2.24a. This observation confirmed that propagating chains in the newly developed *t*-butylbenzene functionalization strategy are prominently driven by α-helical conformation. Since the kinetics is relatively fast in polycysteine-3, the chains exhibited the conformational transformation at n=15-mers. CD spectroscopic analysis was applied to validate α-helical secondary structure in the *t*-butylbenzene substituted polyserine-2 and polycysteine-3. The isolated polymer samples were re-dissolved in THF and dichloromethane (DCM) and the spectra were recorded and shown in Figure 2.24c (in THF), 2.25a and 2.25b (in DCM). CD spectra of polyserine-2 and polycysteine-3 in THF showed a double minimum at 216 nm and 228 nm corresponding to the α-helical conformation of the polymer chains (due to solvent cut off, CD was recorded till 210 nm). Only a second minima at 230 nm was observed in DCM (due to the solvent UV cut off at 220 nm) which is quite similar to that for α-helical poly-L-glutamate samples as reported by Cheng and cowerkers.[137] CD spectra of polyserine-1 also showed similar feature for α-helical conformation in Figure 2.25c and 2.25d. CD analysis was evident for the existence of α-helical conformation of *t*-butylbenzene substituted polypeptides in both L-serine and L-cysteine systems.

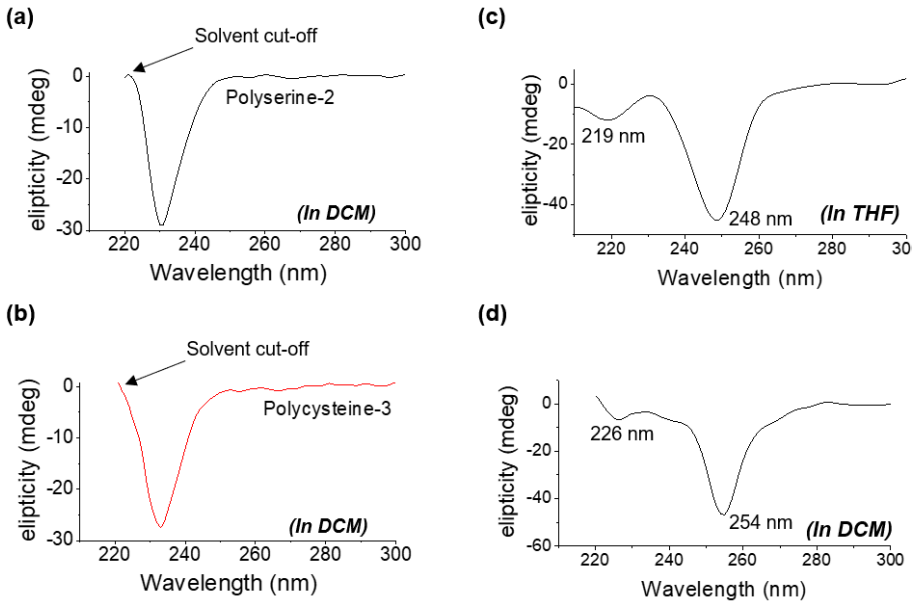

Figure 2.25: *CD spectra of (a) polyserine-2 in DCM (b) polycysteine-3 in DCM (c) polyserine-1 in THF and (d) polyserine-1 in DCM.*

FT-IR spectra of the isolated polyserine-2 (with *t*-butylbenzyl side chains) and polyserine-5 (with simple benzyl substitution) were recorded in Figure 2.24d to elucidate

the role of the *t*-butylbenzene substitution on the secondary structures of the final products. Polyserine-2 with *t*-butylbenzene unit showed the existence of polymers in α-helix conformation whereas the insoluble polypeptides without *t*-butylbenzene unit (polyserine-5) showed signals at 1626 -1636 cm^{-1} with respect to the formation of exclusively β-sheet conformations. A similar trend was clearly evident for the comparison of polycysteine-3 and polyserine-1 with their insoluble polypeptides (polycysteine-6 and polyserine-4) in Figure 2.24e and 2.26 respectively. These data clearly support the trend that *t*-butylbenzene substitution in polyserines and polycysteines drove the polymer structures to adopt α-helix conformation to build high molecular weight polypeptides. On the other hand, polyserines and polycysteines with conventional protecting group adopts β-sheet conformations which drastically reduces their solubility.

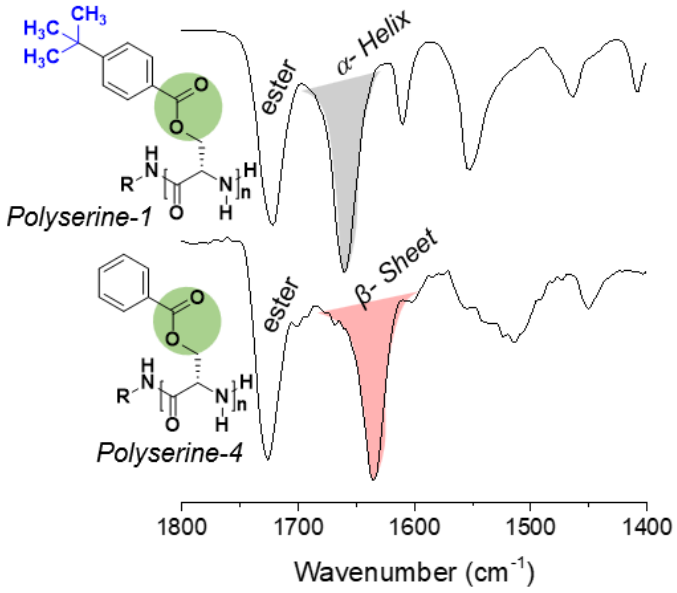

Figure 2.26: *FT-IR spectra of polyserine-1 and polyserine-4.*

2.3.4. Conformational Reversibility & Mechanism

To support the above proposed mechanism, reversible transformation of α-helical to fully β-sheet conformation was established by post polymerization deprotection method as shown in Figure 2.27a. The *t*-butylbenzyl ether unit in the polyserine-2 was readily deprotected using HBr in acetic acid as shown in Figure 2.27a. The deprotected polyserine-2D (D-refers deprotected polymer) was insoluble in all the solvents except trifluoroacetic acid. ^{1}H-NMR analysis of the polyserine-2D showed complete disappearance of protecting unit in Figure 2.28. The degree of polymerization of polyserine-2D was estimated as n = 90

by comparing the intensities of peaks in the polymer-C**H**-CH_2OH (at 5.11 ppm) and the initiator protons at 0.88 ppm. The number of units in the polyserine backbone did not change by the deprotection.

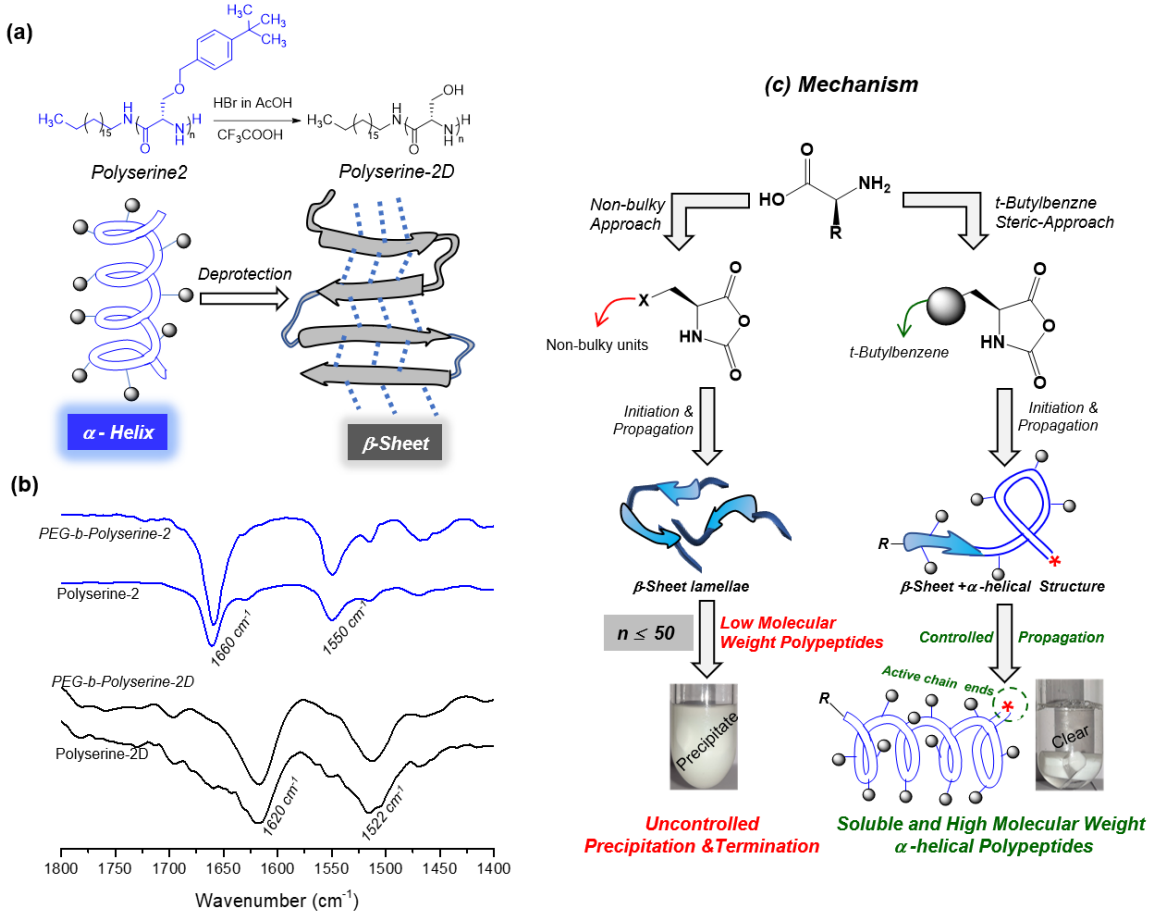

Figure 2.27. *(a) Post polymerization deprotection methodology for reversible conformational switch from α-helix to β-sheet structures and scheme for deprotection of polyserine-2. (b) FT-IR spectra of polyserine-2, polyserine-2D and corresponding PEG diblock-copolymers. (c) Mechanism of t-butylbenzene functionalization strategy for synthesis of* β-sheet polypeptides.

FT-IR analysis of the polyserine-2 and polyserine-2D are compared in Figure 2.27b. The α-helix conformation peaks in the amide I and amide II signals at 1660 cm^{-1} and 1550 cm^{-1} in polyserine-2 completely vanished and new peaks at 1620 cm^{-1} and 1522 cm^{-1} in polyserine-2D appeared with respect to the reversible restoration of β-sheet conformation in poly(L-serine). It is important to note that such high molecular weight poly(L-serine) (without any substitution) is nearly impossible to synthesize. The present approach is unique in accomplishing the above task by cleverly making soluble poly(L-serine) polypeptide in α-helix conformation and reverse the conformational transition to β-sheet by post-

polymerization de-protection. Attempt to deprotect the ester-linkage in *t*-butyl-benzoate in polyserine-1 and thioether linkages in polycysteine-3 showed partial success; thus, the data is not provided here (efforts are continued). Nevertheless, the deprotection strategy is successfully demonstrated in polyserine-2 to validate the synthetic strategy and proof-of-concept is established to support the proposed idea in Figure 2.1.

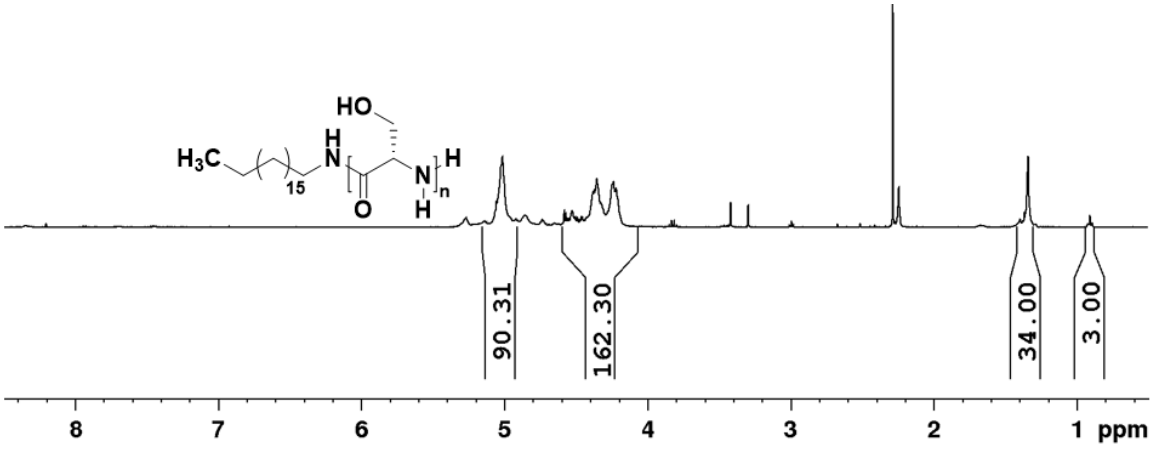

Figure 2.28: *^{1}H NMR of poly(L-serine)-2D in Trifluoroacetic acid-D*

Based on these evidences, an appropriate mechanism for this newly developed *t*-butylbenzene functionalization approach for β-sheet polypeptides is shown in Figure 2.27c. The polymerization of *t*-butylbenzene substituted NCA monomers produced both β-sheet and α-helical structures in the short oligomeric chains by the inherent characteristic of the L-serine and L-cysteine residues. Interestingly, the propagation was predominately controlled by the steric-hindrance induced by the *t*-butylbenzene bulky units which largely suppressed β-sheet secondary interaction and facilitated in-situ formation of α-helix secondary structures in the propagating front. The α-helix structures substantially enhanced the solubility of the propagating polypeptide chains and enabled the formation of higher molecular weight soluble polypeptides. The entire process in the *t*-butylbenzene substituted NCA monomer was driven by homogeneous polymerization and there were no traces of polymer precipitation. The precise role of the *t*-butylbenzene unit on the polymer secondary structure is not clear at present and more efforts are further required. On the other hand, the NCA monomers having conventional substitution such as simple benzyl unit in the L-serine and L-cysteine monomer was not capable of inducing undergoing conformation-transformation; as a result, the growth of the polymer chains continued in the β-sheet

structures which resulted in the uncontrolled precipitation with low degree of control in molecular weight build-up.

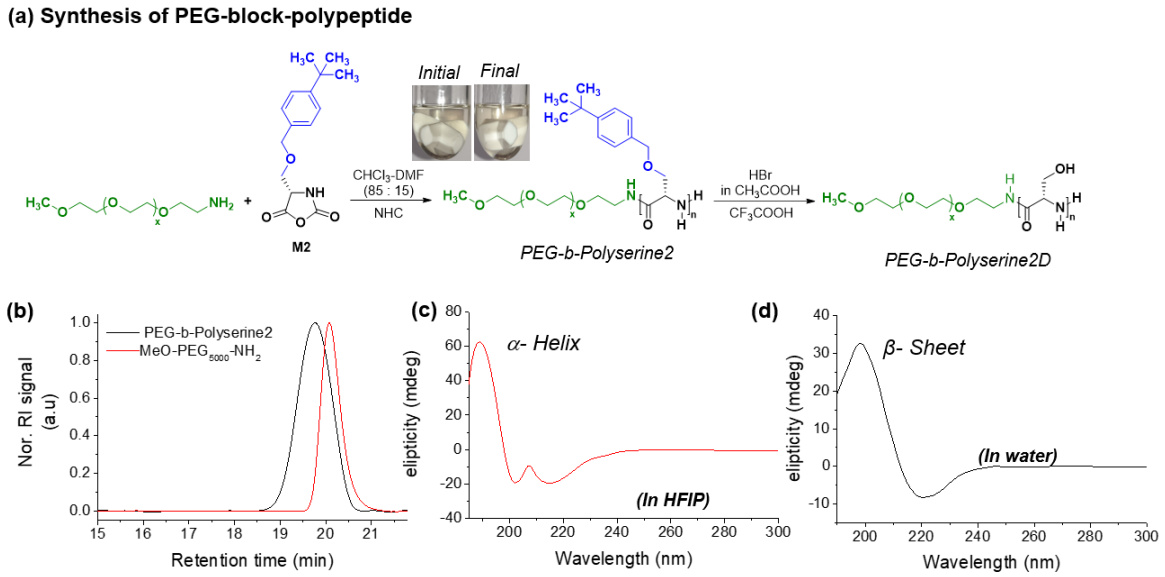

Figure 2.29. *(a) Synthesis of PEG-b-polyserine2 and its deprotection to PEG-b-polyserine2D. (b) SEC traces of MeO-PEG$_{5000}$-NH$_2$ and PEG-b-polyserine2 in THF as eluent. (c) CD spectra of PEG-b-polyserine2 (in HFIP). (d) CD spectra of PEG-b-polyserine2D (in water).*

To study the role of the PEG chains in the present strategy, MeO-PEG$_{5000}$-NH$_2$ was employed as initiator for the ROP of *t*-buylbenzene substituted serine monomer **M2** and its benzyl substituted counterpart **M5** in $CHCl_3$+DMF solvent mixture for M/I = 100 using NHC catalyst as shown in Figure 2.29a and Figure 2.30a. Surprisingly, precipitation of polymer was noticed in the formation of PEGlated serine diblock copolymer produced from monomer **M5** (with simple benzyl substitution) and the polymer was also found to be insoluble in organic solvents for molecular weight determination (See Figure 2.30a for photograph). The *t*-butylbenzene substituted monomer **M2** exhibited homogeneous polymerization throughout and produced soluble PEG-*b*-polyserine2 with high molecular weight (See Figure 2.29a for photograph). The *t*-butylbenzene substitution has enabled the polyserine to become soluble in $CHCl_3$ or THF irrespective of PEG$_{5000}$-NH$_2$ or simple octadecyl amine were employed as initiator in the synthesis. This observation reiterates that the solubility of the polypeptides in the given strategy was primarily achieved by the precise control of the secondary structures by the *t*-butylbenzene substitution and it cannot be merely possible by choosing more soluble initiator such as PEG$_{5000}$.

(a)

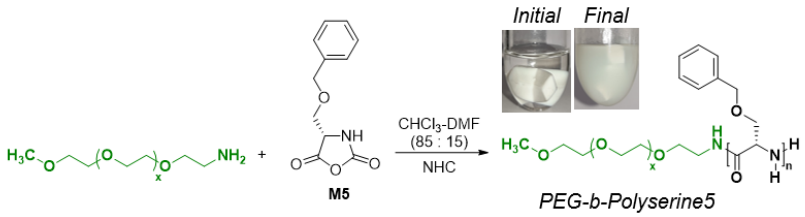

(b)

Monomer	n (^{1}H-NMR)[a]	M_n NMR[b] (g/mol)	M_n SEC[c] (g/mol)	M_w SEC[c] (g/mol)	Đ[c]	% Conversion[d]
PEG-block-Polyserine5	82	19500	Insoluble	-	-	> 99
PEG-block-Polyserine2	99	28100	10800	12400	1.2	> 99

Polymerization was carried out in $CHCl_3$+DMF (85:15, v/v) using MeO-PEG_{5000}-NH_2 as an initiator (M/I = 100) and in-situ generated N,N-dimesitylene substituted carbene as a catalyst. [a] Degree of polymerization (n) was determined from ^{1}H-NMR. [b] NMR based number average molar mass (M_n = 5000 + n × repeating unit mass). [c] molar mass and dispersity (Đ) were determined by size exclusion chromatography in tetrahydrofuran at 25 ºC. [d] Determined using FT-IR spectroscopy from integration of NCA anhydride peak at ~1780 cm^{-1} at the beginning and end of reaction.

Figure 2.30: *(a) Scheme for synthesis of PEG-polyserine5 along with photographs of reaction vial at the beginning and end of reaction. (b) Table contain the polymerization conditions, degree of polymerization (n) and M_n determined by ^{1}H-NMR and SEC molecular weights and percent conversion.*

PEG-*b*-polyserine2 was further successfully deprotected using HBr in acetic acid to yield PEG-*b*-polyserine2D. ^{1}H-NMR analysis further confirmed the complete deprotection of the polymer and also retaining the expected degree of polymerization (see Figure 2.31 for ^{1}H-NMR of PEG-*b*-polyserine5, PEG-*b*-polyserine2 and PEG-*b*-polyserine2D, also see Figure 2.29b for SEC of PEG-*b*-polyserine2). FT-IR analysis of the deprotected sample in Figure 2.27b again supported the expected conformational transformation from α-helix to β-sheet structure in the post-polymerization deprotection. PEG-*b*-polyserine2 was soluble in hexafluoroisopropanol (HFIP) that facilitated its secondary structure determination by CD in HFIP, which showed one positive signal at 189 nm and two negative signals at 202 nm and 216 nm with respect to the perfect α-helical conformation (see Figure 2.29c).[172] CD spectrum of deprotected sample PEG-*b*-polyserine2D in water showed one positive signal at 198 nm and a negative signal at 220 nm corresponding to typical β-sheet structure (see Figure 2.29d).[172] CD spectroscopic signals with respect to α-helical structure in PEG-*b*-polyserine2 having *t*-butylbenzene side chains and β-sheet structure in de-protected PEG-*b*-polyserine2D (or simply PEG-*b*-polyserine) reiterated the conformational transitions from the α-helix to β-sheet structure by the post polymerization deprotection strategy.

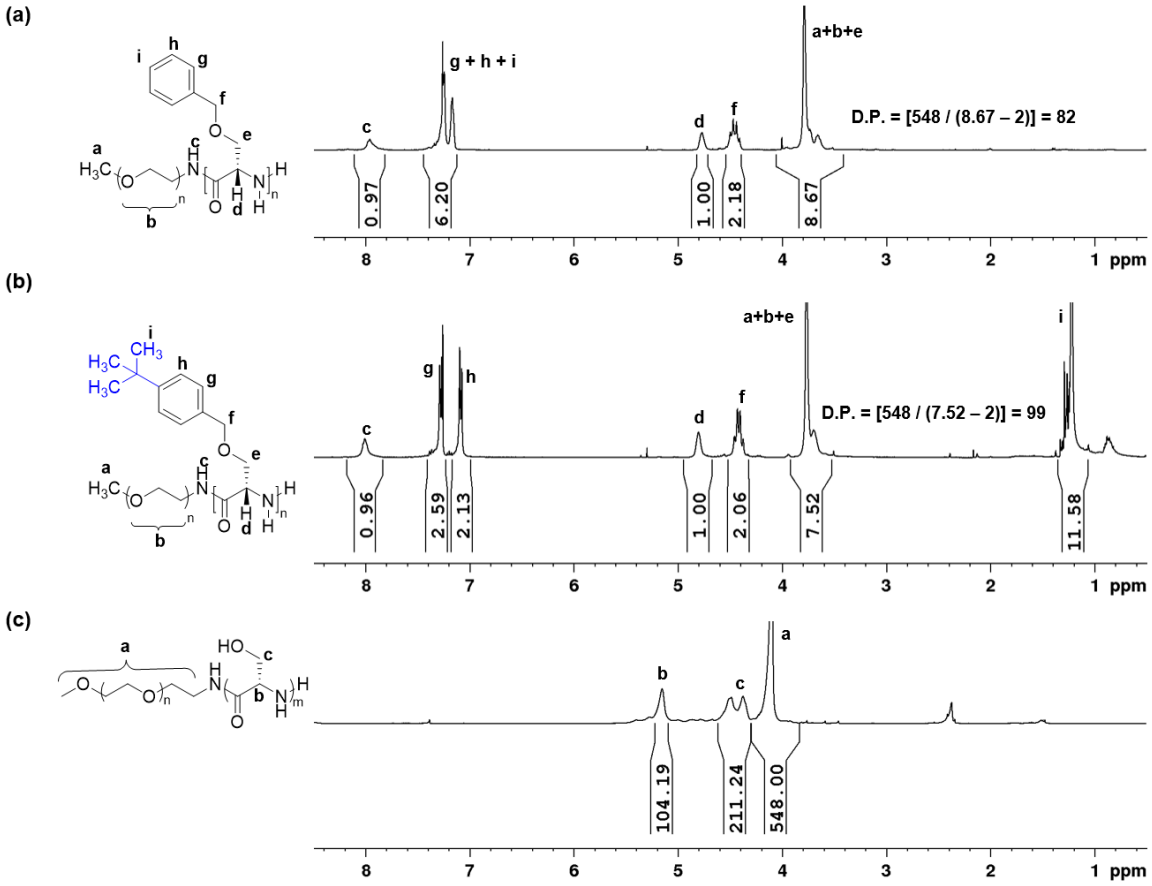

Figure 2.31: *(a) ^{1}H NMR of spectrum of PEG-b-polyserine5 in $CDCl_3$+Trifluoroacetic acid (6:1, v/v). (b) ^{1}H NMR of spectrum of PEG-b-polyserine2 in $CDCl_3$+Trifluoroacetic acid (6:1, v/v). (c) ^{1}H NMR of spectrum of PEG-b-polyserine-2D in Trifluoroacetic acid-D.*

These astonishing results suggest that the *controlled polymerization* of *t*-butylbenzene substituted serine and cysteine monomers produced soluble polyserines and polycysteines whose chain lengths can be controlled. These glimpses of results are exciting and could open up new avenues for synthesis of higher order block copolymers, star shaped polymers and graft copolymers from polyserines and polycysteines. Currently efforts are being taken to expand the scope of this methodology to other β-sheet forming polypeptides and block copolymers to explore their application in drug delivery and antimicrobial research.

2.4. Conclusion

In summary we have designed and developed new *t-butylbenzene functionalization* strategy for synthesis of high molecular weight β-sheet forming polypeptides based on polyserines and polycysteines. NCA monomers of serine and cysteine with bulky protecting groups bearing *t*-butylbenzene unit were designed and tailor made via multistep organic synthesis without involving any column chromatographic purification step. These monomers successfully underwent ROP to obtain soluble, high molecular weight polyserines and polycysteines with narrow dispersity (Đ). Detailed optimization on solvent and catalyst for ROP of the serine and cysteine NCA monomers were established in $CHCl_3$ or $CHCl_3$+DMF using NHC catalyst. Solubility of these new polymers in common organic solvents allowed their complete characterization by NMR and SEC. FT-IR based detailed secondary structure analysis of polymerization reaction mixture in $CHCl_3$ revealed that the *t*-butylbenzene functionalized serine and cysteine monomers produced polypeptides in β-sheet conformation at oligomeric stage and in-situ conformational transition of polypeptide propagating chains in α-helix conformation. FT-IR and CD spectroscopic analysis was evident for the existence of α-helical conformation in the propagating chain front and established their controlled ROP characteristics. *t*-Butylbenzene masking unit was successfully deprotected to restore the high molecular weight polyserine in native β-sheet conformation. The approach demonstrated here is not restricted to only these few examples, and in principle, it could be extended to wide ranges of other polypeptides for application in material science and biomedical field at large.

Chapter 3

Development of β-Sheet Polypeptide Block copolymer Nano-assemblies and their Delivery Aspects In vitro and In vivo

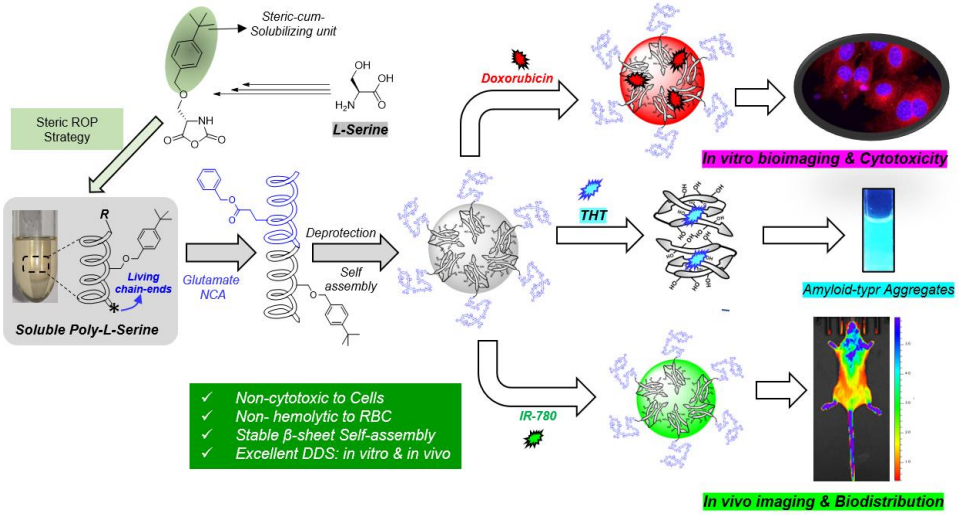

Abstract

Polyserine based block copolymers are one of the least explored macromolecular architectures due to uncontrolled precipitation associated with polyserines in the form β-sheet. Herein, we report serine-based polypeptide block copolymer synthesized by employing soluble α-helical polyserine based macroinitiator for ROP of glutamate NCA monomer. The molecular weight of diblock copolymer was in agreement with expected molecular weight and the SEC profile was monomodal with very low dispersity (Đ = 1.03) suggesting the great control over polymerization process. The diblock copolymer adopted α-helical conformation and it underwent α-helix to β-sheet conformational transition upon deprotection. The deprotected serine-glutamate diblock copolymer was highly water soluble and was able to self-assemble in to tiny spherical nanoparticles of size ~ 30 nm having negative zeta potential (-50 mV). The size of nanoparticles was found to be unaffected by pH (from pH 4 to 9), while their zetapotential became less negative with decreasing the pH. The pH mediated helix to coil conformational transition was observed upon increasing pH above 5. The β-sheet assemblies in di-block copolymer were validated by ThT fluorescence assay and it was found to enhance ThT fluorescence by ~15 times. The serine-glutamate di-block copolymer was non-toxic to mammalian cells and non-hemolytic to RBCs. The diblock copolymer was found to encapsulate anticancer drug doxorubicin (DOX, DLC = 6.1%) and near IR dye (IR-780, DLC = 1.6%). The DOX loaded nanoparticles were utilized for *in vitro* applications such as to study the uptake of nanoparticles by mammalian cells with the help of confocal microscopy. The IR-780 loaded polymer nanoparticles were employed for *in vivo* biodistribution studies using IVIS. The *in vivo* biodistribution studies revealed the better circulation time and *in vivo* stability of dye loaded polymer nanoparticles. All in all, both *in vitro* and *in vivo* study reveals the biocompatible nature of these novel serine-glutamate di-block copolymers which makes them a strong candidate in future biomedical applications.

3.1. Introduction

The block copolymers are fascinating macromolecular architecture formed by covalent attachment of two or more polymeric chains of different types.[182] The block copolymers are typically synthesized by mainly two strategies: 1) sequential addition of monomers in living/controlled polymerization techniques; and 2) coupling of two different homopolymers by chemoselective reactions.[183] The segmented nature of block copolymers gives rise to unique set of properties which are not achievable by random copolymers and hence block copolymers are exploited in plethora of applications.[184-187] The dissimilarity between the block segments results in phase separation and hence the amphiphilic block copolymers can be easily created by choosing the proper hydrophobic/hydrophilic segment blocks.[188] The amphiphilic block copolymers when dispersed in water can form self-assembled structures like micelles or vesicles which are extensively used in biomedical applications (see Figure 3.1 for self-assembly and drug encapsulation in block copolymer micelle for biomedical application).[189, 190]

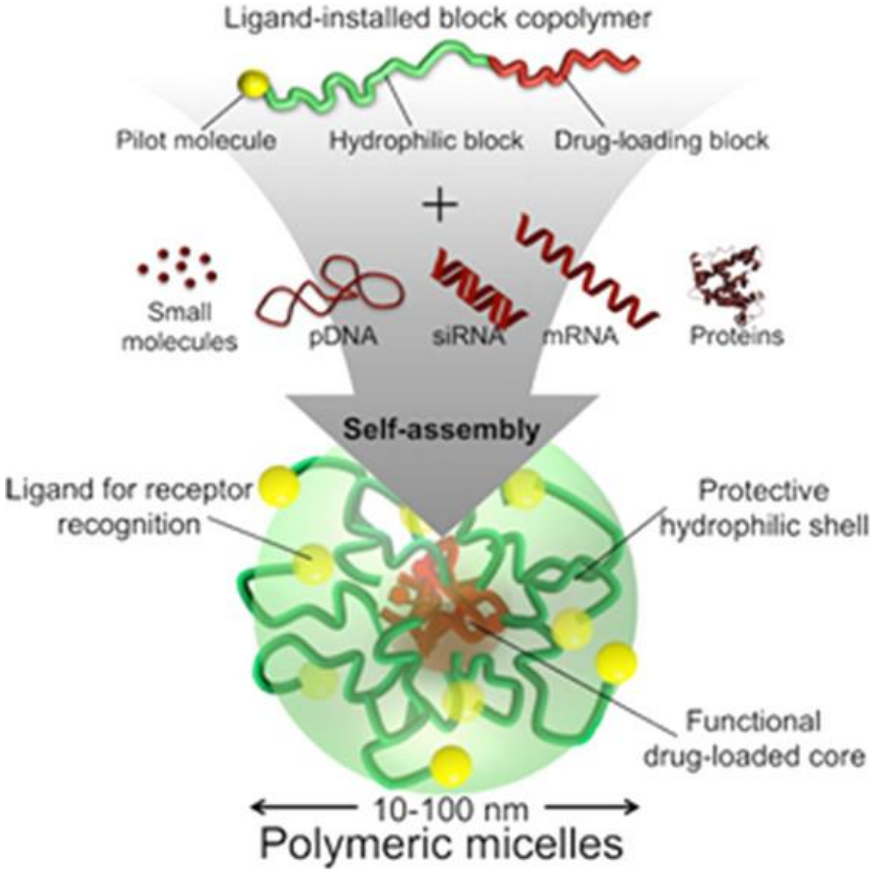

Figure 3.1. *Scheme demonstrating the loading of drug molecules in self-assembled block copolymer micelle. (adapted from Cabral, H. et.al. Chem. Rev.* ***2018,*** *118, 6844-6892).*

Although, the block copolymer architectures are nearly part of all kinds of polymers, the polypeptide-based block copolymers are inimitable entity due to protein mimicking ability of polypeptides in terms of their ability to form secondary structures.[129, 172] The polypeptides are synthetic polymers derived from amino acids and typically synthesized by ring opening polymerization (ROP) of N-carboxyanhydride (NCA) monomers.[10, 11] Although the ROP of NCA is more than hundred years old chemistry, primarily homo-polypeptides or random co-polypeptides were known until the discovery of nickel or cobalt based organometallic catalysts for controlled NCA polymerization.[13, 14] Since then, there has been growing attention in development of catalysts or methodologies for controlled NCA polymerization to make block copolymers by sequential monomer addition.[37, 39, 44, 50, 55, 56, 134, 138, 191] The polypeptide-based block copolymers can be composed of only amino acids or they can be hybrid copolymers consisting of polypeptide segment with other synthetic polymer chain. The hybrid copolymer can be synthesized by ROP of amino acid NCA using non-polypeptide based macroinitiator and notable example of these macroinitiator includes, polyethylene glycol (PEG),[192-194] polystyrene (PS),[195-197] polycaprolactone (PCL),[57, 198, 199] polylactides (PLA),[200-202] polybutadienes,[203-205] polyisobutylenes,[206] polyacetylenes,[207] polythiophenes,[208] polyoxazolines (POx),[153, 209] polysarcosines,[210] etc. Another way to synthesize hybrid block copolymers is by joining polypeptide block with other synthetic polymer using chemoselective reactions such as click chemistry,[211-214] diels alder reaction,[215] native chemical ligation,[216] etc. (see Figure 3.2). Due to these synthetic advancements, plethora of polypeptide-based block copolymers were synthesized for wide variety of applications such as 3D-printing,[75, 217, 218] protein patterning,[219] drug delivery,[118, 123, 220] gene delivery,[221, 222] anti-microbial applications,[84, 223, 224] hydrogels,[225-227] organogel,[228, 229] etc.

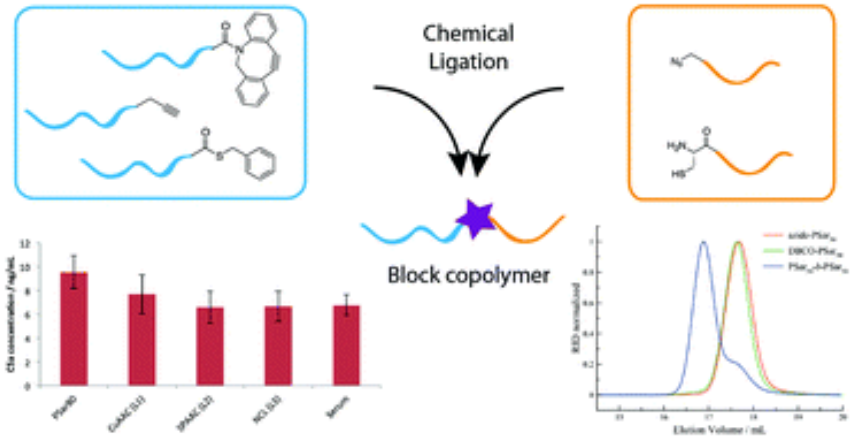

***Figure 3.2**. Scheme demonstrating the synthesis of block copolymer by chemoselective linking of two blocks. (adapted from Klinker, K. et.al. Polym. Chem. **2015,** 6, 4612-4623).*

The most important property of polypeptide-based block copolymers is their tendency to adopt secondary structures such as α-helices and β-sheets which regulate the aqueous self-assembly of amphiphilic polypeptide block copolymers and that in turn plays a vital role in polymer properties such as, self-assembly,[230] gelation,[227] pH responsiveness,[231, 232] AIE property,[233] etc. In addition to self-assembly related properties, the secondary structures play a key role in properties of polypeptide block copolymers related to biomedical application such as drug delivery.[108] Moreover, the secondary structure of growing polymer chain plays a key role in synthesis of block copolymer architectures. If growing polymer chain adopts α-helical conformation then polymerization proceeds homogeneously due to excellent solubility of helical chains, furthermore, their self-catalyzed propagation remarkably accelerates the polymerization,[133] as a result the growing helical polymer chain is living and upon addition of another monomer, block copolymer can be synthesized. In such scenario, sequential addition of NCA monomer from amino acid with propensity to form α-helices (e.g. glutamate or lysine based NCA monomer) can be done several times and multi-block polypeptides can be synthesized in controlled manner (see Figure 3.3).[44, 191, 234]

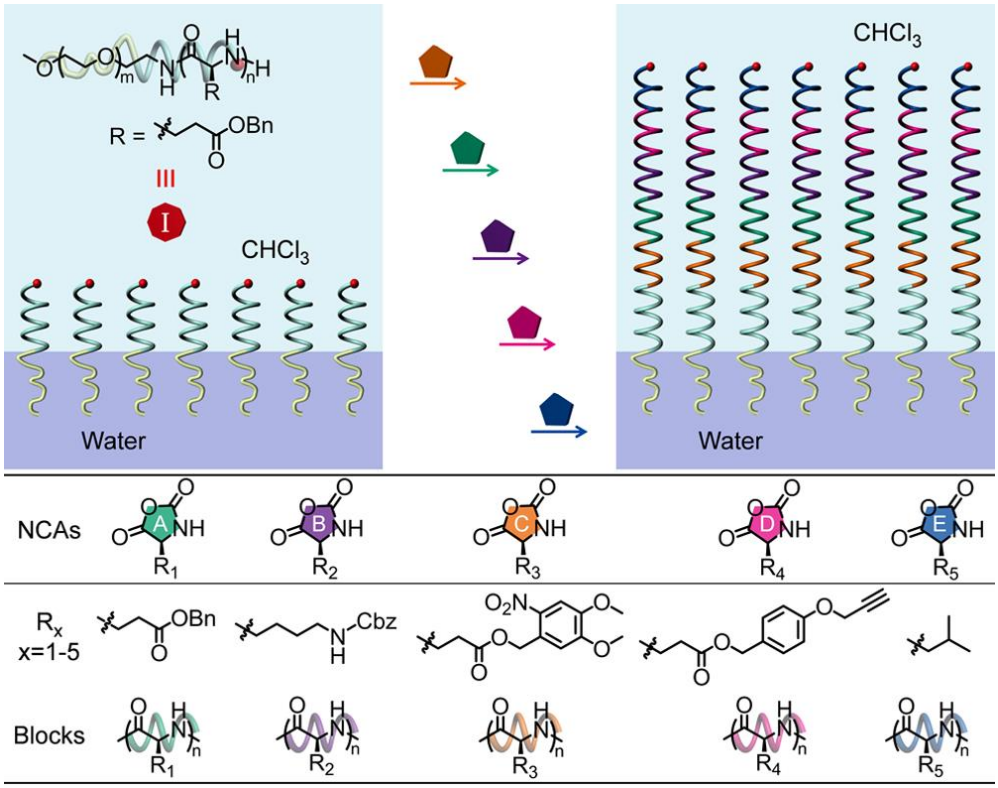

Figure 3.3. *Scheme demonstrating the synthesis of helical multiblock copolypeptides via rapid polymerization of NCAs. (adapted from Xuefang Wang, et. al. ACS Macro Lett.* ***2019****, 8, 1517–1521)*

On the contrary, if growing polymer chain adopts β-sheet conformation then it is almost impractical to make block copolymers from it due to uncontrolled precipitation of propagating chains and non-availability of the active-chain ends to initiate the second block.[12] As a result, polypeptide block copolymer synthesis starting from amino acid having propensity to form β-sheet structures is rarely practiced and it is also restricted to shorter chain length of β-sheet block (~10 units).[235] Consequently, the polypeptide block copolymers are primarily synthesized from amino acids having tendency to form α-helices such as glutamate or lysine. Although, NCA of amino acid with propensity to form β-sheet can be added to grown α-helical living polymer chain to make di-block copolymer consisting of β-sheet block but it is also limited to length of β-sheet block as it can hamper the solubility of growing block co-polymer chain.

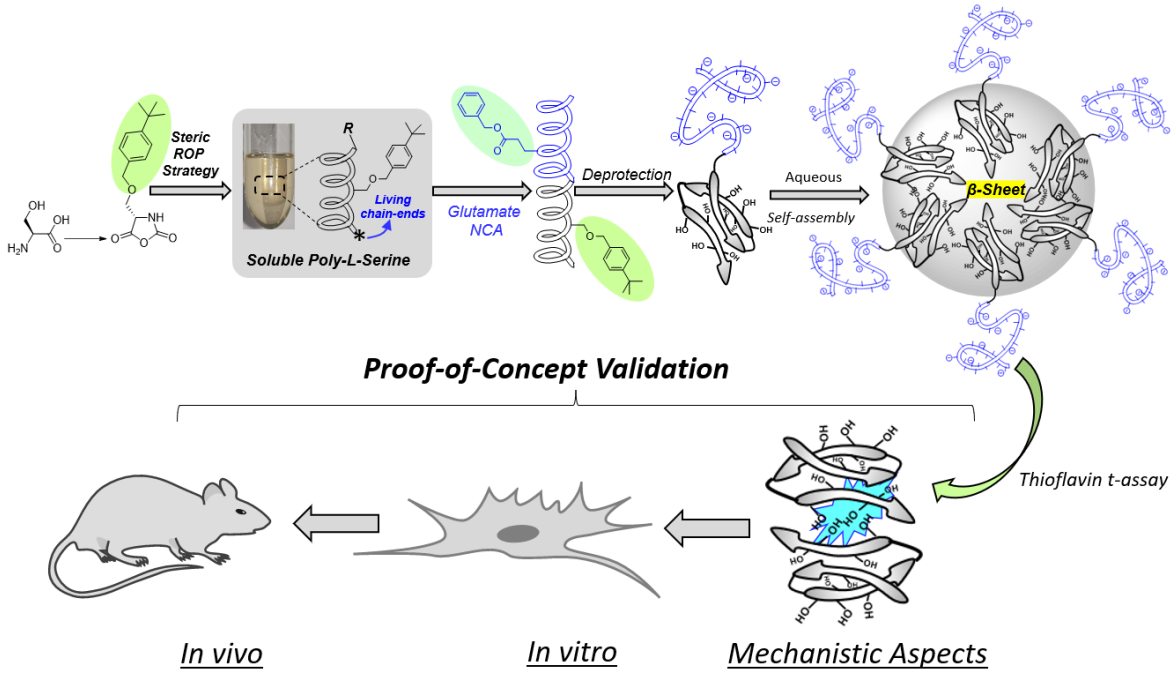

***Figure 3.4**. Schematic representation of the synthesis of serine-glutamate di-block copolymer and its utilization in various applications.*

Considering these factors, the polypeptide block copolymers with long β-sheet architectures are difficult to make. Taking this as a challenge, we decided to make block copolymer composed of long β-sheets of polyserine motif. Since, there has been no reports on utilization of Poly(L-serine) as macro-initiator in the synthesis of polypeptide block copolymers and it would be interesting to study these unexplored β-sheet structures from poly(L-serine) motif for various applications. In the first chapter it has been shown that the

bulky *t*-butyl benzene substitution in poly(L-serine) imparts the helicity to growing poly(L-serine) chain as a results polymerization proceeds homogeneously and the growing poly(L-serine) chains are living in nature. In the present chapter, we expanded the scope of the steric ROP approach to open new avenue for the building inaccessible block copolymer macromolecular architecture based on Poly(L-serine) and the concept is shown in Figure 3.4.

As a proof of concept, the *t*-butyl benzene functionalized serine NCA monomer was polymerized to produce soluble helical poly(L-serine) based macroinitiator which was then used for ROP of glutamate NCA monomer to produce a di-block copolymer consisting of polyserine and polyglutamate blocks having α-helix conformation in both segments as shown in Figure 3.4. The control in polymerization process resulted in the formation of di-block copolymer with expected degree of polymerization and having narrow polydispersity. The resultant di-block copolymer was deprotected to obtain highly water-soluble serine-glutamate diblock copolymer which found to adopt β-sheet conformation in water. The ser-glu diblock copolymer nano assemblies were found to undergo helix to coil conformational transition upon increasing pH above 5. The β-sheet motif in serine-glutamate diblock copolymer was validated by ThT assay and the di-block copolymer was found to enhance fluorescence of ThT by ~ 15-fold. The serine-glutamate diblock copolymer was not cytotoxic and non-hemolytic in nature that makes it potential candidate for biomedical application. In order to explore it for biomedical applications, anticancer drug doxorubicin (DOX) was encapsulated by polymer nano assemblies and, while the cytotoxic activity of DOX is retained while being in nano assemblies. The confocal microscopy revealed the successful uptake of drug loaded nano assemblies by mammalian cells. Towards end, the di-block copolymer nanoparticles were found to encapsulate NIR dye IR-780 and explored for *in vivo* biodistribution studies by IVIS imaging. We strongly believe that, this serine-glutamate di-block copolymer would open up new horizons for unexplored serine based diblock copolymer architectures for drug delivery applications.

3.2. Experimental Methods

3.2.1. Materials: Chloropropyl amine hydrochloride, 4-methoxy phenol, Thioflavin T (ThT), anhydrous chloroform, DAPI, Doxorubicin, IR-780 iodide, paraformaldehyde, EDTA, 3-(4, 5 dimethylthiazolyl)-2,5 diphenyltetrazolium bromide (MTT) were obtained from Sigma Aldrich chemicals. L-Serine, L-glutamic acid, triphosgene, propylene oxide, di-*t*-butyl dicarbonate (Boc_2O), trifluoroacetic acid (TFA), HBr in acetic acid (33 wt %) were purchased from local vendors and directly used without further purification. Wild-type mouse embryonic fibroblast cells (WT-MEF) were maintained in DMEM (phenol red free medium: Gibco) containing fetal bovine serum (FBS) (10 %, v/v) and penicillin–streptomycin (1 %, v/v) at 37 °C in an atmosphere humidified with CO_2 (5 %). Trypsinization of cells was done using trypsin (0.05 %, Gibco) and cells were seeded in desired flat bottomed plastic plates (Eppendorf) for all assays. The female balb/c and C57B1/6 male mice were obtained from the IISER Animal House facility, National Facility for Gene function in Health and Disease (NFGFHD).

3.2.2. Methods: Most methods are same that mentioned in Chapter 2 of this thesis. dn/dc of P(Bn-ser)-*b*-P(Bn-glu) was determined as per protocol mentioned in methods section of Chapter 2 and it was found to be 0.0984 ml/g. Circular dichroism (CD) analysis of the polymer samples (0.1 mg/mL) was performed on a JASCO J-815 CD spectrometer at 25 °C in HFIP or water as solvent. pH dependent CD analysis was performed by recording CD spectra of polymer samples in Britton-Robinson buffer of various pH (2 to 12). Dynamic light scattering (DLS) and zetapotential measurements were performed in water as solvent using Nano ZS-90 setup from Malvern. The concentration of polymer used for zetapotential measurements is 1 mg/mL and the DLS measurements were carried at 0.1 mg/mL concentration. For DLS and zetapotential measurements at various pH, the solution pH was adjusted using 0.1 N HCl or 0.1 N NH_3 (aq.) Schimadzu UV1900 spectrophotometer was used for absorbance measurements. The ThT fluorescence assays were performed in miliQ water with the exception of assay in various pH where Britton-Robinson buffer was used. The fluorescence spectra were recorded on SPEX Fluorolog HORIBA JOBIN VYON fluorescence spectrophotometer using slit width of 2 nm and excitation wavelength of 444 nm. FE-SEM analysis was performed using Zeiss Ultra Plus scanning electron microscope. The dilute sample solution (0.1 mg/mL in miliQ water) was drop casted on silicon wafer. For AFM analysis, polymer solution (0.1 mg/mL in miliQ water) was also drop casted on silicon wafer and the AFM imaging was performed using Agilent instruments. For HR-TEM

analysis, samples (0.1 mg/mL in miliQ water) were drop casted on copper TEM grids and imaging was performed using Jeol JEM2200FS 200 KeV systems. Leica SP8 was used for Confocal microscopic analysis.

3.2.3. Synthetic procedures

Synthesis of tert-butyl (3-chloropropyl)carbamate (11): To a solution of di-*t*-butyl dicarbonate (4.2 mL, 4.0 g, 18.3 mmol) in THF-water (1:1, v/v, 80 mL) was added sodium bicarbonate (3.4 g, 40.3 mmol). Subsequently, the solution of chloropropyl amine hydrochloride (2.9 g, 22.0 mmol) in water (40 mL) was added and the reaction mixture was stirred at 25 °C overnight. Eventually, the layers were separated and aqueous layer was extracted with ethyl acetate (3 × 60 mL). The organic layers were combined, washed with 2N HCl (50 mL), aqueous saturated $NaHCO_3$ (50 mL) and brine (50 mL) before drying over anhydrous Na_2SO_4 and then concentrated on a rotary evaporator to get a pure desired product tert-butyl (3-chloropropyl)carbamate (**11**) as a colourless oil. Yield: 3.3 g (94 %). ^{1}H NMR (400 MHz, $CDCl_3$) δ 4.68 (bs, 1H, N**H**), 3.58 (t, *J* = 6.4 Hz, 2H, Cl-C**H**$_2$), 3.27 (q, *J* = 6.5 Hz, 2H, NH-C**H**$_2$), 1.96 (p, *J* = 6.0 Hz, 2H, CH_2C**H**$_2$$CH_2$), 1.43 (s, 9H, C(C**H**$_3$)$_3$). ^{13}C NMR (101 MHz, $CDCl_3$) δ 156.1, 79.5, 42.5, 38.0, 32.7, 28.5. ATR-FTIR (cm^{-1}): 3350, 2977, 1687, 1513, 1450, 1392, 1366, 1250, 1165, 1082, 992, 907, 854, 780, 730, 652. HRMS (ESI) $[M+Na]^+$ calculated for $C_8H_{16}ClNNaO_2$, 216.0767; found, 216.0754.

Synthesis of tert-butyl (3-(4-methoxyphenoxy)propyl)carbamate (12): A flame dried Schlenk tube was charged with 4-methoxy phenol (3.1 g, 24.8 mmol), potassium iodide (0.5 g, 3.3 mmol), and potassium carbonate (3.4 g, 24.8 mmol). After drying under vacuum for 1 h, the mixture was diluted with anhydrous DMF (10 mL) and the mixture was stirred at 25 °C for 30 min. Subsequently the solution of tert-butyl (3-chloropropyl)carbamate (**11**) (3.2 g, 16.5 mmol) in anhydrous DMF (10 mL) was added to it and the reaction mixture was stirred at 70 °C for 24 h. Reaction mixture was slowly added to aqueous 2N NaOH (100 mL) at 0 °C and stirred for 15 min at 0 °C and then filtered. The solid product residue was washed with water (200 mL) and then dried in a vacuum to give pure tert-butyl (3-(4-methoxyphenoxy)propyl)carbamate (**12**) as pale brown solid. Yield: 3.7 g (80 %). ^{1}H NMR (400 MHz, $CDCl_3$) δ 6.83 (s, 4H, Ar-H), 4.78 (bs, 1H, N**H**), 3.97 (t, *J* = 6.0 Hz, 2H, O-C**H**$_2$), 3.77 (s, 3H, O-C**H**$_3$), 3.32 (q, *J* = 6.4 Hz, 2H, NH-C**H**$_2$), 1.95 (p, *J* = 6.2 Hz, 2H, CH_2C**H**$_2$$CH_2$), 1.44 (s, 9H, C(C**H**$_3$)$_3$). ^{13}C NMR (101 MHz, $CDCl_3$) δ 156.2, 154.0, 153.0, 115.6, 114.8, 79.3, 66.7, 55.9, 38.3, 29.7, 28.5. ATR-FTIR (cm^{-1}): 3367, 2933, 1691, 1505,

1469, 1391, 1366, 1227, 1166, 1108, 1038, 980, 825, 781, 736, 638, 621. HRMS (ESI) $[M+Na]^+$ calculated for $C_{15}H_{23}NNaO_4$, 304.1525; found, 304.1514.

Synthesis of 3-(4-methoxyphenoxy)propan-1-amine (initiator, R-NH_2) (13): To a solution of tert-butyl (3-(4-methoxyphenoxy)propyl)carbamate (**12**) (1.2 g, 4.3 mmol) in THF (2 mL) was added aq. phosphoric acid (85 %, w/w, 64 mmol, 4.4 mL) and the mixture was stirred at 25 °C for 18 h. Subsequently, the reaction mixture was diluted with water (10 mL) and extracted with ethyl acetate (1 × 20 mL). The aqueous layer was cooled to 0 °C and then aqueous NaOH (50 %, w/v) was slowly added to it till pH of resulting mixture becomes ~ 8. The resulting turbid solution was extracted with ethyl acetate (3 × 30 mL). The organic layers were combined, washed with brine (30 mL), dried over anhydrous Na_2SO_4 and then concentrated on a rotary evaporator to get a pure desired product 3-(4-methoxyphenoxy)propan-1-amine (initiator, R-NH_2) (**13**) as a colourless solid. Yield: 0.5 g (63 %). ^{1}H NMR (400 MHz, $CDCl_3$) δ 6.81 (s, 4H, Ar-H), 3.99 (t, *J* = 6.0 Hz, 2H, O-C**H**$_2$), 3.76 (s, 3H, O-C**H**$_3$), 2.90 (t, *J* = 7.0 Hz, 2H, NH-C**H**$_2$), 1.90 (p, *J* = 6.4 Hz, 2H, CH_2C**H**$_2$$CH_2$), 1.53 (bs, 2H, N**H**). ^{13}C NMR (101 MHz, $CDCl_3$) δ 154.1, 152.9, 115.6, 114.8, 66.2, 55.8, 38.3, 30.3. ATR-FTIR (cm^{-1}): 3300, 2953, 1586, 1511, 1444, 1395, 1359, 1292, 1239, 1178, 1114, 1034, 935, 826, 724, 668, 639, 618. HRMS (ESI) $[M+H]^+$ calculated for $C_{10}H_{16}NO_2$, 182.1181; found, 182.1165.

Synthesis of γ-Benzyl-L-glutamate (14): A suspension of L-glutamic acid (24.0 g, 163.1 mmol) and benzyl alcohol (25.4 mL, 26.5 g, 244.7 mmol) in toluene (25 mL) was stirred at 45 °C for 15 min. Subsequently, methane sulphonic acid (12.7 mL, 18.8 g, 195.7 mmol) was added to it very slowly using addition funnel and mixture was continued to stir at 45 °C for 3 h to obtain clear solution which was further stir at 25 °C for 12 h. Eventually, water (50 mL) was added and layers were separated using separating funnel. The organic layer was discarded while, aqueous layer was diluted with ethanol (100 mL) and pH of resulting mixture was adjusted to neutral pH (pH = 7) using conc. aqueous ammonia to obtain crude product as white precipitate. The crude product was isolated by precipitation and recrystallised using mixture of water and ethanol (150 mL, 2:1, v/v) to obtain γ-Benzyl-L-glutamate (**14**) as white shiny crystals. Yield: 16.5 g (43 %). ^{1}H NMR (400 MHz, $CDCl_3$ – TFA (0.7 mL, 6:1, v/v) δ 7.77 (bs, 3H, N**H**), 7.43 – 7.29 (m, 5H, Ar-**H**), 5.17 (s, 2H, ArOC**H**$_2$), 4.32 (bs, 1H, C**H**CH_2), 2.81 (t, *J* = 6.3 Hz, 2H, COC**H**$_2$$CH_2$CH), 2.51 – 2.14 (m, 2H, $COCH_2$C**H**$_2$CH). ^{13}C NMR (101 MHz, $CDCl_3$ – TFA (0.7 mL, 6:1, v/v)) δ 176.2, 172.8,

134.1, 129.3, 129.0, 128.7, 69.1, 53.7, 31.1, 24.8. HRMS (ESI) $[M+H]^+$ calculated for $C_{12}H_{16}NO_4$, 238.1079; found, 238.1073.

Synthesis of Glutamate NCA (M7): To a suspension of γ-Benzyl-L-glutamate (**14**) (2.0 g, 8.43 mmol) in THF (40 mL) was sequentially added propylene oxide (2.3 mL, 1.96 g, 33.7 mmol) and triphosgene (1.25 g, 4.22 mmol) and mixture was stirred at 25 °C for 2 h in a closed vessel to get clear solution. Subsequently, the mixture was cooled to 0 °C on ice and then water (20 mL) was added to quench the excess phosgene. After stirring the mixture at 0 °C for 1 min, it was extracted with ethyl acetate (2 × 40 mL). The organic layers were combined, extracted with brine (20 mL), dried over anhydrous Na_2SO_4, and concentrated on rotary evaporator (below 45 °C) to get an oil. The resulting oily residue was dissolved in THF (20 mL), layered with hexane (100 mL) and left undisturbed at -20 °C for overnight to precipitate the product. The precipitated product was isolated by filtration, washed with hexane (100 mL) and dried in vacuum to obtain pure product as white solid. The obtained product was further repurified by recrystallization from ethyl acetate – hexane (1:4, v/v, 100 mL) to get pure Glutamate NCA (**M7**) as white crystalline solid. Yield: 1.5 g (69 %). ^{1}H NMR (400 MHz, $CDCl_3$) δ 7.51 – 7.29 (m, 5H, Ar-**H**), 6.65 (s, 1H, N**H**), 5.14 (s, 2H, ArOC**H**$_2$), 4.44 – 4.32 (m, 1H, C**H**CH_2), 2.59 (t, *J* = 6.9 Hz, 2H, COC**H**$_2CH_2CH$), 2.39 – 1.98 (m, 2H, $COCH_2C$**H**$_2CH$). ^{13}C NMR (101 MHz, $CDCl_3$) δ 172.5, 169.5, 151.9, 135.3, 128.9, 128.7, 128.5, 67.3, 57.1, 30.0, 27.0. ATR-FTIR (cm^{-1}): 3334, 2900, 1853, 1779, 1728, 1361, 1274, 1171, 1107, 924, 751, 699. HRMS (ESI) $[M+Na]^+$ calculated for $C_{13}H_{13}NNaO_5$, 286.0691; found, 286.0699.

Synthesis of P(*t*-Bu-Bn-ser)-*b*-P(Bn-glu): The serine NCA monomer (**M2**) (0.56 g, 2.00 mmol) was dissolved in anhydrous chloroform (8 mL) and 3-(4-methoxyphenoxy)propan-1-amine (**13**) (20 mM in anhydrous chloroform, 1 mL, 0.02 mmol) was added to it under inert atmosphere. Subsequently, the solution of IMes.HCO_3 [1,3-Bis(2,4,6-trimethylphenyl) imidazolium bicarbonate] (8 mM , 1 mL, 8 µmol) in anhydrous chloroform was added, and the mixture was stirred under inert conditions at 25 °C for 18 h. FT-IR of an aliquot (5 µL) of the reaction mixture indicated complete monomer consumption. A small portion of the reaction mixture (0.5 mL) was taken out to characterize the first block (i.e., P(*t*-Bu-Bn-ser)). Eventually, glutamate NCA monomer (**M7**) (0.50 g, 1.9 mmol) was directly added to the reaction mixture under inert atmosphere. After stirring the reaction under the nitrogen atmosphere for 2 h, FT-IR analysis on a small portion of reaction mixture (5 µL) indicated

NCA monomer's total consumption. Finally, the solvent was removed by rotary evaporation, and the precipitation of polymer was carried out by adding diethyl ether (40 mL). The precipitated polymer was isolated by centrifugation (4000 rpm for 10 min), washed with diethyl ether and finally dried under high vacuum to obtain P(*t*-Bu-Bn-ser)-*b*-P(Bn-glu) as a white solid. Yield: 0.77 g (87 %). ^{1}H NMR (400 MHz, $CDCl_3$ – TFA (0.7 mL, 6:1, v/v) δ 8.03 (bs, 93H, N**H**), 7.84 (d, *J* = 6.73 Hz, 97H, N**H**), 7.42 – 7.20 (m, 723H, Ar-**H**), 7.10 (d, *J* = 8.41 Hz, 191H, Ar-**H**), 6.95 – 6.77 (m, 4H, Ar-**H**), 5.14 – 5.00 (m, 199H, ArC**H**$_2$OCO), 4.91 – 4.69 (m, 94H, OCH_2C**H**), 4.69 – 4.53 (m, 101H, $(CH_2)_2$C**H**CO), 4.53 – 4.33 (m, 185H, ArC**H**$_2$$OCH_2$), 3.91 – 3.56 (m, 189H, CHC**H**$_2$O), 2.57 – 2.28 (m, 202H, $CHCH_2$C**H**$_2$), 2.20 – 1.79 (m, 203H, CHC**H**$_2$$CH_2$), 1.41 – 1.04 (m, 859H, C(C**H**$_3$)$_3$). ^{13}C NMR (101 MHz, $CDCl_3$ – TFA (0.7 mL, 6:1, v/v)) δ 175.3, 173.1, 171.7, 152.0, 134.6, 132.8, 128.8, 128.4, 128.1, 126.1, 125.7, 73.9, 68.4, 68.2, 53.9, 53.6, 34.6, 31.2, 30.2, 27.0. ATR-FTIR (cm^{-1}):3287, 2961, 2866, 1732, 1656, 1547, 1456, 1361, 1314, 1266, 1217, 1165, 1107, 1016, 837, 819, 749, 697, 666.

Synthesis of P(ser)-*b*-P(glu): A Schlenk tube was charged with P(*t*-Bu-Bn-ser)-*b*-P(Bn-glu) (0.2 g, 8.55 µmol) and it was dissolved in trifluoroacetic acid (5 mL) at 0 °C. After getting clear solution, HBr in acetic acid (2 mL, 33 % solution, w/w) was added carefully and mixture was stirred at 0 °C for initial 2 h and then at 25 °C for overnight. Subsequently, the diethyl ether (40 mL) was added to precipitate the deprotected polymer. The precipitated product was isolated by centrifugation (4000 rpm for 10 min) and after discarding supernatant, precipitate was triturated with diethyl ether and dried in vacuum. The resulting solid was dissolved in aq. sodium bicarbonate (0.5 M, 15 mL) and dialysed against miliQ water for 48 h with frequent change of water. Finally, dialysed solution was lyophilised to get sodium salt of P(ser)-*b*-P(glu) as white fluffy solid. Yield: 0.1 g (94 %). ^{1}H NMR (400 MHz, Trifluoro Acetic Acid-D) δ 5.04 (bs, 1H, C**H**CH_2OH), 4.98 – 4.89 (m, 1H, C**H**CH_2CH_2CO), 4.52 – 4.11 (m, 2H, CHC**H**$_2$OH), 2.76 (t, *J* = 7.1 Hz, 2H, $CHCH_2$C**H**$_2$CO), 2.53 – 2.15 (m, 2H, CHC**H**$_2$$CH_2$CO). ATR-FTIR ($cm^{-1}$): 3293, 3276, 1647, 1540, 1435, 1410, 1363, 1307, 1289, 1247, 1231, 1208, 1068, 1054, 1023.

Synthesis of P(*t*-Bu-Bn-ser)-*r*-P(Bn-glu): The Schlenk tube was charged with serine NCA monomer (**M2**) (0.27 g, 1.00 mmol) and glutamate NCA monomer (**M7**) (0.26 g, 1.00 mmol) and anhydrous chloroform (4 mL) was added to make homogeneous solution of NCA monomers. Subsequently, the solution of 3-(4-methoxyphenoxy)propan-1-amine (**13**) (20

mM , 0.5 mL, 0.01 mmol) in anhydrous chloroform under nitrogen atmosphere was added to above solution of NCA monomers. Immediately, the solution of IMes.HCO_3 [1,3-Bis(2,4,6-trimethylphenyl) imidazolium bicarbonate] (8 mM , 0.5 mL, 4 µmol) in anhydrous chloroform was added, and the reaction mixture was stirred under inert conditions at 25 °C for 18 h. FT-IR of an aliquot (5 µL) of the reaction mixture indicated complete monomer consumption. Finally, the solvent was removed by rotary evaporation, and the precipitation of polymer was carried out by adding hexane (40 mL). The precipitated polymer was isolated by centrifugation (4000 rpm for 10 min), washed with hexane and finally dried under high vacuum to obtain P(*t*-Bu-Bn-ser)-*r*-P(Bn-glu) as a white solid. Yield: 0.41 g (91 %). ^{1}H NMR (400 MHz, $CDCl_3$ – TFA (0.7 mL, 6:1, v/v) δ 8.03 (bs, 186H, N**H**), 7.42 – 7.20 (m, 684H, Ar-**H**), 7.10 (d, *J* = 8.41 Hz, 197H, Ar-**H**), 6.95 – 6.77 (m, 4H, Ar-**H**), 5.14 – 5.00 (m, 193H, ArC**H**$_2$OCO), 4.91 – 4.69 (m, 94H, OCH_2C**H**), 4.69 – 4.53 (m, 104H, $(CH_2)_2$C**H**CO), 4.53 – 4.33 (m, 188H, ArC**H**$_2$$OCH_2$), 3.91 – 3.56 (m, 188H, CHC**H**$_2$O), 2.57 – 2.28 (m, 187H, $CHCH_2$C**H**$_2$), 2.20 – 1.79 (m, 188H, CHC**H**$_2$$CH_2$), 1.41 – 1.04 (m, 892H, C(C**H**$_3$)$_3$). ATR-FTIR (cm^{-1}):3283, 2959, 2866, 1732, 1652, 1546, 1516, 1454, 1361, 1313, 1293, 1256, 1214, 1165, 1109, 1097, 751, 697.

Synthesis of P(ser)-*r*-P(glu): A similar procedure to that for P(ser)-*b*-P(glu) is employed using P(*t*-Bu-Bn-ser)-*r*-P(Bn-glu) (0.1 g, 4.33 µmol), HBr in acetic acid (1 mL, 33 % solution, w/w) and trifluoroacetic acid as solvent (2 mL). After precipitation of deprotected polymer using diethyl ether (30 mL), it was isolated by centrifugation (4000 rpm for 10 min), triturated using diethyl ether and dried in vacuum to get crude P(ser)-*r*-P(glu) as pale-yellow solid. The resulting solid was dissolved in aq. sodium bicarbonate (0.5 M, 5 mL) and dialysed against miliQ water for 48 h with frequent change of water. Finally, dialysed solution was lyophilised to get sodium salt of P(ser)-*r*-P(glu) as white fluffy solid. Yield: 0.05 g (94 %). ^{1}H NMR (400 MHz, D_2O) δ 4.55 – 4.36 (m, 1H, C**H**CH_2OH), 4.36 – 4.16 (m, 1H, C**H**CH_2CH_2CO), 3.99 – 3.68 (m, 2H, CHC**H**$_2$OH), 2.31 – 2.09 (m, 2H, $CHCH_2$C**H**$_2$CO), 2.09 – 1.68 (m, 2H, CHC**H**$_2$$CH_2$CO). ATR-FTIR ($cm^{-1}$): 3245, 2928, 2860, 1648, 1538, 1445, 1398, 1307, 1256, 1068.

3.2.4. Drug Encapsulation in the Copolymer Scaffolds

A representative protocol is given for Doxorubicin (DOX) loading. To a solution of P(ser)-*b*-P(glu) (5.0 mg) in miliQ water (4.0 mL) was added a solution of doxorubicin hydrochloride (DOX.HCl, prior treated with triethyl amine) (0.5 mg) in DMSO (1.0 mL)

slowly in dropwise manner. The mixture was stirred for 2 h and subsequently transferred in to a dialysis tube (MWCO = 3500D) and dialyzed against large excess of miliQ water in dark with frequent change of miliQ water for 48 h. The dialysed solution was then filtered and stored at 4 °C. Weight of encapsulated DOX was determined using UV-visible spectroscopy by measuring absorbance at 490 nm (ε = 11500 $L.M^{-1}.cm^{-1}$). The DLC (drug loading content) and DLE (drug loading efficiency) were determined by using the following equations:

DLC = [weight of encapsulated DOX / weight of polymer] x 100

DLE = [weight of encapsulated DOX / weight of total DOX added] x 100

In the similar manner, the encapsulation of IR-780 dye was carried out.

3.2.5. Stability of Dox-loaded nanoparticles by release studies

The DOX loaded polymer nanoparticles were subjected to release studies at pH = 7.4 and pH = 5.0 to understand their stability. The DOX loaded polymer solution was taken (1.0 mL) in dialysis tube (MWCO = 3500D) and immersed in 3.0 mL of buffer solution (PBS pH = 7.4 or pH = 5) and incubated at 37 °C. At periodic intervals, 2.0 mL of solution was withdrawn from reservoir for absorbance measurements and immediately it was transferred back to the reservoir and incubation is continued. The absorbance reading at each time interval was used to calculate amount of drug released. The cumulative drug release (%) was calculated by following equation.

Cumulative drug release (%) = [[Amount of drug released at time 't'] / [actual amount of drug present in nanoparticles when taken in dialysis tube]] X 100.

3.2.6. Cell Viability Assay (MTT Assay)

In ordered to validate the cytotoxicity of polymer alone, DOX loaded polymer nanoparticles, and free drug (DOX), the cell viability assay was performed in wild type MEF cell line and SKOV3 ovarian cancer cells using the well-known tetrazolium salt, 3-(4,5-dimethylthiazol-2-yl)-2,5-diphenyltetrazolium bromide (MTT). In the typical procedure, each well of a 96-well plate (Corning, U.S.A.) was seeded with thousand cells in DMEM (100 μL) with 10 % fetal bovine serum (FBS) and incubated for 16 h to adhere. The media from every well was aspirated before feeding the sample and then cells were fed with various concentrations of

polymer, free DOX and DOX loaded polymer. The cells fed with only media (DMEM with FBS only, no compound added), was used as control for all experiments. The experiment was performed in triplicates. After compound addition, cells were incubated for 72 h without changing the media. Subsequently the media was aspirated from each well and a freshly prepared stock solution of MTT (100 μL, 0.5 mg/mL in sterile DMEM) was added to each well and the cells were incubated for 4 h at 37 °C. Again, the media was removed by aspiration and DMSO (100 μL) was added to each well to dissolve the purple-coloured formazan crystals [the formazan crystals are the resultant product of reduction of MTT by the mitochondrial dehydrogenase enzyme]. Immediately, the absorbance at 570 nm of resultant formazan solution in each well was measured using the microplate reader (Perkin-Elmer Ensight microplate reader). Mean absorbance of the triplicate set was used for further calculations and it is representative of the number of viable cells per well. The absorbance value corresponding to the control well was considered to be 100 % and accordingly the relative percentage values for the sample treated wells were determined.

3.2.7. Cellular Uptake of DOX-loaded Polymer nanoparticles by Confocal Microscopy

Wild type MEF cells or SKOV3 ovarian cancer cells were seeded (cell density was 0. million) on sterile coverslips kept in 6-well plates having media (DMEM) containing fetal bovine serum (FBS, 10%), 1 % Penicillin-Streptomycin and incubated for 16 h at 37 °C in CO_2 incubator prior to compound addition. The cells were further treated with required concentrations of free DOX and DOX-loaded polymer nanoparticles (solutions in media) and the incubation was continued for further 4 h or 8 h under same conditions. Subsequently, the media was removed and cells were washed with PBS (2 x 1 mL) and fixed using 3.5 % paraformaldehyde solution in PBS for 15 min at 25 °C. Again, the cells were washed with PBS (2 x 1 mL) and immediately stained with DAPI solution in PBS by incubating with it in dark for 2 min. Finally, the PBS washings were given (2 x 1 mL) to remove excess dye from the plate. Coverslips were fixed onto the glass slides (from borosil) with the help of glycerol and then dried for 30 min in dark at 37 °C. The cells were then imaged using confocal microscopy by employing λ 405 nm and λ 488 nm lasers and the obtained images were analysed using Image J software.

3.2.8. Hemolysis Assay

The blood (0.4 mL) was procured from ~ 9 weeks old male mice (C57B1/6) via the retro-orbital plexus puncture and collected in 5 % EDTA coated centrifuge tubes. The red blood cells (RBCs) were separated from blood plasma by centrifugation (8000 rpm) at 25 °C. The supernatant (plasma) was removed carefully leaving behind the pellet of RBCs and which was then washed carefully with freshly prepared PBS (pH = 7.4) buffer three times. The RBCs were diluted with PBS to make 5 % solution (v/v). This freshly prepared RBC solution was taken in 96-well plate (100 µL in each well) and treated with polymer solution (100 µL, 200 µg/mL), PBS (100 µL, as negative control) and Triton X-100 (100 µL, 1% solution in PBS, as positive control) and the corresponding 96-well plate was incubated at 37 °C for 1 h. Please note that, all the samples were prepared in triplicates. Subsequently, the solutions in each well were transferred to separate centrifuge tubes and centrifuged at 1400 rpm for 10 min. The photographs of centrifuge tubes were taken and carefully without disturbing much, the supernatant (100 µL) was transferred to another 96-well plate and subjected to absorbance measurements at 576 nm using plate reader. Hemolysis (%) was determined using the formula:

Hemolysis (%) = [[(O.D.$_{576nm}$ for polymer treated sample - O.D.$_{576nm}$ for PBS treated sample)] / [(O.D.$_{576nm}$ for Triton X-100 treated sample - O.D.$_{576nm}$ for PBS treated sample)]] × 100

3.2.9. IVIS mediated biodistribution analysis and *whole-organ* imaging

Female balb/c mice of 8-12 week old (~ 25 g in weight) were used for the biodistribution studies using IVIS. Total 8 mice were randomly divided into 3 groups. The first group (n=3) were injected with free IR-780 dye, the second group (n=3) were injected with IR-780 loaded polymer nanoparticles and the last group (n=2) were injected with PBS. All the injections of free IR-780 or IR-780 loaded nanoparticles in PBS (100 µL) were done intraperitonially while maintaining the IR-780 dosage at 0.5 mg/kg. The blood was collected from anesthetized mice via retro-orbital plexus puncture at the various time points (4 h, 24 h, 48 h post injection) from alternate sides. In case of bleeding the absorbable hemostatic gelatin sponge (AbGel) was used. The biodistribution of the free IR-780 dye and the dye loaded polymer nanoparticles were monitored in real time by employing IVIS spectrum (Perkin Elmer). Wherein, the mice were anesthetized and imaged at time points 4 h, 24 h,

and 48 h to capture both the dorsal and ventral view using the excitation and emission filter of λ_{exc} = 745 nm and λ_{em} = 820 nm respectively. At the end of 48 h, the Mice were euthanized by overdose of anaesthesia (isoflurane) and perfused with PBS prior to organ harvesting. The harvested organs were used for *whole-organ* imaging analysis employing the same excitation and emission filters. From the collected blood, plasma samples were isolated by centrifugation and inoculated (10 µL) in each well of 96-well plate and subsequently diluted 10 times with PBS (n=3). These samples were then subjected to the IVIS imaging using similar filters (as mentioned above). The average radiance was calculated from the instrument software and used to quantify the amount of the dye IR-780.

3.3. Results and Discussion

3.3.1. Synthesis of Initiator and NCA monomers for polymerization

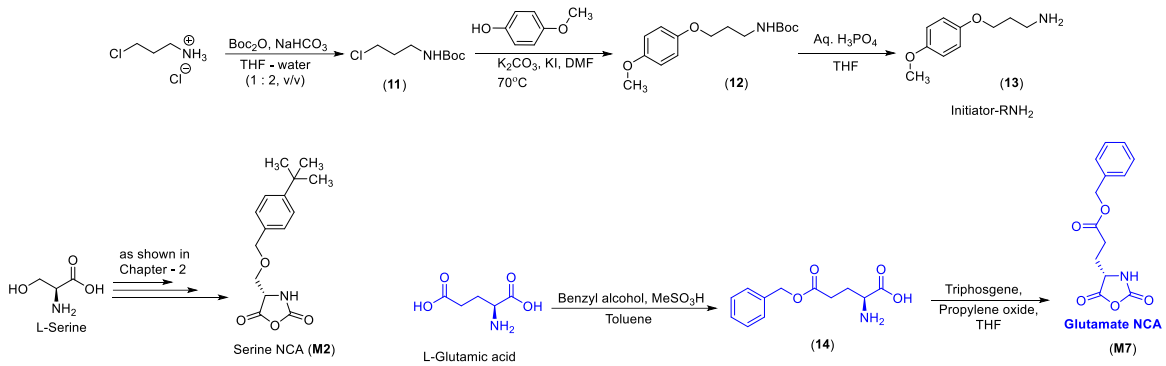

Scheme 3.1. *Synthesis of initiator-R-NH₂ (**13**) and NCA monomers*

For ring opening polymerization of NCA, primary amines are considered to be one of the best initiators and we chose compound **13** as an initiator for our polymerization studies as it has characteristic aromatic protons for determining degree of polymerization, also it is solid at room temperature, which makes it easy to handle and accurately weigh. The synthesis of compound **13** is shown in scheme 3.1 and it starts with Boc-protection of chloropropyl amine hydrochloride to get product **11** which was then subjected to nucleophilic substitution with 4-methoxy phenol to get **12**. At the end, compound **12** was deprotected using aqueous phosphoric acid to obtain compound **13**. The compound **13** was characterized by ^{1}H-NMR, ^{13}C-NMR and HRMS (^{1}H and ^{13}C NMRs are given in Appendix). After synthesis of initiator, desired NCA monomers for polymerization were synthesized and their synthesis is also shown in scheme 3.1. Serine NCA monomer (**M2**) is obtained from L-serine by multi-step organic synthesis as described in Chapter 2 of this thesis.

Glutamate NCA monomer (**M7**) is synthesized in two steps from L-glutamic acid, wherein in the first step, L-glutamic acid was converted to its mono benzyl ester (**14**) using methane sulphonic acid and benzyl alcohol. The compound **14** was further treated with triphosgene in presence of propylene oxide as a HCl quencher to afford glutamate NCA monomer (**M7**). Efficient trapping of HCl generated during phosgenation reaction by propylene oxide allowed us to carry out NCA synthesis without use of stringent anhydrous conditions as reported recently.[25]

3.3.2. Synthesis of block and random copolymers of serine and glutamate

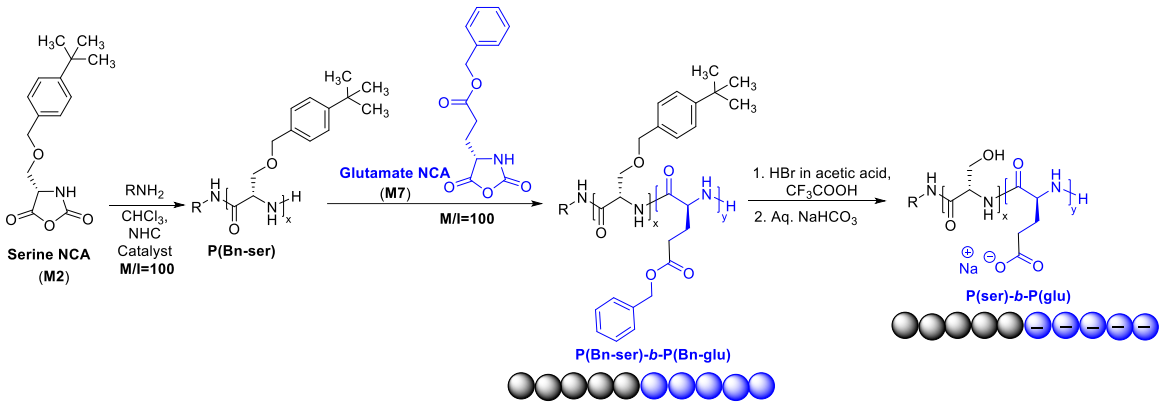

***Scheme 3.2**. Synthesis of Poly(serine)-b-poly(glutamate)*

The di-block copolymer Poly(L-serine)-*b*-poly(L-glutamate) (P(ser)-*b*-P(glu)) is synthesized from two sequential ROP processes followed by post-polymerization deprotection as shown in scheme 3.2. The serine NCA monomer (**M2**) was subjected to polymerization in chloroform using compound **13** as an initiator by maintaining M/I = 100 in the feed and IMes.HCO_3 was used as a catalyst to generate soluble Poly(*t*-Bu-benzyl-L-serine) [P(Bn-ser)] macro-initiator. The complete consumption of the first monomer (**M2**) was monitored by ATR-FTIR (see Figure 3.5a); then, the second monomer glutamate NCA (**M7**) was charged into the polymerization reactor by keeping same M/I = 100 in the feed to make diblock copolymer Poly(*t*-Bu-benzyl-L-serine)-*b*-Poly(benzyl-L-glutamate) [P(Bn-ser)-*b*-P(Bn-glu)]. The polymerization was proceeded till the complete disappearance of the second monomer (monitored by ATR-FTIR, see Figure 3.5a). The degree of polymerization of macroinitiator and di-block copolymer was determined using ^{1}H-NMR by comparing the integration of proton "**b**" in serine segment and proton "**c**" of glutamate segment with that of an initiator proton ("**a**" proton) as shown in Figure 3.5b. The ^{1}H-NMR spectra in Figure

3.5b reveals the existence of the expected chemical structure having degree of polymerization (n) as 94 and 100 for first and second block, respectively.

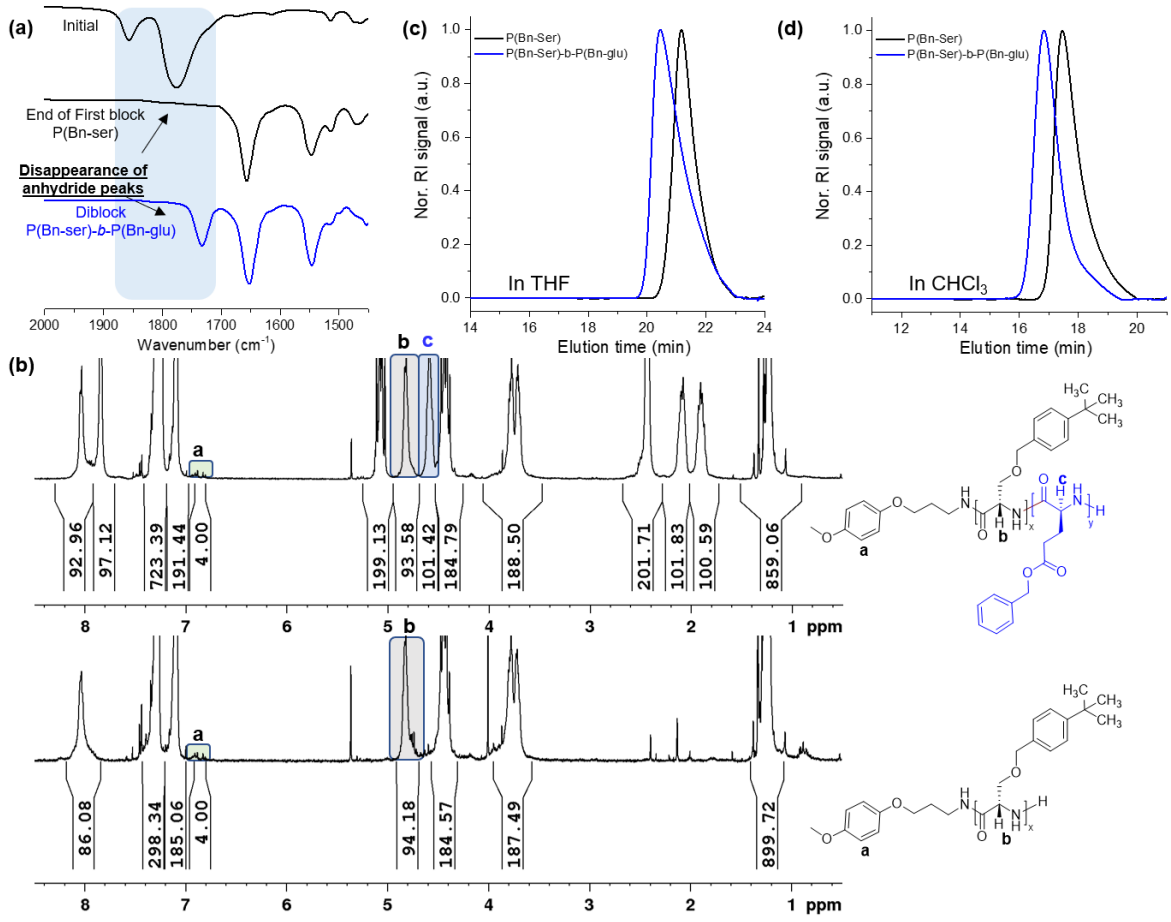

Figure 3.5*. Synthesis of P(Bn-ser)-b-P(Bn-glu). (a) FT-IR spectra of the polymer aliquots at initial, end of first block (macroinitiator) and di-block stage. (b) ^{1}H-NMR spectrum of macroinitiator P(Bn-ser) (bottom panel) and di-block copolymer P(Bn-ser)-b-P(Bn-glu) (top panel) in $CDCl_3$+CF_3COOH. SEC for P(Bn-ser) macroinitiator and P(Bn-ser)-b-P(Bn-glu) diblock copolymer (c) in THF and (d) in $CHCl_3$ respectively.*

The SEC analysis of macroinitiator P(Bn-ser) and di-block copolymer P(Bn-ser)-*b*-P(Bn-glu) was carried out in both THF and $CHCl_3$ as eluents and the corresponding SEC traces are given in Figure 3.5c and 3.5d respectively. SEC traces for both macroinitiator and diblock copolymer exhibited monomodal peaks with narrow dispersity (Đ) and the diblock copolymer appeared at low retention time compared to macroinitiator which clearly indicates the formation of diblock copolymers in controlled manner. From SEC in THF, the molecular weight and dispersity (Đ) were determined based on polystyrene standards using differential refractive index (DRI) detector signals and the values are reported in table 3.1. It was found that, the molecular weight determined from SEC analysis in THF was much lower than that determined by ^{1}H-NMR, this could be attributed to difference in

hydrodynamic volume of polypeptide and polystyrene. On the other hand, the absolute molecular weight estimated using triple detector setup comprising of RALS, LALS and RI detectors for SEC in $CHCl_3$ was found to be in good correlation with ^{1}H-NMR based molecular weight and the data is given in table 3.1. The *t*-butyl benzyl ether and benzyl ester units in diblock copolymer P(Bn-ser)-*b*-P(Bn-glu) were removed using HBr in acetic acid and subsequent basification resulted in the formation of sodium salt of P(ser)-*b*-P(glu) as shown in scheme 3.2. The disappearance of aromatic protons and benzylic proton in ^{1}H NMR as shown in Figure 3.6 clearly indicates the complete deprotection. Also, ^{1}H NMR of deprotected polymer reveals that upon deprotection, the ratio of serine and glutamate units is still remained 1:1 (e.g., see protons **b** and **c** in Figure 3.6) indicating the backbone was intact upon deprotection. After deprotection of P(Bn-ser)-*b*-P(Bn-glu) under acidic conditions, the poly(serine)-b-poly(glutamate) is initially isolated as poly(serine)-*b*-poly(glutamic acid), i.e., side chain of glutamic acid component exists in the form of carboxylic acid moiety and in this form it is insoluble in water at neutral pH. The obtained poly(serine)-*b*-poly(glutamic acid) has to be dissolved in aq. $NaHCO_3$ solution and after dialysis it results in aqueous solution of sodium salt of poly(serine)-*b*-poly(glutamic acid). The sodium salt of poly(serine)-*b*-poly(glutamic acid) [or simply, P(ser)-*b*-P(glu)] can be isolated in powder form after lyophilization of dialyzed solution and the resultant P(ser)-*b*-P(glu) is highly water soluble (checked up to 30 mg/mL). Additionally, selective deprotection of benzyl ester over benzyl ether was attempted using base hydrolysis but the resultant polymer P(Bn-Ser)-b-P(glu) was insoluble in water (even under alkaline conditions), hence not suitable for biological applications.

Table 3.1. *Details of degree of polymerization, NMR Molecular weight and SEC molecular weight for synthesis of P(Bn-ser)-b-P(Bn-glu) and P(Bn-ser)-r-P(Bn-glu).*

Entry	Polymer[a]	n (NMR)[b]		M_n NMR (g/mol)[e]	SEC in THF[f]			SEC in $CHCl_3$[g]			Conv (%)[h]
		x[c]	y[d]		M_n (g/mol)	M_w (g/mol)	Đ	M_n (g/mol)	M_w (g/mol)	Đ	
1	P(Bn-ser)	94	-	21900	5900	6500	1.1	23100	23800	1.03	> 99
2	P(Bn-ser)-*b*-P(Bn-glu)	94	101	44000	6700	9400	1.4	35300	36400	1.03	> 99
3	P(Bn-ser)-*r*-P(Bn-glu)	94	104	44700	9600	12800	1.3	36300	38100	1.05	> 99

[a] Polymerization was carried out in $CHCl_3$ using insitu generated N,N-dimesytlene substituted carbene as a catalyst and 3-(4-methoxyphenoxy)propan-1-amine (**13**) was used as an initiator while maintaining the concentration of monomer [M] to 0.2 M. The monomer/Initiator ratio was maintained as 100 in the feed for both blocks. [b] Degree of polymerization (n) was determined from ^{1}H-NMR [c] x = degree of polymerization for serine segment in polymer. [d] y = degree of polymerization for glutamate segment in polymer. [e] Sum of M_n (NMR) for all both blocks wherein, M_n = (n × repeating unit mass). [f] molar mass and dispersity (Đ) were determined by size exclusion chromatography in THF at 25 ºC with respect to polystyrene standards. [g] molar mass and dispersity (Đ) were obtained by size exclusion chromatography in $CHCl_3$ at 25 ºC using triple detector (RI, RALS and LALS) setup. [h] Determined using FT-IR spectroscopy from integration of NCA anhydride peak at ~1780 cm^{-1} at the beginning and end of reaction.

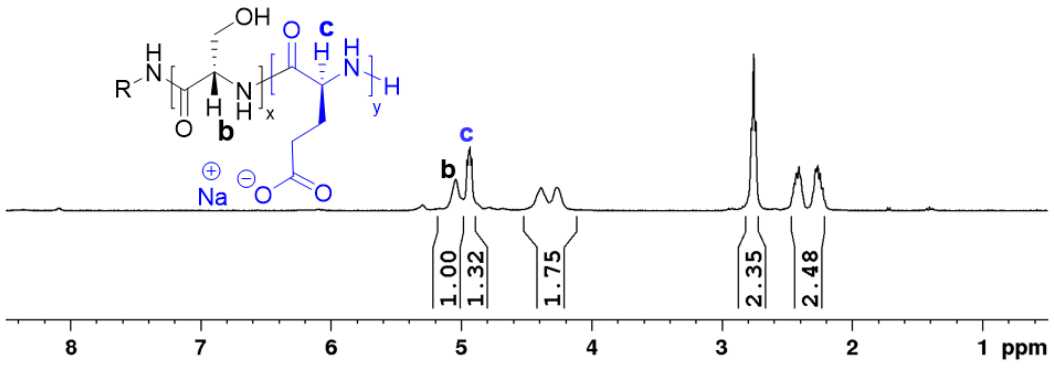

***Figure 3.6**. [1]H-NMR of deprotected di-block copolymer P(ser)-b-P(glu) in TFA-D.*

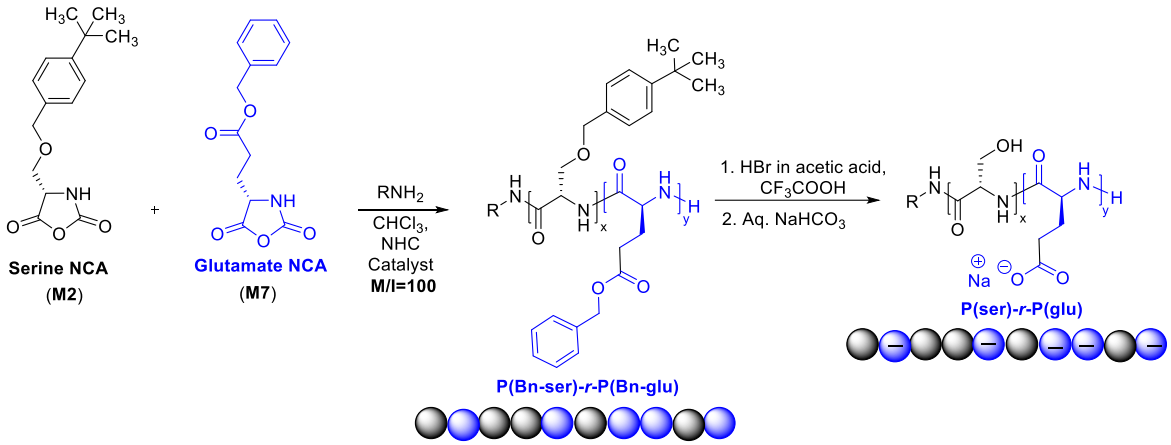

***Scheme 3.3**. Synthesis of Poly(serine)-r-poly(glutamate)*

In the similar manner, the random copolymer Poly(L-serine)-*r*-poly(L-glutamate) (P(ser)-*r*-P(glu)) is synthesized from one pot ROP of monomers **M2** and **M7** followed by deprotection as shown in scheme 3.3. The complete consumption of monomers was confirmed by FT-IR as shown in Figure 3.7a and the degree of polymerization (n) was found to be 94 and 99 for serine and glutamate component respectively based on ^{1}H-NMR analysis as shown in Figure 3.7b (bottom panel) which is excellent for M/I = 100 (for both monomers) in the feed. The SEC chromatogram of random copolymer in THF and $CHCl_3$ as eluent was monomodal and given in Figure 3.7c and 3.7d respectively. In this case also, the molecular weight obtained from SEC analysis in THF was much lower than that obtained by ^{1}H-NMR. On the other hand, the absolute molecular weight estimated using triple detector setup for SEC in $CHCl_3$ was found to be in good correlation with molecular weight determined by ^{1}H NMR and the data is given in table 3.1. The molecular weights of both di-block copolymer and random copolymer was almost similar hence these two polymers can be compared for their properties effectively. At the end, the deprotection of random

copolymer was carried out using HBr in acetic acid to obtain P(ser)-*r*-P(glu) and ^{1}H-NMR of deprotected random copolymer shown in Figure 3.7b (top panel) confirms the complete deprotection. The ratio of serine and glutamate in the deprotected random copolymer was found to be 1:1 as determined by ^{1}H NMR given in top panel of Figure 3.7b, indicating the backbone is intact after deprotection.

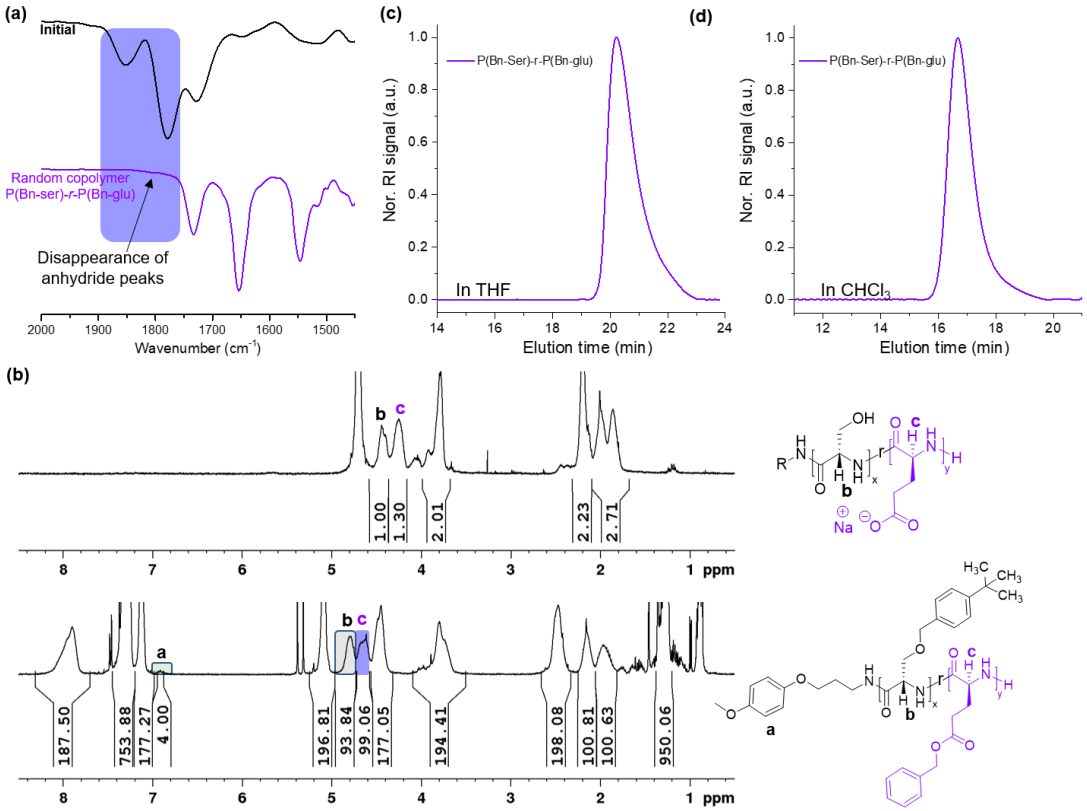

Figure 3.7*. Synthesis of P(ser)-r-P(glu) (a) FT-IR spectra of the polymer aliquots at initial and final random copolymer stage. (b) ^{1}H-NMR spectrum of protected random copolymer P(Bn-ser)-r-P(Bn-glu) in $CDCl_3$+CF_3COOH (bottom panel) and deprotected random copolymer P(ser)-r-P(glu) in D_2O. SEC for random copolymer P(Bn-ser)-r-P(Bn-glu) (c) in THF and (d) in $CHCl_3$ respectively.*

3.3.3. Secondary structure and Self-assembly of di-block copolymers

The CD spectroscopy was employed to validate the secondary structure of di-block copolymers. CD spectra of protected diblock copolymer P(Bn-ser)-*b*-P(Bn-glu) in HFIP is given in Figure 3.8a reveals the existence of double minimum at 216 nm and 206 nm and single maximum at 191 nm corresponding to α-helical conformation. Excellent water solubility of deprotected di-block copolymer P(ser)-*b*-P(glu) allowed us to carry out CD spectroscopic measurement in water and the spectra is given in Figure 3.8b. The CD spectra

of P(ser)-*b*-P(glu) shows single minimum at 220 nm and single maximum at 193 nm corresponding to β-sheet conformation. These astonishing results clearly illustrates that the bulky *t*-butyl benzene unit imparts helicity to polyserine (as shown in Chapter 2) and the helicity is retained upon further chain extension to block copolymer and upon removal of bulky *t*-butyl benzene unit, polyserine comes back to native β-sheet conformation and it overall determines the secondary structure of di-block copolymer. The deprotected polymer P(ser)-*b*-P(glu) was self-assembled by directly dissolving in water and subjected to dynamic light scattering (DLS) measurements to determine the size of resultant nano assemblies. It was found that the di-block copolymer can self-assembled in to tiny nanoparticles (< 50 nm) as shown in histogram given in Figure 3.8c. Zeta potential measurements were performed in order to determine the surface charge of the nano assemblies and it was found that these nano assemblies exhibit zetapotential of -50 mV as shown in Figure 3.8d. The high negative zeta potential of P(ser)-*b*-P(glu) was anticipated as the polymer was isolated in anionic form (sodium salt of glutamate). Based on these results, we envisioned that P(ser)-*b*-P(glu) could form nano-assemblies as represented in Figure 3.8e. The hydrophobic β-sheet domain of polyserine moiety would form core of nanoparticles and negatively charged hydrophilic polyglutamate moiety would project outward in random coil conformation.

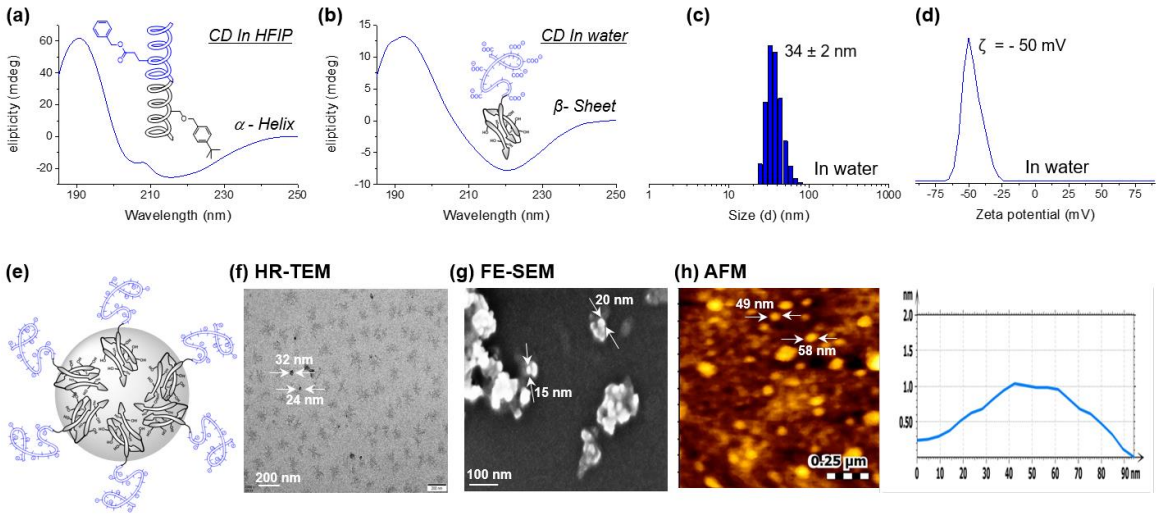

Figure 3.8*. (a) CD spectrum of P(Bn-ser)-b-P(Bn-glu) in HFIP, (b) CD spectrum of P(ser)-b-P(glu) in water, (c) DLS histogram of P(ser)-b-P(glu), (d) Zetapotential plot for P(ser)-b-P(glu), (e) Schematic representation of nano-assemblies formed by P(ser)-b-P(glu), (f) HR-TEM, (g) FE-SEM, (h) AFM images along with height profile of self-assembled P(ser)-b-P(glu) in water.*

To investigate the morphology of this block copolymer nano-assembly, the sample was analyzed by high resolution transmission electron microscope (HR-TEM), field

emission scanning electron microscope (FE-SEM), and atomic force microscope (AFM). HR-TEM image in Figure 3.8f gave clear evidence for the existence of spherical nano-assemblies with sizes around 30 nm. FE-SEM images of P(ser)-*b*-P(glu) exhibited spherical nanoparticle morphology with size ~ 15 - 20 nm (see Figure 3.8g). AFM image of the of P(ser)-*b*-P(glu) showed the spherical nanoparticle morphology with sizes around 80 nm (see Figure 3.8h). Overall, the sizes of the nanoparticles as measured from DLS were in good agreement with that obtained from HR-TEM, FE-SEM, and AFM analysis.

3.3.4. pH dependent self-assembly and secondary structure of di-block copolymers

In case of P(ser)-*b*-P(glu), serine block is expected to be insensitive to pH while glutamate block is known to undergo conformational changes depending upon pH.[231, 232] In acidic medium (pH ≤ 5), carboxylate group of glutamate will be protonated and remains in carboxylic acid form (-COOH) and known to adopt α-helical conformation. On the other hand, at pH ≥ 5, it remains in carboxylate anion (COO^-) form and known to exists in random coil conformation because of destabilization of α-helix due to charge repulsion. Based on this, we envisioned that, di-block copolymer P(ser)-*b*-P(glu) would form nano assemblies as represented in Figure 3.9a wherein, β-sheet core of the particle will be insensitive to pH changes while, outer glutamate component will change its conformation and surface charge depending on pH. To investigate the effect of pH on size of nanoparticles, DLS measurements were performed at various pH and the data is represented in Figure 3.9b. It was found that the size of nanoparticles does not changes significantly in the pH range of 4 to 9. On the other hand, the nano assemblies were destabilized in highly acidic pH (pH ~ 3) and polymer precipitation resulted in formation of large aggregates at pH ~ 3. The polymer precipitation is the result of dramatic reduction in water solubility of polymer due to charge neutralization at extremely acidic pH. The influence of pH on surface charge of nano assemblies was studied by carrying out zeta potential measurements at various pH and the data is given in Figure 3.9c. The zeta potential was almost zero at pH ~ 3 corresponding to charge neutralization as a result of complete protonation of carboxylate groups. Upon increase in pH from 4 to 9, the zetapotential of nano assemblies was found to become more negative with increase in pH due to deprotonation of carboxylic acid group. These important findings show that, pH can indeed have huge influence on size and surface charge of nano assemblies formed by block copolymer. To substantiate the influence of pH on secondary structure of di-block copolymer P(ser)-*b*-P(glu), we performed CD analysis at different pH

ranging from pH = 2 to pH = 9 and the spectra are shown in Figure 3.9d. As anticipated, the clear secondary structure transition from α-helix to random coil was observed upon increasing pH above 5. As mentioned earlier, the carboxylic acid pendant groups of glutamate exist in -COOH form at pH ≤ 5 and polymer adopts α-helical conformation. On the other hand, upon further increasing the pH above 5, pendent -COOH group in glutamate starts deprotonating and exists in COO^- form and due charge repulsion, helical conformation is destabilized and it adopts random coil conformation as shown in Figure 3.9a. These results clearly shows that the pH dependent conformational transition in polyglutamate regulate the overall secondary structure of di-block copolymer in buffer.

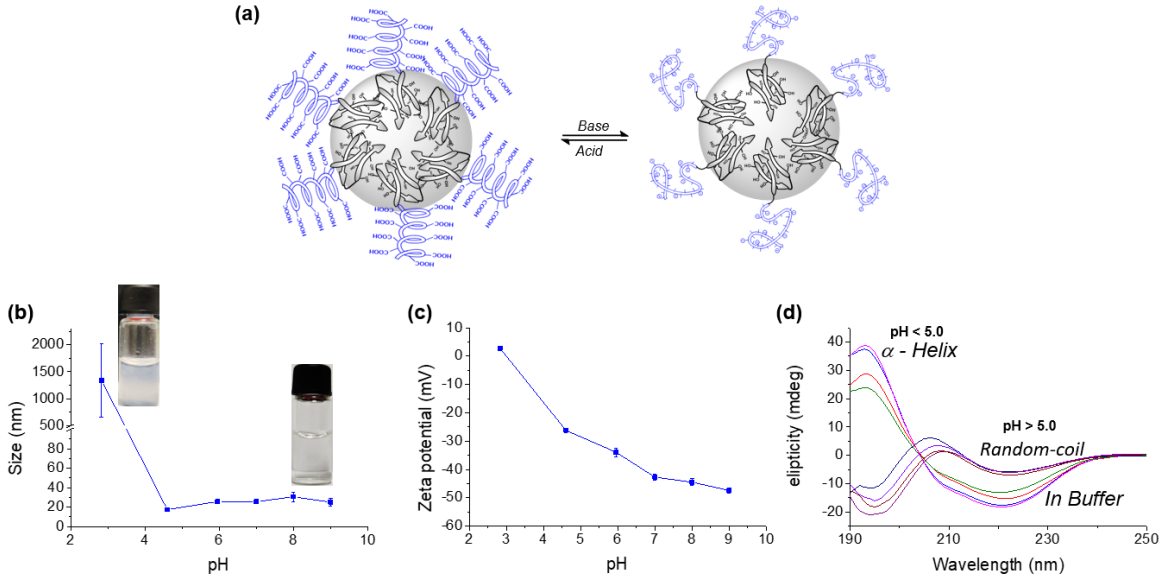

Figure 3.9*. (a) pH dependent changes in nano-assemblies of P(ser)-b-P(glu), (b) DLS size and (c) Zetapotential of P(ser)-b-P(glu) nano-assemblies in different pH, wherein pH of polymer solution was adjusted to desired pH using 0.1 N HCl or 0.1 N aq. NH_3. (d) CD spectra of P(ser)-b-P(glu) in Britton-Robinson buffer of different pH.*

3.3.5. Thioflavin T assay to support β-sheet assemblies

Thioflavin T (ThT) is a classical dye used to detect amyloid fibrils by fluorescence assay.[236, 237] ThT is a part of special class of fluorophores called molecular rotors wherein fluorescence arises due to restriction of bond rotation.[238, 239] The structure of ThT as shown in Figure 3.10a comprises of benzothiozole (BzT) ring and dimethyl aniline ring joined by C-C single bond. In case of free ThT in solution, free rotation of rings occurs about C-C single bond that leads to quenching of excited state generated by photoexcitation resulting in transition from luminescent locally excited state (LE) to non-luminescent twisted internal

charge transfer state (TICT) causing weak emission for free ThT. On the other hand, when ThT binds to β-sheet rich amyloid fibrils, the rotation about C-C single bond is hampered which preserves the excited state generate by photoexcitation and leads to strong fluorescence.[238, 240] Apart from fluorescence enhancement, ThT shows a dramatic red shift of the excitation (from 385 nm to 450 nm) and emission maxima (from 445 nm to 490 nm) when bound to amyloid fibrils.[240, 241] In addition to amyloid fibrils, ThT can become fluorescent in presence of many other amyloid-like fibrils from proteins like α-Synuclein, prion protein, tau proteins, etc.[242] The common feature among most of ThT binding proteins/peptides is the presence of β-sheet motif in them. In the present investigation, the di-block copolymer P(ser)-*b*-P(glu) forms nano-assemblies having β-sheet structure in water and we anticipated that ThT can bind to these β-sheet motif in di-block copolymer and that can result in enhancement in ThT fluorescence as shown in Figure 3.10b. To validate this hypothesis, we decided to perform ThT assay on di-block copolymer and the results are given in Figure 3.10c. The di-block copolymer P(ser)-*b*-P(glu) (1 mg/mL) was mixed with ThT (50 μM) and fluorescence spectrum was recorded by exciting at 444 nm. As anticipated, a very strong fluorescence signal was observed with an emission maximum of 490 nm which is characteristic of typical ThT fluorescence in β-sheet motifs. The photograph of ThT solution along with P(ser)-*b*-P(glu) under UV light is shown in Figure 3.10b and it indicates the existence of strong blue fluorescence. On the other hand, minimal fluorescence was observed for free ThT under similar conditions (see Figure 3.10a for photograph of free ThT solution in water under UV light). The fluorescence intensity for mixture of P(ser)-*b*-P(glu) and ThT was 15 times higher compared to free ThT indicating the binding of ThT to di-block copolymer. In the similar manner we performed ThT assay for polyglutamate, P(glu) and random copolymer P(ser)-*r*-P(glu) and we could not see substantial increase in ThT fluorescence and the fluorescence intensity was comparable to free ThT. Polyglutamate is known to form random coil structure and random copolymer P(ser)-*r*-P(glu) does not have organized β-sheet structures which makes both of them insensitive towards ThT. These astonishing results depicts that, perfectly ordered β-sheet motif is present in di-block copolymer P(ser)-*b*-P(glu) which makes it sensitive towards ThT fluorescence. To further validate the concept, ThT assay was performed on P(ser)-*b*-P(glu) (1 mg/mL, 43 μM) by varying ThT concentration from 5 μM to 100 μM and the data is given in Figure 3.10d. The fluorescence spectra of free ThT at various concentration was also measured as control. The fluorescence intensity at 490 nm was plotted against concentration of ThT and shown in Figure 3.10e. It is evident that for free ThT, only a minimal increase in fluorescence was

observed for increase in concentration. On the other hand, for P(ser)-*b*-P(glu) with various ThT concentration, the fluorescence intensity was found to increase with increase in concentration of ThT and it reached to maximum at 50 µM ThT concentration and later it remained almost constant with further increase in ThT concentration. The saturation in fluorescence intensity is observed at 50 µM ThT and 43 µM diblock copolymer indicating the ~ 1:1 binding stoichiometry of polymer and ThT.

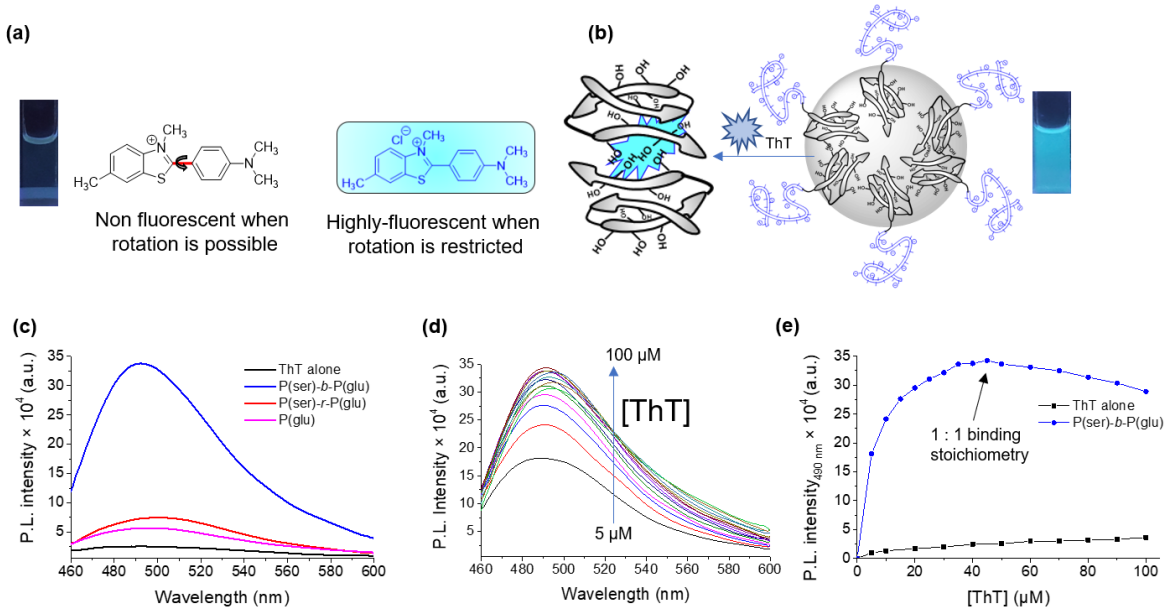

Figure 3.10*. ThT assay (a) Structure of ThT. The C-C single bond about which the rotation of rings is possible is shown in red and the photograph of aqueous ThT solution under UV is also shown. (b) Anticipated interaction of ThT with nano assemblies of P(ser)-b-P(glu), (c) Fluorescence spectra for free ThT (50µM), P(ser)-b-P(glu) (1 mg/mL) + ThT (50µM), P(ser)-r-P(glu) (1 mg/mL) + ThT (50µM) and P(glu) (1 mg/mL) + ThT (50µM). (d) Fluorescence spectra for various concentration of ThT (5 to 100 µM) with fixed concentration of polymer, [P(ser)-b-P(glu)] = 1 mg/mL. (e) PL intensity at 490 nm vs concentration of ThT for [P(ser)-b-P(glu) (1 mg/mL) + ThT] and free ThT. For all fluorescence measurements, excitation wavelength of 444 nm was used.*

In order to further substantiate the interaction of ThT with di-block copolymer P(ser)-*b*-P(glu), the ThT fluorescence assay was performed at fixed concentration of ThT (50 µM), while the concentration of P(ser)-*b*-P(glu) was varied from 0.03 mg/mL to 1 mg/mL and the data is shown in Figure 3.11 It was observed that, in the beginning for very low concentration of polymer (0.03 mg/mL to 0.14 mg/mL) the emission maxima was observed at 557 nm corresponding to ThT excimer emission.[243] Upon further increase in polymer concentration, the emission intensity at 557 nm started to decrease and increase in

emission intensity at 490 nm corresponding to monomeric ThT emission was observed. The plot of emission intensity at 490 nm against the concentration of polymer was found to be linear in nature, indicating that ThT fluorescence increases linearly with increase in polymer concentration.

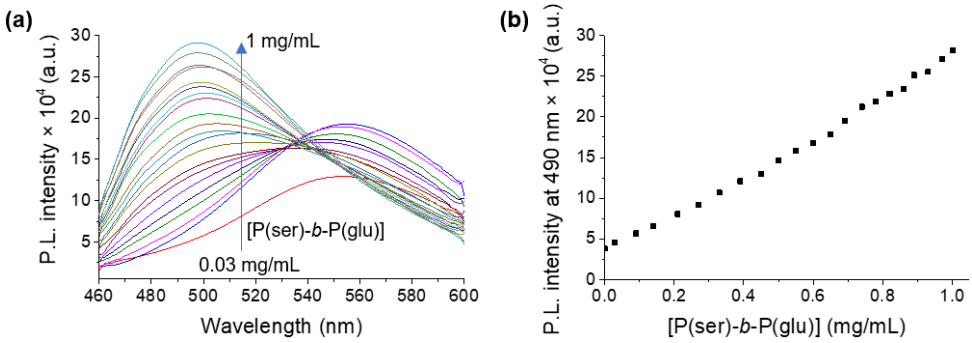

Figure 3.11. *(a) Fluorescence spectra for ThT (50 µM) with various concentration of polymer, [P(ser)-b-P(glu)]* = 0.03 to 1.00 mg/mL. *(b) PL intensity at 490 nm vs concentration of P(ser)-b-P(glu) for [ThT (50 µM) + polymer P(ser)-b-P(glu) (0.03 mg/ml to 1.00 mg/mL)]. Here, excitation wavelength of 444 nm was used for fluorescence measurements.*

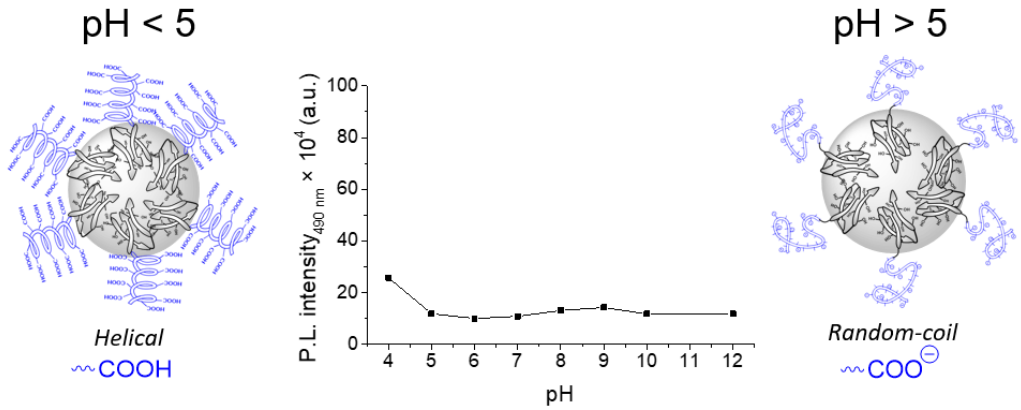

Figure 3.12. *PL intensity at 490 nm vs pH for [ThT (50 µM) + polymer P(ser)-b-P(glu) (0.5 mg/mL) in buffers of various pH]. Here, excitation wavelength of 444 nm was used for fluorescence measurements. Britton-Robinson buffers of different pH were used for this assay.*

To study the effect of pH on polymer-ThT interactions, we performed ThT assay in buffers of various pH for fixed concentration of di-block copolymer P(ser)-*b*-P(glu) (0.5 mg/mL) and ThT (50 µM) and the data is given in Figure 3.12. It was observed that the

fluorescence intensity at 490 nm was almost constant with respect to pH indicating that pH has no role on ThT-polymer interactions. In nano assemblies of P(ser)-*b*-(glu), only the outer core of glutamate will undergo conformational transitions depending on pH while the polyserine core in β-sheet conformation will be unchanged with respect to pH (as shown previously in Figure 3.9d). The ThT fluorescence is associated with interaction of ThT with β-sheet motif in the polymer and as the β-sheet core in P(ser)-*b*-(glu) diblock copolymer remains unchanged with respect to pH, the ThT fluorescence remains constant for wide range of pH.

3.3.6. Drug encapsulation for biomedical applications

The di-block copolymer P(ser)-*b*-P(glu) was subjected to encapsulation of anticancer drug doxorubicin (DOX) by dialysis method. DOX is purchased as hydrochloride salt (DOX.HCl) which is hydrophilic molecule and hence, difficult to load in hydrophobic core of micelle. As a result, DOX.HCl was neutralized using triethyl amine before loading. The solution of di-block copolymer and DOX in a mixture of DMSO and water (1: 4 v/v) was dialyzed against miliQ water for 48 h with the help of semi-permeable membrane of MWCO = 3500 D. The efficient removal of unencapsulated DOX, DMSO, triethyl amine and its hydrochloride salt was assisted by frequent change of water for 48 h. After dialysis, solution was filtered through whatmann filter paper and stored at stored at 4 °C for subsequent studies. The photograph of the vial containing the DOX loaded polymer sample is shown in Figures 3.13a. UV-Visible spectroscopy was employed for determination of drug loading content (DLC) and it was found that the di-block copolymer was able to load 6.1 % DOX with drug loading efficiency (DLE) of 30.5 %. To measure the size of DOX loaded nano-assemblies they were subjected to DLS measurements and the histogram is given in Figure 3.13b. The histogram shows monomodal distribution and average size of 52 ± 8 nm. The surface charge of DOX loaded nano-assemblies was determined by zeta potential measurements and it was found to be -30.1 mV as shown in Figure 3.13c. The morphology of DOX-loaded polymer nano particles was studied by AFM and FE-SEM analysis as shown in Figure 3.13d and 3.13e respectively and they were found to be spherical nano particles. The size of DOX loaded nano particles from FE-SEM and AFM analysis were matching close to size determined by DLS. The stability of DOX-loaded polymer sample was studied by release studies under physiological conditions (in PBS pH 7.4 at 37°C) and also in pH 5 at 37°C. The DOX-loaded polymer solution was taken in semi-permeable membrane (MWCO = 1000) and incubated at 37°C in PBS (pH 7.4) or pH 5 buffer. In order to estimate

the amount of DOX released, the reservoir solution was subjected to absorbance measurements at various time intervals. The % DOX-released from nano-assemblies is plotted against time and shown in Figure 3.13f and 3.13g. It was found that, DOX-loaded polymer nano assemblies are very stable under physiological conditions as well as in pH 5 as only < 20 % DOX release was observed which makes them suitable for biomedical applications. The release studies by using protease enzymes will be done in subsequent future to validate the enzymatic biodegradation of polymer.

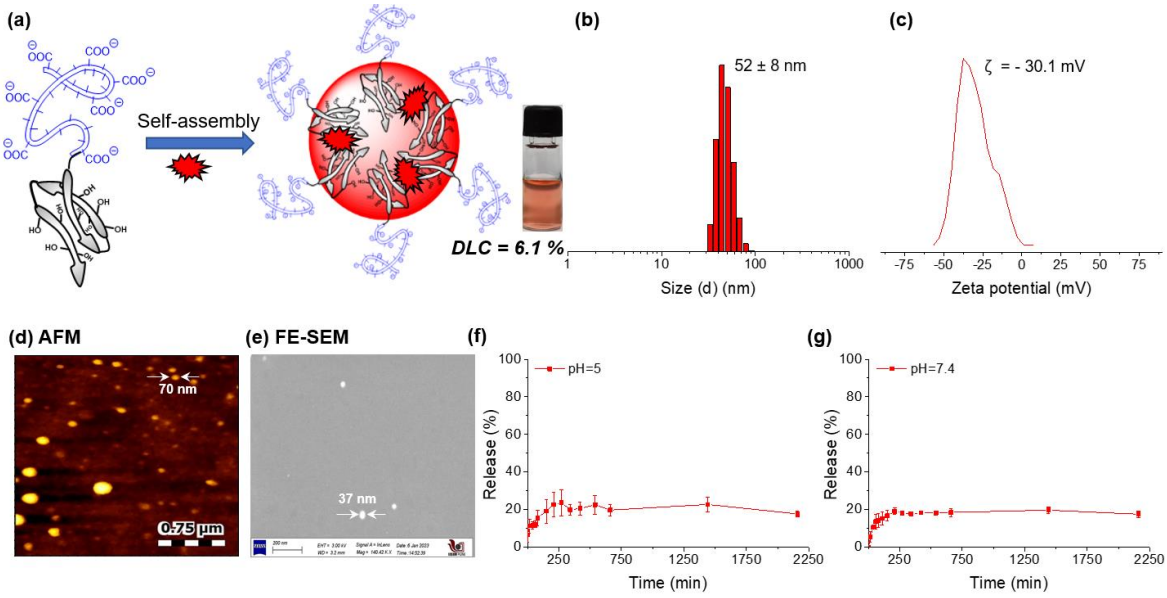

Figure 3.13*. (a) Schematic representation for encapsulation of DOX in di-block copolymer. The photograph of DOX-loaded polymer sample is shown. (b) DLS histogram, (c) Zetapotential plot, (d) AFM image for DOX-loaded polymer sample. (e) FE-SEM image for DOX-loaded polymer sample, Cumulative release of DOX (f) in pH 5 and (g) in PBS, pH 7.4 at* 37°C.

3.3.7. Cell viability and cellular uptake

The cytotoxicity of nascent polymer nanoparticles, DOX loaded polymer nanoparticles and free DOX was studied in wild type MEF cell line by MTT assay. The nascent di-block copolymer P(ser)-*b*-(glu) was non-toxic to cells up to 100 µg/mL concentration as shown in Figure 3.14a. For free DOX, the IC_{50} value was found to be < 0.1 µg/mL and nearly complete killing was observed at 1 µg/mL as shown in Figure 3.14b. In case of DOX-loaded polymer sample, IC_{50} value was found to be ~ 0.2 µg/mL and ~80% killing was observed at 1 µg/mL as given in Figure 3.14b. The cellular uptake of the DOX-loaded polymer nanoparticles and free DOX was investigated in wild type MEF cell line with the help of confocal laser scanning microscopy (CLSM). The CLSM images for free DOX, DOX-loaded polymer nanoparticles are given in Figure 3.14c. The DAPI stained nuclei and DOX (or DOX-loaded polymer nanoparticles) were visualized at blue (λ_{exc} = 405 nm) channels and red (λ_{exc} = 488 nm) channel respectively. In case of free DOX treated sample, the red fluorescence of DOX was predominately observed from the nucleus and partially from the cytoplasm (first panel in Figure 3.14c). In the merged image, it showed a magenta colour in nuclear region due to overlapping of blue and red fluorescence corresponding to DAPI stained nucleus and DOX respectively. This result indicates the accumulation of free DOX in nucleus of cell and it is not surprising since, the free DOX is DNA intercalator and binds DNA. In case of DOX loaded polymer nanoparticles, strong red fluorescence was observed mostly in cytoplasm as shown in second panel of Figure 3.14c which clearly indicates the DOX-loaded polymer nano-assembly is intact and DOX is not released much inside cell in 4h. In order to quantify the uptake of free DOX and DOX loaded polymer nanoparticles, the mean CTCF (corrected total cell fluorescence) values were estimated for three different regions of interest (ROIs) from each image and these values were in plotted in the form of histogram in Figure 3.14d. Based on these CTCF measurements, it is clearly evident that the cellular uptake of DOX-loaded nanoparticles is nearly 4 fold higher compared to free DOX which makes di-block copolymer P(ser)-*b*-(glu) suitable for biomedical applications.

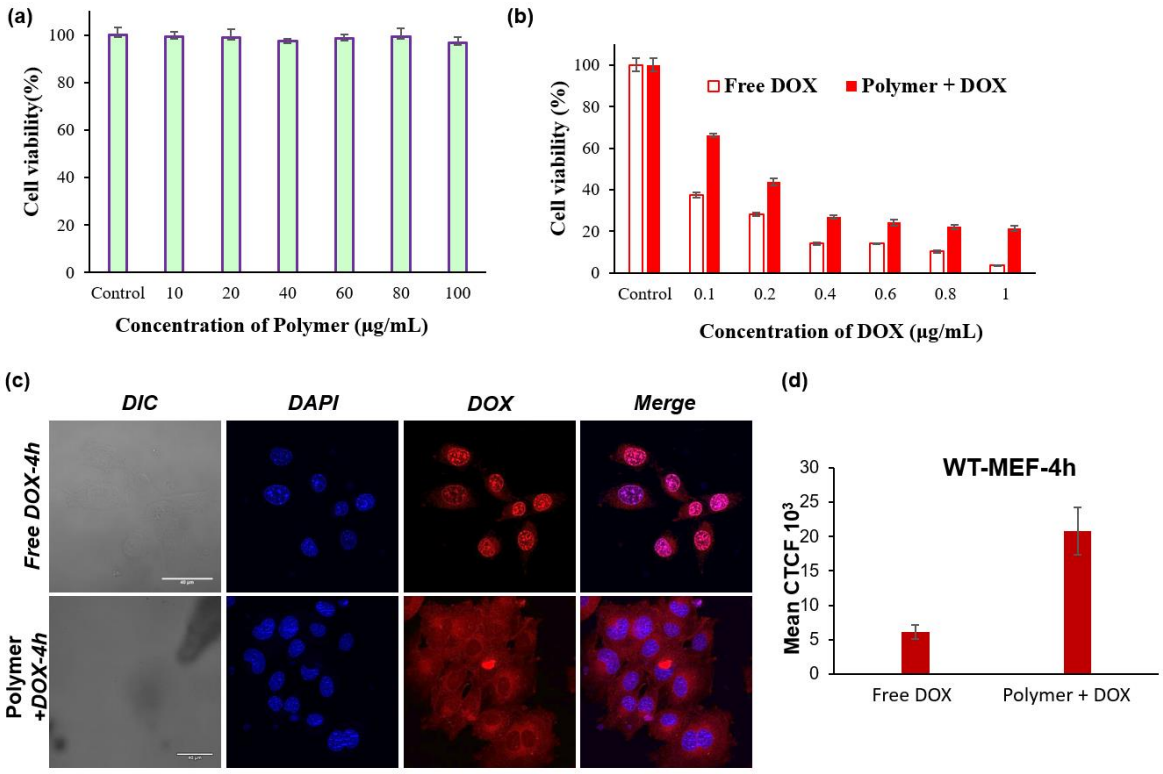

Figure 3.14. *(a)Plot showing the cytotoxicity assay of P(ser)-b-P(glu) in wild type MEF cell line. (b) Plot showing the cytotoxicity assay of DOX loaded P(ser)-b-P(glu) and free DOX in wild type MEF cell line. (c) CLSM images of wild type MEF cells incubated with DOX alone (in first panel) and dox loaded P(ser)-b-P(glu) (in second panel). The nucleus of cells was counterstained with DAPI and visualised in blue channel (labelled as DAPI in figure). The red channel (labelled as DOX in image) was used to visualise DOX fluorescence. (d) CTCF corresponding to CLSM images of wild type MEF cells incubated with free DOX and dox loaded P(ser)-b-P(glu) (Note: The data was provided by Shahid Khan Pathan from our lab)*

In the similar manner, cytoxicity and cellular uptake studies were performed in SKOV3 ovarian cancer cell line (see Figure 3.15) and the results were almost similar to that in wild type MEF cell line. The nascent polymer was found to be non-toxic to SKOV3 cells while free DOX exhibited ~ 70% cellular killing at 1 µg/mL concentration and the activity of DOX towards SKOV3 cells was retained in polymer-DOX nano-formulation (see Figure 3.15a). In case of the cellular uptake studies in SKOV3 cell line, free DOX was mostly accumulated in the nucleus while polymer-DOX nano-formulation was mostly localised in cytoplasm (see Figure 3.15b). Based on CTCF measurements, the uptake of DOX loaded

nanoparticles was slightly higher till 4 h incubation but in 8 h, both free DOX and DOX-loaded nanoparticles exhibited similar uptake (see Figure 3.15c).

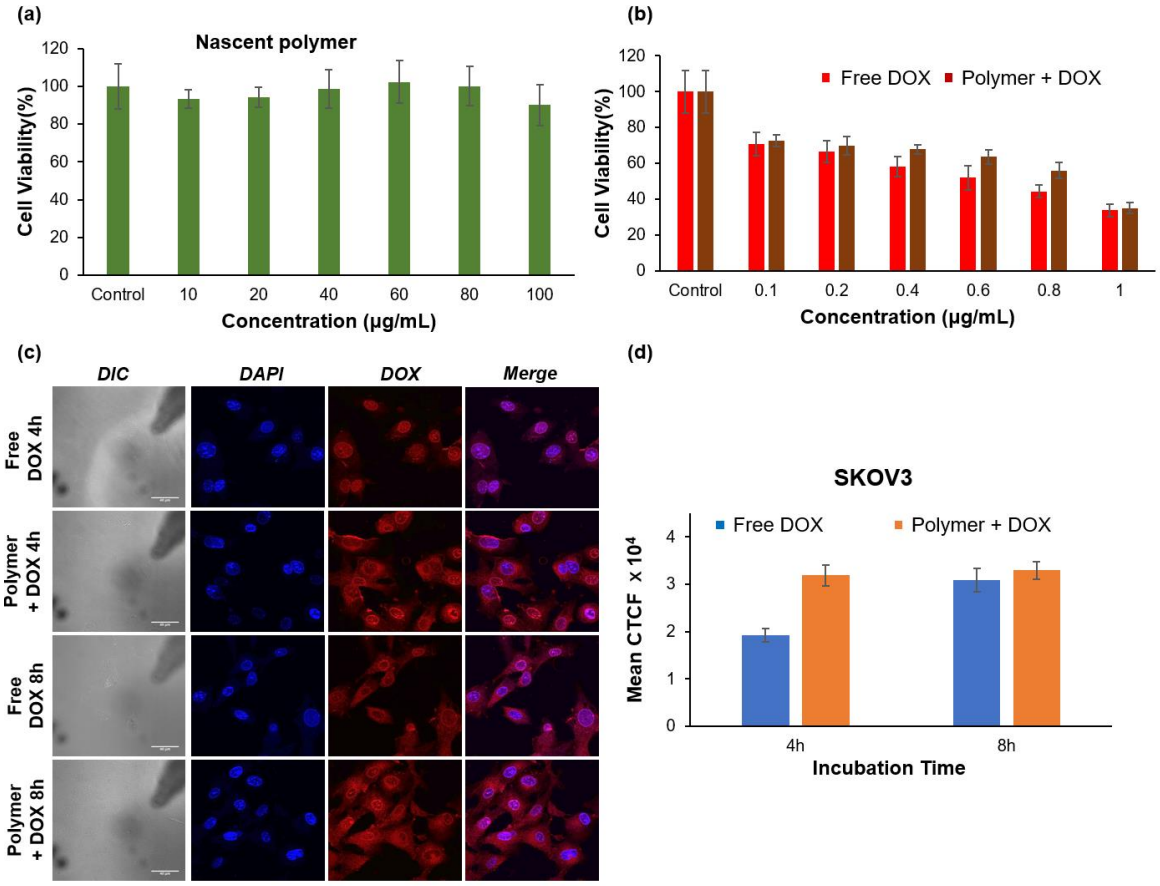

Figure 3.15. *(a)Plot showing the cytotoxicity assay of P(ser)-b-P(glu) in SKOV3 ovarian cancer cell line. (b) Plot showing the cytotoxicity assay of DOX loaded P(ser)-b-P(glu) and free DOX in SKOV3 ovarian cancer cell line. (c) CLSM images of SKOV3 ovarian cancer cells incubated with DOX alone for 4 h (in first panel, from top), dox loaded P(ser)-b-P(glu) for 4 h (in second panel, from top), DOX alone for 8 h (in third panel, from top) and dox loaded P(ser)-b-P(glu) for 8 h (in fourth panel, from top). The nucleus of cells was counterstained with DAPI and visualised in blue channel (labelled as DAPI in figure). The red channel (labelled as DOX in image) was used to visualise DOX fluorescence. (d) CTCF corresponding to CLSM images of SKOV3 ovarian cancer cells incubated with free DOX and dox loaded P(ser)-b-P(glu) for 4h and 8 h. (Note: The data was provided by Shahid Khan Pathan from our lab)*

3.3.8. Hemolysis assay of di-block copolymer

One of the crucial pre-requisites for a nano-formulation is non hemolytic nature, i.e. compatibility towards red blood cells (RBCs). To investigate this, we subjected the di-block copolymer P(ser)-*b*-P(glu) for hemolysis assay. In hemolysis assay, polymer sample is incubated with RBC solution in PBS and then centrifuged to separate RBCs. If sample is non-hemolytic then RBCs remain intact and a red pellet is formed at the bottom and supernatant liquid is colourless. On the other hand, if RBCs breaks due to polymer interaction, the hemoglobin comes out from RBCs and upon centrifugation red colour is observed in supernatant liquid and this rupture of RBCs (erythrocytes) is quantified by measuring the amount of hemoglobin released based on absorbance measurement of supernatant liquid. In this case for hemolysis assay, PBS buffer was used as a negative control while Triton X-100 was positive control. Triton X-100 is nonionic surfactant and causes lysis of RBCs due to osmosis, as a result 100 % hemoglobin is released which is evident from red colored plasma (see Figure 3.16a last centrifuge tube). In the presence of PBS and the di-block copolymer P(ser)-*b*-P(glu), the RBCs remained stable and settled at bottom in the form of pellet after centrifugation post incubation while no significant red color was observed in the plasma as shown in Figure 3.16a (first two centrifuge tubes). The % hemolysis is plotted in the form of histogram and shown in Figure 3.16b which clearly shows that the di-block copolymer P(ser)-*b*-P(glu) is non-hemolytic to RBCs.

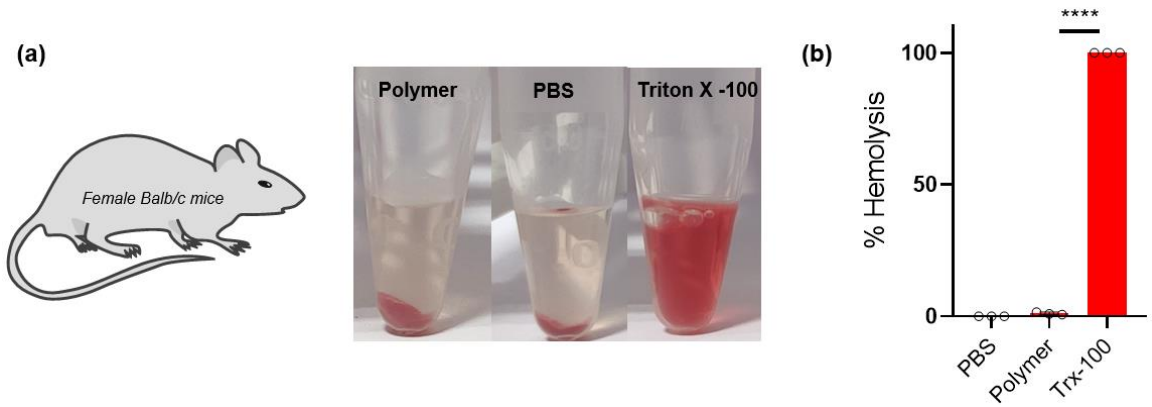

Figure 3.16 *Hemolysis assay. (a) Photographs of centrifuge tubes after centrifugation post incubation of sample with RBC solution. Appearance of intact pellet indicate RBC stability. (b) Plot showing % hemolysis for polymer (P(ser)-b-P(glu) along with PBS (negative control) and 1% Triton X-100 (positive control), (****P<0.0001) each point represents mean* ± SEM, n=3). *(Note: The experiment was performed with help of Ruma Ghosh and Shahid Khan Pathan).*

3.3.9. Encapsulation of IR-780 dye and biodistribution studies by *in vivo* imaging

NIR dyes are the fluorophores having excitation wavelength in the near-infrared region. NIR dyes are extensively used for *in vivo* imaging studies due to greater tissue penetration ability of IR radiations compared to UV-visible light, and negligible cellular autofluorescence for excitation in the near-infrared region. In order to utilize our di-block copolymer scaffold for *in vivo* imaging and to study it's *in vivo* biodistribution we encapsulated NIR dye called IR-780 in our polymer scaffold as shown in Figure 3.17a. The encapsulation of dye was done in the similar manner as that for DOX and DLC was found to be 1.6 % which is quite great for *in vivo* imaging applications. The photograph of IR-780 loaded polymer sample is given in Figure 3.17a. The DLS measurements of IR-780 loaded nanoparticles revealed the existence of nano-assemblies of sizes ~ 37 nm which is similar to nascent nanoparticle (see Figure 3.17a). For *in vivo* imaging and biodistribution studies, three mice were used in each experiment (and the experiment was performed in triplicate), one mouse was injected with IR-780 loaded polymer nanoparticles, second mouse was injected with free IR-780 dye while as a control, third mouse was injected with 1X PBS. The *in vivo* whole-body imaging was carried out at 4 h, 24 h and 48 h post injection using In Vivo Imaging System (IVIS, PerkinElmer) for biodistribution analysis and the images are given in Figure 3.17b for dorsal view. As expected, no fluorescence was observed for control mouse injected with PBS. On the other hand, the intense fluorescence was observed from the body of mouse injected with IR-780 loaded nanoparticles or free IR-780 dye. Quantification of this signal was carried out and as a measure of fluorescence readout signal, the average radiance was plotted against time and shown in Figure 3.17c. It was found that at all time points, signal was much higher for mouse injected with IR-780 loaded particles than that injected with free IR-780 dye, indicating the better uptake of IR-780 loaded nanoparticles compared to free IR-780 dye. In case of mouse injected with free IR-780 dye, the total radiance at 48 h was slightly less compared to that at 24 h, indicating the clearance of IR-780 dye from the body. On the contrary, the total radiance at 48 h and 24 h was same for mouse injected with IR-780 loaded polymer nanoparticle, indicating the greater *in vivo* stability of IR-780 loaded nanoparticles.

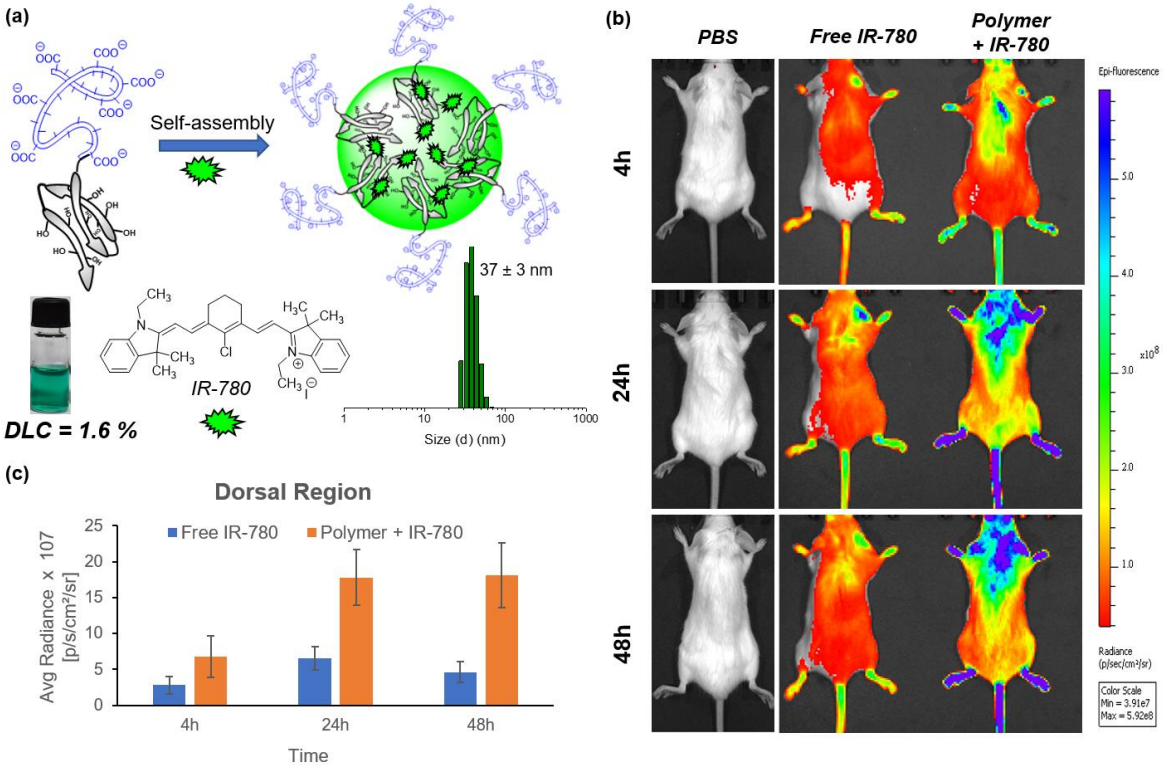

Figure 3.17. *(a) Schematic for encapsulation of IR-780 dye and DLS histogram for IR-780 loaded nanoparticles (b) Time-dependent IVIS images (dorsal view) of mice injected with PBS (control), free IR-780 dye and IR-780 loaded polymer nanoparticles. (c) Histogram representing amount of IR-780 dye (quantified as average radiance) at various time points in the body of mouse injected with free IR-780 and IR-780 loaded polymer nanoparticles. (Note: The data was provided by Shahid Khan Pathan and Uttareshwar Gavhane).*

For any drug formulation, circulation time in the blood stream is crucial factor. In order to study the ability of polymer nanoparticles to remain in the blood stream, the plasma samples were analysed by IVIS imaging. The blood sample of mouse was collected at 4h, 24h and 48 h post injection of IR-780-loaded nanoparticles or free IR-780 dye or PBS and plasma was isolated at each time point. The isolated plasma was then imaged in 96-well plate using IVIS to estimate the amount of IR-780 dye and the image is shown in Figure 3.18a. The fluorescence signal was quantified from plasma samples and plotted in the form of histogram for various time interval as shown in Figure 3.18b. It is quite evident that, IR-780 loaded nanoparticles were sustained for longer duration in blood compared to free IR-780 dye suggesting the better circulation time and *in vivo* stability of these nanoparticles.

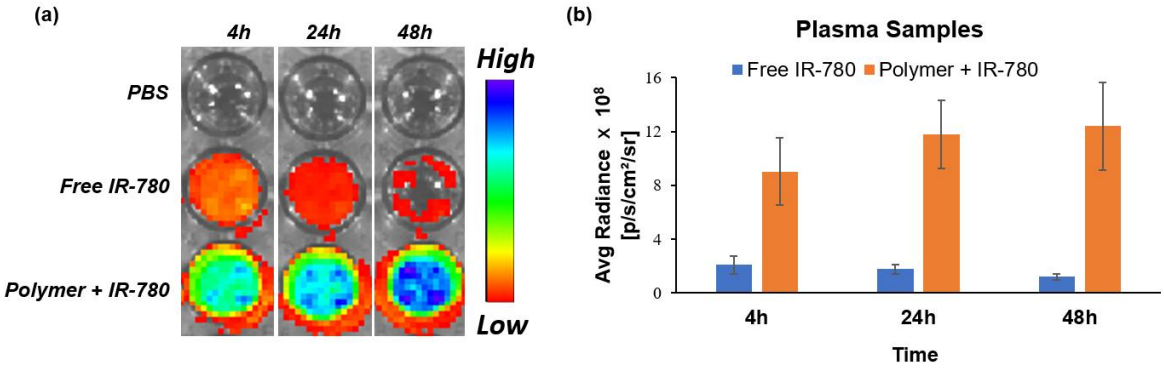

***Figure 3.18**. (a) Representative time-dependent photograph of the plasma samples captured in a 96-well plate using IVIS. (b) Histogram representing amount of IR-780 dye (quantified as average radiance) at various time points in plasma samples. (Note: The data was provided by Shahid Khan Pathan and Uttareshwar Gavhane)*

In order to study the biodistribution in more details, the injected mice were sacrificed post 48 h of injection and their organs were harvested. The collected organs were imaged using IVIS and the image is shown in Figure 3.19a. The quantification of fluorescence signal from image was carried out and represented in Figure 3.19b in the form of histogram. The fluorescence signals were much lower for free IR-780 injected mouse compared to that for IR-780 loaded polymer nanoparticles injected mouse reiterating the better *in vivo* stability of polymer nanoparticles. More fluorescence signal was observed from kidney, liver, lungs and heart indicating more uptake of IR-780 loaded nanoparticles in these organs.

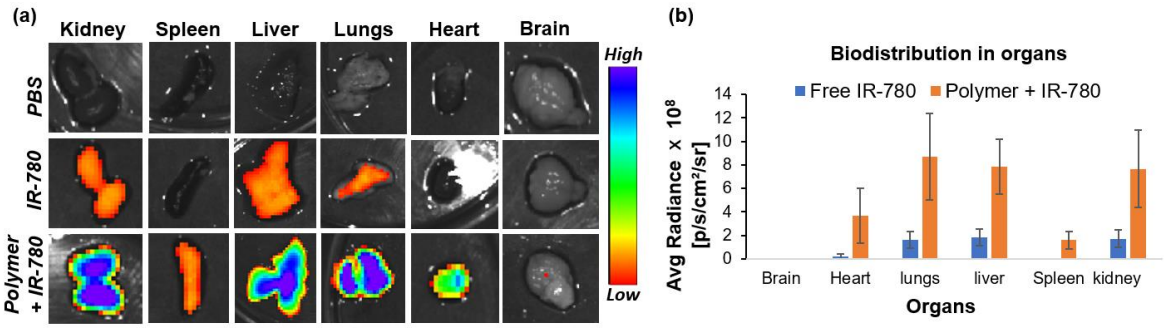

***Figure 3.19**. (a) Photographs of the various organs (harvested post 48 h injection) captured using IVIS. (b) Histogram representing amount of IR-780 dye (quantified as average radiance) in various organs. (Note: The data was provided by Shahid Khan Pathan and Uttareshwar Gavhane)*

These astonishing results are exciting and can open up new avenues for serine-based block copolymer architectures for biomedical applications. Currently, the serine based diblock copolymers with lysine diblock copolymers are being explored for antibacterial

research and results are seems to be promising. The other higher order architectures such as tri-block copolymer or multi diblock copolymers based on serine are being explored further for various applications.

3.5. Conclusion

In the nutshell, for the first-time serine based macroinitiator was used for ROP of glutamate NCA to make protected di-block copolymer P(Bn-ser)-*b*-P(Bn-glu). The polymerization occurred in controlled manner to yield resultant di-block copolymer with expected degree of polymerization and having narrow polydispersity. The resultant di-block copolymer was found to adopt α-helical conformation based on CD spectroscopic measurements. The deprotection of di-block copolymer P(Bn-ser)-*b*-P(Bn-glu) resulted in formation of highly water-soluble serine-glutamate diblock copolymer P(ser)-*b*-P(glu) that found to adopt β-sheet conformation in water and it was found to self-assemble in to tiny nanoparticles (~30 nm size). The morphology of P(ser)-*b*-P(glu) nano-assemblies were investigated by HR-TEM, FE-SEM and AFM analysis and it was found to exists in the form of spherical nanoparticles. The CD spectroscopic analysis at various pH revealed that the P(ser)-*b*-P(glu) nano-assemblies were found to undergo helix to coil conformational transition upon increasing pH above 5 which is characteristic of polyglutamate segment. The DLS analysis at various pH revealed that these nano assemblies were stable and retained their size in the pH range of 5 to 9. The surface charge of these nano assemblies was determined by zetapotential measurements and it was found to be highly negative (-50 mV) and also found to change with pH. The zetapotential value was nearly zero at pH = 3 and upon increasing the pH, zetapotential tend to become more negative. ThT fluorescence assay was performed to support the β-sheet structures in these assemblies and it was found that, P(ser)-*b*-P(glu) diblock copolymer enhances the ThT fluorescence by ~15 fold. While, random copolymer having same composition was unable to enhance ThT fluorescence indicating the importance of block copolymer architecture over random copolymers in terms of perfect self-assembly. The di-block copolymer P(ser)-*b*-P(glu) was found to be nontoxic to mammalian cells as well as it was non hemolytic to RBCs thus making it valuable candidate for biomedical applications. As a proof of concept, it was subjected to anticancer drug (DOX) encapsulation and found to encapsulate 6.1% DOX. The DOX loaded nanoparticles were stable in pH 5 and pH 7.4. The DOX loaded polymer nanoparticles were able to retain the DOX activity and were able to up taken by mammalian cells based on confocal microscopy studies. Furthermore, successful encapsulation of NIR dye (IR-780)

by polymer nano assemblies enabled us to study the *in vivo* biodistribution of polymer by IVIS imaging and these studies revealed that IR-780 loaded polymer nanoparticles were retained in the body of mice for longer duration compared to free IR-780 dye suggesting the better circulation time and *in vivo* stability of these nanoparticles.

Chapter 4

Ring Opening Polymerization-induced Self-assembly (ROPISA) Strategy for In-situ Cargoes Entrapment in Poly(L-serine) Nanoparticles

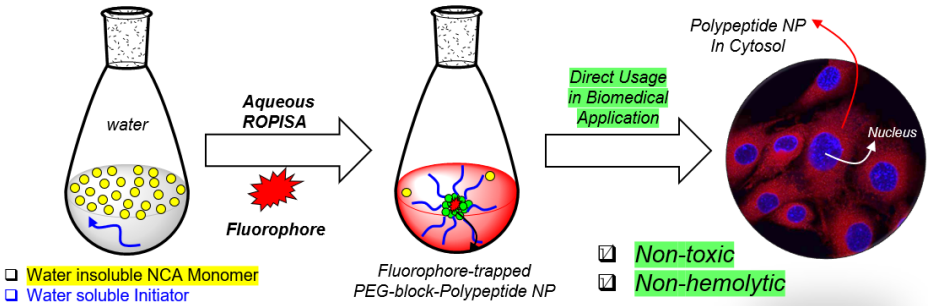

Abstract

Polymerization induced self-assembly (PISA) is very powerful way to make polymer nano objects in single step. In this chapter, the ring opening polymerization induced self-assembly (ROPISA) strategy was employed for polymerization of tert-butyl benzene functionalized NCA monomer using amine terminated PEG as a hydrophilic macroinitiator to obtain polypeptide di-block copolymer nano assemblies. The variation of M/I feed ratio revealed that, ROPISA of serine derived NCA monomer at M/I = 10 or 25 afforded stable polymer emulsions in the form of opalescent solutions. The amphiphilic di-block copolymers isolated from these stable polymer emulsions were exhibited monomodal, narrow dispersed SEC profile and their molecular weight was in close agreement with expected molecular weight indicating the controlled polymerization process. These polypeptide emulsions were composed of nano assemblies of sizes around 20 to 30 nm having spherical nano particle morphology. Five different dyes such as curcumin, HPTS, Nile red, rhodamine B and IR-780 were encapsulated in-situ by adding them in the beginning of ROPISA mediated polymerization to afford dye loaded polypeptide nanoparticle's emulsions in various colors. The nascent polypeptide nanoparticles were nontoxic and non-hemolytic in nature, while dye loaded polypeptide nanoparticles were also nontoxic to mammalian cells. As a proof of concept, the cellular uptake of Nile red loaded nanoparticles was shown using confocal microscopy. This newly developed insitu dye loading method during ROPISA process can open up new platform for polypeptide based nano formulations for biomedical applications.

4.1. Introduction

Molecular self-assembly is the fundamental phenomenon that occurs everywhere in our life.[244] The self-assembly is nothing but the reversible, spontaneous arrangements of molecules in to well defined ordered structure with the help of non-covalent interactions. The molecules which undergo self-assembly in water, usually consists of hydrophilic group and hydrophobic group and they are known as amphiphiles. The amphiphile can be small molecules like common detergents that we use (soap, SDS, etc.) or it can be a large macromolecule like protein or polymer. The polymer self-assembly is traditionally performed by post polymerization processing of synthesized polymer using various techniques such as nano-precipitation, dialysis method, film hydration method, etc.[245] and over so many decades these methods are in practice to prepare several kinds of nano objects such as micelles, vesicles, worms, rods, torroids, etc.[188, 244, 246] These traditional methods for polymer self-assembly are performed under dilute conditions (typically at < 1 wt% concentration) and this limitation keeps most of them away from commercial application since their industrial scalability is usually not cost effective. Addition to cost factor, these methods are sometimes sensitive to scale and that makes it extremely hard to scale up.

To overcome this issue, a method called polymerization induced self-assembly (PISA) is developed to directly create nano-objects from polymers during polymerization.[247] Typical PISA process in water involves the chain extension of soluble hydrophilic macroinitiator by insoluble hydrophobic monomer resulting in the formation of amphiphilic block copolymer that simultaneously grows and self-assembles in to various kinds of nano objects (see Figure 4.1 for schematic representation).[248] Interestingly, the reverse sequence PISA has been recently shown wherein, the water soluble hydrophilic block is propagated from initially formed hydrophobic block.[249] The PISA is possible in organic solvents also, wherein chain extension of soluble macroinitiator is carried out using monomer whose homopolymer is insoluble in the polymerization solvent.[250] PISA process was first reported in 2002[251] and the term PISA was coined for the first time in 2009.[252] PISA is extremely efficient polymerization process and can be performed at very high concentrations (up to 50 wt%) and hence easily scalable.[247]

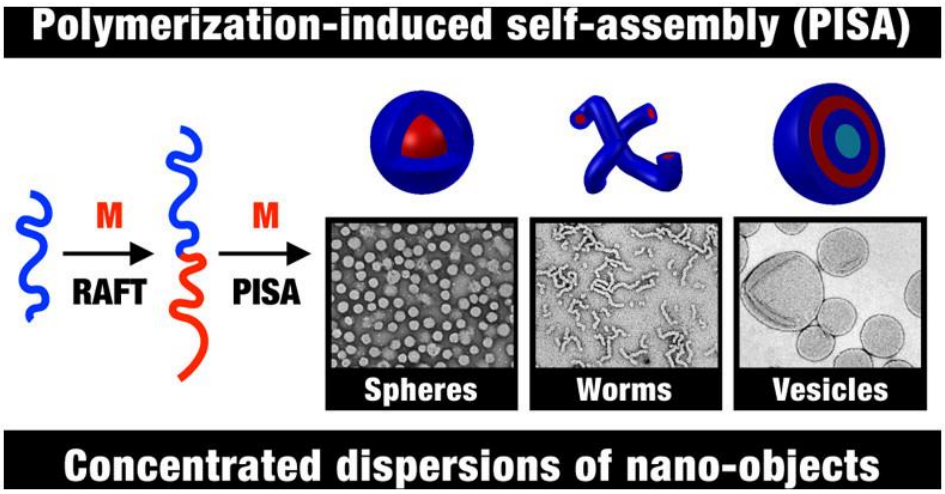

Figure 4.1. *Preparation of different nano-objects by PISA approach. (adapted from Sarah L. et al. Macromolecules* **2016**, *49*, 1985−2001).

The PISA process has been extensively utilized for radical polymerization of wide range of vinyl monomers in several solvents such as water,[253-257] ethanol,[258-260] n-alkanes,[261-264] ionic liquids,[265] silicon fluids[266] and supercritical CO_2[267, 268] and several polymer morphologies have been produced. Majority of PISA synthesis is based on thermally initiated controlled radical polymerization, however there has been growing interest in utilizing non-thermal ways[269] such as visible light,[270-274] ultrasound,[275, 276] micro waves,[277] or even enzymes[278] as an initiation trigger. Using PISA approach various stimuli responsive such as thermoresponsive,[262, 274, 279] pH responsive,[280-282] photo responsive,[273] and redox responsive[282, 283] block copolymer nano objects were prepared. Additionally, various hybrid materials such as organic-inorganic hybrid materials,[284] polymer-protein/peptide biohybrid nano objects[285-287] were prepared using PISA approach. Furthermore, the PISA process is now made automated by coupling it to high throughput robotics.[288, 289] Another notable advancement in PISA process is the use of flow chemistry for PISA.[290, 291] As a result of these recent developments in the PISA process in the past decade or so, the PISA has been a unique way to create materials that have been explored in catalysis, as an imaging agents, as lubricants, etc.[292, 293] The high solid content and in-situ self-assembly in PISA has paved a way for making nano formulations by in-situ encapsulation of drugs, dyes or even protein molecules[256] during polymerization process and these formulations were used extensively in biomedical applications.[294] Notable example among drug formulations made by PISA is in-situ encapsulation of a protein drug molecule (asparginase) for leukemia treatment (see

Figure 4.2) and the encapsulated protein was found to have greater proteolytic stability compared to unencapsulated protein as well as PEGylated protein indicating advantage of encapsulation over PEGylation of this protein therapeutic.

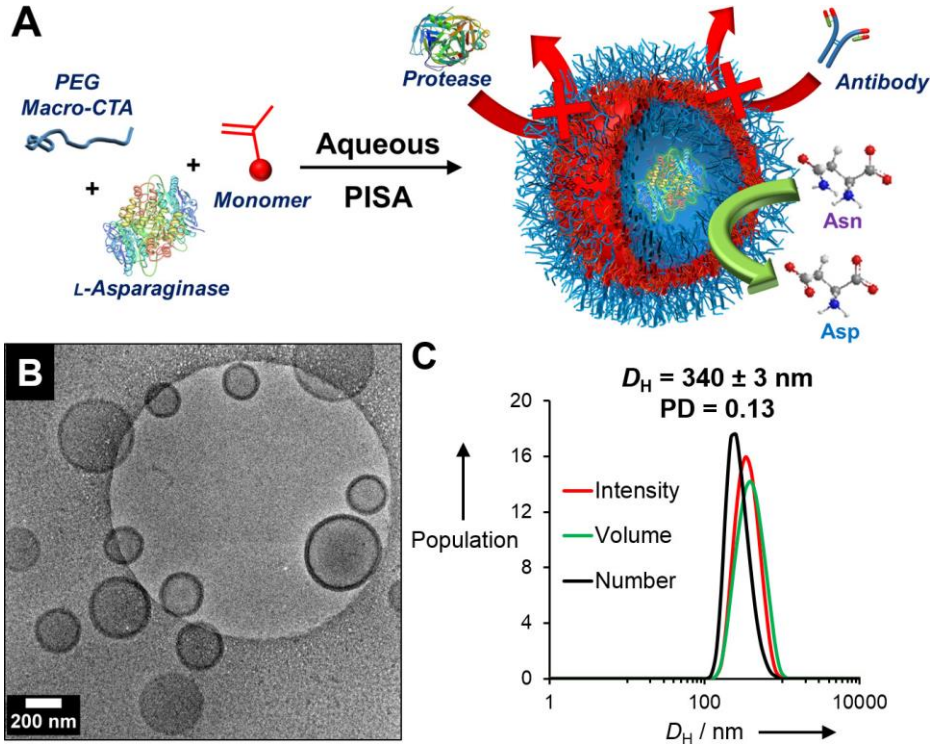

Figure 4.2. *(A) Schematic representation for the ASNS-loaded vesicle preparation by aqueous PISA (B) cryo-TEM image and (C) DLS size distribution of purified asparginase-loaded vesicles. (adapted from Lewis D. et al. ACS Cent. Sci.* ***2018****, 4, 718–723*)

The PISA process has been primarily explored using reversible addition fragmentation chain transfer (RAFT) polymerization (called as RAFT-PISA) while, the other controlled radical polymerizations such as atom transfer radical polymerization (ATRP) (PISA process is called as ATRPISA), nitroxide mediated polymerization (NMP) (PISA process is called as NMPISA) are also explored to some extent.[295, 296] Recently, ring opening metathesis polymerization is utilized for PISA (called as ROMPISA).[297-299] Despite these advancement in PISA process, it suffers from major drawback that, in all of these cases, the resultant polymers are non-biodegradable making it questionable to use in biomedical applications.[300] To overcome the biodegradability issue, the radical ring opening polymerization induced self-assembly (rROPISA) was developed to prepare biodegradable ester containing nano-objects from co-polymerization of cyclic-ketene acetals (CKAs) with conventional vinyl monomers.[301-303] The high sensitivity of cyclic-ketals towards traces of

water or protic solvents makes the rROPISA process of CKAs impossible in water and it has been only shown in n-alkanes (hydrocarbons) which makes it extremely difficult to make water based self-assembled structures from it for biomedical applications. Additionally, water based self-assembled structures were prepared using two step process, wherein first rROPISA of CKAs was carried out in DMF then it was transferred to water based system to make nano objects which were biodegradable.[304] Additionally, rROPISA of cyclic allylic sulfide (a 15-membered macrocycle) was shown in water to make nano-objects degradable by TCEP.[305] Although these few reports on degradable nano-assemblies from vinyl monomers are quite exciting, they have a limitation of utilization of petroleum based acrylic monomers and also synthesis of these CKAs or cyclic allylic sulfide is extremely challenging.

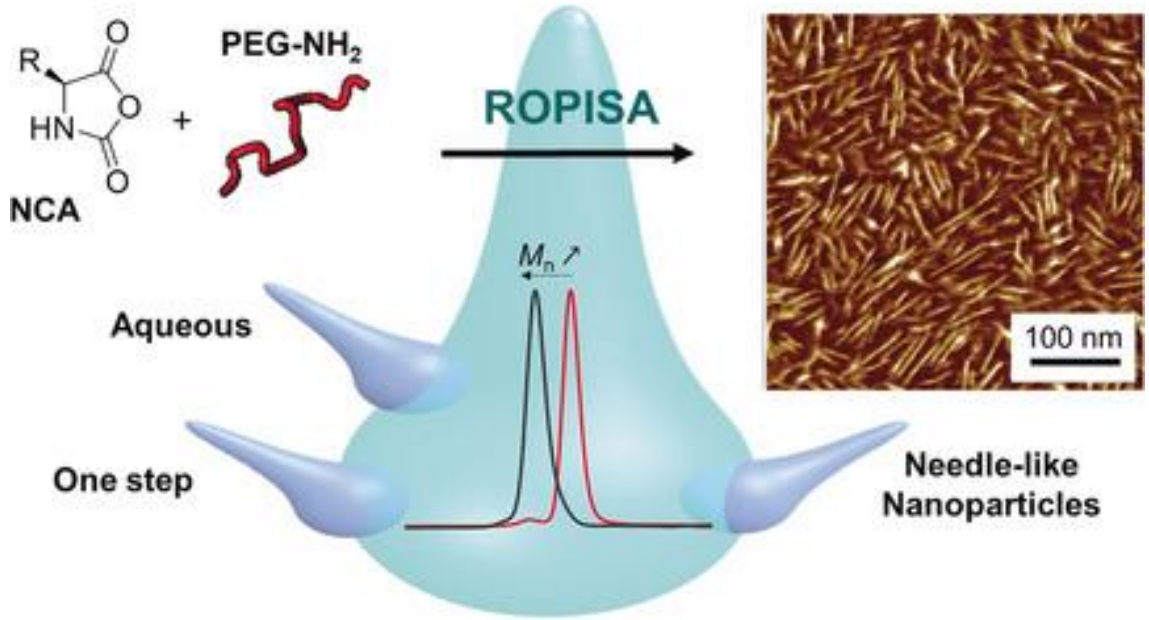

***Figure 4.3**. Schematic representation for the aqueous ROPISA process of NCA to afford needle like nanoparticles. (adapted from C. Grazon et al. Angew. Chem. Int. Ed. **2020**, 59, 622–626*).

To make bio-based nano objects by PISA approach, the ring opening polymerization induced self-assembly (ROPISA) of amino acid derived NCA monomers is developed to prepare polypeptide nano assemblies. There are only handful of reports demonstrating the ROPISA concept for making polypeptides. In particular, ROPISA for phenyl alanine NCA has been shown in THF using PEG amine as an initiator to make polypeptide vesicles in THF.[62] The insitu thermally generated methionine NCA was polymerized under ROPISA

conditions in DMSO and several oxidation responsive nano-objects were prepared in DMSO.[63] These two recent reports have shown ROPISA for NCA monomers in organic solvents and hence restricts their use for biomedical applications. On the other hand, Colin Bonduelle and co-worker shown for the first time the ROPISA of NCA monomer in water (See Figure 4.3 for schematic representation).[64, 65] The aqueous "Ring Opening Polymerization Induced Self-assembly" (ROPISA) results in the formation of polymer emulsion in situ. In this process, the water insoluble monomer is polymerized using water soluble initiator (such as PEG) and the resultant growing polymer chain becomes amphiphilic in nature which simultaneously grows and self-assembles throughout the course of polymerization. The final polymerization mixture appeared as opalescent solution which is characteristic of emulsion polymerization. Hence, the addition of external surfactant is not required in the ROPISA process. In case of suspension polymerization, monomer, initiator and polymer are water insoluble and hence it is much different than ROPISA process. Colin Bonduelle and co-worker utilized water soluble amine functionalized PEG as an initiator for ring opening of benzyl glutamate NCA monomer to produce polypeptide emulsion of PEG-*b*-benzyl glutamate and it was found to exhibit worm like morphology. It was hypothesized that, the water-soluble amine functionalized PEG initiator will initiate the polymerization of NCA, and upon formation of oligomers, they will self-assemble and encapsulates the remaining NCA molecules inside their hydrophobic cavity, that protects these NCA molecules from hydrolysis. The polymerization will still proceed inside the cavity of nano assemblies till the consumption of monomer. The similar strategy was explored for lysine and leucine based NCA monomers and worm like nano objects were prepared. In these two reports, only self-assembly aspects of polypeptide di-block copolymer emulsion were studied and there has been no emphasis on the application of these polypeptide emulsions.

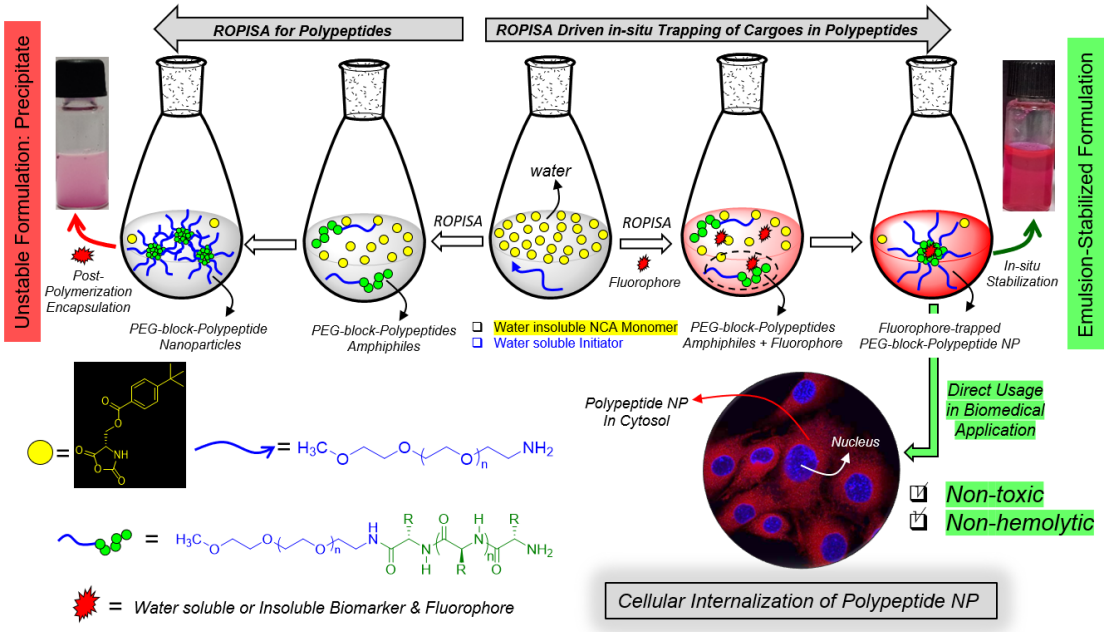

Figure 4.4. *Development of ROPISA driven in-situ encapsulation strategy for making polypeptide nano formulations.*

Considering these only two literature reports and on aqueous ROPISA of NCA we decided to utilize tert-butyl functionalized serine NCA monomer for ROPISA process to create nano objects from polyserine based scaffolds. Additionally, we envisioned that, upon addition of cargo molecule such as dye molecule during ROPISA process, it will get encapsulated during polymerization and dye loaded polypeptide emulsion will be generated. This concept has been shown in Figure 4.4. In this study, the serine ester monomer (**M1**) was polymerized in 50 mM aq. $NaHCO_3$ using amine functionalized PEG as an initiator at various M/I ratios and it was found that for M/I = 10 and 25, the polymer emulsions were produced as an indication from formation of opalescent solution at the end of polymerization. Also, the isolated di-block copolymers from these polymer emulsions (P-10 and P-25) were exhibited monomodal, narrow dispersed SEC chromatogram and their molecular weight was matching very well to expected value. While polymerization with higher M/I ratio produced turbid solutions indicating colloidal instability. The DLS measurements performed on emulsions produced by P-10 ad P-25 revealed the existence of tiny nano assemblies of sizes around 20 to 30 nm. The FE-SEM, HR-TEM and AFM analysis of these polymer emulsions revealed the existence of spherical nanoparticles of sizes matching to DLS measurements. Next, five different dye molecules were successfully encapsulated during ROPISA process by adding them in to the polymerization medium at the beginning of polymerization indicating the robustness of the process. The nascent

polymer was nontoxic to mammalian cells and non-hemolytic to RBCs. The dye loaded polymer emulsions were also nontoxic to mammalian cells indicating their biocompatibility. As a proof of concept, the cellular uptake of Nile red loaded polypeptide nanoparticles was studied using confocal microscopy and result revealed the successful uptake of NR loaded nanoparticles by mammalian cells. We are firmly confident that this approach will open up new horizons for polypeptide based nano formulations for potential biomedical applications.

4.2. Experimental Methods

4.2.1. Materials : Nile red (NR), curcumin (Cur) and IR-780 iodide, Rhodamine B (Rh B), 8-Hydroxypyrene-1,3,6-trisulfonic acid tri-sodium salt (HPTS), 4',6-diamidino-2-phenylindole (DAPI), paraformaldehyde, EDTA, 3-(4,5-dimethylthiazolyl)-2,5 diphenyltetrazolium bromide (MTT) were obtained from Sigma Aldrich chemicals. Wild-type mouse embryonic fibroblast cells (WT-MEF) were maintained in DMEM (phenol red free medium: Gibco) containing fetal bovine serum (FBS) (10 %, v/v) and penicillin–streptomycin (1 %, v/v) at 37 °C in an atmosphere humidified with CO_2 (5 %). Trypsinization of cells was done using trypsin (0.05 %, Gibco) and cells were seeded in desired flat bottomed plastic plates (Eppendorf) for all assays. MeO-PEG_{5000}-NH_2 and monomers **M1** and **M4** were synthesized as per procedures mentioned in Chapter 2 of this thesis.

4.2.2. Methods : Circular dichroism (CD) analysis of the polymer samples (0.1 mg/mL) was performed on a JASCO J-815 CD spectrometer at 25 °C in water as solvent. Dynamic light scattering (DLS) measurements were performed in water as solvent using Nano ZS-90 setup (Malvern instruments). The concentration of polymer used for DLS measurements was 0.1 mg/mL concentration. Schimadzu UV1900 spectrophotometer was used for absorbance measurements. The fluorescence spectra were recorded on SPEX Fluorolog HORIBA JOBIN VYON fluorescence spectrophotometer using slit width of 2 nm. FE-SEM analysis was performed using Zeiss Ultra Plus scanning electron microscope. The dilute sample solution (0.1 mg/mL in miliQ water) was drop casted on silicon wafer. For AFM analysis, polymer solution (0.1 mg/mL in miliQ water) was also drop casted on silicon wafer and the AFM imaging was performed using Agilent instruments. For HR-TEM analysis, samples (0.1 mg/mL in miliQ water) were drop casted on copper TEM grids and imaging was

performed using Jeol JEM2200FS 200 KeV systems. Leica SP8 was used for Confocal microscopic analysis.

4.2.3. ROPISA Polymerization procedure : The procedure is explained in detail for M/1 = 25. To a cylindrical polymerization tube, 50 mM aq. $NaHCO_3$ (10 mL) was added and it was cooled on ice bath at 4 °C. MeO-PEG_{5000}-NH_2 (313 mg, 1.57 mmol) was added to the polymerization tube and it was stirred at 4 °C to get clear solution. Subsequently, serine monomer (**M1**) (456 mg, 0.063 mmol) was added and polymerization mixture was stirred vigorously at 4 °C for 8 h and then at 25 °C for 40 h. At the end of 48 h, it was opalescent solution. To monitor the reaction progress by FT-IR, a small aliquot (100 µL) was taken out and extracted with DCM (200 µL) and DCM layer was used for FT-IR measurements. Upon complete consumption of monomer (disappearance of anhydride peaks) the opalescent reaction mixture was dialyzed against miliQ water with frequent change of water. For ^{1}H-NMR and SEC measurements, 1 mL of dialyzed solution was lyophilized and the white powder thus obtained was used for ^{1}H-NMR and SEC analysis. ^{1}H NMR (400 MHz, $CDCl_3$ – TFA (0.7 mL, 6:1, v/v) δ 8.35 (bs, 21H, N**H**CO), 7.85 – 7.67 (m, 52H, Ar-**H**), 7.44 – 7.28 (m, 51H, Ar-**H**), 5.08 (bs, 25H, COC**H**NH), 4.84 – 4.51 (m, 54H, COCHC**H**$_2$), 3.77 (s, 337H, OC**H**$_2$C**H**$_2$O), 3.51 (s, 3H, C**H**$_3$OCH$_2$CH$_2$), 1.47 – 1.02 (m, 234H, C(C**H**$_3$)$_3$). ATR-FTIR (cm^{-1}): 3289, 2921, 2854, 1726, 1661, 1640, 1610, 1555, 1506, 1463, 1353, 1274, 1189, 1116, 950, 855, 771, 704.

For polymerization at M/I = 10, Same procedure was employed as that for M/I = 25 as mentioned above using 50 mM aq. $NaHCO_3$ (10 mL), MeO-PEG_{5000}-NH_2 (468 mg, 0.094 mmol) and serine monomer (**M1**) (273 mg, 0.94 mmol). ^{1}H NMR (400 MHz, $CDCl_3$ – TFA (0.7 mL, 6:1, v/v) δ 8.35 (bs, 9H, N**H**CO), 7.85 – 7.67 (m, 26H, Ar-**H**), 7.44 – 7.28 (m, 24H, Ar-**H**), 5.08 (bs, 10H, COC**H**NH), 4.84 – 4.51 (m, 25H, COCHC**H**$_2$), 3.77 (s, 377H, OC**H**$_2$C**H**$_2$O), 3.51 (s, 3H, C**H**$_3$OCH$_2$CH$_2$), 1.47 – 1.02 (m, 109H, C(C**H**$_3$)$_3$). ATR-FTIR (cm^{-1}): 3297, 2880, 1726, 1660, 1639, 1611, 1557, 1506, 1468, 1345, 1278, 1110, 962, 843, 771, 705.

For polymerization at M/I = 50, Same procedure was employed as that for M/I = 25 as mentioned above using 50 mM aq. $NaHCO_3$ (10 mL), MeO-PEG_{5000}-NH_2 (202 mg, 0.040 mmol) and serine monomer (**M1**) (587 mg, 2.016 mmol). Polymer was not characterized as the reaction mixture was highly turbid solution which made the isolation difficult.

For polymerization at M/I = 100, Same procedure was employed as that for M/I = 25 as mentioned above using 50 mM aq. $NaHCO_3$ (10 mL), MeO-PEG_{5000}-NH_2 (118 mg, 0.024 mmol) and serine monomer (**M1**) (686 mg, 2.355 mmol). Polymer was not characterized as the reaction mixture was highly turbid solution which made its isolation difficult.

4.2.4. ROPISA procedure for in-situ encapsulation of Dyes: The procedure is explained for encapsulation of Nile red. To a cylindrical polymerization tube, 50 mM aq. $NaHCO_3$ (5 mL) was added and it was cooled on ice bath at 4 °C. MeO-PEG_{5000}-NH_2 (157 mg, 0.785 mmol) was added to the polymerization tube and it was stirred at 4 °C to get clear solution. Subsequently, the Nile red (17 mg) and serine monomer (**M1**) (228 mg, 0.032 mmol) were added and polymerization mixture was stirred vigorously in dark at 4 °C for 8 h and then at 25 °C for 40 h. At the end of 48 h, the resultant coloured suspension was filtered through Whatman filter paper to get rid of unencapsulated water insoluble Nile red particles. Then, 1 mL of resultant filtered solution was diluted with miliQ water (2 mL) and the solution was dialyzed against miliQ water in dark for 48 h. The dialyzed solution was stored at 4 °C and used for DLS, AFM, FE-SEM, HR-TEM analysis. Also, the dialyzed solution was used for quantification of amount of Nile red encapsulated (DLC or DLE parameters). To do so, the small fraction of this dialyzed solution (500 µL) was lyophilized to get solid powder composed of polymer and encapsulated Nile red which was weighed (to know how much polymer + Nile red is present) and dissolved in DMSO (1 mL). Weight of encapsulated dye in the resultant solution was determined by measuring absorbance at 552 nm (ε = 19600 $L.M^{-1}.cm^{-1}$). The DLC (dye loading content) and DLE (dye loading efficiency) were determined by using the following equations:

DLC = [weight of encapsulated dye / weight of polymer] x 100

DLE = [weight of encapsulated dye / weight of total dye added] x 100

Similar procedure was utilized for encapsulation of other dye molecules. The absorption maxima and molar absorption coefficient for each dye are as follows: HPTS (ε = 21600 $L.M^{-1}.cm^{-1}$ at 403 nm), Curcumin (ε = 55000 $L.M^{-1}.cm^{-1}$ at 416 nm), Rhodamine B (ε = 116000 $L.M^{-1}.cm^{-1}$ at 553 nm), IR-780 (ε = 265000 $L.M^{-1}.cm^{-1}$ at 795 nm).

4.2.5. Cellular Uptake of Nile red (NR)-loaded Polymer nanoparticles by Confocal Microscopy

Wild type MEF cells were seeded (cell density was 10^5) on flame-dried coverslips kept in 6-well plates containing DMEM media with 10 % FBS and incubated for 16 h at 37 °C. Cells were incubated with the required concentrations of nile red (NR)-loaded polymer nanoparticles for 3 h, 6 h and 9 h in a CO_2 incubator at 37 °C. Subsequently the media was aspirated and cells were washed with PBS (2 x 1 mL) and fixed using 4 % paraformaldehyde solution in PBS for 10 min at 25 °C. Again, the cells were washed with PBS (2 x 1 mL) and immediately stained with DAPI solution in PBS by incubating with it in dark for 2 min. Finally, the PBS washings were given (2 x 1 mL) to remove excess dye from the plate. Coverslips were fixed onto the glass slides (from borosil) with the help of glycerol and then dried for 30 min in dark at 37 °C. The cells were then imaged using confocal microscopy by employing λ 405 nm (blue channel) and λ 568 nm (red channel) lasers and the obtained images were analysed using Image J software.

For hemolysis assay and cell viability assay (MTT Assay) similar protocol was employed as mentioned in Chapter-3.

4.3. Results and Discussion

4.3.1. Optimization of Polymerization using ROPISA

The serine-ester monomer (**M1**) was subjected to polymerization in water at slightly basic pH (pH ~ 8.5) using polyethylene glycol monomethyl ether amine (M_n ~ 5000) (MeO-PEG_{5000}-NH_2) as a hydrophilic macroinitiator at various M/I ratios (M/I = 10, 25, 50 and 100). The reaction was performed at slightly basic pH, since the hydrolysis of NCA (ring opening of NCA by water) is slower than the aminolysis of NCA (ring opening of NCA by amine) at slight basic pH ~ 8.5 and it was maintained by using 50 mM aq. $NaHCO_3$ solution as a solvent for polymerization. Additionally, the amount of monomer and initiator for polymerization reaction were taken in such a manner that at the end of polymerization it would produce emulsion of total solid content 7 wt.% (means, 700 mg polymer would be produced in 10 mL of reaction, assuming complete consumption of monomer) and while doing so, desired monomer to initiator ration (M/I) was also maintained.

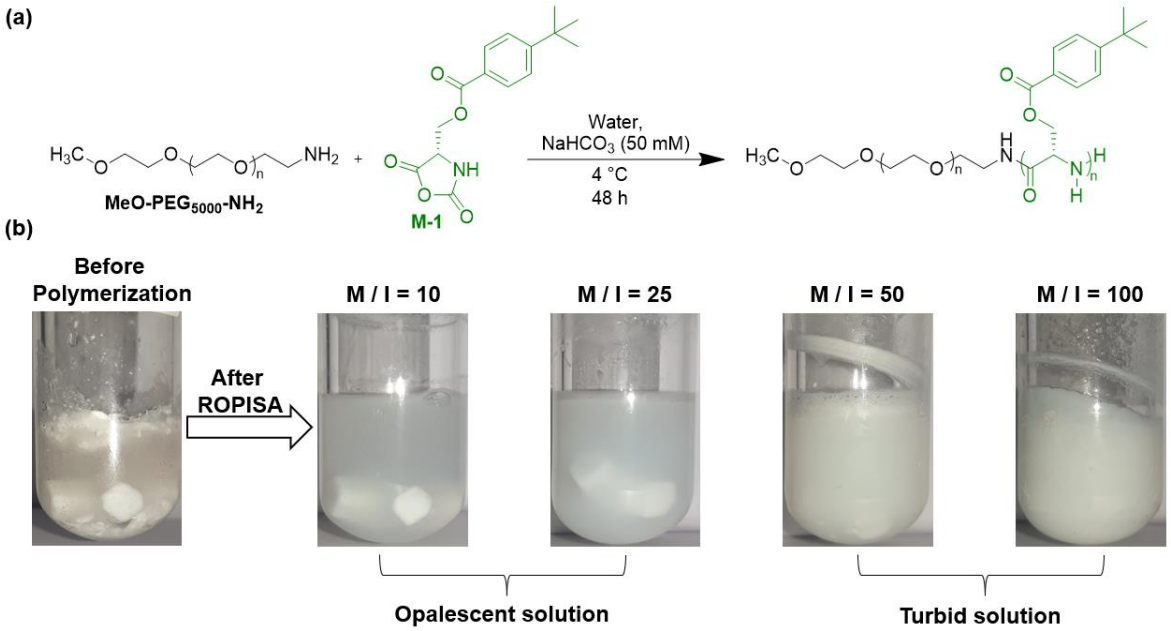

Figure 4.5*. (a) Synthetic scheme for ROPISA mediated polymerization of* ***M1*** *using MeO-PEG_{5000}-NH_2 as an initiator. (b) Photographs of polymerization reaction mixture at the beginning and at the end of polymerization for various M/I ratios.*

In a typical experiment, serine-ester NCA monomer (**M1**) was added to solution of MeO-PEG_{5000}-NH_2 in 50 mM aq. $NaHCO_3$ at 4°C and it was stirred vigorously for 48 h (it is represented in scheme in Figure 4.5a). In the beginning of reaction, due to insolubility of monomer in water, the reaction mixture was a turbid solution as shown in photograph given in Figure 4.5b on the other hand, at the end of 48 h stirring, the reaction mixtures were

opalescent solutions for polymerization at M/I = 10 and 25 (see Figure 4.5b for photograph). On the other hand, for polymerization at M/I = 50 and M/I = 100, the reaction medium was turbid, indicating loss of colloidal stability for higher feed ratios and hence they were not studied further.

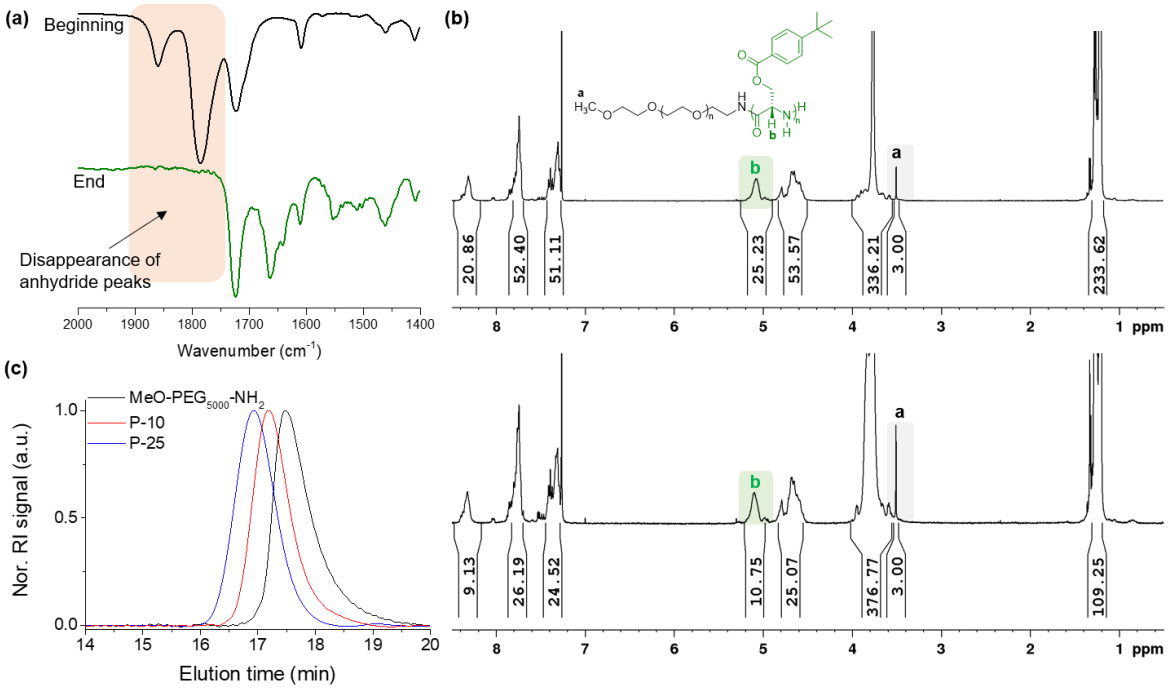

***Figure 4.6**. (a) FT-IR spectra of the polymer aliquots at the beginning and at the end of polymerization. (b) ^{1}H-NMR spectrum of isolated di-block copolymer P-10 and P-25. (c) Sec chromatograms for MeO-PEG5000-NH_2, P-10 and P-25.*

The polymerization was monitored by ATR-FTIR (see Figure 4.6a, for both polymerization at M/I = 10 and 25) and the disappearance of NCA anhydride peaks at the end of reaction confirms the complete consumption of monomer. The polymerization for feed ratio of M/I = 50 and M/I = 100 was incomplete even after 72 h and hence not considered for further studies. The resultant di-block copolymers, PEG-*b*-P(Bz-serine)$_n$, (will be named as P-10 for polymer obtained from polymerization at M/I = 10 and P-25 for polymer obtained from polymerization at M/I =25 in the rest of chapter) were isolated by dialysis followed by lyophilization and then subjected to ^{1}H NMR analysis as shown in Figure 4.6b. The degree of polymerization was determined by comparing the initiator proton (methoxy proton at the end of PEG chain, proton "a") with polymer proton (α C-H proton, proton "b") and it was found that, the degree of polymerizations were obtained to be 11 and 25 for P-10 and P-25 respectively, indicating the control in polymerization process as the

degree of polymerization is perfectly matching to feed M/I ratio. Then, P-10 and P-25 were subjected to SEC analysis in $CHCl_3$ as an eluent and the SEC chromatograms are given in Figure 4.6c. The SEC chromatograms were monomodal, narrow-dispersed and the molecular weights obtained from SEC were in quite good agreement with ^{1}H-NMR (see table 4.1.). The P-25 eluted earlier than P-10 which was eluted earlier than MeO-PEG_{5000}-NH_2, thus following a perfect trend in elution pattern as per molecular weights.

Table 4.1 *Table containing the molecular weight data from NMR and SEC for P-10, P-25, P-50 and P-100.*

.

Polymer[a]	M/I	n (^{1}H-NMR)[b]	M_n NMR (g/mol)[c]	M_n SEC (g/mol)[d]	M_w SEC (g/mol)[d]	Đ[d]
P-10	10	11	7700	8200	10800	1.3
P-25	25	25	11200	9300	10800	1.2
P-50	50	-[e]	-	-[e]	-	-
P-100	100	-	-	-	-	-

[a)] Polymerization was carried out in 50 mM Aq. $NaHCO_3$ using MeO-PEG_{5000}-NH_2 as an initiator while maintaining total solid content at 7 wt%. [b)] Degree of polymerization (n) was determined from ^{1}H-NMR [c)] M_n (NMR) = 5000 + (n × repeating unit mass). [d)] molar mass and dispersity (Đ) were determined by size exclusion chromatography in $CHCl_3$ at 25 ºC with respect to polystyrene standards. [d)] Not determined due to incompletion of reaction and difficulty in isolation due to turbidity.

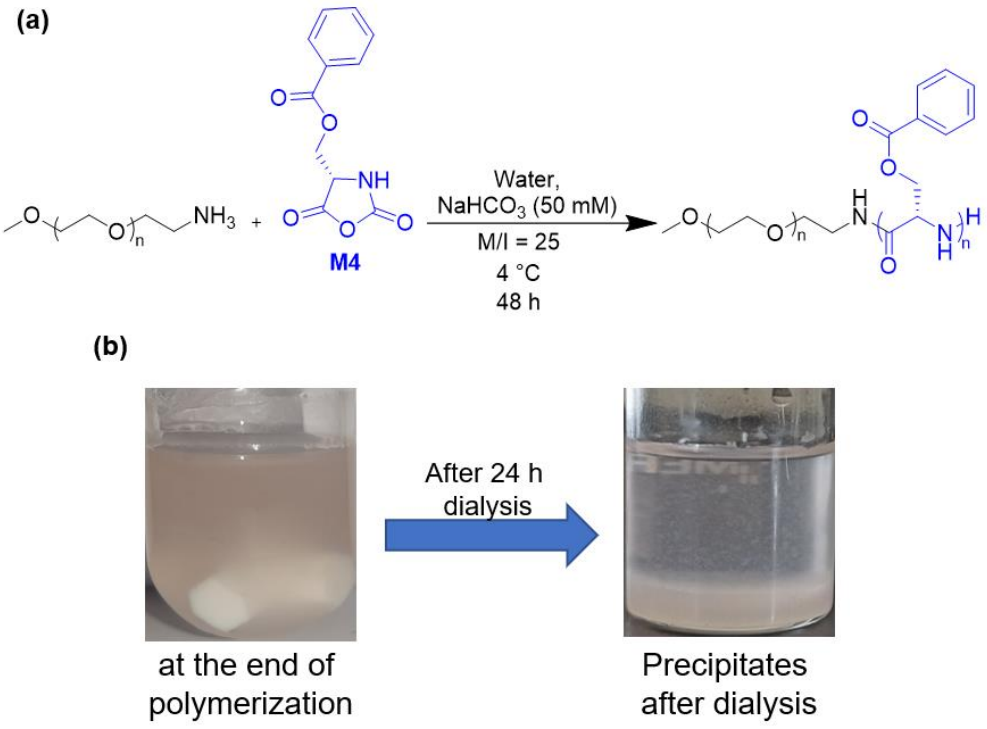

Figure 4.7*. (a) Scheme for ROPISA driven polymerization of non tert-butyl benzene functionalized monomer (**M4**) using MeO-PEG5000-NH2 as an initiator. (b) Photographs*

*at the end of polymerization and after dialysis for ROPISA driven polymerization of non tert-butyl benzene functionalized monomer (**M4**) using MeO-PEG5000-NH2 as an initiator.*

As mentioned in chapter-2, the polymerization of serine-ester monomer without tert-butyl benzene substitution (**M4**) in organic solvent leads to uncontrolled precipitation. Keeping it mind, to study the role of tert-butyl benzene substitution in ROPISA, we decided to polymerize monomer **M4** under ROPISA conditions (see Figure 4.7a). the polymerization was carried out under similar conditions mentioned above at feed of M/I = 25. The polymerization went alright and at the end emulsion was obtained but upon dialysis, the emulsion got destabilized and polymer crashed out as a precipitate as shown in Figure 4.7b. This astonishing results clearly suggests that, serine-monomer without tert-butyl benzene unit is not polymerizable even under tested ROPISA conditions and reiterates the importance of tert-butyl benzene group.

4.3.2. Secondary structure analysis by CD and FT-IR spectroscopy

We employed FT-IR spectroscopy to investigate the secondary structures of isolated polymer and the spectra are given in Figure 4.8a. in the FT-IR spectra for both polymers, peak at 1725 cm^{-1} corresponding to ester carbonyl is observed, indicating the ester functionality is intact during ROPISA process. In case of P-10 polymer, the amide I region in FT-IR spectra revealed the existence of both peaks at 1660 cm^{-1} and 1639 cm^{-1} in nearly equal proportions indicating the mixed α-helical and β-sheet structures. While on the other hand, for P-25 polymer, predominantly peak at 1660 cm^{-1} corresponding to α-helical conformation was observed, although a small hump at 1639 cm^{-1} is also observed indicating some β-sheet structures are also present. Overall, the FT-IR-based secondary structure analysis reveals that the P-10 adopts mixed α-helical and β-sheet structures while P-25 predominantly exists in α-helical conformation. To study the secondary structure di-block copolymers (P-10 and P-25) in the emulsion state, they were subjected to CD-spectroscopy analysis and the spectra are given in Figure 4.8b and Figure 4.8c. The CD spectra for both P-10 and P-25 were similar and it revealed the existence of positive peak at 193 nm and negative peat at 220 nm corresponding to β-sheet structure but un recognised positive signal at 208 nm and 245 nm were observed. This makes CD spectra difficult to predict and it cannot be assigned to any perfect secondary structures and supports the existence of mixed structures.

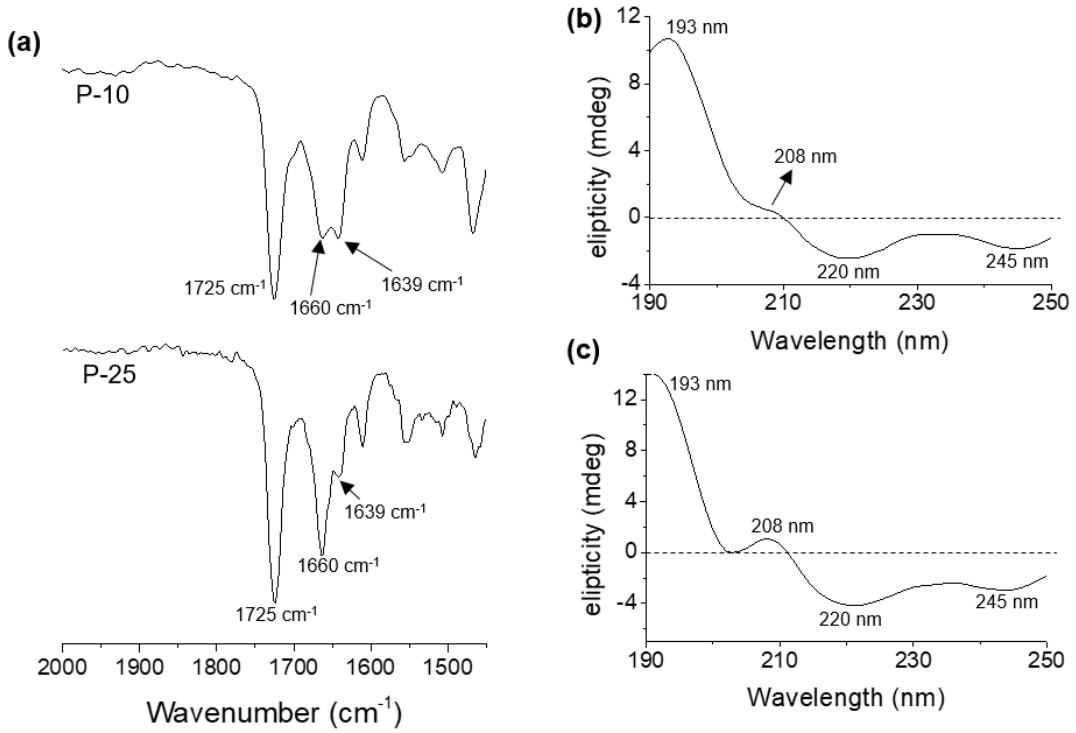

Figure 4.8*. (a) Stacked ATR-FT-IR spectra of P-10 and P-25 polymers. CD spectra of (b) P-10 and (c) P-25 in water.*

4.3.3. Size and morphology of nano assemblies

To investigate the stability and size of nano assemblies generated by ROPISA, they were subjected to DLS measurements before and after dialysis and the data is given in Figure 4.9a for P-25 polymer. The DLS histograms reveals existence of tiny nano assemblies of sizes around 30 nm. Importantly, DLS analysis before and after dialysis reveals the existence of nano assemblies of similar sizes since the DLS histogram was almost similar for sample before and after dialysis indicating the stability of emulsions generated by ROPISA method. Additionally, we have checked the stability of emulsions up to six months by DLS and they were found to be stable. In order to examine the morphology of these nano assemblies, samples were subjected to FE-SEM, HR-TEM and AFM analysis and the data is given in Figure 4.9b to 4.9d, respectively. Both FE-SEM and HR-TEM analysis revealed the existence of spherical nano particles of sizes matching close to DLS data. Similarly, AFM analysis revealed the existence of spherical nanoparticles but sizes were slightly higher than that obtained from DLS measurements. The existence of spherical morphology is in stark contrast to existence of worm like nano assemblies for PEG-*b*-benzyl glutamate, PEG-*b*-Z-Lys and PEG-*b*-leucine generated by ROPISA under similar conditions.[64, 65] This result

clearly depicts the role of amino acid in dictating the morphology of nano assemblies generated by ROPISA.

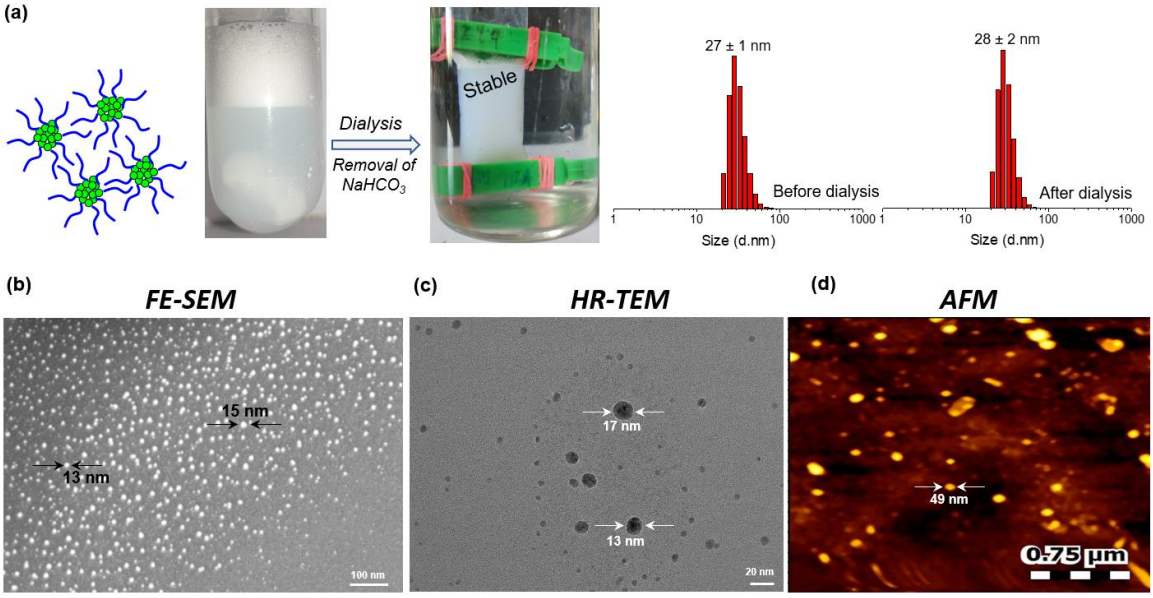

***Figure 4.9**. (a) Scheme depicting stability of nano assemblies generated by ROPISA for P-25. DLS histograms for DLS measurements before and after dialysis are given for P-25 polymer. (b) FE-SEM, (c) HR-TEM and (d) AFM images for P-25 polymer.*

In the similar manner, the P-10 polymer was subjected to DLS analysis before and after dialysis and the corresponding DLS histograms are given in Figure 4.10a and 4.10b respectively. The DLS analysis reveals the existence of tiny nano assemblies of sizes around 20 nm and it was unchanged upon dialysis thus indicating the stability of emulsion. The morphology of nano-assemblies of P-10 were investigated by FE-SEM, HR-TEM and AFM analysis (see Figure 4.10c to 4.10e for FE-SEM, HR-TEM and AFM images respectively) and it was found to exhibit spherical nanoparticle morphology similar to that obtained from P-25. The size of nano particles obtained by FE-SEM and HR-TEM was very well matching to size determined by DLS while the AFM analysis revealed slightly higher sized nanoparticles.

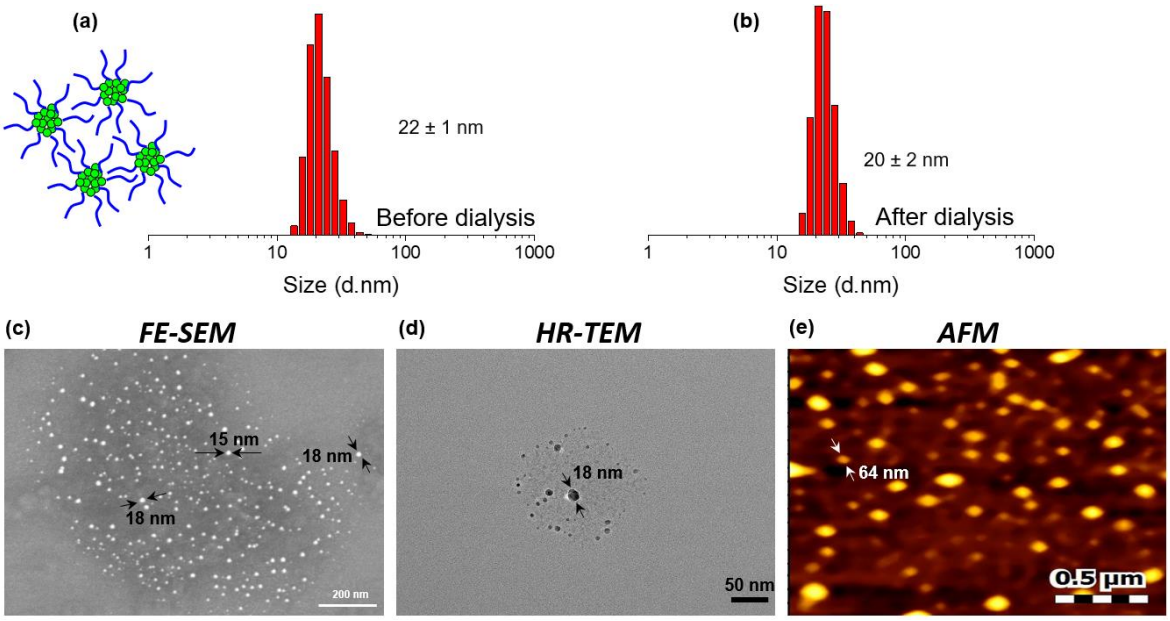

Figure 4.10. *(a) DLS histograms for DLS measurements before and (b) after dialysis are given for P-10 polymer. (c) FE-SEM, (d) HR-TEM and (e) AFM images for P-10 polymer.*

4.3.4. ROPISA Driven Encapsulation Strategy

To utilize this ROPISA methodology for making drug-formulations we decided to first investigate our ROPISA approach for encapsulation of dye molecules and it is schematically represented in Figure 4.11a. We envisioned that, if dye molecule is added at the beginning of ROPISA mediated polymerization then along with monomer, they will also get trapped (encapsulated) inside the initially formed nano assemblies of amphiphilic oligomers. Furthermore, polymerization will be going on till the consumption of monomer and at the end emulsion will be produced consisting of encapsulated dye molecules in the nano-assemblies of polymer. We chose total five dyes for these studies and their structures are given in Figure 4.11b. Among them, three dyes are water insoluble (Nile red (NR), curcumin (Cur) and IR-780) while two dyes are water soluble dyes (Rhodamine B (Rh B) and 8-Hydroxypyrene-1,3,6-trisulfonic acid tri-sodium salt (HPTS)).

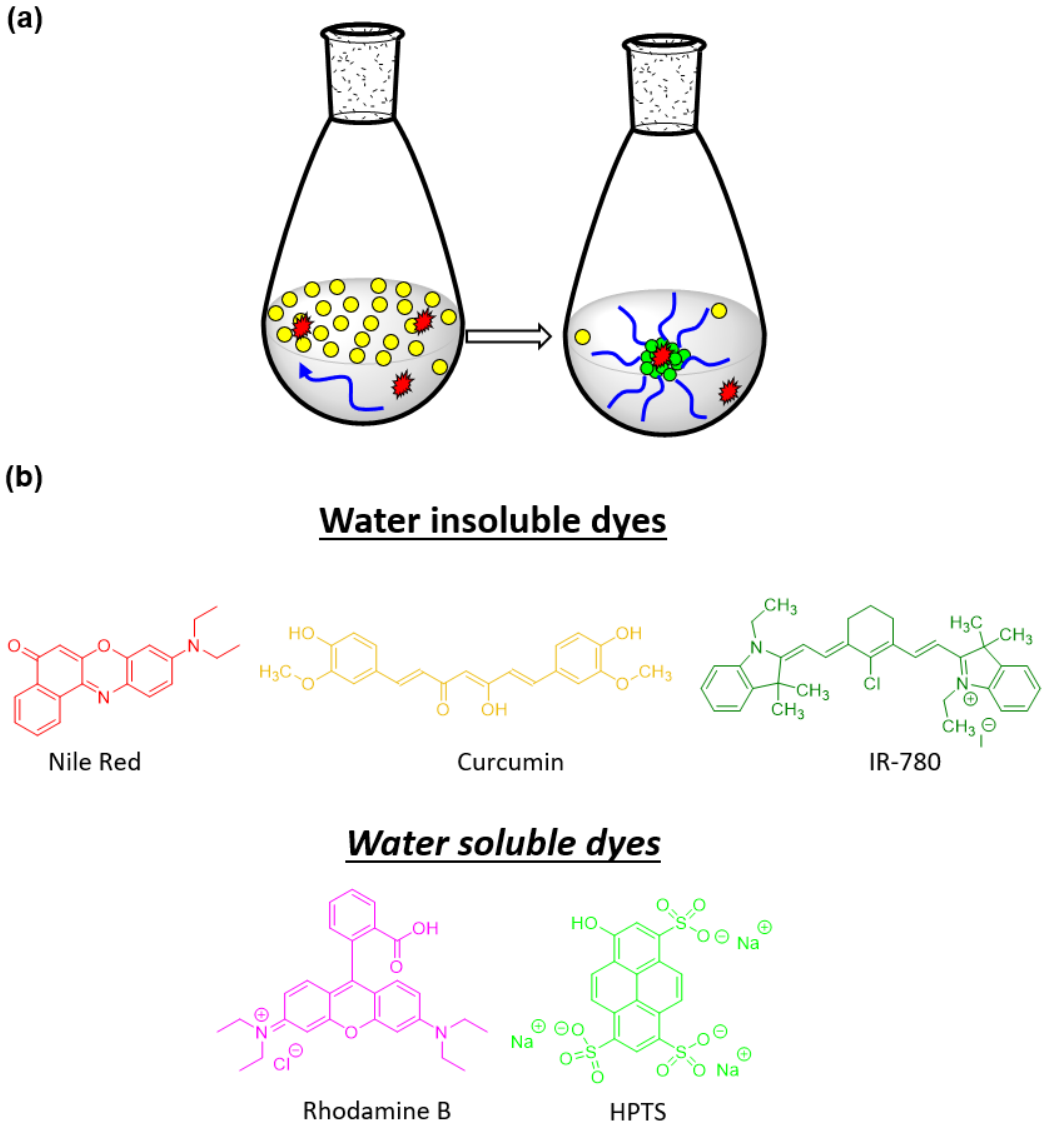

Figure 4.11. *(a) Scheme depicting the ROPISA driven encapsulation strategy. (b) Structure of water insoluble and water-soluble dyes chosen for the study.*

For this purpose, the monomer **M1** was polymerised using MeO-PEG$_{5000}$-NH$_2$ as macroinitiator at the M/I = 25 under similar conditions as mentioned above and the dye molecule was added at the beginning of ROPISA driven polymerization. At the end of polymerization, the reaction mixture was filtered to remove unencapsulated water insoluble dye molecules and then it was extensively dialysed for 48 h to remove adsorbed dye molecules and unencapsulated water soluble dye molecules. Finally, the dialysed suspension was filtered once again and used for subsequent analysis. The photographs of dye loaded polymer emulsions under day light and under UV lamp are given in Figure 4.12a. The appearance of coloured emulsion in day light and glowing of emulsion due to dye fluorescence under UV lamp indicates the successful encapsulation. This is remarkable as

the dye molecules can be encapsulated in polymer nano-assemblies during polymerization itself. In addition to this, we have tried loading Rhodamine B and IR-780 dyes in preformed PEG-block-polypeptide nanoparticles but the loading did not happen, indicating the importance of in situ encapsulation of dye molecules during polymerization process.

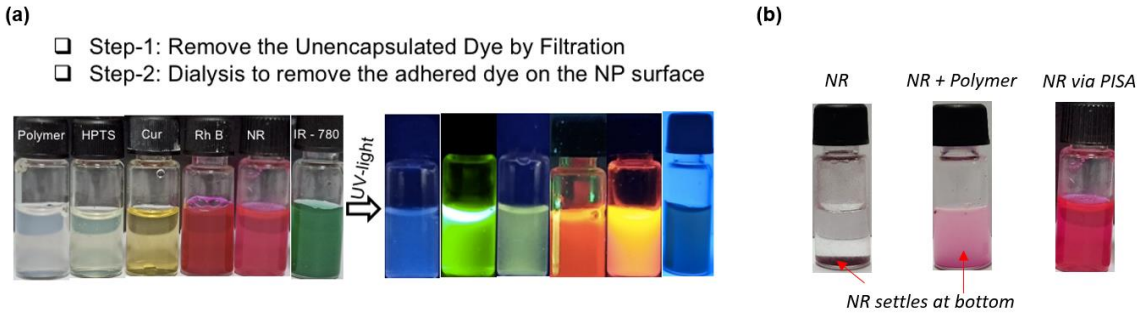

***Figure 4.12**. (a) Photographs of dye loaded polymer emulsions prepared by ROPISA driven encapsulation strategy in day light and under UV light. (b) Photograph of vial containing Nile red suspended in water (left side), Nile red suspended in aqueous polymer (P-25) solution (middle vial) and Nile red loaded polymer emulsion prepared via ROPISA driven encapsulation strategy.*

The significance of the dye encapsulation during polymerization is emphasized in Figure 4.12b. When hydrophobic, water insoluble dye such as Nile red (NR) is added to water, it does not dissolve and settles at bottom (see left side vial photograph in Figure 4.12b) as result the heterogeneous turbid solution is obtained which cannot be used for any applications. Also, when Nile red is added to polymer (P-25 polymer) solution in water and sonicated it results in turbid pinkish solution (see middle vial photograph in Figure 4.12b) indicating no encapsulation and hence cannot be used for any application. On the other hand, when Nile red is added at the beginning of ROPISA mediated polymerization then it gets encapsulated and clear dark reddish coloured solution is obtained (see right side vial photograph in Figure 4.12b) which can be useful for bioimaging applications. This data clearly emphasizes the importance of dye encapsulation during polymerization.

Furthermore, to quantify the amount of dye loaded in polymer emulsions, the polymer emulsions were subjected to UV-visible spectroscopy and dye loading content (DLC) and dye loading efficiency (DLE) was calculated (see experimental section for detailed procedure) and tubulised in Figure 4.13a. The DLC and DLE values were quite good and signifies the potential of this method. The dye loaded emulsions of P-25 polymer were subjected to DLS measurements and the sizes of resultant dye loaded nano assemblies

are given in table in Figure 4.13a. Except for curcumin loaded emulsion, the sizes of dye loaded nano assemblies were almost matching to that of nascent polymer nano assemblies. Furthermore, dye loaded emulsion were subjected to absorbance and fluorescence measurements and the absorbance and fluorescence spectra are given in Figure 4.13b to 4.13f. The HPTS loaded emulsion gave the absorption maxima at 403 nm and fluorescence maxima at 511 nm (see Figure 4.13b). For curcumin loaded emulsion, the broad absorption spectrum was observed with maxima at 416 nm and the fluorescence spectra of curcumin loaded emulsion exhibited maxima at 514 nm (see Figure 4.13c). The rhodamine B and Nile red loaded polymer emulsions exhibited absorption maxima at ~550 nm but their fluorescence maxima appeared at 577 nm and 614 nm respectively, indicating higher stoke shift for Nile red loaded emulsion (see Figure 4.13d and 4.13e for rhodamine B and Nile red loaded assemblies respectively). IR-780 dye is NIR dye and can be used for *in vivo* biodistribution studies as shown in chapter 3 of this thesis. IR-780 loaded emulsion exhibited absorption maxima at 795 nm which is characteristic of NIR dye and emission maxima of 826 nm (see Figure 4.13f).

(a)

Dye	DLC (%)	DLE (%)	Size (nm)
HPTS	1.4	28	28.4 ± 2.4
Curcumin	0.06	1.2	122.4 ± 1.1
Rhodamine b	2.10	42	25.6 ± 1.2
Nile Red	1.3	26	27.7 ± 5.1
IR-780	2.6	52	29.6 ± 1.4

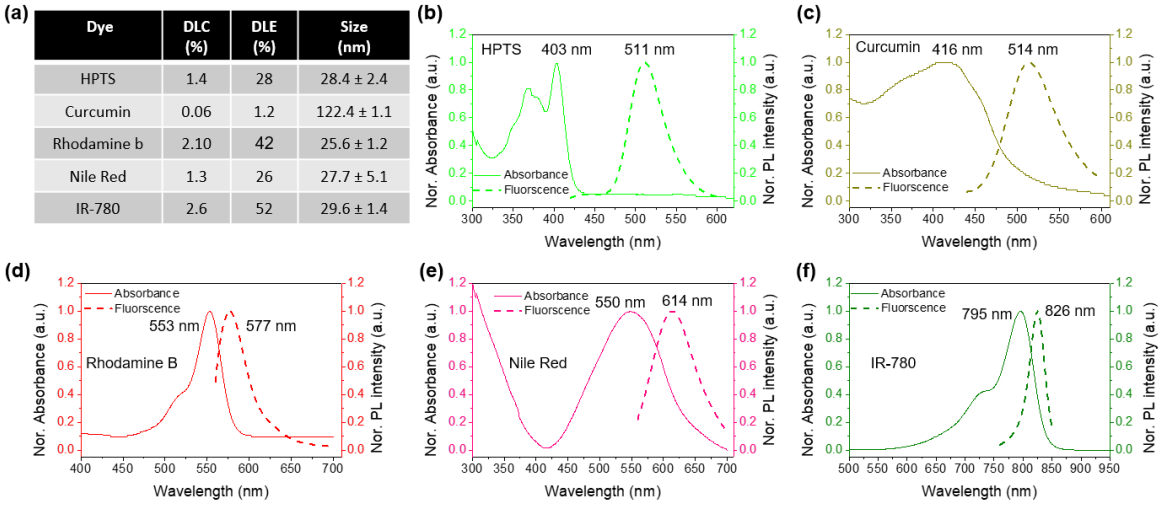

Figure 4.13. *(a) Table containing DLC, DLE and sizes for various dye loaded polymer emulsion prepared by ROPISA driven encapsulation strategy. Absorption and Emission spectra for (b) HPTS loaded polymer emulsion, (c) curcumin loaded polymer emulsion, (d) Rhodamine B loaded polymer emulsion, (e) Nile red polymer emulsion and (f) IR-780 polymer emulsion.*

4.3.5. Morphology of Nile red loaded polymer emulsion

To investigate the morphology of dye loaded polymer emulsions, we chose Nile red loaded polymer emulsion and it was subjected to FE-SEM, HR-TEM and AFM analysis and the images are given in Figure 4.14a to 4.14c respectively. Both FE-SEM and HR-TEM revealed the existence of spherical nanoparticles of sizes similar to that obtained from DLS. AFM analysis also revealed the existence of spherical nano particles but sizes were slightly higher than DLS.

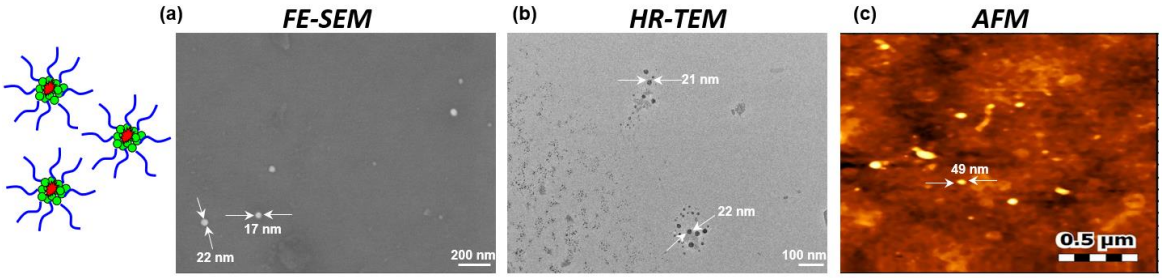

***Figure 4.14**. (a) FE-SEM, (b) HR-TEM and (c) AFM images for Nile red loaded P-25 polymer.*

4.3.6. Cytotoxicity and Hemolysis Assay

For any polymer nano carrier to be used in biomedical applications the most important criteria to follow is its non-toxic nature to cells. To investigate the toxicity of P-25 and the dye loaded P-25 nanoparticles we subjected the corresponding polymer emulsions for MTT assay and the data is given in Figure 4.15. The MTT assay reveals the more than 90% cell viability upon treatment of cells with P-25 or dye loaded P-25 nano particles indicating the nontoxic nature of P-25 and dye loaded P-25 nanoparticles. The MTT assay reveals that, up to 100 µg/mL, the P-25 nano particles and dye loaded P-25 nanoparticles were nontoxic to WT-MEF cells.

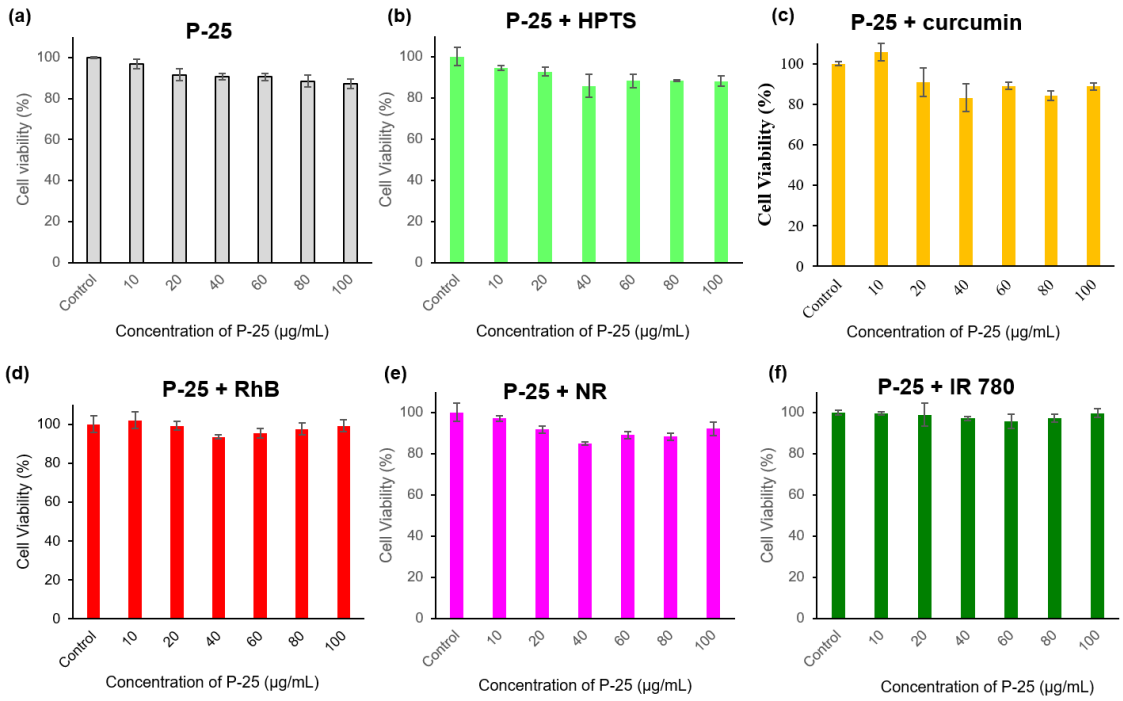

***Figure 4.15**. Plot showing the cytotoxicity assay of (a) P-25 polymer, (b) P-25 + HPTS, (c) P-25 + curcumin, (d) P-25 + Rhodamine B (RhB), (e) P-25 + Nile red (NR) and (f) P-25 + IR-780. (Note: The data was provided by Shahid Khan Pathan)*

In addition to nontoxic nature, the another most important crucial pre-requisites for a nano-formulation are non-hemolytic nature, i.e. compatibility towards red blood cells (RBCs). To investigate this, we subjected the P-25 for hemolysis assay and PBS buffer was used as a negative control while Triton X-100 was positive control. Triton X-100 is nonionic surfactant and causes lysis of RBCs due to osmosis, as a result 100 % hemoglobin is released which is evident from red colored plasma (see Figure 4.16a last centrifuge tube). In the presence of PBS and the P-25, the RBCs remained stable and settled at bottom in the form of pellet while no significant red color was observed in the plasma as shown in Figure 4.16a (first two centrifuge tubes). The % hemolysis is plotted in the form of histogram and shown in Figure 4.16b which clearly shows the that P-25 is non-hemolytic to RBCs.

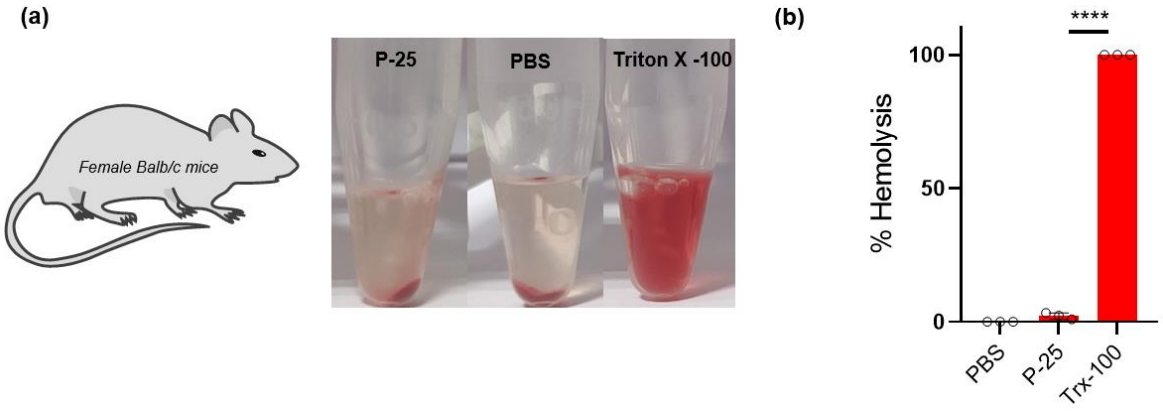

Figure 4.16. *Hemolysis assay. (a) Photographs of centrifuge tubes after centrifugation post incubation of sample with RBC solution. Appearance of intact pellet indicate RBC stability. (b) Plot showing % hemolysis for P-25 along with PBS (negative control) and 1% Triton X-100 (positive control) (****P<0.0001) each point represents mean* ± SEM, n=3). *(Note: The experiment was performed with help of Ruma Ghosh and Shahid Khan Pathan).*

4.3.7. Cellular uptake of Nile red (NR) loaded polymer emulsion

In order to investigate the uptake of the Nile red (NR)-loaded polymeric nanoparticles, NR loaded polymer emulsion was subjected to cellular uptake in wild type MEF cell line and it was studied using Confocal laser scanning microscopy (CLSM) at various time points. The CLSM images for NR-loaded nanoparticle and DAPI stained nuclei were visualized at red (λ = 568 nm) and blue (λ = 405 nm) channels, respectively and the images are given in Figure 4.17a. The first panel in Figure 4.17a represents the images for cells incubated with NR loaded nano particles for 3 h and it clearly demonstrates the DAPI stained nuclei in blue channel while in red channel, red fluorescence corresponding to NR loaded polymer nanoparticles was observed from cytoplasm of cells. The similar images were observed for cells incubated with NR loaded nanoparticles for 6h (second panel) and 9h (third panel). The red fluorescence from cells indicates the uptake of NR loaded nanoparticles by cells. The red fluorescence was present only in cytoplasm of cells and it did not come from nuclei (it is also evident from merge image; no magenta color is present in nucleus in merge image) indicating the localization of NR loaded nanoparticles in cytoplasm only and not in nucleus. In order to quantify the uptake of NR loaded polymer nanoparticles, the mean CTCF (corrected total cell fluorescence) values were estimated for three different regions of interest (ROIs) from each image and these values were in plotted

in the form of histogram in Figure 4.17b. Based on these CTCF measurements, it is clearly evident that the cellular uptake of NR-loaded nanoparticles is gradually increasing with time.

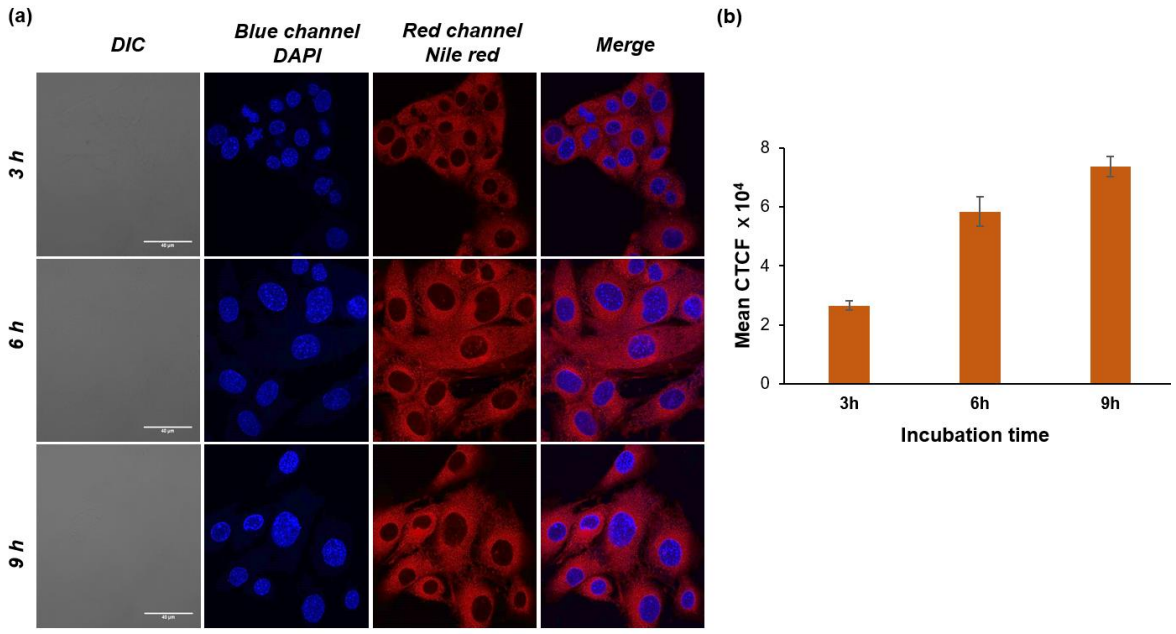

Figure 4.17 *(a) CLSM images of wild type MEF cells incubated with NR loaded P-25 nano particles for 3 h (first panel), 6 h (second panel) and 9 h (third panel). The nucleus of cells was counterstained with DAPI (blue). The red fluorescence of the NR was visualized using the red channel. (b) CTCF corresponding to CLSM images of wild type MEF cells incubated with NR loaded P-25 nano particles for 3 h, 6 h and 9 h. (Note: The data was provided by Shahid Khan Pathan)*

In addition to this, further *in vivo* biodistribution studies for IR-780 loaded samples are under progress. The approach demonstrated here is not only limited to in-situ loading of dye molecules during ROPISA process but in principle it can be applicable to other cargoes like drug molecules and our lab is putting efforts towards these directions.

4.4. Conclusion

To conclude, we have demonstrated the aqueous ROPISA approach for polymerization of tert-butyl benzene functionalized serine based NCA monomer in 50 mM aq. $NaHCO_3$ using amine functionalized PEG as an initiator at various M/I ratios and the stable polymer emulsions were produced for polymerization performed at M/I = 10 and 25 and the resultant emulsions—opalescent solution with bluish tinch were stable for months. The degree of polymerization of isolated diblock copolymers from these stable polymer emulsions (P-10 and P-25) were in close agreement with feed M/I ratio, also their SEC

chromatograms were monomodal and narrow disperse and SEC based molecular weight was matching well to NMR based molecular weight. On the other hand, for ROPISA mediated polymerization of **M1** at M/I = 50 and 100 resulted in turbid solutions indicative of loss of colloidal stability and the SEC chromatograms for isolated di-block copolymers from these turbid solutions were bimodal. Importantly, ROPISA mediated polymerization of serine-based monomer without tert-butyl benzene functionality resulted in polymer precipitation during dialysis process indicating loss of colloidal stability and the importance of *tert*-butyl benzene functionality in giving stable polymer emulsions. The stable polymer emulsions from P-10 and P-25 were subjected to DLS analysis and it revealed the existence of nano-assemblies of sizes around 20 to 30 nm and these nano-assemblies were found to be spherical nanoparticle objects based on our FE-SEM, HR-TEM and AFM analysis. Using this approach, in-situ encapsulation of five dyes (HPTS, curcumin, Nile Red, Rhodamine B and IR-780) were successfully carried out by adding dye in the beginning of polymerization. The size and morphology of resultant dye loaded nano assemblies were found to be similar to nascent polymer nano assemblies. The biocompatibility of nascent polymer emulsion and dye loaded polymer emulsions were studied by MTT assay and they were found to be non-toxic mammalian cells. Additionally, nascent polymer emulsion was found to be non-hemolytic to RBCs indicating its biocompatible nature. Our confocal based imaging assay revealed successful time dependent uptake of Nile red loaded polymer nanoparticles by mammalian cells. These results are exciting and shows that the polypeptide based nano formulations with very high solid content (7 wt%) can be directly made from polymerization of NCA monomers in water. This green approach of making polypeptide-based formulations expands the boundaries of polypeptide-based nanomaterials in biomedical applications.

5. Summary and Future perspectives

In summary we have designed and developed new *"steric hinderance ROP strategy"* for synthesis of high molecular weight β-sheet forming polypeptides based on polyserines and polycysteines. NCA monomers of serine and cysteine with bulky protecting groups bearing *t*-butylbenzene unit were designed and synthesized via multistep organic synthesis without need of any column chromatographic purification step. These monomers successfully underwent ROP to obtain soluble, high molecular weight polyserines and polycysteines with narrow dispersity (Đ). Detailed optimization on solvent and catalyst for ROP of the serine and cysteine NCA monomers were established in $CHCl_3$ or $CHCl_3$+DMF using NHC catalyst. Solubility of these new polymers in common organic solvents allowed their complete characterization by NMR and SEC. The detailed secondary structure analysis of polymerization reaction mixture in $CHCl_3$ by FT-IR revealed that the *t*-butylbenzene functionalized serine and cysteine monomers produced polypeptides in β-sheet conformation at initial oligomeric stage and in-situ conformational transition of polypeptide propagating chains in α-helix conformation. FT-IR and CD spectroscopic analysis was evident for the existence of α-helical conformation in the propagating chain front and established their controlled ROP characteristics. *t*-Butylbenzene masking unit was successfully deprotected to restore the high molecular weight polyserine in native β-sheet conformation.

The steric hinderance strategy developed here was expanded to make block copolymer architectures. For the first-time ever, serine based macroinitiator was used for ROP of glutamate NCA to make protected di-block copolymer P(Bn-ser)-*b*-P(Bn-glu). The polymerization occurred in controlled manner to yield resultant di-block copolymer with expected degree of polymerization and having narrow polydispersity. The resultant di-block copolymer was found to adopt α-helical conformation based on CD spectroscopic measurements. The deprotection of di-block copolymer P(Bn-ser)-*b*-P(Bn-glu) resulted in formation of highly water-soluble serine-glutamate diblock copolymer P(ser)-*b*-P(glu) that adopted β-sheet conformation in water and it was found to self-assemble in to tiny nanoparticles of sizes around ~30 nm. The P(ser)-*b*-P(glu) nano-assemblies were found to exists in the form of spherical nanoparticles based on our investigation by HR-TEM, FE-SEM and AFM analysis. The CD measurements at various pH revealed that the P(ser)-b-P(glu) nano-assemblies were found to undergo helix to coil conformational transition upon increasing pH above 5 which is characteristic of polyglutamate segment. The DLS analysis at various pH discovered that these nano assemblies were stable and retained their size in

the pH range of 5 to 9. The surface charge of these nano assemblies was found to be highly negative (-50 mV) and also found to change with pH. The zetapotential value of these nano-assemblies was nearly zero at pH = 3 and upon increasing the pH, zetapotential tend to become more negative. ThT fluorescence assay was performed to support the β-sheet structures in these assemblies and it was found that, P(ser)-*b*-P(glu) diblock copolymer enhances the ThT fluorescence by ~15 times. On the other hand, random copolymer having same composition was unable to enhance ThT fluorescence, highlighting the importance of block copolymer architecture over random copolymers in terms of perfect self-assembly. The di-block copolymer P(ser)-*b*-P(glu) was nontoxic to mammalian cells as well as non hemolytic to RBCs thus making it a great candidate for biomedical applications. It was found to encapsulate 6.1% DOX and the DOX loaded polymer nanoparticles were able to retain the DOX activity and were able to up taken by mammalian cells based on confocal microscopy studies. Further, the di-block copolymer nanoparticles were found to encapsulate NIR dye IR-780 and it was explored for *in vivo* biodistribution studies by IVIS imaging. The IVIS studies reveals that IR-780 loaded polymer nanoparticles were able to retain in mouse for longer period of time compared to free IR-780, that indicates the polymer nanoparticles have longer circulation time and better *in vivo* stability.

Lastly the aqueous ROPISA approach was employed for polymerization of tert-butyl benzene functionalized serine based NCA monomer in 50 mM aq. $NaHCO_3$ using MeO-PEG_{5000}-NH_2 as an initiator at various M/I ratios and the stable emulsions were produced for polymerization performed at M/I = 10 and 25 and the resultant emulsions—opalescent solution with bluish tinch were stable for months. The degree of polymerization of isolated diblock copolymers from these stable emulsions were in close agreement with feed M/I ratio, and exhibited monomodal and narrow disperse SEC profile. Importantly, ROPISA mediated polymerization of serine-based monomer without tert-butyl benzene functionality resulted in precipitation or polymer during dialysis process indicating loss of colloidal stability and signifies the importance of *tert*-butyl benzene functionality in giving stable emulsions. The stable emulsions from P-10 and P-25 were composed of nano-assemblies of sizes around 20 to 30 nm based on DLS measurements and these nano-assemblies were found to exists in spherical nanoparticle morphology based on our FE-SEM, HR-TEM and AFM analysis. Using this approach, nano-formulations of five dyes (HPTS, curcumin, Nile Red, Rhodamine B and IR-780) were successfully made by adding dye at the beginning of polymerization. The size and morphology of resultant dye loaded nano assemblies were

found to closely resemble the corresponding nascent polymer nano assemblies. The nascent polymer emulsion and dye loaded polymer emulsions were non-toxic mammalian cells. Additionally, nascent polymer emulsion was non-hemolytic to RBCs highlighting its biocompatible nature. The Nile red loaded polymer nanoparticles were successfully up taken by mammalian cells based on Confocal microscopy-based imaging assay.

These results are exciting, and the approach demonstrated here be extended to wide ranges of other polypeptides for application in material science and biomedical field at large. The biocompatible nature of the synthesized serine-glutamate diblock copolymer make its way for future exploration in biomedical field. Aqueous ROPISA of tert-butyl benzene functionalized serine NCA monomers demonstrated that the polypeptide based nano formulations with very high solid content (7 wt%) can be directly made from polymerization of NCA monomers in water. This green approach of making polypeptide-based formulations would expand the boundaries of polypeptide-based nanomaterials in biomedical applications.

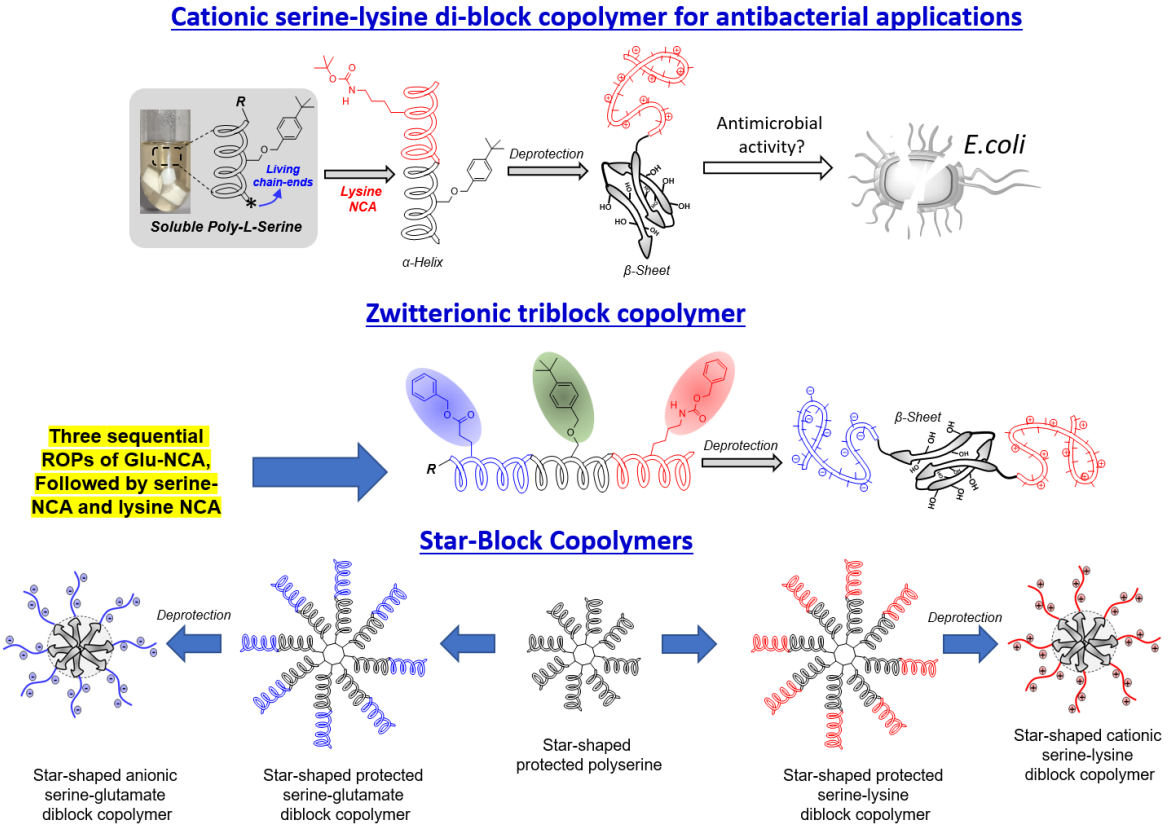

Figure 5.1. *Scheme demonstrating the future perspectives of steric controlled ROP strategy for making serine-lysine diblock copolymers for antimicrobial applications, zwitterionic triblock copolymers and star shaped polyserine based architectures*

The Figure 5.1 demonstrates few approaches for the next obvious steps in the field of β-sheet polypeptides. As demonstrated in Chapter 2, in the similar manner serine lysine block copolymers can be synthesized for antimicrobial applications and the effect of β-sheet structures arising from polyserine on antibacterial activity can be studied. Also, zwitterionic triblock copolymer can be synthesized from three sequential ROPs of glutamate NCA, serine NCA and lysine NCA. The architecture would be interesting and very difficult to make by any other strategy as the β-sheet segment is in middle and hence it would be very difficult to grow polypeptide chain from middle β-sheet block. The steric hinderance ROP strategy demonstrated was applied for synthesis of linear β-sheet polypeptides but it can be expanded to start shaped architectures using appropriate star shaped initiators. Similarly, the star shaped di-block copolymer architectures with β-sheet structures can be made and explored for biomedical applications.

6. References

(1) Nelson, D. L.; Lehninger, A. L.; Cox, M. M., *Lehninger principles of biochemistry*. Macmillan: 2008.
(2) Litwack, G., Chapter 11 - Protein Biosynthesis. In *Human Biochemistry (Second Edition)*, Litwack, G., Ed. Academic Press: Boston, 2022; pp 357-375.
(3) Behrendt, R.; White, P.; Offer, J., Advances in Fmoc solid-phase peptide synthesis. *J. Pept. Sci.* **2016,** *22*, 4-27.
(4) Merrifield, R. B. J. J. o. t. A. C. S., Solid phase peptide synthesis. I. The synthesis of a tetrapeptide. *J. Am. Chem. Soc.* **1963,** *85*, 2149-2154.
(5) Merrifield, R. J. B., Solid-phase peptide synthesis. III. An improved synthesis of bradykinin. *Biochemistry* **1964,** *3*, 1385-1390.
(6) Kent, S. B. H., Total chemical synthesis of proteins. *Chem. Soc. Rev.* **2009,** *38*, 338-351.
(7) Harmand, T. J. R.; Murar, C. E.; Bode, J. W., New chemistries for chemoselective peptide ligations and the total synthesis of proteins. *Curr. Opin. Chem. Biol.* **2014,** *22*, 115-121.
(8) Torbeev, V. Y.; Kent, S. B. H., Convergent Chemical Synthesis and Crystal Structure of a 203 Amino Acid "Covalent Dimer" HIV-1 Protease Enzyme Molecule. *Angew. Chem. Int. Ed.* **2007,** *46*, 1667-1670.
(9) He, C.; Kulkarni, S. S.; Thuaud, F.; Bode, J. W., Chemical Synthesis of the 20 kDa Heme Protein Nitrophorin 4 by α-Ketoacid-Hydroxylamine (KAHA) Ligation. *Angew. Chem. Int. Ed.* **2015,** *54*, 12996-13001.
(10) Hadjichristidis, N.; Iatrou, H.; Pitsikalis, M.; Sakellariou, G., Synthesis of well-defined polypeptide-based materials via the ring-opening polymerization of alpha-amino acid N-carboxyanhydrides. *Chem. Rev.* **2009,** *109*, 5528-5578.
(11) Rasines Mazo, A.; Allison-Logan, S.; Karimi, F.; Chan, N. J.; Qiu, W.; Duan, W.; O'Brien-Simpson, N. M.; Qiao, G. G., Ring opening polymerization of alpha-amino acids: advances in synthesis, architecture and applications of polypeptides and their hybrids. *Chem. Soc. Rev.* **2020,** *49*, 4737-4834.
(12) Kricheldorf, H. R., Polypeptides and 100 years of chemistry of alpha-amino acid N-carboxyanhydrides. *Angew. Chem. Int. Ed. Engl.* **2006,** *45*, 5752-5784.
(13) Deming, T. J., Facile synthesis of block copolypeptides of defined architecture. *Nature* **1997,** *390*, 386-389.
(14) Deming, T. J., Cobalt and iron initiators for the controlled polymerization of α-amino acid-N-carboxyanhydrides. *Macromolecules* **1999,** *32*, 4500-4502.
(15) Deming, T. J., Synthesis of Side-Chain Modified Polypeptides. *Chem. Rev.* **2016,** *116*, 786-808.
(16) Deng, C.; Wu, J.; Cheng, R.; Meng, F.; Klok, H.-A.; Zhong, Z., Functional polypeptide and hybrid materials: Precision synthesis via α-amino acid N-carboxyanhydride polymerization and emerging biomedical applications. *Prog. Polym. Sci.* **2014,** *39*, 330-364.
(17) Aliferis, T.; Iatrou, H.; Hadjichristidis, N., Living polypeptides. *Biomacromolecules* **2004,** *5*, 1653.
(18) Poché, D. S.; Moore, M. J.; Bowles, J. L., an unconventional method for purifying the N-carboxyanhydride derivatives of γ-alkyl-L-glutamates. *Synth. Commun.* **1999,** *29*, 843.
(19) Kramer, J. R.; Deming, T. J., General Method for Purification of α-Amino acid-N-carboxyanhydrides Using Flash Chromatography. *Biomacromolecules* **2010,** *11*, 3668-3672.
(20) Semple, J. E.; Sullivan, B.; Sill, K. N., Large-scale synthesis of α-amino acid-N-carboxyanhydrides. *Synth. Commun.* **2017,** *47*, 53-61.
(21) Yamada, S.; Sudo, A.; Goto, M.; Endo, T., Phosgene-free synthesis of polypeptides using activated urethane derivatives of α-amino acids: an efficient synthetic approach to hydrophilic polypeptides. *RSC Adv.* **2014,** *4*, 29890-29896.

(22) Kamei, Y.; Sudo, A.; Nishida, H.; Kikukawa, K.; Endo, T., Synthesis of polypeptides from activated urethane derivatives of α-amino acids. *J. Polym. Sci. A Polym. Chem.* **2008,** *46*, 2525-2535.
(23) Tao, X.; Li, M.-H.; Ling, J., α-Amino acid N-thiocarboxyanhydrides: A novel synthetic approach toward poly(α-amino acid)s. *Eur. Polym. J.* **2018,** *109*, 26-42.
(24) Otake, Y.; Nakamura, H.; Fuse, S., Rapid and mild synthesis of amino acid N-carboxy anhydrides: basic-to-acidic flash switching in a microflow reactor. *Angew. Chem., Int. Ed.* **2018,** *57*, 11389.
(25) Tian, Z.-Y.; Zhang, Z.; Wang, S.; Lu, H., A moisture-tolerant route to unprotected α/β-amino acid N-carboxyanhydrides and facile synthesis of hyperbranched polypeptides. *Nat. Commun.* **2021,** *12*, 5810.
(26) Cheng, J.; Deming, T. J., Synthesis of Polypeptides by Ring-Opening Polymerization of α-Amino Acid N-Carboxyanhydrides. In *Peptide-Based Materials. Top Curr Chem*, Deming, T., Ed. Springer Berlin Heidelberg: Berlin, Heidelberg, 2012; pp 1-26.
(27) Detwiler, R. E.; Schlirf, A. E.; Kramer, J. R., Rethinking Transition Metal Catalyzed N-Carboxyanhydride Polymerization: Polymerization of Pro and AcOPro N-Carboxyanhydrides. *J. Am. Chem. Soc.* **2021,** *143*, 11482-11489.
(28) Curtin, S. A.; Deming, T. J., Initiators for End-Group Functionalized Polypeptides via Tandem Addition Reactions. *J. Am. Chem. Soc.* **1999,** *121*, 7427-7428.
(29) Song, Z.; Han, Z.; Lv, S.; Chen, C.; Chen, L.; Yin, L.; Cheng, J., Synthetic polypeptides: from polymer design to supramolecular assembly and biomedical application. *Chem. Soc. Rev.* **2017,** *46*, 6570-6599.
(30) Dimitrov, I.; Schlaad, H., Synthesis of nearly monodisperse polystyrene–polypeptide block copolymers via polymerisation of N-carboxyanhydrides. *Chem. Commun.* **2003**, 2944-2945.
(31) Vacogne, C. D.; Schlaad, H., Primary ammonium/tertiary amine-mediated controlled ring opening polymerisation of amino acid N-carboxyanhydrides. *Chem. Commun.* **2015,** *51*, 15645-15648.
(32) Conejos-Sánchez, I.; Duro-Castano, A.; Birke, A.; Barz, M.; Vicent, M. J., A controlled and versatile NCA polymerization method for the synthesis of polypeptides. *Polym. Chem.* **2013,** *4*, 3182-3186.
(33) Zhang, H.; Nie, Y.; Zhi, X.; Du, H.; Yang, J., Controlled ring-opening polymerization of α-amino acid N-carboxy-anhydride by frustrated amine/borane Lewis pairs. *Chem. Commun.* **2017,** *53*, 5155-5158.
(34) Nie, Y.; Zhi, X.; Du, H.; Yang, J., Zn(OAc)2-Catalyzing Ring-Opening Polymerization of N-Carboxyanhydrides for the Synthesis of Well-Defined Polypeptides. *Molecules* **2018,** *23*, 760.
(35) Lu, H.; Cheng, J., Hexamethyldisilazane-mediated controlled polymerization of alpha-amino acid N-carboxyanhydrides. *J. Am. Chem. Soc.* **2007,** *129*, 14114-14115.
(36) Lu, H.; Cheng, J., N-Trimethylsilyl Amines for Controlled Ring-Opening Polymerization of Amino Acid N-Carboxyanhydrides and Facile End Group Functionalization of Polypeptides. *J. Am. Chem. Soc.* **2008,** *130*, 12562-12563.
(37) Yuan, J.; Sun, Y.; Wang, J.; Lu, H., Phenyl Trimethylsilyl Sulfide-Mediated Controlled Ring-Opening Polymerization of alpha-Amino Acid N-Carboxyanhydrides. *Biomacromolecules* **2016,** *17*, 891-896.
(38) Hou, Y.; Zhou, Y.; Wang, H.; Sun, J.; Wang, R.; Sheng, K.; Yuan, J.; Hu, Y.; Chao, Y.; Liu, Z.; Lu, H., Therapeutic Protein PEPylation: The Helix of Nonfouling Synthetic Polypeptides Minimizes Antidrug Antibody Generation. *ACS Cent. Sci.* **2019,** *5*, 229-236.

(39) Yuan, J.; Zhang, Y.; Li, Z.; Wang, Y.; Lu, H., A S-Sn Lewis pair-mediated ring-opening polymerization of α-amino acid N-carboxyanhydrides: fast kinetics, high molecular weight, and facile bioconjugation. *ACS Macro Lett.* **2018,** *7*, 892-897.
(40) Zhao, W.; Gnanou, Y.; Hadjichristidis, N., From competition to cooperation: a highly efficient strategy towards well-defined (co)polypeptides. *Chem. Commun. (Camb).* **2015,** *51*, 3663-3666.
(41) Zhao, W.; Gnanou, Y.; Hadjichristidis, N., Fast and living ring-opening polymerization of α-amino acid N-carboxyanhydrides triggered by an "alliance" of primary and secondary amines at room temperature. *Biomacromolecules* **2015,** *16*, 1352-1357.
(42) Wu, Y.; Zhang, D.; Ma, P.; Zhou, R.; Hua, L.; Liu, R., Lithium hexamethyldisilazide initiated superfast ring opening polymerization of alpha-amino acid N-carboxyanhydrides. *Nat. Commun.* **2018,** *9*, 5297.
(43) Wu, Y.-M.; Zhang, W.-W.; Zhou, R.-Y.; Chen, Q.; Xie, C.-Y.; Xiang, H.-X.; Sun, B.; Zhu, M.-F.; Liu, R.-H., Facile Synthesis of High Molecular Weight Polypeptides via Fast and Moisture Insensitive Polymerization of α-Amino Acid N-Carboxyanhydrides. *Chin J Polym Sci* **2020,** *38*, 1131-1140.
(44) Wu, Y.; Chen, K.; Wu, X.; Liu, L.; Zhang, W.; Ding, Y.; Liu, S.; Zhou, M.; Shao, N.; Ji, Z.; Chen, J.; Zhu, M.; Liu, R., Superfast and Water-Insensitive Polymerization on α-Amino Acid N-Carboxyanhydrides to Prepare Polypeptides Using Tetraalkylammonium Carboxylate as the Initiator. *Angew. Chem. Int. Ed.* **2021,** *60*, 26063-26071.
(45) Jeong, W.; Shin, E. J.; Culkin, D. A.; Hedrick, J. L.; Waymouth, R. M., Zwitterionic Polymerization: A Kinetic Strategy for the Controlled Synthesis of Cyclic Polylactide. *J. Am. Chem. Soc.* **2009,** *131*, 4884-4891.
(46) Culkin, D. A.; Jeong, W.; Csihony, S.; Gomez, E. D.; Balsara, N. P.; Hedrick, J. L.; Waymouth, R. M., Zwitterionic polymerization of lactide to cyclic poly(lactide) by using N-heterocyclic carbene organocatalysts. *Angew. Chem., Int. Ed.* **2007,** *46*, 2627.
(47) Connor, E. F.; Nyce, G. W.; Myers, M.; Möck, A.; Hedrick, J. L., First Example of N-Heterocyclic Carbenes as Catalysts for Living Polymerization: Organocatalytic Ring-Opening Polymerization of Cyclic Esters. *J. Am. Chem. Soc.* **2002,** *124*, 914-915.
(48) Sun, Y.; Hou, Y.; Zhou, X.; Yuan, J.; Wang, J.; Lu, H., Controlled Synthesis and Enzyme-Induced Hydrogelation of Poly(l-phosphotyrosine)s via Ring-Opening Polymerization of α-Amino Acid N-Carboxyanhydride. *ACS Macro Lett.* **2015,** *4*, 1000-1003.
(49) Fèvre, M.; Pinaud, J.; Leteneur, A.; Gnanou, Y.; Vignolle, J.; Taton, D.; Miqueu, K.; Sotiropoulos, J.-M., Imidazol(in)ium Hydrogen Carbonates as a Genuine Source of N-Heterocyclic Carbenes (NHCs): Applications to the Facile Preparation of NHC Metal Complexes and to NHC-Organocatalyzed Molecular and Macromolecular Syntheses. *J. Am. Chem. Soc.* **2012,** *134*, 6776-6784.
(50) Zhang, Y.; Liu, R.; Jin, H.; Song, W.; Augustine, R.; Kim, I., Straightforward access to linear and cyclic polypeptides. *Commun. Chem.* **2018,** *1*, 40.
(51) Zou, J.; Fan, J.; He, X.; Zhang, S.; Wang, H.; Wooley, K. L., A facile glovebox-free strategy to significantly accelerate the syntheses of well-defined polypeptides by N-Carboxyanhydride (NCA) ring-opening polymerizations. *Macromolecules* **2013,** *46*, 4223-4226.
(52) Li, K.; Li, Z.; Shen, Y.; Fu, X.; Chen, C.; Li, Z., Organobase 1,1,3,3-tetramethyl guanidine catalyzed rapid ring-opening polymerization of α-amino acid N-carboxyanhydrides adaptive to amine, alcohol and carboxyl acid initiators. *Polym. Chem.* **2022,** *13*, 586-591.

(53) Chan, B. A.; Xuan, S.; Horton, M.; Zhang, D., 1,1,3,3-Tetramethylguanidine-Promoted Ring-Opening Polymerization of N-Butyl N-Carboxyanhydride Using Alcohol Initiators. *Macromolecules* **2016,** *49*, 2002-2012.
(54) Zhao, W.; Gnanou, Y.; Hadjichristidis, N., Organocatalysis by hydrogen-bonding: a new approach to controlled/living polymerization of α-amino acid N-carboxyanhydrides. *Polym. Chem.* **2015,** *6*, 6193-6201.
(55) Zhao, W.; Lv, Y.; Li, J.; Feng, Z.; Ni, Y.; Hadjichristidis, N., A Synthetic Method for Site-Specific Functionalized Polypeptides: Metal-Free, Highly Active, and Selective at Room Temperature. *Angew. Chem. Int. Ed. Engl.* **2021,** *60*, 889-895.
(56) Zhao, W.; Lv, Y.; Li, J.; Feng, Z.; Ni, Y.; Hadjichristidis, N., Fast and selective organocatalytic ring-opening polymerization by fluorinated alcohol without a cocatalyst. *Nat. Commun.* **2019,** *10*, 3590.
(57) Gradišar, Š.; Žagar, E.; Pahovnik, D., Ring-Opening Polymerization of N-Carboxyanhydrides Initiated by a Hydroxyl Group. *ACS Macro Lett.* **2017,** *6*, 637-640.
(58) Gradišar, Š.; Žagar, E.; Pahovnik, D., Hybrid block copolymers of polyesters/polycarbonates and polypeptides synthesized via one-pot sequential ring-opening polymerization. *Polym. Chem.* **2018,** *9*, 4764-4771.
(59) Habraken, G. J. M.; Peeters, M.; Dietz, C. H. J. T.; Koning, C. E.; Heise, A., How controlled and versatile is N-carboxy anhydride (NCA) polymerization at 0 °C? Effect of temperature on homo-, block- and graft (co)polymerization. *Polym. Chem.* **2010,** *1*, 514.
(60) Habraken, G. J. M.; Wilsens, K. H. R. M.; Koning, C. E.; Heise, A., Optimization of N-carboxyanhydride (NCA) polymerization by variation of reaction temperature and pressure. *Polym. Chem.* **2011,** *2*, 1322-1330.
(61) Jacobs, J.; Pavlović, D. E.; Prydderch, H.; Moradi, M. A.; Ibarboure, E.; Heuts, J. P.; Lecommandoux, S.; Heise, A., Polypeptide nanoparticles obtained from emulsion polymerization of amino acid N-carboxyanhydrides. *J. Am. Chem. Soc.* **2019,** *141*, 12522-12526.
(62) Jiang, J.; Zhang, X.; Fan, Z.; Du, J., Ring-Opening Polymerization of N-Carboxyanhydride-Induced Self-Assembly for Fabricating Biodegradable Polymer Vesicles. *ACS Macro Lett.* **2019,** *8*, 1216-1221.
(63) Duro-Castano, A.; Rodríguez-Arco, L.; Ruiz-Pérez, L.; De Pace, C.; Marchello, G.; Noble-Jesus, C.; Battaglia, G., One-Pot Synthesis of Oxidation-Sensitive Supramolecular Gels and Vesicles. *Biomacromolecules* **2021,** *22*, 5052-5064.
(64) Grazon, C.; Salas-Ambrosio, P.; Ibarboure, E.; Buol, A.; Garanger, E.; Grinstaff, M. W.; Lecommandoux, S.; Bonduelle, C., Aqueous Ring-Opening Polymerization-Induced Self-Assembly (ROPISA) of N-Carboxyanhydrides. *Angew. Chem. Int. Ed. Engl.* **2020,** *59*, 622-626.
(65) Grazon, C.; Salas-Ambrosio, P.; Antoine, S.; Ibarboure, E.; Sandre, O.; Clulow, A. J.; Boyd, B. J.; Grinstaff, M. W.; Lecommandoux, S.; Bonduelle, C., Aqueous ROPISA of α-amino acid N-carboxyanhydrides: polypeptide block secondary structure controls nanoparticle shape anisotropy. *Polym. Chem.* **2021,** *12*, 6242-6251.
(66) Nguyen, T. P.; Easley, A. D.; Kang, N.; Khan, S.; Lim, S.-M.; Rezenom, Y. H.; Wang, S.; Tran, D. K.; Fan, J.; Letteri, R. A.; He, X.; Su, L.; Yu, C.-H.; Lutkenhaus, J. L.; Wooley, K. L., Polypeptide organic radical batteries. *Nature* **2021,** *593*, 61-66.
(67) Chen, J.; Guan, X.; Hu, Y.; Tian, H.; Chen, X., Peptide-Based and Polypeptide-Based Gene Delivery Systems. In *Polymeric Gene Delivery Systems*, Cheng, Y., Ed. Springer International Publishing: Top. Curr. Chem., 2018; pp 85-112.
(68) Ahmed, M., Peptides, polypeptides and peptide–polymer hybrids as nucleic acid carriers. *Biomater. Sci.* **2017,** *5*, 2188-2211.

(69) Yin, H.; Kanasty, R. L.; Eltoukhy, A. A.; Vegas, A. J.; Dorkin, J. R.; Anderson, D. G., Non-viral vectors for gene-based therapy. *Nat. Rev. Genet.* **2014,** *15*, 541-555.
(70) Wang, H.-X.; Song, Z.; Lao, Y.-H.; Xu, X.; Gong, J.; Cheng, D.; Chakraborty, S.; Park, J. S.; Li, M.; Huang, D. J. P. o. t. N. A. o. S., Nonviral gene editing via CRISPR/Cas9 delivery by membrane-disruptive and endosomolytic helical polypeptide. *Proc. Natl. Acad. Sci. U. S. A.* **2018,** *115*, 4903-4908.
(71) Walsh, D. P.; Raftery, R. M.; Castaño, I. M.; Murphy, R.; Cavanagh, B.; Heise, A.; O'Brien, F. J.; Cryan, S.-A., Transfection of autologous host cells in vivo using gene activated collagen scaffolds incorporating star-polypeptides. *J. Control. Release* **2019,** *304*, 191-203.
(72) Chen, B.; Yu, L.; Li, Z.; Wu, C., Design of Free Triblock Polylysine-b-Polyleucine-b-Polylysine Chains for Gene Delivery. *Biomacromolecules* **2018,** *19*, 1347-1357.
(73) Liarou, E.; Varlas, S.; Skoulas, D.; Tsimblouli, C.; Sereti, E.; Dimas, K.; Iatrou, H., Smart polymersomes and hydrogels from polypeptide-based polymer systems through α-amino acid N-carboxyanhydride ring-opening polymerization. From chemistry to biomedical applications. *Prog. Polym. Sci.* **2018,** *83*, 28-78.
(74) Zhou, X.; Li, Z., Advances and Biomedical Applications of Polypeptide Hydrogels Derived from α-Amino Acid N-Carboxyanhydride (NCA) Polymerizations. *Adv. Healthcare Mater.* **2018,** *7*, 1800020.
(75) Murphy, R.; Walsh, D. P.; Hamilton, C. A.; Cryan, S.-A.; in het Panhuis, M.; Heise, A., Degradable 3D-Printed Hydrogels Based on Star-Shaped Copolypeptides. *Biomacromolecules* **2018,** *19*, 2691-2699.
(76) Li, C.; Faulkner-Jones, A.; Dun, A. R.; Jin, J.; Chen, P.; Xing, Y.; Yang, Z.; Li, Z.; Shu, W.; Liu, D.; Duncan, R. R., Rapid Formation of a Supramolecular Polypeptide–DNA Hydrogel for In Situ Three-Dimensional Multilayer Bioprinting. *Angew. Chem. Int. Ed.* **2015,** *54*, 3957-3961.
(77) Patel, M.; Lee, H. J.; Park, S.; Kim, Y.; Jeong, B., Injectable thermogel for 3D culture of stem cells. *Biomaterials* **2018,** *159*, 91-107.
(78) Yan, S.; Wang, T.; Feng, L.; Zhu, J.; Zhang, K.; Chen, X.; Cui, L.; Yin, J., Injectable In Situ Self-Cross-Linking Hydrogels Based on Poly(l-glutamic acid) and Alginate for Cartilage Tissue Engineering. *Biomacromolecules* **2014,** *15*, 4495-4508.
(79) Bozokalfa, G.; Akbulut, H.; Demir, B.; Guler, E.; Gumus, Z. P.; Odaci Demirkol, D.; Aldemir, E.; Yamada, S.; Endo, T.; Coskunol, H.; Timur, S.; Yagci, Y., Polypeptide Functional Surface for the Aptamer Immobilization: Electrochemical Cocaine Biosensing. *Anal. Chem.* **2016,** *88*, 4161-4167.
(80) Celikbas, E.; Guler Celik, E.; Odaci Demirkol, D.; Yamada, S.; Endo, T.; Timur, S.; Yagci, Y., Surface Modification with a Catechol-Bearing Polypeptide and Sensing Applications. *Biomacromolecules* **2018,** *19*, 3067-3076.
(81) Gao, Q.; Yu, M.; Su, Y.; Xie, M.; Zhao, X.; Li, P.; Ma, P. X., Rationally designed dual functional block copolymers for bottlebrush-like coatings: In vitro and in vivo antimicrobial, antibiofilm, and antifouling properties. *Acta Biomater.* **2017,** *51*, 112-124.
(82) Yilmaz, T.; Guler, E.; Gumus, Z. P.; Akbulut, H.; Aldemir, E.; Coskunol, H.; Goen Colak, D.; Cianga, I.; Yamada, S.; Timur, S.; Endo, T.; Yagci, Y., Synthesis and application of a novel poly-l-phenylalanine electroactive macromonomer as matrix for the biosensing of 'Abused Drug' model. *Polym. Chem.* **2016,** *7*, 7304-7315.
(83) Zhang, C.; Lu, J.; Hou, Y.; Xiong, W.; Sheng, K.; Lu, H., Investigation on the Linker Length of Synthetic Zwitterionic Polypeptides for Improved Nonfouling Surfaces. *ACS Appl. Mater. Interfaces* **2018,** *10*, 17463-17470.
(84) Yoo, J.; Birke, A.; Kim, J.; Jang, Y.; Song, S. Y.; Ryu, S.; Kim, B.-S.; Kim, B.-G.; Barz, M.; Char, K., Cooperative Catechol-Functionalized Polypept(o)ide Brushes and Ag

Nanoparticles for Combination of Protein Resistance and Antimicrobial Activity on Metal Oxide Surfaces. *Biomacromolecules* **2018,** *19*, 1602-1613.
(85) Zhang, C.; Yuan, J.; Lu, J.; Hou, Y.; Xiong, W.; Lu, H., From neutral to zwitterionic poly(α-amino acid) nonfouling surfaces: Effects of helical conformation and anchoring orientation. *Biomaterials* **2018,** *178*, 728-737.
(86) Lu, D.; Wang, H.; Li, T. e.; Li, Y.; Wang, X.; Niu, P.; Guo, H.; Sun, S.; Wang, X.; Guan, X.; Ma, H.; Lei, Z., Versatile Surgical Adhesive and Hemostatic Materials: Synthesis, Properties, and Application of Thermoresponsive Polypeptides. *Chem. Mater.* **2017,** *29*, 5493-5503.
(87) Lu, D.; Wang, H.; Li, T. e.; Li, Y.; Dou, F.; Sun, S.; Guo, H.; Liao, S.; Yang, Z.; Wei, Q.; Lei, Z., Mussel-Inspired Thermoresponsive Polypeptide–Pluronic Copolymers for Versatile Surgical Adhesives and Hemostasis. *ACS Appl. Mater. Interfaces* **2017,** *9*, 16756-16766.
(88) Lu, D.; Li, Y.; Wang, X.; Li, T. e.; Zhang, Y.; Guo, H.; Sun, S.; Wang, X.; Zhang, Y.; Lei, Z., All-in-one hyperbranched polypeptides for surgical adhesives and interventional embolization of tumors. *J. Mater. Chem. B.* **2018,** *6*, 7511-7520.
(89) Wyrsta, M. D.; Cogen, A. L.; Deming, T. J., A Parallel Synthetic Approach for the Analysis of Membrane Interactive Copolypeptides. *J. Am. Chem. Soc.* **2001,** *123*, 12919-12920.
(90) Zhou, C.; Qi, X.; Li, P.; Chen, W. N.; Mouad, L.; Chang, M. W.; Leong, S. S. J.; Chan-Park, M. B., High Potency and Broad-Spectrum Antimicrobial Peptides Synthesized via Ring-Opening Polymerization of α-Aminoacid-N-carboxyanhydrides. *Biomacromolecules* **2010,** *11*, 60-67.
(91) Xiong, M.; Lee, M. W.; Mansbach, R. A.; Song, Z.; Bao, Y.; Peek, R. M.; Yao, C.; Chen, L. F.; Ferguson, A. L.; Wong, G. C. L.; Cheng, J., Helical antimicrobial polypeptides with radial amphiphilicity. *Proc. Natl. Acad. Sci. U. S. A.* **2015,** *112*, 13155.
(92) Chen, Y.-F.; Lai, Y.-D.; Chang, C.-H.; Tsai, Y.-C.; Tang, C.-C.; Jan, J.-S., Star-shaped polypeptides exhibit potent antibacterial activities. *Nanoscale* **2019,** *11*, 11696-11708.
(93) Pranantyo, D.; Xu, L. Q.; Hou, Z.; Kang, E.-T.; Chan-Park, M. B., Increasing bacterial affinity and cytocompatibility with four-arm star glycopolymers and antimicrobial α-polylysine. *Polym. Chem.* **2017,** *8*, 3364-3373.
(94) Lam, S. J.; O'Brien-Simpson, N. M.; Pantarat, N.; Sulistio, A.; Wong, E. H. H.; Chen, Y.-Y.; Lenzo, J. C.; Holden, J. A.; Blencowe, A.; Reynolds, E. C.; Qiao, G. G., Combating multidrug-resistant Gram-negative bacteria with structurally nanoengineered antimicrobial peptide polymers. *Nat. Microbiol.* **2016,** *1*, 16162.
(95) Shirbin, S. J.; Insua, I.; Holden, J. A.; Lenzo, J. C.; Reynolds, E. C.; O'Brien-Simpson, N. M.; Qiao, G. G., Architectural Effects of Star-Shaped "Structurally Nanoengineered Antimicrobial Peptide Polymers" (SNAPPs) on Their Biological Activity. *Adv. Healthcare Mater.* **2018,** *7*, 1800627.
(96) Zhang, Y.; Song, W.; Li, S.; Kim, D.-K.; Kim, J. H.; Kim, J. R.; Kim, I., Facile and scalable synthesis of topologically nanoengineered polypeptides with excellent antimicrobial activities. *Chem. Commun.* **2020,** *56*, 356-359.
(97) Gao, J.; Wang, M.; Wang, F.; Du, J., Synthesis and Mechanism Insight of a Peptide-Grafted Hyperbranched Polymer Nanosheet with Weak Positive Charges but Excellent Intrinsically Antibacterial Efficacy. *Biomacromolecules* **2016,** *17*, 2080-2086.
(98) Li, P.; Zhou, C.; Rayatpisheh, S.; Ye, K.; Poon, Y. F.; Hammond, P. T.; Duan, H.; Chan-Park, M. B., Cationic Peptidopolysaccharides Show Excellent Broad-Spectrum Antimicrobial Activities and High Selectivity. *Adv. Mater.* **2012,** *24*, 4130-4137.

(99) Nakamura, R.; Aoi, K.; Okada, M., Controlled Synthesis of a Chitosan-Based Graft Copolymer Having Polysarcosine Side Chains Using the NCA Method with a Carboxylic Acid Additive. *Macromol. Rapid Commun.* **2006,** *27*, 1725-1732.
(100) Gao, Q.; Li, P.; Zhao, H.; Chen, Y.; Jiang, L.; Ma, P. X., Methacrylate-ended polypeptides and polypeptoids for antimicrobial and antifouling coatings. *Polym. Chem.* **2017,** *8*, 6386-6397.
(101) Xiong, M.; Han, Z.; Song, Z.; Yu, J.; Ying, H.; Yin, L.; Cheng, J., Bacteria-assisted activation of antimicrobial polypeptides by a random-coil to helix transition. *Angew. Chem., Int. Ed.* **2017,** *56*, 10826.
(102) Xiong, M.; Bao, Y.; Xu, X.; Wang, H.; Han, Z.; Wang, Z.; Liu, Y.; Huang, S.; Song, Z.; Chen, J.; Peek, R. M.; Yin, L.; Chen, L. F.; Cheng, J., Selective killing of Helicobacter pylori with pH-responsive helix–coil conformation transitionable antimicrobial polypeptides. *Proc. Natl. Acad. Sci. U. S. A.* **2017,** *114*, 12675.
(103) Hong, Y.; Xi, Y.; Zhang, J.; Wang, D.; Zhang, H.; Yan, N.; He, S.; Du, J., Polymersome–hydrogel composites with combined quick and long-term antibacterial activities. *J. Mater. Chem. B.* **2018,** *6*, 6311-6321.
(104) Wan, Y.; Liu, L.; Yuan, S.; Sun, J.; Li, Z., pH-Responsive Peptide Supramolecular Hydrogels with Antibacterial Activity. *Langmuir* **2017,** *33*, 3234-3240.
(105) Shirbin, S. J.; Lam, S. J.; Chan, N. J.-A.; Ozmen, M. M.; Fu, Q.; O'Brien-Simpson, N.; Reynolds, E. C.; Qiao, G. G., Polypeptide-Based Macroporous Cryogels with Inherent Antimicrobial Properties: The Importance of a Macroporous Structure. *ACS Macro Lett.* **2016,** *5*, 552-557.
(106) Gao, Q.; Feng, T.; Huang, D.; Liu, P.; Lin, P.; Wu, Y.; Ye, Z.; Ji, J.; Li, P.; Huang, W., Antibacterial and hydroxyapatite-forming coating for biomedical implants based on polypeptide-functionalized titania nanospikes. *Biomater. Sci.* **2020,** *8*, 278-289.
(107) Xu, H.; Yao, Q.; Cai, C.; Gou, J.; Zhang, Y.; Zhong, H.; Tang, X., Amphiphilic poly(amino acid) based micelles applied to drug delivery: The in vitro and in vivo challenges and the corresponding potential strategies. *J. Control. Release* **2015,** *199*, 84-97.
(108) Mochida, Y.; Cabral, H.; Miura, Y.; Albertini, F.; Fukushima, S.; Osada, K.; Nishiyama, N.; Kataoka, K., Bundled assembly of helical nanostructures in polymeric micelles loaded with platinum drugs enhancing therapeutic efficiency against pancreatic tumor. *ACS Nano* **2014,** *8*, 6724.
(109) Sill, K. N.; Sullivan, B.; Carie, A.; Semple, J. E., Synthesis and Characterization of Micelle-Forming PEG-Poly(Amino Acid) Copolymers with Iron-Hydroxamate Cross-Linkable Blocks for Encapsulation and Release of Hydrophobic Drugs. *Biomacromolecules* **2017,** *18*, 1874-1884.
(110) Gu, X.; Qiu, M.; Sun, H.; Zhang, J.; Cheng, L.; Deng, C.; Zhong, Z., Polytyrosine nanoparticles enable ultra-high loading of doxorubicin and rapid enzyme-responsive drug release. *Biomater. Sci.* **2018,** *6*, 1526-1534.
(111) Yi, H.; Liu, P.; Sheng, N.; Gong, P.; Ma, Y.; Cai, L., In situ crosslinked smart polypeptide nanoparticles for multistage responsive tumor-targeted drug delivery. *Nanoscale* **2016,** *8*, 5985-5995.
(112) Shirbin, S. J.; Ladewig, K.; Fu, Q.; Klimak, M.; Zhang, X.; Duan, W.; Qiao, G. G., Cisplatin-Induced Formation of Biocompatible and Biodegradable Polypeptide-Based Vesicles for Targeted Anticancer Drug Delivery. *Biomacromolecules* **2015,** *16*, 2463-2474.
(113) Jeannot, V.; Mazzaferro, S.; Lavaud, J.; Vanwonterghem, L.; Henry, M.; Arboléas, M.; Vollaire, J.; Josserand, V.; Coll, J.-L.; Lecommandoux, S.; Schatz, C.; Hurbin, A., Targeting CD44 receptor-positive lung tumors using polysaccharide-based nanocarriers: Influence of nanoparticle size and administration route. *Nanomedicine* **2016,** *12*, 921-932.

(114) Duan, H.; Donovan, M.; Foucher, A.; Schultze, X.; Lecommandoux, S., Multivalent and multifunctional polysaccharide-based particles for controlled receptor recognition. *Sci. Rep.* **2018,** *8*, 14730.
(115) Pati, D.; Das, S.; Patil, N. G.; Parekh, N.; Anjum, D. H.; Dhaware, V.; Ambade, A. V.; Sen Gupta, S., Tunable Nanocarrier Morphologies from Glycopolypeptide-Based Amphiphilic Biocompatible Star Copolymers and Their Carbohydrate Specific Intracellular Delivery. *Biomacromolecules* **2016,** *17*, 466-475.
(116) Gu, X.; Wei, Y.; Fan, Q.; Sun, H.; Cheng, R.; Zhong, Z.; Deng, C., cRGD-decorated biodegradable polytyrosine nanoparticles for robust encapsulation and targeted delivery of doxorubicin to colorectal cancer in vivo. *J Control Release* **2019,** *301*, 110-118.
(117) Chen, P.; Qiu, M.; Deng, C.; Meng, F.; Zhang, J.; Cheng, R.; Zhong, Z., pH-Responsive Chimaeric Pepsomes Based on Asymmetric Poly(ethylene glycol)-b-Poly(l-leucine)-b-Poly(l-glutamic acid) Triblock Copolymer for Efficient Loading and Active Intracellular Delivery of Doxorubicin Hydrochloride. *Biomacromolecules* **2015,** *16*, 1322-1330.
(118) Han, S.-S.; Li, Z.-Y.; Zhu, J.-Y.; Han, K.; Zeng, Z.-Y.; Hong, W.; Li, W.-X.; Jia, H.-Z.; Liu, Y.; Zhuo, R.-X.; Zhang, X.-Z., Dual-pH Sensitive Charge-Reversal Polypeptide Micelles for Tumor-Triggered Targeting Uptake and Nuclear Drug Delivery. *Small* **2015,** *11*, 2543-2554.
(119) Quader, S.; Cabral, H.; Mochida, Y.; Ishii, T.; Liu, X.; Toh, K.; Kinoh, H.; Miura, Y.; Nishiyama, N.; Kataoka, K., Selective intracellular delivery of proteasome inhibitors through pH-sensitive polymeric micelles directed to efficient antitumor therapy. *J. Control. Release* **2014,** *188*, 67-77.
(120) Ding, Y.; Du, C.; Qian, J.; Zhou, L.; Su, Y.; Zhang, R.; Dong, C.-M., Tumor pH and intracellular reduction responsive polypeptide nanomedicine with a sheddable PEG corona and a disulfide-cross-linked core. *Polym. Chem.* **2018,** *9*, 3488-3498.
(121) Yen, H.-C.; Cabral, H.; Mi, P.; Toh, K.; Matsumoto, Y.; Liu, X.; Koori, H.; Kim, A.; Miyazaki, K.; Miura, Y.; Nishiyama, N.; Kataoka, K., Light-Induced Cytosolic Activation of Reduction-Sensitive Camptothecin-Loaded Polymeric Micelles for Spatiotemporally Controlled in Vivo Chemotherapy. *ACS Nano* **2014,** *8*, 11591-11602.
(122) Huang, K.; Shi, B.; Xu, W.; Ding, J.; Yang, Y.; Liu, H.; Zhuang, X.; Chen, X., Reduction-responsive polypeptide nanogel delivers antitumor drug for improved efficacy and safety. *Acta Biomater.* **2015,** *27*, 179-193.
(123) Yoo, J.; Sanoj Rejinold, N.; Lee, D.; Jon, S.; Kim, Y.-C., Protease-activatable cell-penetrating peptide possessing ROS-triggered phase transition for enhanced cancer therapy. *J. Control. Release* **2017,** *264*, 89-101.
(124) Deepagan, V. G.; Kwon, S.; You, D. G.; Nguyen, V. Q.; Um, W.; Ko, H.; Lee, H.; Jo, D.-G.; Kang, Y. M.; Park, J. H., In situ diselenide-crosslinked polymeric micelles for ROS-mediated anticancer drug delivery. *Biomaterials* **2016,** *103*, 56-66.
(125) Bacinello, D.; Garanger, E.; Taton, D.; Tam, K. C.; Lecommandoux, S., Tailored drug-release from multi-functional polymer-peptide hybrid vesicles. *Eur. Polym. J.* **2015,** *62*, 363-373.
(126) Liu, G.; Zhou, L.; Guan, Y.; Su, Y.; Dong, C., Multi-Responsive Polypeptidosome: Characterization, Morphology Transformation, and Triggered Drug Delivery. *Macromol. Rapid Commun.* **2014,** *35*, 1673.
(127) Song, Z.; Kim, H.; Ba, X.; Baumgartner, R.; Lee, J. S.; Tang, H.; Leal, C.; Cheng, J., Polypeptide vesicles with densely packed multilayer membranes. *Soft Matter* **2015,** *11*, 4091-4098.
(128) Fujiwara, Y.; Mukai, H.; Saeki, T.; Ro, J.; Lin, Y.-C.; Nagai, S. E.; Lee, K. S.; Watanabe, J.; Ohtani, S.; Kim, S. B.; Kuroi, K.; Tsugawa, K.; Tokuda, Y.; Iwata, H.;

Park, Y. H.; Yang, Y.; Nambu, Y., A multi-national, randomised, open-label, parallel, phase III non-inferiority study comparing NK105 and paclitaxel in metastatic or recurrent breast cancer patients. *Br. J. Cancer* **2019,** *120*, 475-480.
(129) Song, Z.; Fu, H.; Wang, R.; Pacheco, L. A.; Wang, X.; Lin, Y.; Cheng, J., Secondary structures in synthetic polypeptides from N-carboxyanhydrides: design, modulation, association, and material applications. *Chem. Soc. Rev.* **2018,** *47*, 7401-7425.
(130) Deming, T. J., Synthesis and Self-Assembly of Well-Defined Block Copolypeptides via Controlled NCA Polymerization. In *Hierarchical Macromolecular Structures: 60 Years after the Staudinger Nobel Prize II*, Percec, V., Ed. Springer International Publishing: Cham, 2013; pp 1-37.
(131) Deming, T. J., Synthetic polypeptides for biomedical applications. *Prog. Polym. Sci.* **2007,** *32*, 858-875.
(132) Chen, J.; Ding, J.; Wang, Y.; Cheng, J.; Ji, S.; Zhuang, X.; Chen, X., Sequentially Responsive Shell-Stacked Nanoparticles for Deep Penetration into Solid Tumors. *Adv. Funct. Mater.* **2017,** *29*, 1701170.
(133) Song, Z.; Fu, H.; Baumgartner, R.; Zhu, L.; Shih, K. C.; Xia, Y.; Zheng, X.; Yin, L.; Chipot, C.; Lin, Y.; Cheng, J., Enzyme-mimetic self-catalyzed polymerization of polypeptide helices. *Nat. Commun.* **2019,** *10*, 5470.
(134) Xia, Y.; Song, Z.; Tan, Z.; Xue, T.; Wei, S.; Zhu, L.; Yang, Y.; Fu, H.; Jiang, Y.; Lin, Y.; Lu, Y.; Ferguson, A. L.; Cheng, J., Accelerated polymerization of N-carboxyanhydrides catalyzed by crown ether. *Nat. Commun.* **2021,** *12*, 732.
(135) Baumgartner, R.; Fu, H.; Song, Z.; Lin, Y.; Cheng, J., Cooperative polymerization of alpha-helices induced by macromolecular architecture. *Nat. Chem.* **2017,** *9*, 614-622.
(136) Chen, C.; Fu, H.; Baumgartner, R.; Song, Z.; Lin, Y.; Cheng, J., Proximity-induced cooperative polymerization in "hinged" helical polypeptides. *J. Am. Chem. Soc.* **2019,** *141*, 8680-8683.
(137) Lv, S.; Kim, H.; Song, Z.; Feng, L.; Yang, Y.; Baumgartner, R.; Tseng, K. Y.; Dillon, S. J.; Leal, C.; Yin, L.; Cheng, J., Unimolecular Polypeptide Micelles via Ultrafast Polymerization of N-Carboxyanhydrides. *J. Am. Chem. Soc.* **2020,** *142*, 8570-8574.
(138) Song, Z.; Fu, H.; Wang, J.; Hui, J.; Xue, T.; Pacheco, L. A.; Yan, H.; Baumgartner, R.; Wang, Z.; Xia, Y.; Wang, X.; Yin, L.; Chen, C.; Rodriguez-Lopez, J.; Ferguson, A. L.; Lin, Y.; Cheng, J., Synthesis of polypeptides via bioinspired polymerization of in situ purified N-carboxyanhydrides. *Proc. Natl. Acad. Sci. U. S. A.* **2019,** *116*, 10658-10663.
(139) Kricheldorf, H. R., *α-aminoacid-N-carboxy-anhydrides and related heterocycles: syntheses, properties, peptide synthesis, polymerization*. Springer Science & Business Media: 2012.
(140) Khuphe, M.; Mukonoweshuro, B.; Kazlauciunas, A.; Thornton, P. D., A vegetable oil-based organogel for use in pH-mediated drug delivery. *Soft Matter* **2015,** *11*, 9160-9167.
(141) Canning, A.; Pasquazi, A.; Fijten, M.; Rajput, S.; Buttery, L.; Aylott, J. W.; Zelzer, M., Tuning the conformation of synthetic co-polypeptides of serine and glutamic acid through control over polymer composition. *J. Polym. Sci., Part A: Polym.Chem.* **2016,** *54*, 2331-2336.
(142) Price, D. J.; Khuphe, M.; Davies, R. P. W.; McLaughlan, J. R.; Ingram, N.; Thornton, P. D., Poly(amino acid)-polyester graft copolymer nanoparticles for the acid-mediated release of doxorubicin. *Chem. Commun.* **2017,** *53*, 8687-8690.
(143) Tooney, N. M.; Fasman, G. D., Synthesis of poly-O-tert-butyl-L-serine and poly-L-serine. *Biopolymers* **1968,** *6*, 81-96.
(144) Tai, W.; Mo, R.; Di, J.; Subramanian, V.; Gu, X.; Gu, Z., Bio-Inspired Synthetic Nanovesicles for Glucose-Responsive Release of Insulin. *Biomacromolecules* **2014,** *15*, 3495-3502.

(145) Yu, J.; Qian, C.; Zhang, Y.; Cui, Z.; Zhu, Y.; Shen, Q.; Ligler, F. S.; Buse, J. B.; Gu, Z., Hypoxia and H_2O_2 Dual-Sensitive Vesicles for Enhanced Glucose-Responsive Insulin Delivery. *Nano Lett.* **2017,** *17*, 733-739.
(146) Qian, C.; Feng, P.; Yu, J.; Chen, Y.; Hu, Q.; Sun, W.; Xiao, X.; Hu, X.; Bellotti, A.; Shen, Q.-D.; Gu, Z., Anaerobe-Inspired Anticancer Nanovesicles. *Angew. Chem. Int. Ed.* **2017,** *56*, 2588-2593.
(147) Hu, X.; Yu, J.; Qian, C.; Lu, Y.; Kahkoska, A. R.; Xie, Z.; Jing, X.; Buse, J. B.; Gu, Z., H_2O_2-Responsive Vesicles Integrated with Transcutaneous Patches for Glucose-Mediated Insulin Delivery. *ACS Nano* **2017,** *11*, 613-620.
(148) Xiao, Y.; Tang, C.; Chen, Y.; Lang, M., Dual stimuli-responsive polypeptide prepared by thiol-ene click reaction of poly(l-cysteine) and N, N-dimethylaminoethyl acrylate. **2019,** *110*, e23318.
(149) Liu, G.; Dong, C.-M., Photoresponsive Poly(S-(o-nitrobenzyl)-l-cysteine)-b-PEO from a l-Cysteine N-Carboxyanhydride Monomer: Synthesis, Self-Assembly, and Phototriggered Drug Release. *Biomacromolecules* **2012,** *13*, 1573-1583.
(150) Liu, G.; Zhou, L.; Su, Y.; Dong, C.-M., An NIR-responsive and sugar-targeted polypeptide composite nanomedicine for intracellular cancer therapy. *Chem. Commun.* **2014,** *50*, 12538-12541.
(151) Wu, X.; Zhou, L.; Su, Y.; Dong, C.-M., Comb-like poly(l-cysteine) derivatives with different side groups: synthesis via photochemistry and click chemistry, multi-responsive nanostructures, triggered drug release and cytotoxicity. *Polym. Chem.* **2015,** *6*, 6857-6869.
(152) Sun, J.; Chen, X.; Lu, T.; Liu, S.; Tian, H.; Guo, Z.; Jing, X., Formation of Reversible Shell Cross-Linked Micelles from the Biodegradable Amphiphilic Diblock Copolymer Poly(l-cysteine)-block-Poly(l-lactide). *Langmuir* **2008,** *24*, 10099-10106.
(153) Obeid, R.; Scholz, C., Synthesis and Self-Assembly of Well-Defined Poly(amino acid) End-Capped Poly(ethylene glycol) and Poly(2-methyl-2-oxazoline). *Biomacromolecules* **2011,** *12*, 3797-3804.
(154) Si, J.; Liang, D.; Kong, D.; Wu, S.; Yuan, L.; Xiang, Y.; Jiang, L., A low-toxic artificial fluorescent glycoprotein can serve as an efficient cytoplasmic labeling in living cell. *Carbohydr. Polym.* **2015,** *117*, 211-214.
(155) Xu, W.; Ding, J.; Chen, X., Reduction-Responsive Polypeptide Micelles for Intracellular Delivery of Antineoplastic Agent. *Biomacromolecules* **2017,** *18*, 3291-3301.
(156) Schäfer, O.; Huesmann, D.; Barz, M., Poly(S-ethylsulfonyl-L-cysteines) for Chemoselective Disulfide Formation. *Macromolecules* **2016,** *49*, 8146-8153.
(157) Schäfer, O.; Huesmann, D.; Muhl, C.; Barz, M., Rethinking Cysteine Protective Groups: S-Alkylsulfonyl-l-Cysteines for Chemoselective Disulfide Formation. *Chem. Eur. J.* **2016,** *22*, 18085-18091.
(158) Zheng, Y.; Wang, Z.; Li, Z.; Liu, H.; Wei, J.; Peng, C.; Zhou, Y.; Li, J.; Fu, Q.; Tan, H.; Ding, M., Ordered Conformation-Regulated Vesicular Membrane Permeability. *Angew. Chem. Int. Ed.* **2021,** *60*, 22529-22536.
(159) Liu, H.; Wang, R.; Wei, J.; Cheng, C.; Zheng, Y.; Pan, Y.; He, X.; Ding, M.; Tan, H.; Fu, Q., Conformation-Directed Micelle-to-Vesicle Transition of Cholesterol-Decorated Polypeptide Triggered by Oxidation. *J. Am. Chem. Soc.* **2018,** *140*, 6604-6610.
(160) Tang, H.; Yin, L.; Lu, H.; Cheng, J., Water-soluble poly(L-serine)s with elongated and charged side-chains: synthesis, conformations, and cell-penetrating properties. *Biomacromolecules* **2012,** *13*, 2609-2615.
(161) Liu, G.; Dong, C. M., Photoresponsive poly(S-(o-nitrobenzyl)-L-cysteine)-b-PEO from a L-cysteine N-carboxyanhydride monomer: synthesis, self-assembly, and phototriggered drug release. *Biomacromolecules* **2012,** *13*, 1573-1583.

(162) Bauer, T. A.; Muhl, C.; Schollmeyer, D.; Barz, M., Racemic S-(ethylsulfonyl)-dl-cysteine N-Carboxyanhydrides Improve Chain Lengths and Monomer Conversion for beta-Sheet-Controlled Ring-Opening Polymerization. *Macromol. Rapid. Commun.* **2021,** *42*, e2000470.
(163) Kramer, J. R.; Onoa, B.; Bustamante, C.; Bertozzi, C. R., Chemically tunable mucin chimeras assembled on living cells. *Proc. Natl. Acad. Sci. U. S. A.* **2015,** *112*, 12574-12579.
(164) Zhou, M. N.; Delaveris, C. S.; Kramer, J. R.; Kenkel, J. A.; Engleman, E. G.; Bertozzi, C. R., N-carboxyanhydride polymerization of glycopolypeptides that activate antigen-presenting cells through Dectin-1 and Dectin-2. *Angew. Chem., Int. Ed.* **2018,** *57*, 3137-3142.
(165) Hwang, J.; Deming, T. J., Methylated mono- and di(ethyleneglycol)-functionalized β-sheet forming polypeptides. *Biomacromolecules* **2001,** *2*, 17-21.
(166) Yakovlev, I.; Deming, T. J., Controlled synthesis of phosphorylcholine derivatives of poly(serine) and poly(homoserine). *J. Am. Chem. Soc.* **2015,** *137*, 4078-4081.
(167) Kramer, J. R.; Deming, T. J., Glycopolypeptides with a redox-triggered helix-to-coil transition. *J. Am. Chem. Soc.* **2012,** *134*, 4112-4115.
(168) Fu, X.; Shen, Y.; Fu, W.; Li, Z., Thermoresponsive Oligo(ethylene glycol) Functionalized Poly-L-cysteine. *Macromolecules* **2013,** *46*, 3753-3760.
(169) Hayakawa, T.; Kondo, Y.; Matsuyama, M., Syntheses and conformational studies of poly(S-menthyloxycarbonylmethyl l- and d-cysteines). *Polymer* **1976,** *17*, 1009-1012.
(170) Benavides, I.; Raftery, E. D.; Bell, A. G.; Evans, D.; Scott, W. A.; Houk, K. N.; Deming, T. J., Poly(dehydroalanine): Synthesis, Properties, and Functional Diversification of a Fluorescent Polypeptide. *J. Am. Chem. Soc.* **2022,** *144*, 4214-4223.
(171) Deming, T. J., Methodologies for preparation of synthetic block copolypeptides: materials with future promise in drug delivery. *Adv. Drug Delivery Rev.* **2002,** *54*, 1145-1155.
(172) Bonduelle, C., Secondary structures of synthetic polypeptide polymers. *Polym. Chem.* **2018,** *9*, 1517-1529.
(173) Carlsen, A.; Lecommandoux, S., Self-assembly of polypeptide-based block copolymer amphiphiles. *Curr. Opin. Colloid Interface Sci.* **2009,** *14*, 329-339.
(174) Fasman, G. D.; Blout, E. R., The Synthesis and the Conformation of Poly-L-serine and Poly-O-acetyl-L-serine. *J. Am. Chem. Soc.* **1960,** *82*, 2262-2267.
(175) Ikeda, S., Molecular conformation of poly-S-carboxytmethyl-L-cysteine in aqueous solutions. *Biopolymers* **1967,** *5*, 359-374.
(176) Ma, Y.; Fu, X.; Shen, Y.; Fu, W.; Li, Z., Irreversible Low Critical Solution Temperature Behaviors of Thermal-responsive OEGylated Poly(L-cysteine) Containing Disulfide Bonds. *Macromolecules* **2014,** *47*, 4684-4689.
(177) Das, S.; Kar, M.; Sen Gupta, S., Synthesis of end-functionalized phosphate and phosphonate-polypeptides by ring-opening polymerization of their corresponding N-carboxyanhydride. *Polym. Chem.* **2013,** *4*, 4087.
(178) Fu, X.; Ma, Y.; Shen, Y.; Fu, W.; Li, Z., Oxidation-Responsive OEGylated Poly-l-cysteine and Solution Properties Studies. *Biomacromolecules* **2014,** *15*, 1055-1061.
(179) Wu, C.; Fu, X.; Li, S., New simple and recyclable O-acylation serine derivatives as highly enantioselective catalysts for the large-scale asymmetric direct aldol reactions in the presence of water. *Tetrahedron* **2011,** *67*, 4283-4290.
(180) Boal, A. K.; Guryanov, I.; Moretto, A.; Crisma, M.; Lanni, E. L.; Toniolo, C.; Grubbs, R. H.; O'Leary, D. J., Facile and E-Selective Intramolecular Ring-Closing Metathesis Reactions in 310-Helical Peptides: A 3D Structural Study. *J. Am. Chem. Soc.* **2007,** *129*, 6986-6987.

(181) Milani, P.; Demasi, M.; de Rezende, L.; Amaral, A. T. d.; Andrade, L. H., Synthesis of l-cysteine-based boron compounds and their evaluation as proteasome inhibitors. *New J. Chem.* **2014,** *38*, 4859-4871.
(182) Dau, H.; Jones, G. R.; Tsogtgerel, E.; Nguyen, D.; Keyes, A.; Liu, Y.-S.; Rauf, H.; Ordonez, E.; Puchelle, V.; Basbug Alhan, H.; Zhao, C.; Harth, E., Linear Block Copolymer Synthesis. *Chem. Rev.* **2022,** *122*, 14471-14553.
(183) Hadjichristidis, N.; Pispas, S.; Floudas, G., *Block copolymers: synthetic strategies, physical properties, and applications*. John Wiley & Sons: 2003.
(184) Schacher, F. H.; Rupar, P. A.; Manners, I., Functional Block Copolymers: Nanostructured Materials with Emerging Applications. *Angew. Chem. Int. Ed.* **2012,** *51*, 7898-7921.
(185) Ganda, S.; Stenzel, M. H., Concepts, fabrication methods and applications of living crystallization-driven self-assembly of block copolymers. *Prog. Polym. Sci.* **2020,** *101*, 101195.
(186) Yassar, A.; Miozzo, L.; Gironda, R.; Horowitz, G., Rod–coil and all-conjugated block copolymers for photovoltaic applications. *Prog. Polym. Sci.* **2013,** *38*, 791-844.
(187) Lo, T.-Y.; Krishnan, M. R.; Lu, K.-Y.; Ho, R.-M., Silicon-containing block copolymers for lithographic applications. *Prog. Polym. Sci.* **2018,** *77*, 19-68.
(188) Rodríguez-Hernández, J.; Chécot, F.; Gnanou, Y.; Lecommandoux, S., Toward 'smart' nano-objects by self-assembly of block copolymers in solution. *Prog. Polym. Sci.* **2005,** *30*, 691-724.
(189) Cabral, H.; Miyata, K.; Osada, K.; Kataoka, K., Block Copolymer Micelles in Nanomedicine Applications. *Chem. Rev.* **2018,** *118*, 6844-6892.
(190) Fuks, G.; Mayap Talom, R.; Gauffre, F., Biohybrid block copolymers: towards functional micelles and vesicles. *Chem. Soc. Rev.* **2011,** *40*, 2475-2493.
(191) Wang, X.; Song, Z.; Tan, Z.; Zhu, L.; Xue, T.; Lv, S.; Fu, Z.; Zheng, X.; Ren, J.; Cheng, J., Facile Synthesis of Helical Multiblock Copolypeptides: Minimal Side Reactions with Accelerated Polymerization of N-Carboxyanhydrides. *ACS Macro Lett.* **2019,** *8*, 1517-1521.
(192) Lavasanifar, A.; Samuel, J.; Kwon, G. S., Poly(ethylene oxide)-block-poly(l-amino acid) micelles for drug delivery. *Adv. Drug Deliv. Rev.* **2002,** *54*, 169-190.
(193) Lv, S.; Song, W.; Tang, Z.; Li, M.; Yu, H.; Hong, H.; Chen, X., Charge-Conversional PEG-Polypeptide Polyionic Complex Nanoparticles from Simple Blending of a Pair of Oppositely Charged Block Copolymers as an Intelligent Vehicle for Efficient Antitumor Drug Delivery. *Mol. Pharmaceutics* **2014,** *11*, 1562-1574.
(194) Li, M.; Song, W.; Tang, Z.; Lv, S.; Lin, L.; Sun, H.; Li, Q.; Yang, Y.; Hong, H.; Chen, X., Nanoscaled Poly(l-glutamic acid)/Doxorubicin-Amphiphile Complex as pH-responsive Drug Delivery System for Effective Treatment of Nonsmall Cell Lung Cancer. *ACS Appl. Mater. Interfaces* **2013,** *5*, 1781-1792.
(195) Junnila, S.; Houbenov, N.; Karatzas, A.; Hadjichristidis, N.; Hirao, A.; Iatrou, H.; Ikkala, O., Side-Chain-Controlled Self-Assembly of Polystyrene–Polypeptide Miktoarm Star Copolymers. *Macromolecules* **2012,** *45*, 2850-2856.
(196) Habraken, G. J. M.; Peeters, M.; Thornton, P. D.; Koning, C. E.; Heise, A., Selective Enzymatic Degradation of Self-Assembled Particles from Amphiphilic Block Copolymers Obtained by the Combination of N-Carboxyanhydride and Nitroxide-Mediated Polymerization. *Biomacromolecules* **2011,** *12*, 3761-3769.
(197) Jacobs, J.; Byrne, A.; Gathergood, N.; Keyes, T. E.; Heuts, J. P. A.; Heise, A., Facile Synthesis of Fluorescent Latex Nanoparticles with Selective Binding Properties Using Amphiphilic Glycosylated Polypeptide Surfactants. *Macromolecules* **2014,** *47*, 7303-7310.

(198) Tsai, C.-C.; Gan, Z.; Chen, T.; Kuo, S.-W., Competitive Hydrogen Bonding Interactions Influence the Secondary and Hierarchical Self-Assembled Structures of Polypeptide-Based Triblock Copolymers. *Macromolecules* **2018,** *51*, 3017-3029.
(199) Motala-Timol, S.; Jhurry, D.; Zhou, J.; Bhaw-Luximon, A.; Mohun, G.; Ritter, H., Amphiphilic Poly(l-lysine-b-caprolactone) Block Copolymers: Synthesis, Characterization, and Solution Properties. *Macromolecules* **2008,** *41*, 5571-5576.
(200) Sun, J.; Deng, C.; Chen, X.; Yu, H.; Tian, H.; Sun, J.; Jing, X., Self-Assembly of Polypeptide-Containing ABC-Type Triblock Copolymers in Aqueous Solution and Its pH Dependence. *Biomacromolecules* **2007,** *8*, 1013-1017.
(201) Caillol, S.; Lecommandoux, S.; Mingotaud, A.-F.; Schappacher, M.; Soum, A.; Bryson, N.; Meyrueix, R., Synthesis and Self-Assembly Properties of Peptide−Polylactide Block Copolymers. *Macromolecules* **2003,** *36*, 1118-1124.
(202) Fan, Y.; Chen, G.; Tanaka, J.; Tateishi, T., l-Phe End-Capped Poly(l-lactide) as Macroinitiator for the Synthesis of Poly(l-lactide)-b-poly(l-lysine) Block Copolymer. *Biomacromolecules* **2005,** *6*, 3051-3056.
(203) Lecommandoux, S.; Sandre, O.; Chécot, F.; Rodriguez-Hernandez, J.; Perzynski, R., Magnetic Nanocomposite Micelles and Vesicles. *Adv. Mater.* **2005,** *17*, 712-718.
(204) Chécot, F.; Lecommandoux, S.; Gnanou, Y.; Klok, H.-A., Water-Soluble Stimuli-Responsive Vesicles from Peptide-Based Diblock Copolymers. *Angew. Chem. Int. Ed.* **2002,** *41*, 1339-1343.
(205) Kukula, H.; Schlaad, H.; Antonietti, M.; Förster, S., The Formation of Polymer Vesicles or "Peptosomes" by Polybutadiene-block-poly(l-glutamate)s in Dilute Aqueous Solution. *J. Am. Chem. Soc.* **2002,** *124*, 1658-1663.
(206) Spyridakou, M.; Tsimenidis, K.; Gkikas, M.; Steinhart, M.; Graf, R.; Floudas, G., Effects of Nanometer Confinement on the Self-Assembly and Dynamics of Poly(γ-benzyl-l-glutamate) and Its Copolymer with Poly(isobutylene). *Macromolecules* **2022,** *55*, 2615-2626.
(207) Shiotsuki, M.; Takahashi, K.; Rodriguez Castanon, J.; Sanda, F., Synthesis of block copolymers using end-functionalized polyacetylenes as macroinitiators. *Polym. Chem.* **2018,** *9*, 3855-3863.
(208) Wu, Z.-Q.; Ono, R. J.; Chen, Z.; Li, Z.; Bielawski, C. W., Polythiophene–block–poly(γ-benzyl L-glutamate): synthesis and study of a new rod–rod block copolymer. *Polym. chem.* **2011,** *2*, 300-302.
(209) Osawa, S.; Ishii, T.; Takemoto, H.; Osada, K.; Kataoka, K., A facile amino-functionalization of poly(2-oxazoline)s' distal end through sequential azido end-capping and Staudinger reactions. *Eur. Polym. J.* **2017,** *88*, 553-561.
(210) Birke, A.; Ling, J.; Barz, M., Polysarcosine-containing copolymers: Synthesis, characterization, self-assembly, and applications. *Prog. Polym. Sci.* **2018,** *81*, 163-208.
(211) Schatz, C.; Louguet, S.; Le Meins, J.-F.; Lecommandoux, S., Polysaccharide-block-polypeptide Copolymer Vesicles: Towards Synthetic Viral Capsids. *Angew. Chem. Int. Ed.* **2009,** *48*, 2572-2575.
(212) Agut, W.; Taton, D.; Lecommandoux, S., A Versatile Synthetic Approach to Polypeptide Based Rod−Coil Block Copolymers by Click Chemistry. *Macromolecules* **2007,** *40*, 5653-5661.
(213) Wang, K.; Liang, L.; Lin, S.; He, X., Synthesis of well-defined ABC triblock copolymers with polypeptide segments by ATRP and click reactions. *Eur. Polym. J.* **2008,** *44*, 3370-3376.
(214) Naik, S. S.; Ray, J. G.; Savin, D. A., Temperature- and pH-Responsive Self-assembly of Poly(propylene oxide)-b-Poly(lysine) Block Copolymers in Aqueous Solution. *Langmuir* **2011,** *27*, 7231-7240.

(215) Molev, G.; Lu, Y.; Kim, K. S.; Majdalani, I. C.; Guerin, G.; Petrov, S.; Walker, G.; Manners, I.; Winnik, M. A., Organometallic–Polypeptide Diblock Copolymers: Synthesis by Diels–Alder Coupling and Crystallization-Driven Self-Assembly to Uniform Truncated Elliptical Lamellae. *Macromolecules* **2014,** *47*, 2604-2615.
(216) Klinker, K.; Holm, R.; Heller, P.; Barz, M., Evaluating chemical ligation techniques for the synthesis of block copolypeptides, polypeptoids and block copolypept(o)ides: a comparative study. *Polym. Chem.* **2015,** *6*, 4612-4623.
(217) Murphy, R. D.; Kimmins, S.; Hibbitts, A. J.; Heise, A., 3D-extrusion printing of stable constructs composed of photoresponsive polypeptide hydrogels. *Polym. chem.* **2019,** *10*, 4675-4682.
(218) Wang, Y.; Chang, Y. C., Patterning of Polypeptide Thin Films by the Combination of Surface-Initiated Vapor-Deposition Polymerization and Photolithography. *Adv. Funct. Mater.* **2003,** *15*, 290-293.
(219) Palacios-Cuesta, M.; Cortajarena, A. L.; García, O.; Rodríguez-Hernández, J., Versatile Functional Microstructured Polystyrene-Based Platforms for Protein Patterning and Recognition. *Biomacromolecules* **2013,** *14*, 3147-3154.
(220) Desale, S. S.; Soni, K. S.; Romanova, S.; Cohen, S. M.; Bronich, T. K., Targeted delivery of platinum-taxane combination therapy in ovarian cancer. *J. Control. Release* **2015,** *220*, 651-659.
(221) Christie, R. J.; Matsumoto, Y.; Miyata, K.; Nomoto, T.; Fukushima, S.; Osada, K.; Halnaut, J.; Pittella, F.; Kim, H. J.; Nishiyama, N.; Kataoka, K., Targeted Polymeric Micelles for siRNA Treatment of Experimental Cancer by Intravenous Injection. *ACS Nano* **2012,** *6*, 5174-5189.
(222) Yi, Y.; Kim, H. J.; Mi, P.; Zheng, M.; Takemoto, H.; Toh, K.; Kim, B. S.; Hayashi, K.; Naito, M.; Matsumoto, Y.; Miyata, K.; Kataoka, K., Targeted systemic delivery of siRNA to cervical cancer model using cyclic RGD-installed unimer polyion complex-assembled gold nanoparticles. *J. Control. Release* **2016,** *244*, 247-256.
(223) Shirbin, S. J.; Lam, S. J.; Chan, N. J. A.; Ozmen, M. M.; Fu, Q.; O'Brien-Simpson, N.; Reynolds, E. C.; Qiao, G. G., Polypeptide-based macroporous cryogels with inherent antimicrobial properties: The importance of a macroporous structure. *ACS Macro Lett.* **2016,** *5*, 552.
(224) Xi, Y.; Song, T.; Tang, S.; Wang, N.; Du, J., Preparation and Antibacterial Mechanism Insight of Polypeptide-Based Micelles with Excellent Antibacterial Activities. *Biomacromolecules* **2016,** *17*, 3922-3930.
(225) Sun, Y.; Bentolila, L. A.; Deming, T. J., Self-Sorting Microscale Compartmentalized Block Copolypeptide Hydrogels. *ACS Macro Lett.* **2019,** *8*, 1275-1279.
(226) Skoulas, D.; Mangiapia, G.; Parisi, D.; Kasimatis, M.; Glynos, E.; Stratikos, E.; Vlassopoulos, D.; Frielinghaus, H.; Iatrou, H., Tunable Hydrogels with Improved Viscoelastic Properties from Hybrid Polypeptides. *Macromolecules* **2021,** *54*, 10786-10800.
(227) Nowak, A. P.; Breedveld, V.; Pakstis, L.; Ozbas, B.; Pine, D. J.; Pochan, D.; Deming, T. J., Rapidly recovering hydrogel scaffolds from self-assembling diblock copolypeptide amphiphiles. *Nature* **2002,** *417*, 424-428.
(228) Fan, J.; Zou, J.; He, X.; Zhang, F.; Zhang, S.; Raymond, J. E.; Wooley, K. L., Tunable mechano-responsive organogels by ring-opening copolymerizations of N-carboxyanhydrides. *Chem. Sci.* **2014,** *5*, 141-150.
(229) Kim, K. T.; Park, C.; Vandermeulen, G. W. M.; Rider, D. A.; Kim, C.; Winnik, M. A.; Manners, I., Gelation of Helical Polypeptide–Random Coil Diblock Copolymers by a Nanoribbon Mechanism. *Angew. Chem. Int. Ed.* **2005,** *44*, 7964-7968.
(230) Holowka, E. P.; Pochan, D. J.; Deming, T. J., Charged Polypeptide Vesicles with Controllable Diameter. *J. Am. Chem. Soc.* **2005,** *127*, 12423-12428.

(231) Rodríguez-Hernández, J.; Lecommandoux, S., Reversible Inside−Out Micellization of pH-responsive and Water-Soluble Vesicles Based on Polypeptide Diblock Copolymers. *J. Am. Chem. Soc.* **2005,** *127*, 2026-2027.
(232) Ni, Y.; Sun, J.; Wei, Y.; Fu, X.; Zhu, C.; Li, Z., Two-Dimensional Supramolecular Assemblies from pH-Responsive Poly(ethyl glycol)-b-poly(l-glutamic acid)-b-poly(N-octylglycine) Triblock Copolymer. *Biomacromolecules* **2017,** *18*, 3367-3374.
(233) Ji, S.; Lin, M.; Li, Z.; Xu, L.; Fu, X.; Chen, G.; Li, Z.; Sun, J., Tunable Aggregation-Induced Emission Fluorophore with the Assistance of the Self-Assembly of Block Copolymers by Controlling the Morphology and Secondary Conformation for Bioimaging. *Biomacromolecules* **2022,** *23*, 798-807.
(234) Lavilla, C.; Byrne, M.; Heise, A., Block-Sequence-Specific Polypeptides from α-Amino Acid N-Carboxyanhydrides: Synthesis and Influence on Polypeptide Properties. *Macromolecules* **2016,** *49*, 2942-2947.
(235) Murphy, R. D.; in het Panhuis, M.; Cryan, S.-A.; Heise, A., Disulphide crosslinked star block copolypeptide hydrogels: influence of block sequence order on hydrogel properties. *Polym. chem.* **2018,** *9*, 3908-3916.
(236) Aliyan, A.; Cook, N. P.; Martí, A. A., Interrogating Amyloid Aggregates using Fluorescent Probes. *Chem. Rev.* **2019,** *119*, 11819-11856.
(237) Xue, C.; Lin, T. Y.; Chang, D.; Guo, Z., Thioflavin T as an amyloid dye: fibril quantification, optimal concentration and effect on aggregation. *R. Soc. open sci.* **2017,** *4*, 160696.
(238) Amdursky, N.; Erez, Y.; Huppert, D., Molecular Rotors: What Lies Behind the High Sensitivity of the Thioflavin-T Fluorescent Marker. *Acc. Chem. Res.* **2012,** *45*, 1548-1557.
(239) Stsiapura, V. I.; Maskevich, A. A.; Kuzmitsky, V. A.; Uversky, V. N.; Kuznetsova, I. M.; Turoverov, K. K., Thioflavin T as a Molecular Rotor: Fluorescent Properties of Thioflavin T in Solvents with Different Viscosity. *J. Phys. Chem. B* **2008,** *112*, 15893-15902.
(240) Biancalana, M.; Koide, S., Molecular mechanism of Thioflavin-T binding to amyloid fibrils. *Biochimica et Biophysica Acta* **2010,** *1804*, 1405-1412.
(241) Noël, S.; Cadet, S.; Gras, E.; Hureau, C., The benzazole scaffold: a SWAT to combat Alzheimer's disease. *Chem. Soc. Rev.* **2013,** *42*, 7747-7762.
(242) Lee, D.; Kim, S. M.; Kim, H. Y.; Kim, Y., Fluorescence Chemicals To Detect Insoluble and Soluble Amyloid-β Aggregates. *ACS Chem. Neurosci.* **2019,** *10*, 2647-2657.
(243) Sulatskaya, A. I.; Lavysh, A. V.; Maskevich, A. A.; Kuznetsova, I. M.; Turoverov, K. K., Thioflavin T fluoresces as excimer in highly concentrated aqueous solutions and as monomer being incorporated in amyloid fibrils. *Sci. rep.* **2017,** *7*, 2146.
(244) Mai, Y.; Eisenberg, A., Self-assembly of block copolymers. *Chem. Soc. Rev.* **2012,** *41*, 5969-5985.
(245) Dionzou, M.; Morère, A.; Roux, C.; Lonetti, B.; Marty, J. D.; Mingotaud, C.; Joseph, P.; Goudounèche, D.; Payré, B.; Léonetti, M.; Mingotaud, A. F., Comparison of methods for the fabrication and the characterization of polymer self-assemblies: what are the important parameters? *Soft Matter* **2016,** *12*, 2166-2176.
(246) Lu, Y.; Lin, J.; Wang, L.; Zhang, L.; Cai, C., Self-Assembly of Copolymer Micelles: Higher-Level Assembly for Constructing Hierarchical Structure. *Chem. Rev.* **2020,** *120*, 4111-4140.
(247) Penfold, N. J. W.; Yeow, J.; Boyer, C.; Armes, S. P., Emerging Trends in Polymerization-Induced Self-Assembly. *ACS Macro Lett.* **2019,** *8*, 1029-1054.
(248) Canning, S. L.; Smith, G. N.; Armes, S. P., A Critical Appraisal of RAFT-Mediated Polymerization-Induced Self-Assembly. *Macromolecules* **2016,** *49*, 1985-2001.

(249) Neal, T. J.; Penfold, N. J. W.; Armes, S. P., Reverse Sequence Polymerization-Induced Self-Assembly in Aqueous Media. *Angew. Chem. Int. Ed.* **2022,** *61*, e202207376.
(250) Derry, M. J.; Fielding, L. A.; Armes, S. P., Polymerization-induced self-assembly of block copolymer nanoparticles via RAFT non-aqueous dispersion polymerization. *Prog. Polym. Sci.* **2016,** *52*, 1-18.
(251) Ferguson, C. J.; Hughes, R. J.; Pham, B. T. T.; Hawkett, B. S.; Gilbert, R. G.; Serelis, A. K.; Such, C. H., Effective ab Initio Emulsion Polymerization under RAFT Control. *Macromolecules* **2002,** *35*, 9243-9245.
(252) Wan, W.-M.; Hong, C.-Y.; Pan, C.-Y., One-pot synthesis of nanomaterials via RAFT polymerization induced self-assembly and morphology transition. *Chem. Commun.* **2009**, 5883-5885.
(253) Warren, N. J.; Armes, S. P., Polymerization-Induced Self-Assembly of Block Copolymer Nano-objects via RAFT Aqueous Dispersion Polymerization. *J. Am. Chem. Soc.* **2014,** *136*, 10174-10185.
(254) Blanazs, A.; Madsen, J.; Battaglia, G.; Ryan, A. J.; Armes, S. P., Mechanistic Insights for Block Copolymer Morphologies: How Do Worms Form Vesicles? *J. Am. Chem. Soc.* **2011,** *133*, 16581-16587.
(255) Byard, S. J.; Williams, M.; McKenzie, B. E.; Blanazs, A.; Armes, S. P., Preparation and Cross-Linking of All-Acrylamide Diblock Copolymer Nano-Objects via Polymerization-Induced Self-Assembly in Aqueous Solution. *Macromolecules* **2017,** *50*, 1482-1493.
(256) Blackman, L. D.; Varlas, S.; Arno, M. C.; Houston, Z. H.; Fletcher, N. L.; Thurecht, K. J.; Hasan, M.; Gibson, M. I.; O'Reilly, R. K., Confinement of Therapeutic Enzymes in Selectively Permeable Polymer Vesicles by Polymerization-Induced Self-Assembly (PISA) Reduces Antibody Binding and Proteolytic Susceptibility. *ACS Cent. Sci.* **2018,** *4*, 718-723.
(257) Varlas, S.; Neal, T. J.; Armes, S. P., Polymerization-induced self-assembly and disassembly during the synthesis of thermoresponsive ABC triblock copolymer nano-objects in aqueous solution. *Chem. Sci.* **2022,** *13*, 7295-7303.
(258) Jones, E. R.; Semsarilar, M.; Blanazs, A.; Armes, S. P., Efficient Synthesis of Amine-Functional Diblock Copolymer Nanoparticles via RAFT Dispersion Polymerization of Benzyl Methacrylate in Alcoholic Media. *Macromolecules* **2012,** *45*, 5091-5098.
(259) Pei, Y.; Lowe, A. B., Polymerization-induced self-assembly: ethanolic RAFT dispersion polymerization of 2-phenylethyl methacrylate. *Polymer Chemistry* **2014,** *5*, 2342-2351.
(260) Wang, G.; Schmitt, M.; Wang, Z.; Lee, B.; Pan, X.; Fu, L.; Yan, J.; Li, S.; Xie, G.; Bockstaller, M. R.; Matyjaszewski, K., Polymerization-Induced Self-Assembly (PISA) Using ICAR ATRP at Low Catalyst Concentration. *Macromolecules* **2016,** *49*, 8605-8615.
(261) Derry, M. J.; Fielding, L. A.; Armes, S. P., Industrially-relevant polymerization-induced self-assembly formulations in non-polar solvents: RAFT dispersion polymerization of benzyl methacrylate. *Polym. Chem.* **2015,** *6*, 3054-3062.
(262) Fielding, L. A.; Lane, J. A.; Derry, M. J.; Mykhaylyk, O. O.; Armes, S. P., Thermo-responsive Diblock Copolymer Worm Gels in Non-polar Solvents. *J. Am. Chem. Soc.* **2014,** *136*, 5790-5798.
(263) Houillot, L.; Bui, C.; Save, M.; Charleux, B.; Farcet, C.; Moire, C.; Raust, J.-A.; Rodriguez, I., Synthesis of Well-Defined Polyacrylate Particle Dispersions in Organic Medium Using Simultaneous RAFT Polymerization and Self-Assembly of Block Copolymers. A Strong Influence of the Selected Thiocarbonylthio Chain Transfer Agent. *Macromolecules* **2007,** *40*, 6500-6509.
(264) Pei, Y.; Thurairajah, L.; Sugita, O. R.; Lowe, A. B., RAFT Dispersion Polymerization in Nonpolar Media: Polymerization of 3-Phenylpropyl Methacrylate in n-Tetradecane with

Poly(stearyl methacrylate) Homopolymers as Macro Chain Transfer Agents. *Macromolecules* **2015,** *48*, 236-244.
(265) Zhang, Q.; Zhu, S., Ionic Liquids: Versatile Media for Preparation of Vesicles from Polymerization-Induced Self-Assembly. *ACS Macro Lett.* **2015,** *4*, 755-758.
(266) Rymaruk, M. J.; Hunter, S. J.; O'Brien, C. T.; Brown, S. L.; Williams, C. N.; Armes, S. P., RAFT Dispersion Polymerization in Silicone Oil. *Macromolecules* **2019,** *52*, 2822-2832.
(267) Hasell, T.; Thurecht, K. J.; Jones, R. D. W.; Brown, P. D.; Howdle, S. M., Novel one pot synthesis of silver nanoparticle–polymer composites by supercritical CO2 polymerisation in the presence of a RAFT agent. *Chem. Commun.* **2007**, 3933-3935.
(268) Zong, M.; Thurecht, K. J.; Howdle, S. M., Dispersion polymerisation in supercritical CO2 using macro-RAFT agents. *Chem. Commun.* **2008**, 5942-5944.
(269) An, N.; Chen, X.; Yuan, J., Non-thermally initiated RAFT polymerization-induced self-assembly. *Polym. Chem.* **2021,** *12*, 3220-3232.
(270) Varlas, S.; Georgiou, P. G.; Bilalis, P.; Jones, J. R.; Hadjichristidis, N.; O'Reilly, R. K., Poly(sarcosine)-Based Nano-Objects with Multi-Protease Resistance by Aqueous Photoinitiated Polymerization-Induced Self-Assembly (Photo-PISA). *Biomacromolecules* **2018,** *19*, 4453-4462.
(271) Corrigan, N.; Yeow, J.; Judzewitsch, P.; Xu, J.; Boyer, C., Seeing the Light: Advancing Materials Chemistry through Photopolymerization. *Angew. Chem. Int. Ed.* **2019,** *58*, 5170-5189.
(272) Sun, H.; Cao, W.; Zang, N.; Clemons, T. D.; Scheutz, G. M.; Hu, Z.; Thompson, M. P.; Liang, Y.; Vratsanos, M.; Zhou, X.; Choi, W.; Sumerlin, B. S.; Stupp, S. I.; Gianneschi, N. C., Proapoptotic Peptide Brush Polymer Nanoparticles via Photoinitiated Polymerization-Induced Self-Assembly. *Angew. Chem. Int. Ed.* **2020,** *59*, 19136-19142.
(273) Xu, S.; Yeow, J.; Boyer, C., Exploiting Wavelength Orthogonality for Successive Photoinduced Polymerization-Induced Self-Assembly and Photo-Crosslinking. *ACS Macro Lett.* **2018,** *7*, 1376-1382.
(274) Ren, K.; Perez-Mercader, J., Thermoresponsive gels directly obtained via visible light-mediated polymerization-induced self-assembly with oxygen tolerance. *Polym. Chem.* **2017,** *8*, 3548-3552.
(275) Piogé, S.; Tran, T. N.; McKenzie, T. G.; Pascual, S.; Ashokkumar, M.; Fontaine, L.; Qiao, G., Sono-RAFT Polymerization-Induced Self-Assembly in Aqueous Dispersion: Synthesis of LCST-type Thermosensitive Nanogels. *Macromolecules* **2018,** *51*, 8862-8869.
(276) Wan, J.; Fan, B.; Liu, Y.; Hsia, T.; Qin, K.; Junkers, T.; Teo, B. M.; Thang, S. H., Room temperature synthesis of block copolymer nano-objects with different morphologies via ultrasound initiated RAFT polymerization-induced self-assembly (sono-RAFT-PISA). *Polym. Chem.* **2020,** *11*, 3564-3572.
(277) Garrett, E. T.; Pei, Y.; Lowe, A. B., Microwave-assisted synthesis of block copolymer nanoparticles via RAFT with polymerization-induced self-assembly in methanol. *Polymer Chemistry* **2016,** *7*, 297-301.
(278) Tan, J.; Xu, Q.; Li, X.; He, J.; Zhang, Y.; Dai, X.; Yu, L.; Zeng, R.; Zhang, L., Enzyme-PISA: An Efficient Method for Preparing Well-Defined Polymer Nano-Objects under Mild Conditions. *Macromol. Rapid Commun.* **2018,** *39*, 1700871.
(279) Blanazs, A.; Verber, R.; Mykhaylyk, O. O.; Ryan, A. J.; Heath, J. Z.; Douglas, C. W. I.; Armes, S. P., Sterilizable Gels from Thermoresponsive Block Copolymer Worms. *J. Am. Chem. Soc.* **2012,** *134*, 9741-9748.
(280) Lovett, J. R.; Warren, N. J.; Armes, S. P.; Smallridge, M. J.; Cracknell, R. B., Order–Order Morphological Transitions for Dual Stimulus Responsive Diblock Copolymer Vesicles. *Macromolecules* **2016,** *49*, 1016-1025.

(281) Lovett, J. R.; Warren, N. J.; Ratcliffe, L. P. D.; Kocik, M. K.; Armes, S. P., pH-Responsive Non-Ionic Diblock Copolymers: Ionization of Carboxylic Acid End-Groups Induces an Order–Order Morphological Transition. *Angew. Chem. Int. Ed.* **2015,** *54*, 1279-1283.
(282) Chen, M.; Li, J.-W.; Zhang, W.-J.; Hong, C.-Y.; Pan, C.-Y., pH- and Reductant-Responsive Polymeric Vesicles with Robust Membrane-Cross-Linked Structures: In Situ Cross-Linking in Polymerization-Induced Self-Assembly. *Macromolecules* **2019,** *52*, 1140-1149.
(283) Sobotta, F. H.; Hausig, F.; Harz, D. O.; Hoeppener, S.; Schubert, U. S.; Brendel, J. C., Oxidation-responsive micelles by a one-pot polymerization-induced self-assembly approach. *Polym. Chem.* **2018,** *9*, 1593-1602.
(284) Niu, B.; Chen, Y.; Zhang, L.; Tan, J., Organic–inorganic hybrid nanomaterials prepared via polymerization-induced self-assembly: recent developments and future opportunities. *Polym. Chem.* **2022,** *13*, 2554-2569.
(285) Liu, X.; Gao, W., In Situ Growth of Self-Assembled Protein–Polymer Nanovesicles for Enhanced Intracellular Protein Delivery. *ACS Appl. Mater. Interfaces* **2017,** *9*, 2023-2028.
(286) Dao, T. P. T.; Vezenkov, L.; Subra, G.; Amblard, M.; In, M.; Le Meins, J.-F.; Aubrit, F.; Moradi, M.-A.; Ladmiral, V.; Semsarilar, M., Self-Assembling Peptide—Polymer Nano-Objects via Polymerization-Induced Self-Assembly. *Macromolecules* **2020,** *53*, 7034-7043.
(287) Dao, T. P. T.; Vezenkov, L.; Subra, G.; Ladmiral, V.; Semsarilar, M., Nano-assemblies with core-forming hydrophobic polypeptide via polymerization-induced self-assembly (PISA). *Polym. Chem.* **2021,** *12*, 113-121.
(288) Cockram, A. A.; Bradley, R. D.; Lynch, S. A.; Fleming, P. C. D.; Williams, N. S. J.; Murray, M. W.; Emmett, S. N.; Armes, S. P., Optimization of the high-throughput synthesis of multiblock copolymer nanoparticles in aqueous media via polymerization-induced self-assembly. *React. Chem. Eng.* **2018,** *3*, 645-657.
(289) Tan, J.; Liu, D.; Bai, Y.; Huang, C.; Li, X.; He, J.; Xu, Q.; Zhang, L., Enzyme-Assisted Photoinitiated Polymerization-Induced Self-Assembly: An Oxygen-Tolerant Method for Preparing Block Copolymer Nano-Objects in Open Vessels and Multiwell Plates. *Macromolecules* **2017,** *50*, 5798-5806.
(290) Zaquen, N.; Yeow, J.; Junkers, T.; Boyer, C.; Zetterlund, P. B., Visible Light-Mediated Polymerization-Induced Self-Assembly Using Continuous Flow Reactors. *Macromolecules* **2018,** *51*, 5165-5172.
(291) Peng, J.; Tian, C.; Zhang, L.; Cheng, Z.; Zhu, X., The in situ formation of nanoparticles via RAFT polymerization-induced self-assembly in a continuous tubular reactor. *Polym. Chem.* **2017,** *8*, 1495-1506.
(292) Wan, J.; Fan, B.; Thang, S. H., RAFT-mediated polymerization-induced self-assembly (RAFT-PISA): current status and future directions. *Chem. Sci.* **2022,** *13*, 4192-4224.
(293) Cheng, G.; Pérez-Mercader, J., Polymerization-Induced Self-Assembly for Artificial Biology: Opportunities and Challenges. *Macromol. Rapid Commun.* **2019,** *40*, 1800513.
(294) Phan, H.; Taresco, V.; Penelle, J.; Couturaud, B., Polymerisation-induced self-assembly (PISA) as a straightforward formulation strategy for stimuli-responsive drug delivery systems and biomaterials: recent advances. *Biomater. Sci.* **2021,** *9*, 38-50.
(295) Cornel, E. J.; Jiang, J.; Chen, S.; Du, J., Principles and Characteristics of Polymerization-Induced Self-Assembly with Various Polymerization Techniques. *CCS Chem.* **2021,** *3*, 2104-2125.

(296) Liu, C.; Hong, C.-Y.; Pan, C.-Y., Polymerization techniques in polymerization-induced self-assembly (PISA). *Polym. Chem.* **2020,** *11*, 3673-3689.
(297) Wright, D. B.; Touve, M. A.; Adamiak, L.; Gianneschi, N. C., ROMPISA: Ring-Opening Metathesis Polymerization-Induced Self-Assembly. *ACS Macro Lett.* **2017,** *6*, 925-929.
(298) Varlas, S.; Foster, J. C.; O'Reilly, R. K., Ring-opening metathesis polymerization-induced self-assembly (ROMPISA). *Chem. Commun.* **2019,** *55*, 9066-9071.
(299) Wright, D. B.; Thompson, M. P.; Touve, M. A.; Carlini, A. S.; Gianneschi, N. C., Enzyme-Responsive Polymer Nanoparticles via Ring-Opening Metathesis Polymerization-Induced Self-Assembly. *Macromol. Rapid Commun.* **2019,** *40*, 1800467.
(300) Zhu, C.; Nicolas, J., (Bio)degradable and Biocompatible Nano-Objects from Polymerization-Induced and Crystallization-Driven Self-Assembly. *Biomacromolecules* **2022,** *23*, 3043-3080.
(301) Fielding, L. A.; Derry, M. J.; Ladmiral, V.; Rosselgong, J.; Rodrigues, A. M.; Ratcliffe, L. P. D.; Sugihara, S.; Armes, S. P., RAFT dispersion polymerization in non-polar solvents: facile production of block copolymer spheres, worms and vesicles in n-alkanes. *Chem. Sci.* **2013,** *4*, 2081-2087.
(302) Zhu, C.; Nicolas, J., Towards nanoparticles with site-specific degradability by ring-opening copolymerization induced self-assembly in organic medium. *Polym. Chem.* **2021,** *12*, 594-607.
(303) Guégain, E.; Zhu, C.; Giovanardi, E.; Nicolas, J., Radical Ring-Opening Copolymerization-Induced Self-Assembly (rROPISA). *Macromolecules* **2019,** *52*, 3612-3624.
(304) Zhu, C.; Denis, S.; Nicolas, J., A Simple Route to Aqueous Suspensions of Degradable Copolymer Nanoparticles Based on Radical Ring-Opening Polymerization-Induced Self-Assembly (rROPISA). *Chem. Mater.* **2022,** *34*, 1875-1888.
(305) Ratcliffe, L. P. D.; Couchon, C.; Armes, S. P.; Paulusse, J. M. J., Inducing an Order–Order Morphological Transition via Chemical Degradation of Amphiphilic Diblock Copolymer Nano-Objects. *Biomacromolecules* **2016,** *17*, 2277-2283.

7. List of Publications

1. **Rahul Nisal** and Manickam Jayakannan, Tertiary-Butylbenzene Functionalization as a Strategy for β-Sheet Polypeptides, *Biomacromolecules* 2022, 23 (6), 2667–2684. DOI: 10.1021/acs.biomac.2c00416.

2. Devesh Maurya,[†] **Rahul Nisal**,[†] Ruma Ghosh[†], Parshuram Kambale, Mehak Malhotra, Manickam Jayakannan, Fluorophore-tagged poly(L-Lysine) block copolymer nano-assemblies for real-time visualization and antimicrobial activity, *Eur. Polym. J.* 2023, 183, 111754. *(not included in the thesis, [†]Equal Contribution)* DOI: 10.1016/j.eurpolymj.2022.111754.

3. Debayan Sarkar, Satyajit Mishra, **Rahul Nisal** Sumita Majhi, Rohit Shrivas, Yashaswi Singh, V. S. Anusree and Jeet Kalia, Site-Specific Fluorescent Labeling of the Cysteine-Rich Toxin, DkTx, for TRPV1 Ion Channel Imaging and Membrane Binding Studies. ***Bioconjugate Chem.* 2022**, 33 (9), 1761-1770. (not included in the thesis, From previous work experience). DOI: 10.1021/acs.bioconjchem.2c00355.

4. **Rahul Nisal**, Gregor P. Jose, Shanbhag Chitra, Jeet Kalia, Rapid and reversible hydrazone bioconjugation in cells without the use of extraneous catalysts. ***Org. Biomol. Chem.* 2018**, 16 (23), 4304-4310. (not included in the thesis, From previous work experience). DOI: 10.1039/C8OB00946E.

5. **Rahul Nisal**, Shahid Khan Pathan, Uttareshwar Gavhane, Manickam Jayakannan, Design and Development of β-sheet Polypeptides for Drug and Fluorophore Delivery *in vitro* and *in vivo*, *Manuscript under Preparation*

6. **Rahul Nisal**, Parshuram Kambale, Shahid Khan Pathan, Manickam Jayakannan, ROPISA Driven for in-situ Entrapment for Fluorophores in Poly(L-serine) Nano-emulsion for Cellular Imaging Applications. *Manuscript under Preparation*

7. **Rahul Nisal,** Parshuram Kambale, Ruma Ghosh, Manickam Jayakannan, The Role of α-Helical and β-Sheet Stitched Cationic Polypeptides on the Antimicrobial Activity in E.coli. *Manuscript under Preparation*

BioMACROMOLECULES

pubs.acs.org/Biomac Article

Tertiary-Butylbenzene Functionalization as a Strategy for β-Sheet Polypeptides

Rahul Nisal and Manickam Jayakannan*

Cite This: *Biomacromolecules* 2022, 23, 2667−2684 Read Online

ACCESS | Metrics & More | Article Recommendations | Supporting Information

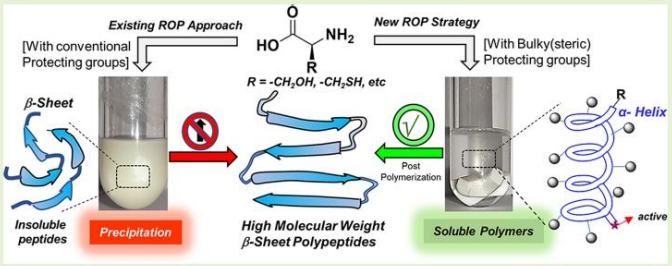

ABSTRACT: β-Sheet forming polypeptides are one of the least explored synthetic systems due to their uncontrolled precipitation in the ring-opening polymerization (ROP) synthetic methodology. Here, a new *t*-butylbenzene functionalization approach is introduced to overcome this limitation by sterically controlling the propagating polymer chains, and homogeneous polymerization with good control over chain growth was accomplished. New bulky *N*-carboxyanhydride monomers were designed having *t*-butylbenzene pendant by multistep organic synthesis, and N-heterocyclic carbene was explored as a catalyst to make high-molecular-weight and narrow polydisperse soluble polypeptides. This ROP process was successfully demonstrated for two β-sheet forming polypeptides such as poly(L-serine) and poly(L-cysteine). These new *t*-butylbenzene-functionalized polypeptides were found to be readily soluble in tetrahydrofuran, chloroform, and so forth, and they were produced in high molecular weights having M_n = 32 kDa with dispersity $Đ \leq 1.3$. ROP kinetics were studied by real-time Fourier transform infrared and ^{1}H NMR to determine the actual content of the secondary structures in the propagating chains. These studies established that the α-helical conformational front in the propagation chain was speeding up the polymerization kinetics with good degree of control in the ROP process. Reversible-conformational transitions in the post-polymerization deprotection were found to restore the β-sheet secondary structures in poly(L-serine)s. The newly developed *t*-butylbenzene-substituted steric-hindrance approach is valuable in yielding soluble polymers, and this approach could be useful for exploring new polypeptide architectures for long-term impact.

INTRODUCTION

Synthetic polypeptides are protein-like polymers having precise control over α-helical and β-sheet conformations for wide range of applications in materials science[1] and biomedical fields.[2−5] Polypeptides are synthesized by ring-opening polymerization (ROP) of *N*-carboxyanhydride (NCA) monomers of L-amino acids by nucleophiles or base initiators,[6−10] and in this process, secondary structures of the propagating polypeptide chains are rationalized as being a foremost deciding factor in determining the kinetics and building the high-molecular-weight polymers.[11] α-Helical polypeptides render excellent solubility in the polymerization medium to speed up the ROP process[12−16] and exhibit "livingness" to make extended block copolymer architectures.[17] α-Helical polypeptides such as poly(L-lysine), poly(L-glutamate), and so forth were reported using nickel- and cobalt-based organometallic catalysts,[18,19] Schreiner's thiourea,[20] N-heterocyclic carbenes (NHCs),[21] fluorinated alcohol,[22] crown-ethers,[23] LiHMDS,[24] and tetra-alkylammonium carboxylates[25] and also methodologies like polymerization-induced self-assembly,[26,27] emulsion polymerization,[12,28] and so on. On the contrary, β-sheet polypeptides were known to undergo uncontrollable precipitation in polymerization medium, which further restricted the polymer chain growth and hampered the molecular-weight buildup.[29] The formation of β-sheet lamellae at the initial stage of the polymerization and strong inter-chain

Received: April 1, 2022
Revised: April 20, 2022
Published: May 3, 2022

https://doi.org/10.1021/acs.biomac.2c00416
Biomacromolecules 2022, 23, 2667−2684

European Polymer Journal 183 (2023) 111754

Contents lists available at ScienceDirect

European Polymer Journal

journal homepage: www.elsevier.com/locate/europolj

Fluorophore-tagged poly(L-Lysine) block copolymer nano-assemblies for real-time visualization and antimicrobial activity

Devesh Maurya [1], Rahul Nisal [1], Ruma Ghosh [1], Parshuram Kambale, Mehak Malhotra, Manickam Jayakannan [*]

Department of Chemistry, Indian Institute of Science Education and Research (IISER Pune), Dr. Homi Bhabha Road, Pune 411008, Maharashtra, India

ARTICLE INFO

Keywords:
Antimicrobial Polypeptides
Fluorescent polymers
Theranostic probe
Poly(L-Lysine)
Ring opening polymerization (ROP)
Coumarin
Cytotoxicity

ABSTRACT

Development of self-reporting polymers having dual-action of membrane disruption for antimicrobial activity and simultaneous visualization and quantification by microscopic imaging techniques are urgently required for early detection and therapeutics. Here, we report a new series of self-reporting coumarin fluorophore-tagged polypeptides based on PEG-*block*-poly(L-lysine) copolymers via ring opening polymerization (ROP) strategy. For this purpose, NHC catalyzed controlled ROP was optimised for ε-Cbz-L-lysine NCA monomer to make desired chain length polypeptides. The resultant cationic polymer was self-assembled into 100 ± 15 nm nanoparticles (NP) having Zeta potentials of +25 to +44 mV associated with strong blue-emission in aqueous medium. The antimicrobial action of these polymers was tested in *E. coli* by colony suspension method and their MIC_{90} values were obtained to be 1×10^{-4} to 3×10^{-4} g/mL. Real-time confocal microscopic imaging enabled the direct visualization of the fluorescent peptide NP action on the *E. coli* membrane, and propidium iodide co-staining assay further established the membrane pore formation mechanism for their antimicrobial activity. *In vitro* cytotoxicity and cellular uptake studies in MCF-7 breast cancer cell lines revealed that the fluorescent polypeptide NP were readily internalized at the cellular level, and they were also found to be nontoxic to cells up to 80 μg/mL and showed minimal haemolysis to RBCs at their MIC concentration which further established their high biocompatibility as suitable biomaterials.

1. Introduction

Pathogenic micro-organisms are continuously throwing new challenges in biomedical field and escalates enormous uncertainty in handling life-threatening diseases and public health care at large [1]. The development of high-speed detection of pathogenic bacteria and virus at the early stage of infection is very crucial for the quick containment as well as for finding new drug formulation in the treatment of the infectious diseases. Some of the most advanced detection-techniques that are currently employed include fluorescent dye labelled antibody detection [2], polymerase chain reaction (PCR) [3], enzyme-linked immunosorbent assay (ELISA) [4], electrochemical methods [5–8] surface enhanced Raman scattering (SERS) [6,9,10], fluorescence confocal microscopic imaging [11–16], and fluorescence (or Förster) resonance energy transfer (FRET) assays [17], etc. Among them, fluorescence assay is most widely utilized non-invasive technique due to its high specificity, sensitivity and real-time imaging in situ [18]. Fluorophore conjugated antibiotics are utilized to understand their intracellular accumulation, mechanism of action, and ultimately detection of resistant microbial infections [19]. In the last two decades, antimicrobial polymers are emerging as an alternative biomaterial due to their scope of substrate modification by functionalization and tunable material properties like hydrogels, polymeric micelles, polymeric vesicles, and so forth [20,21]. In this domain, cationic conjugated polymers have long been used as one of the effective signal amplifiers and non-invasive diagnostic agents [22]. They have been used as photodynamic antimicrobial chemotherapeutic agents (PACT) by enhancing ROS generating activity of photosensitizers [23]. Cationic π-conjugated polymers or oligomers were also employed as FRET probe along with fluorescein [24], green fluorescent protein [25], and porphyrin [26] for screening antibiotic action on *E. coli* and photodynamic therapy via singlet oxygen generation [27], etc. However, a major impediment

* Corresponding author.
E-mail address: jayakannan@iiserpune.ac.in (M. Jayakannan).
[1] Equal contribution.

https://doi.org/10.1016/j.eurpolymj.2022.111754
Received 30 August 2022; Received in revised form 30 November 2022; Accepted 2 December 2022
Available online 13 December 2022

Bioconjugate Chemistry

pubs.acs.org/bc Article

Site-Specific Fluorescent Labeling of the Cysteine-Rich Toxin, DkTx, for TRPV1 Ion Channel Imaging and Membrane Binding Studies

Debayan Sarkar, Satyajit Mishra, Rahul Nisal, Sumita Majhi, Rohit Shrivas, Yashaswi Singh, V. S. Anusree, and Jeet Kalia*

Cite This: *Bioconjugate Chem.* 2022, 33, 1761−1770 Read Online

ACCESS | Metrics & More | Article Recommendations | Supporting Information

ABSTRACT: Peptide toxins secreted by venomous animals bind to mammalian ion channel proteins and modulate their function. The high specificity of these toxins for their target ion channels enables them to serve as powerful tools for ion channel biology. Toxins labeled with fluorescent dyes are employed for the cellular imaging of channels and also for studying toxin-channel and toxin-membrane interactions. Several of these toxins are cysteine-rich, rendering the production of properly folded fluorescently labeled toxins technically challenging. Herein, we evaluate a variety of site-specific protein bioconjugation approaches for producing fluorescently labeled double-knot toxin (DkTx), a potent TRPV1 ion channel agonist that contains an uncommonly large number of cysteines (12 out of a total of 75 amino acids present in the protein). We find that popular cysteine-mediated bioconjugation approaches are unsuccessful as the introduction of a non-native cysteine residue for thiol modification leads to the formation of misfolded toxin species. Moreover, *N*-terminal aldehyde-mediated bioconjugation approaches are also not suitable as the resultant labeled toxin lacks activity. In contrast to these approaches, *C*-terminal bioconjugation of DkTx via the sortase bioconjugation technology yields functionally active fluorescently labeled DkTx. We employ this labeled toxin for imaging rat TRPV1 heterologously expressed in *Xenopus laevis* oocytes, as well as for performing membrane binding studies on giant unilamellar vesicles composed of different lipid compositions. Our studies set the stage for using fluorescent DkTx as a tool for TRPV1 biology and provide an informative blueprint for labeling cysteine-rich proteins.

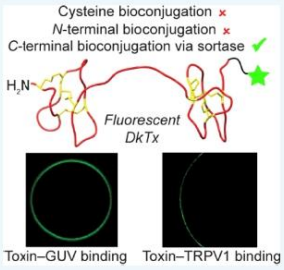

INTRODUCTION

Ion channel-targeting peptide toxins produced by venomous animals have contributed tremendously to ion channel biology. Indeed, these toxins serve as powerful tools for unraveling ion channel structures and gating mechanisms, and as specific pharmacological agents for studying channel activity in their native environments.[1−5] Additionally, radiolabeled toxins are employed for channel imaging using autoradiography techniques[6,7] and serve as the basis for toxin-channel binding assays.[8−11] Notwithstanding their usefulness, radiolabeling-based approaches have inherent limitations including the risk of exposure to damaging radiation and noncompatibility with live cell-based assays. In comparison, fluorescence-based approaches are preferable because they are safe and are ideal for live cell and single molecule studies.[12−16]

Appending fluorescent proteins such as the green fluorescent protein to toxins are not ideal as the former is much larger (>25 kDa) than the latter (5−10 kDa) and, therefore, can result in disruption of the native functional and physicochemical properties of the toxins. In comparison, labeling toxins with small molecule fluorescent dyes is preferable as in addition to imparting minimal alterations to the structure of the toxin, the photochromic properties of these dyes can be synthetically fine-tuned for sensitive imaging applications.[17,18] The production of toxins labeled with fluorophores has been greatly facilitated by the development of a rich toolkit of protein bioconjugation strategies.[19−22] A tabulated summary of previously published reports on the fluorescence labeling of ion channel and receptor-targeting peptide toxins has been provided in the Supporting Information section (Table S1).

The goal of this work was to fluorescently label the TRPV1 ion channel-targeting toxin agonist, the double-knot toxin (DkTx),[23] for imaging TRPV1 in cells, and for studying the toxin's interaction with the membrane which has been demonstrated to play important roles in its activity.[24,25] DkTx consists of two lobes, K1 and K2, each forming an inhibitory cystine knot (ICK) structural motif[26−29] containing three disulfide linkages (Figure 1a). A high-yielding methodology for the recombinant production of DkTx has been reported, and it entails the production of the KSI (ketosteroid isomerase) fusion protein of DkTx in *E. coli* inclusion bodies

Received: July 28, 2022
Revised: August 24, 2022
Published: September 8, 2022

https://doi.org/10.1021/acs.bioconjchem.2c00355
Bioconjugate Chem. 2022, 33, 1761−1770

Organic & Biomolecular Chemistry

PAPER

View Article Online
View Journal | View Issue

Cite this: *Org. Biomol. Chem.*, 2018, **16**, 4304

Rapid and reversible hydrazone bioconjugation in cells without the use of extraneous catalysts†

Rahul Nisal, Gregor P. Jose, Chitra Shanbhag and Jeet Kalia *‡

Received 22nd April 2018,
Accepted 15th May 2018

DOI: 10.1039/c8ob00946e

rsc.li/obc

The amenability of hydrazone linkages to disassemble *via* either hydrolysis in mildly acidic aqueous solutions or transimination upon treatment with amine nucleophiles renders them extremely attractive for applications in chemical biology, drug delivery and materials science. Unfortunately, however, the use of hydrazones is hampered by the extremely slow intrinsic rates of their formation from their hydrazine and carbonyl precursors. Consequently, hydrazone formation is typically performed in the presence of a large excess of cytotoxic aniline-based nucleophilic catalysts, rendering hydrazones unsuitable for biological applications that entail their formation in cells. Herein, we report a hydrazine scaffold—*o*-amino benzyl hydrazine—that rapidly forms hydrazones *via* intramolecular nucleophilic catalysis, thereby obviating the use of extraneous catalysts. We demonstrate the use of this scaffold for rapid and reversible peptide and protein hydrazone bioconjugation and also for reversible fluorescent labeling of sialylated glycoproteins and choline lipids in mammalian cells.

Introduction

Covalent linkages that disassemble when subjected to specific chemical stimuli are extremely attractive for applications in a wide variety of research areas including materials sciences[1] and both clinical and basic biological research.[2–5] Among the handful of such known linkages,[6–15] hydrazones[16] are unique in possessing the ability to undergo breakdown in two ways—hydrolysis to form their hydrazine and aldehyde/ketone precursors under mildly acidic conditions[17] and transimination to form imines, oximes or other hydrazones when treated with amines, alkoxyamines or hydrazines, respectively. The hydrolytic instability of hydrazones has been exploited for a diverse range of applications including drug delivery[18–23] and generating smart polymeric scaffolds.[13,24,25] The transimination of hydrazones, on the other hand, has facilitated the development of dynamic combinatorial libraries[26,27] and has also been employed for chemical biology-based applications.[28,29] Additionally, hydrazones have also been utilized for applications that do not rely on their ability to disassemble, including protein immobilization[30,31] and labeling of proteins with fluorophores,[32–35] affinity tags,[29,33,36,37] mass spectrometry labels[37–39] and polyethylene glycol moieties.[40–42]

Among the previously reported biological applications of hydrazone linkages, very few[32,43,44] involve their formation within cells. Indeed, perhaps the most widely used application of hydrazones is in drug delivery[18–23] that entails conjugate formation *in vitro* followed by administration into cells. A major reason for the lack of use of hydrazones for performing bioconjugation within cells is the slow rate of hydrazone formation in aqueous solutions,[45–47] a drawback that can be partly overcome by the use of large amounts (usually ~50 fold molar excess or more) of aniline or its derivatives that function as nucleophilic catalysts for hydrazone formation (Fig. 1a).[45,48–55] The use of such large amounts of aniline derivatives is undesirable due to their cytotoxicity,[47,56,57] as

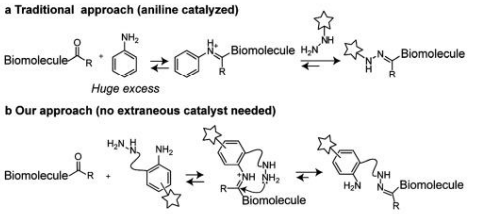

Fig. 1 Hydrazone bioconjugation *via* (a) the traditional aniline-catalyzed approach and (b) our approach involving intramolecular nucleophilic catalysis.

Indian Institute of Science Education and Research (IISER) Pune, Dr. Homi Bhabha Road, Pashan, Pune-411008, Maharashtra, India. E-mail: jeet@iiserb.ac.in; Tel: +91-755-6691437

†Electronic supplementary information (ESI) available. See DOI: 10.1039/c8ob00946e

‡Current address: Department of Biological Sciences, Indian Institute of Science Education and Research (IISER) Bhopal, Bhopal Bypass Road, Bhauri, Bhopal-462066, Madhya Pradesh, India.

8. Animal Usage Approval

Indian Institute of Science Education and Research
(IISER – PUNE)
Dr. Homi Bhabha Road, Pashan, Pune 411 008.

Certificate

This is to certify that the project **"Amino Acid and Sugar Based Biodegradable Polymers for Anticancer Drug Delivery" (IISER_Pune/ IAEC/2022_01/16)** from **Prof. M. Jayakannan** has been approved by the IAEC.

Authorized by	Name	Signature	Date
Chairman:	**Dr. Nixon Abraham**		**04 Mar 2022**
Member Secretary:	**Dr. Suraj Ingle**		**04 Mar 2022**
Main Nominee ofCPCSEA:	**Dr. Shital Suryavanshi**	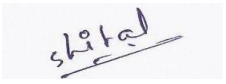	**04 Mar 2022**

9. Appendix

Chapter 2

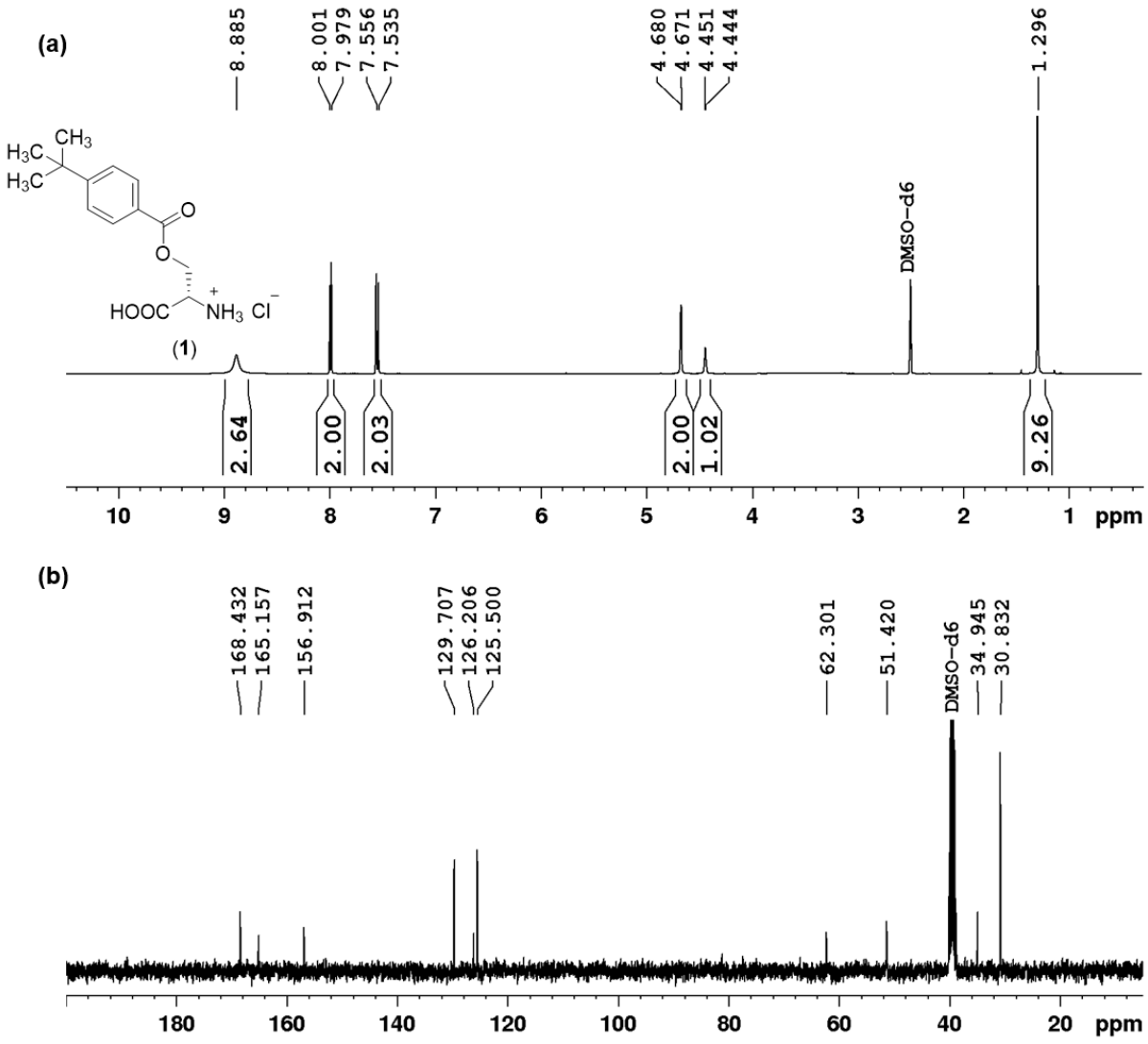

Appendix Figure 2.1: *(a)* ^{1}*H NMR of compound* ***1*** *in DMSO-d6 (b)* ^{13}*C NMR of compound* ***1*** *in DMSO-d6.*

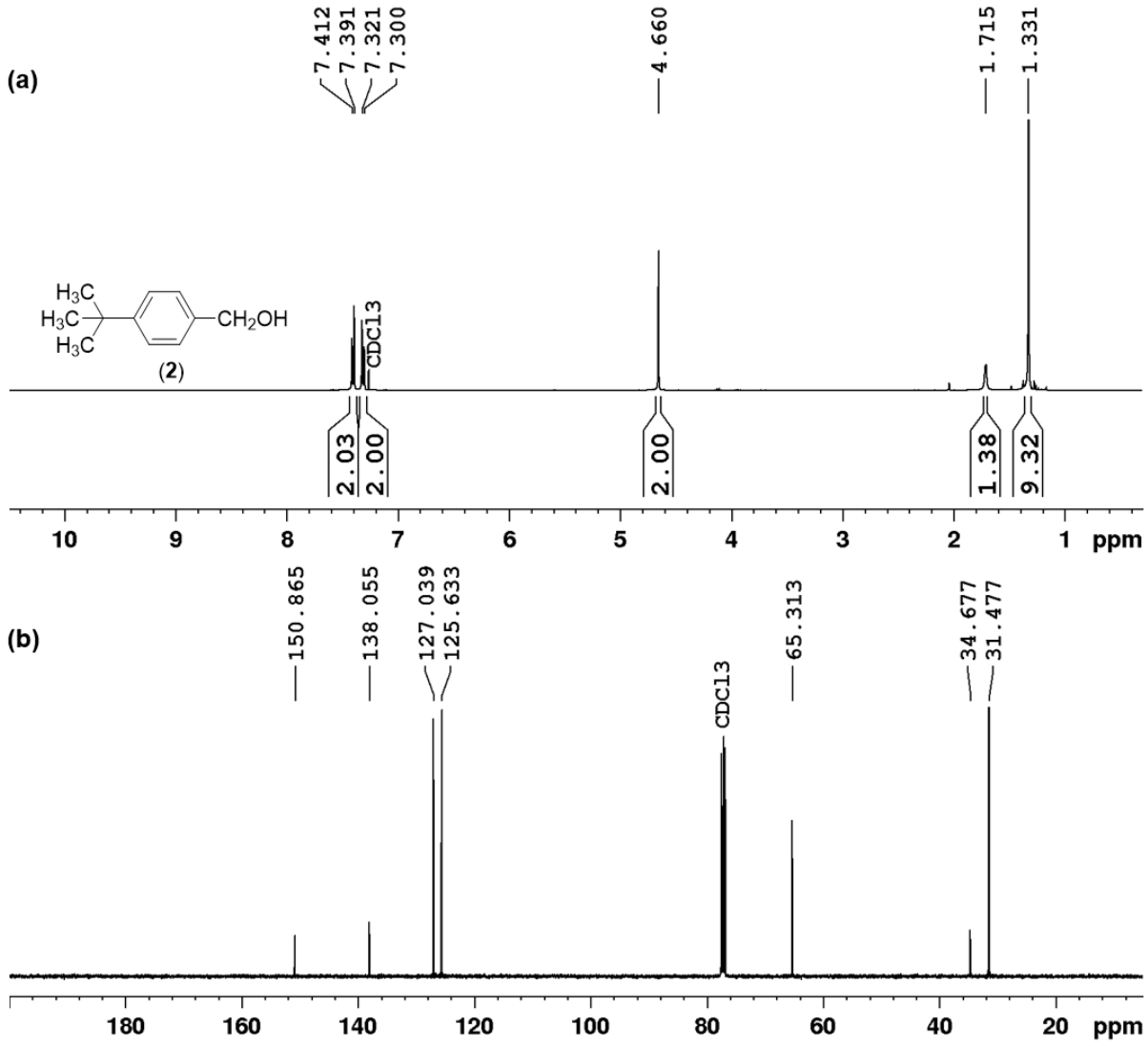

Appendix Figure 2.2: *(a) ^{1}H NMR of compound **2** in $CDCl_3$ (b) ^{13}C NMR of compound **2** in $CDCl_3$*

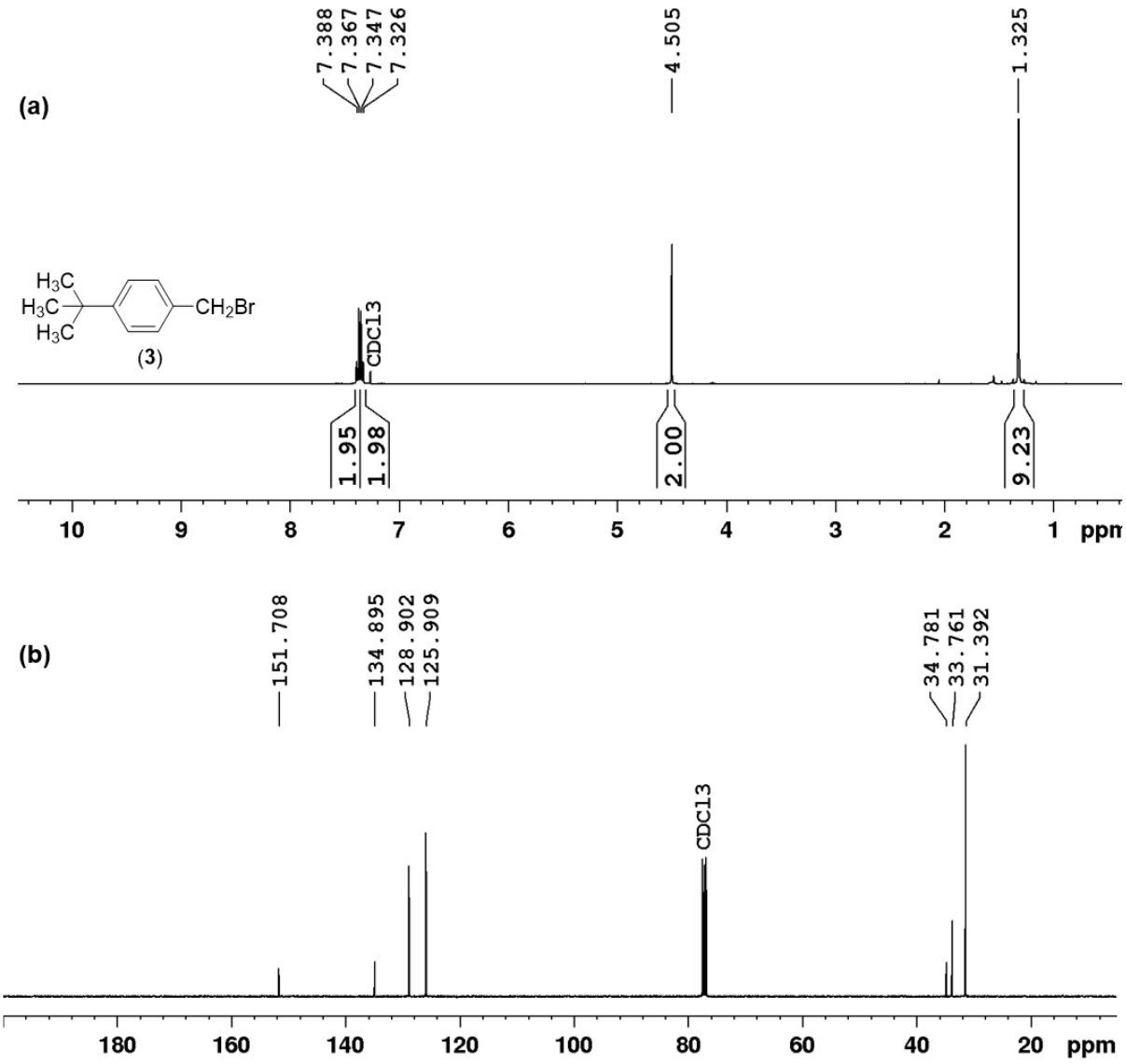

Appendix Figure 2.3: *(a) ^{1}H NMR of compound **3** in $CDCl_3$ (b) ^{13}C NMR of compound **3** in $CDCl_3$*

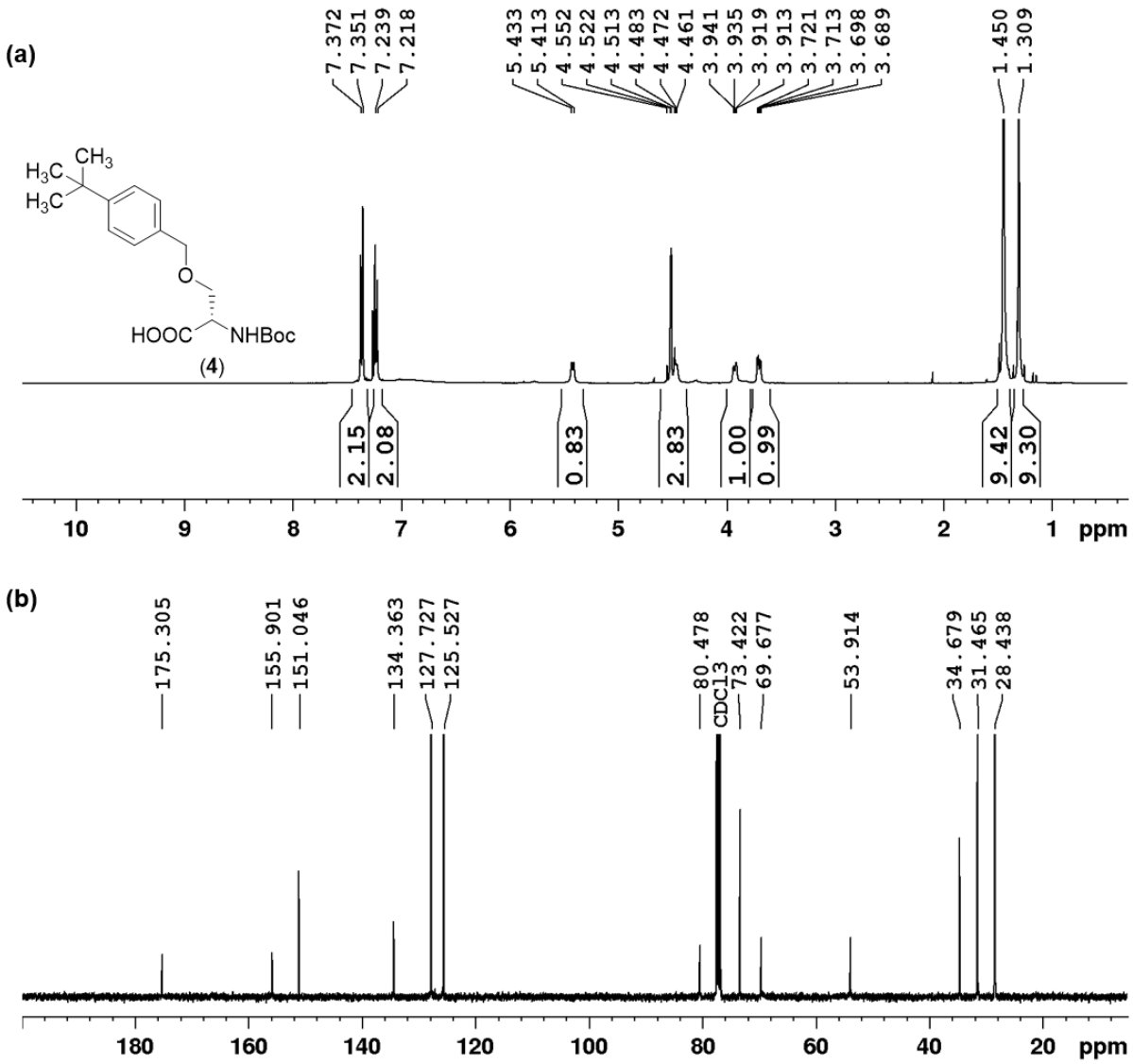

Appendix Figure 2.4: *(a) ^{1}H NMR of compound **4** in $CDCl_3$ (b) ^{13}C NMR of compound **4** in $CDCl_3$*

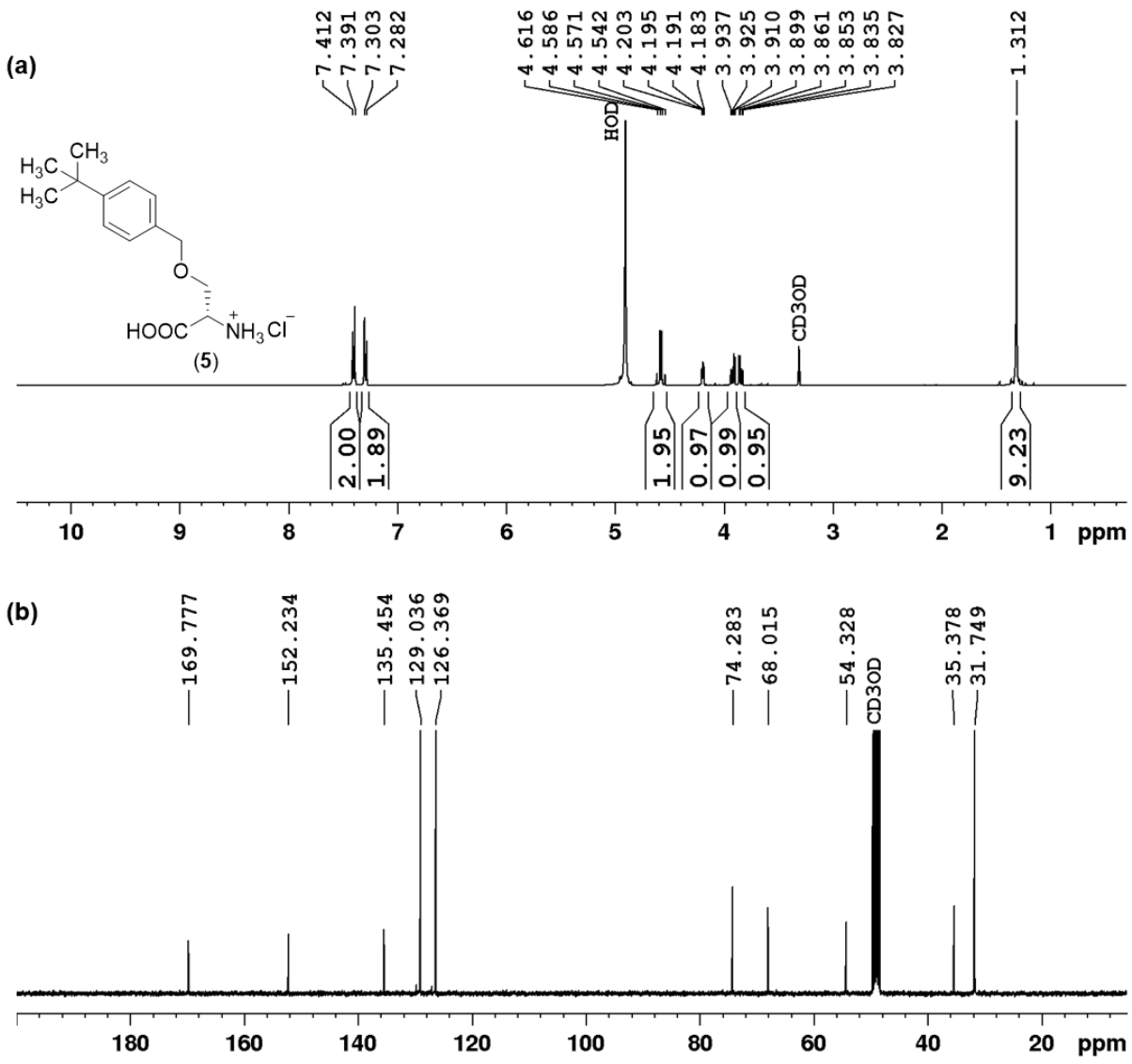

Appendix Figure 2.5: *(a) ^{1}H NMR of compound **5** in CD_3OD (b) ^{13}C NMR of compound **5** in CD_3OD.*

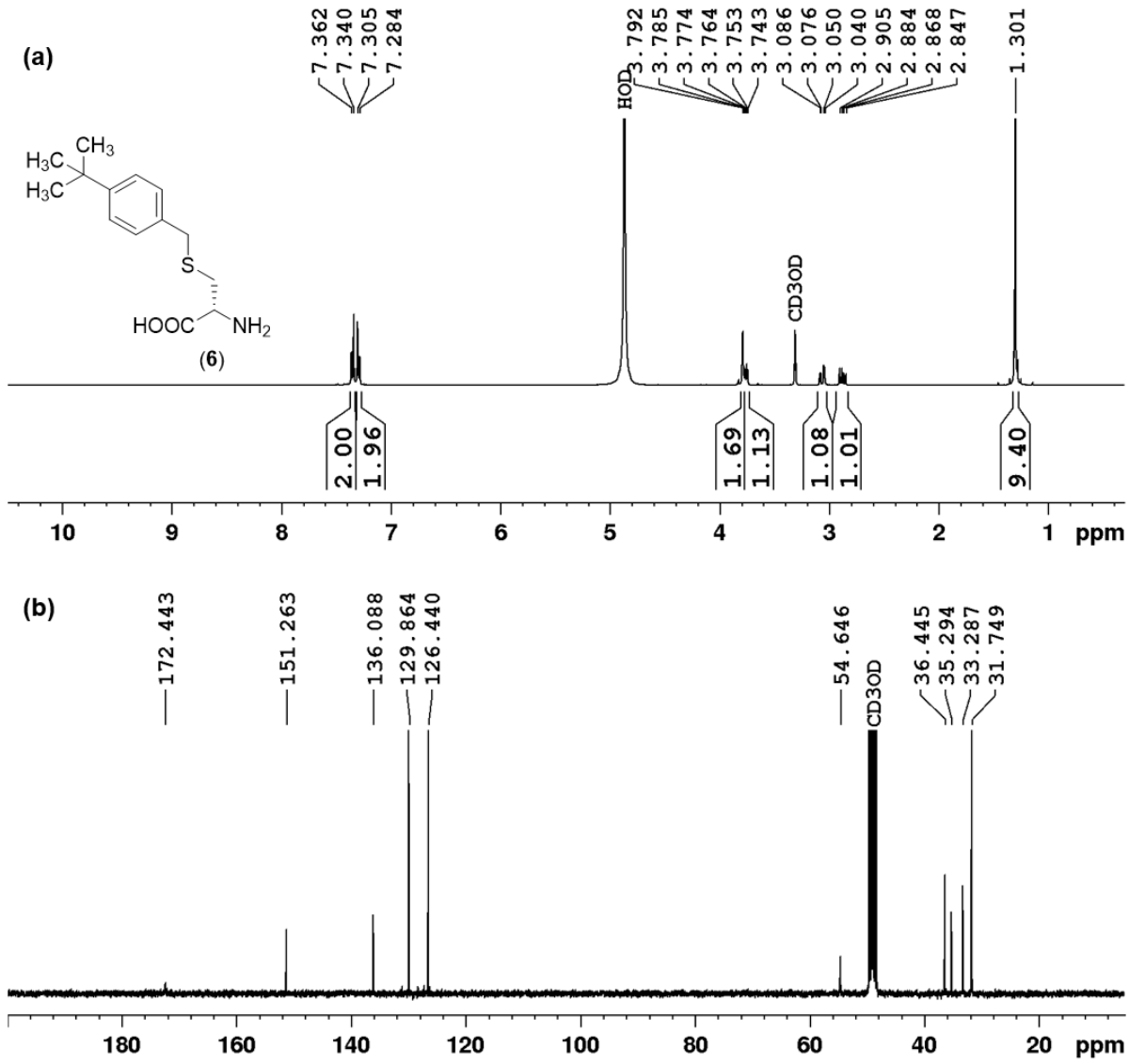

Appendix Figure 2.6: *(a) ^{1}H NMR of compound **6** in CD_3OD (b) ^{13}C NMR of compound **6** in CD_3OD*

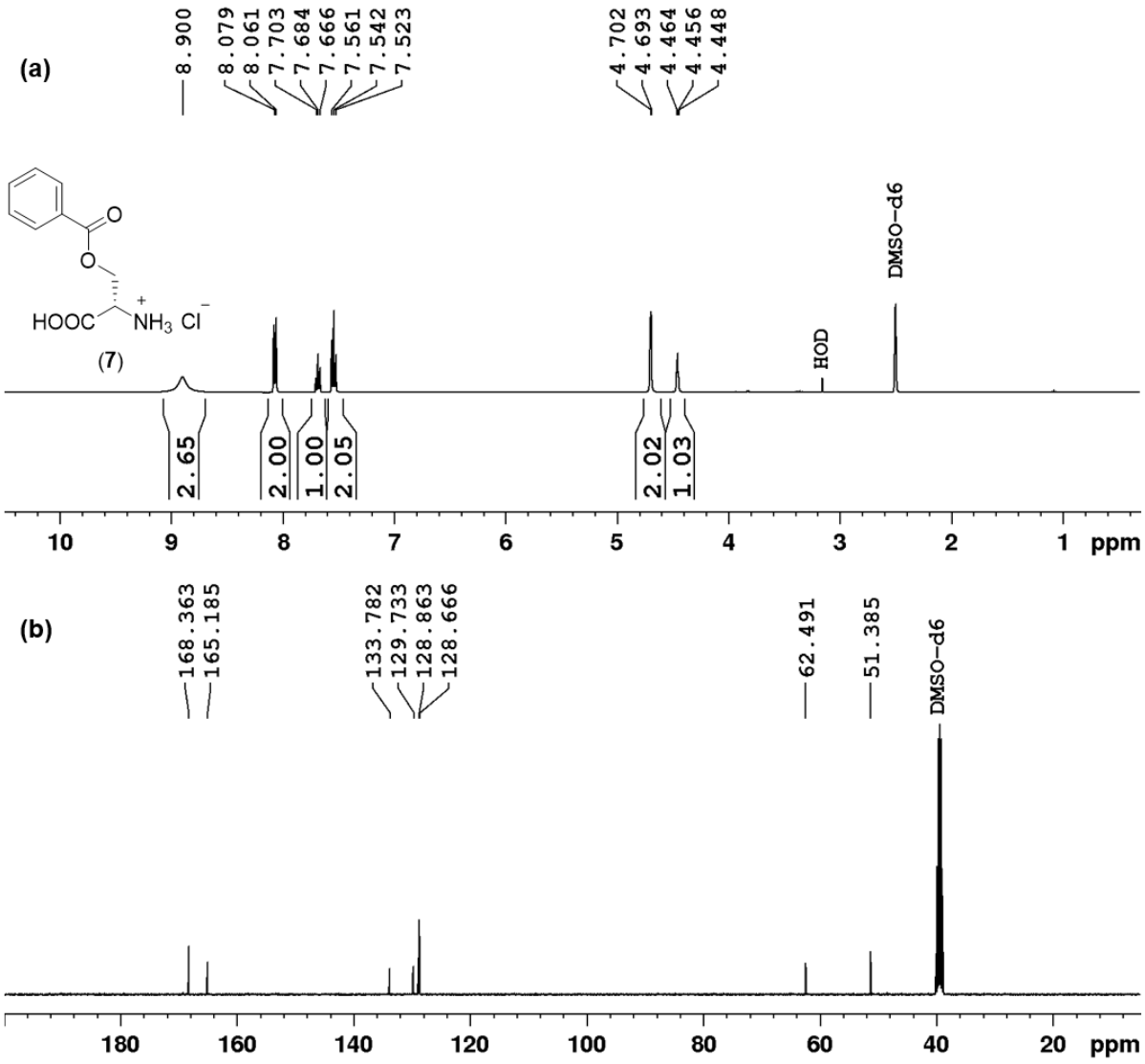

Appendix Figure 2.7: *(a) ^{1}H NMR of compound **7** in DMSO-d_6 (b) ^{13}C NMR of compound **7** in DMSO-d_6*

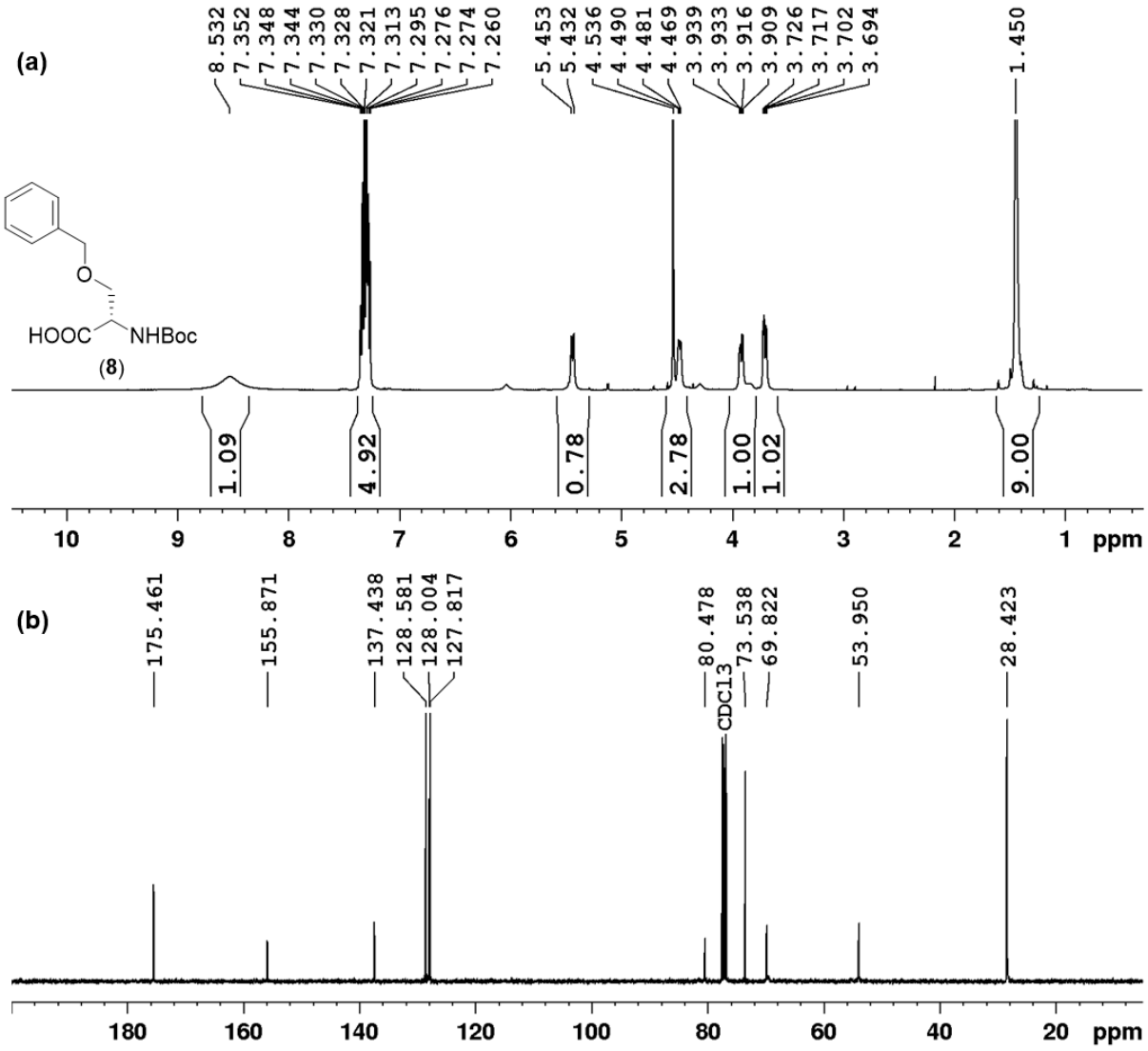

Appendix Figure 2.8: *(a)* ^{1}H *NMR of compound* ***8*** *in* $CDCl_3$ *(b)* ^{13}C *NMR of compound* ***8*** *in* $CDCl_3$

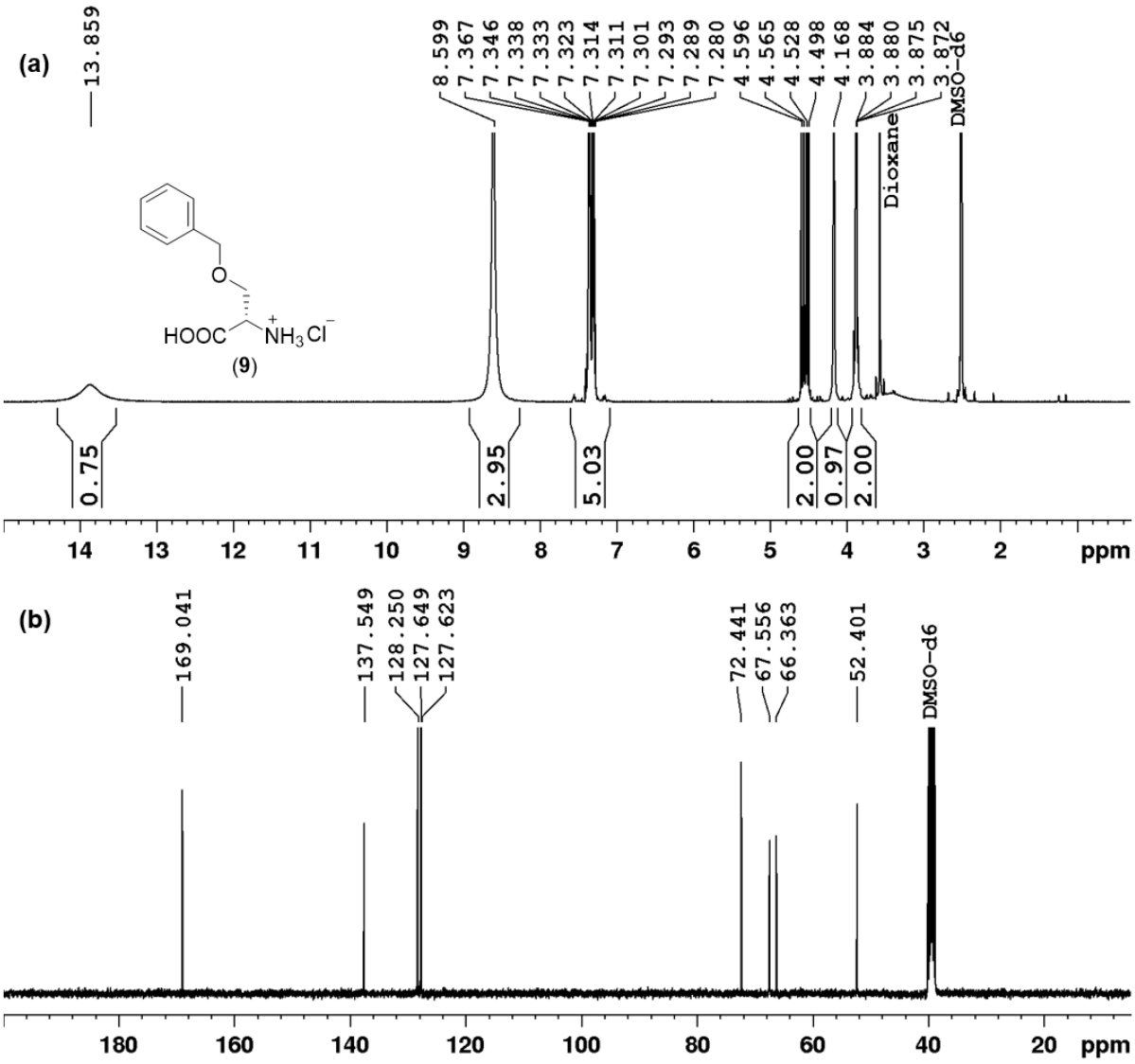

Appendix Figure 2.9: *(a) ^{1}H NMR of compound **9** in DMSO-d_6 (b) ^{13}C NMR of compound **9** in DMSO-d_6*

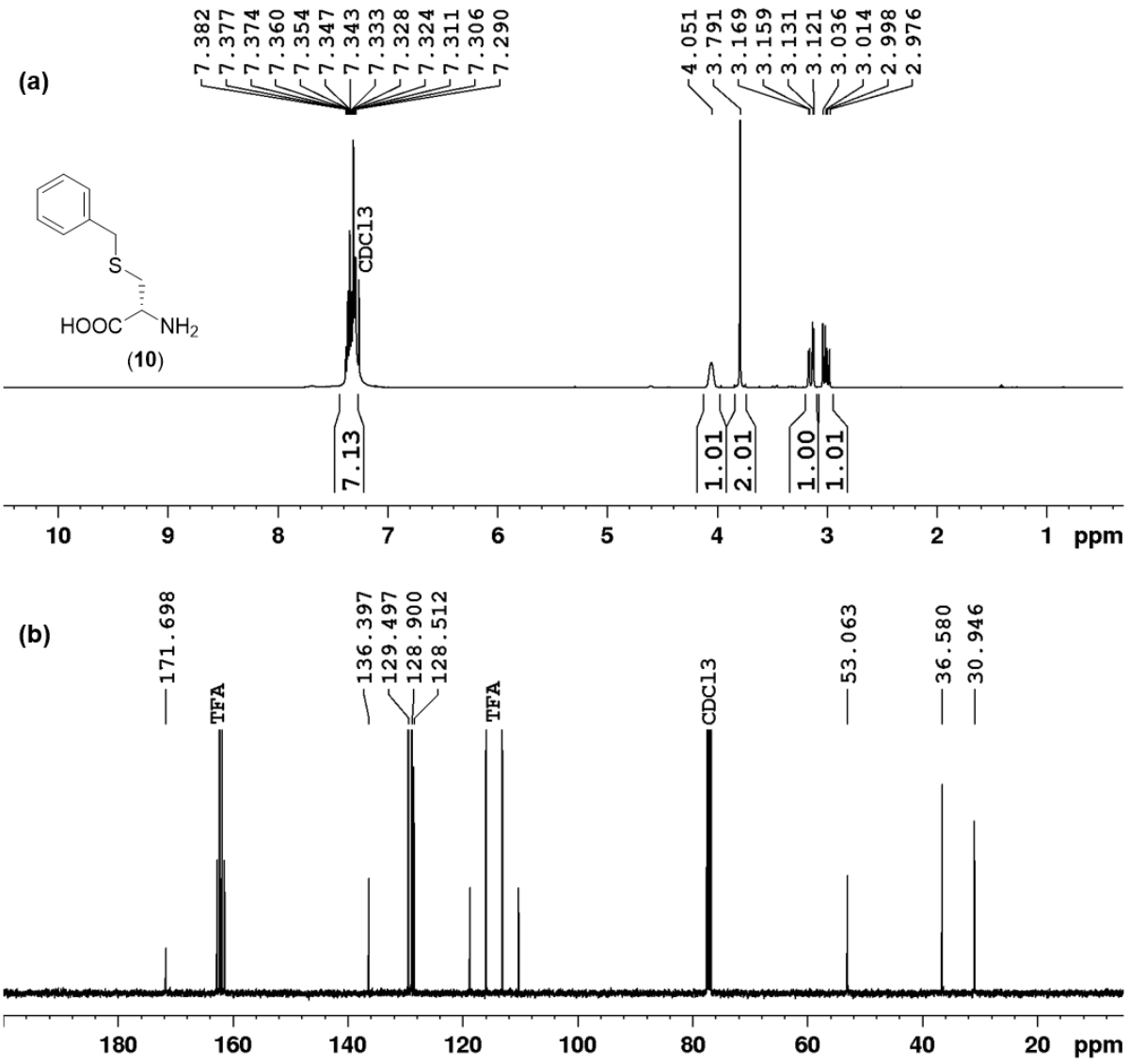

Appendix Figure 2.10: *(a) ^{1}H NMR of compound **10** in $CDCl_3$+Trifluoroacetic acid (6:1, v/v) (b) ^{13}C NMR of compound **10** in $CDCl_3$+Trifluoroacetic acid (6:1, v/v)*

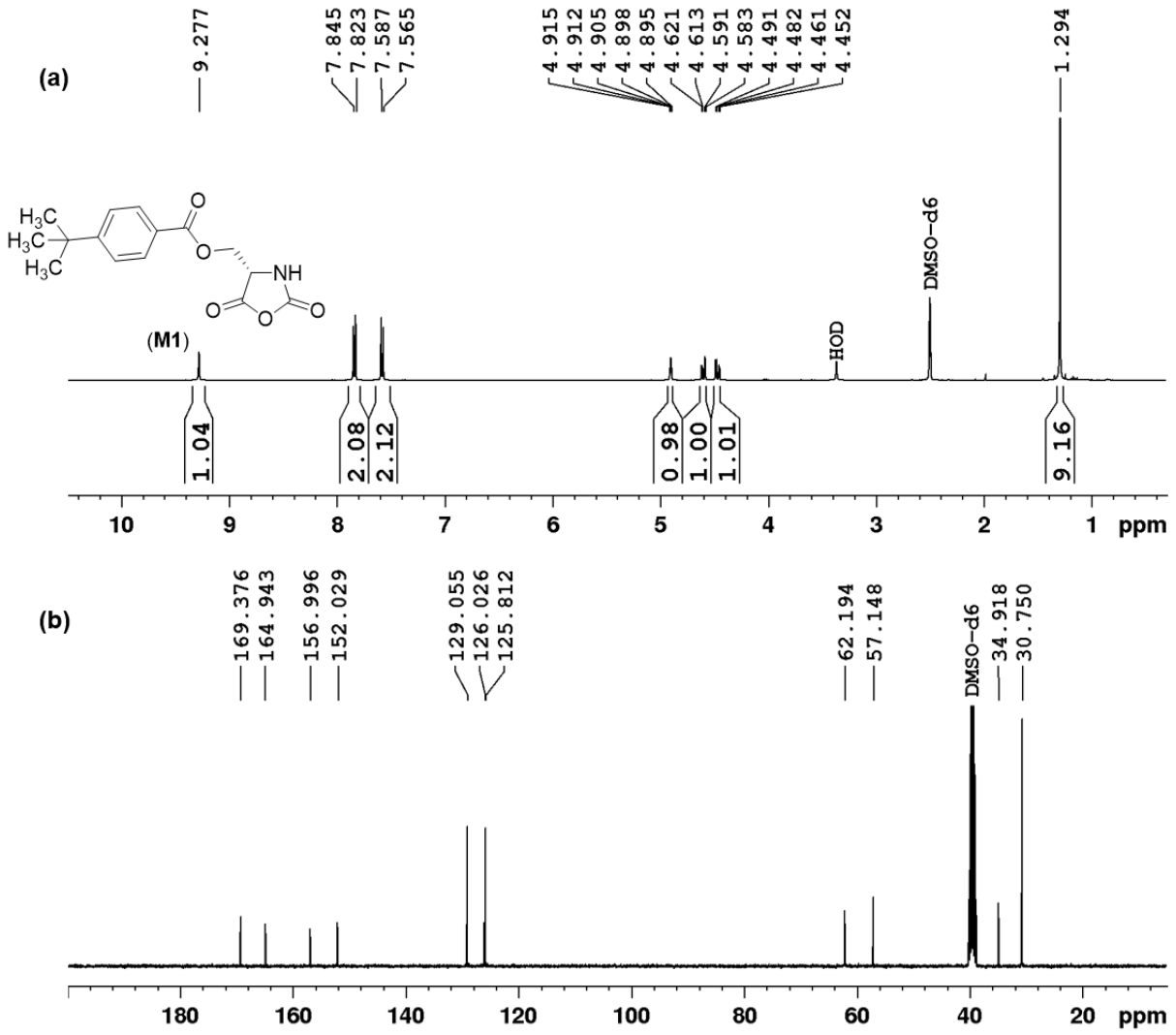

Appendix Figure 2.11: *(a) ^{1}H NMR of serine-ester NCA monomer-**M1** in DMSO-d_6, (b) ^{13}C NMR of serine-ester NCA monomer-**M1** in DMSO-d_6.*

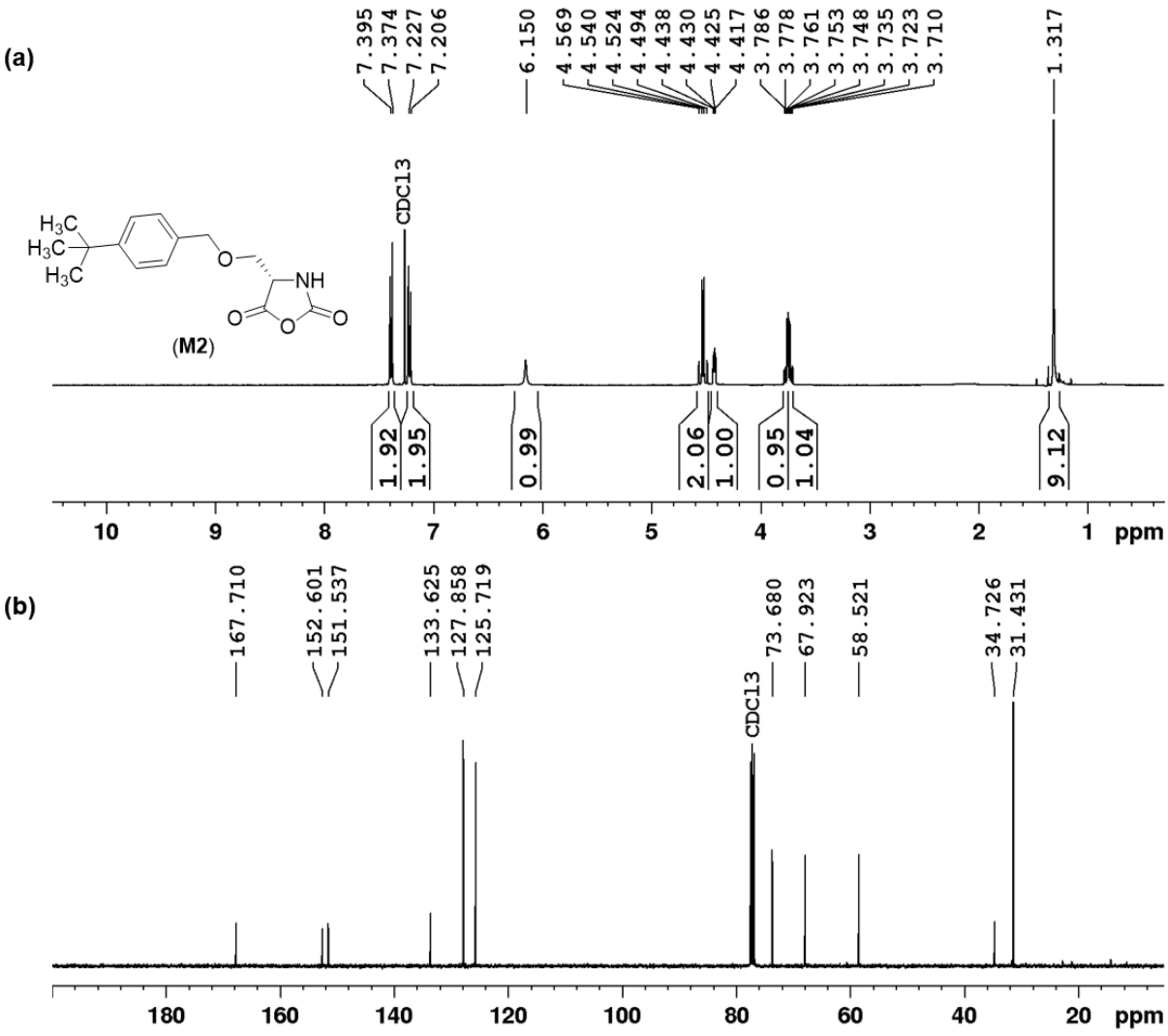

Appendix Figure 2.12: *(a) ^{1}H NMR of serine-ether NCA monomer-**M2** in $CDCl_3$, (b) ^{13}C NMR of serine-ether NCA monomer-**M2** in $CDCl_3$.*

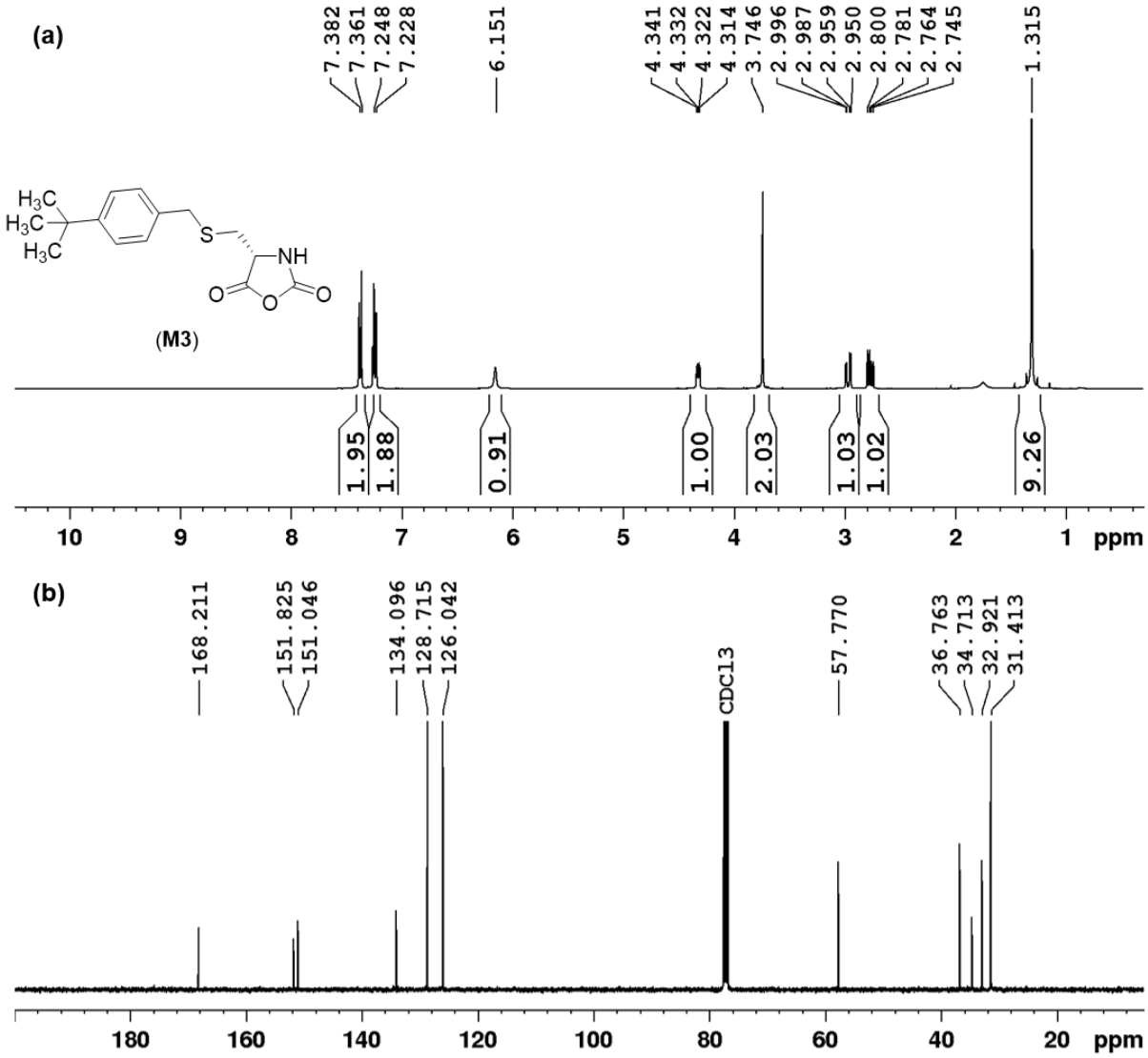

Appendix Figure 2.13: *(a) ^{1}H NMR of cysteine NCA monomer-**M3** in $CDCl_3$, (b) ^{13}C NMR of cysteine NCA monomer-**M3** in $CDCl_3$.*

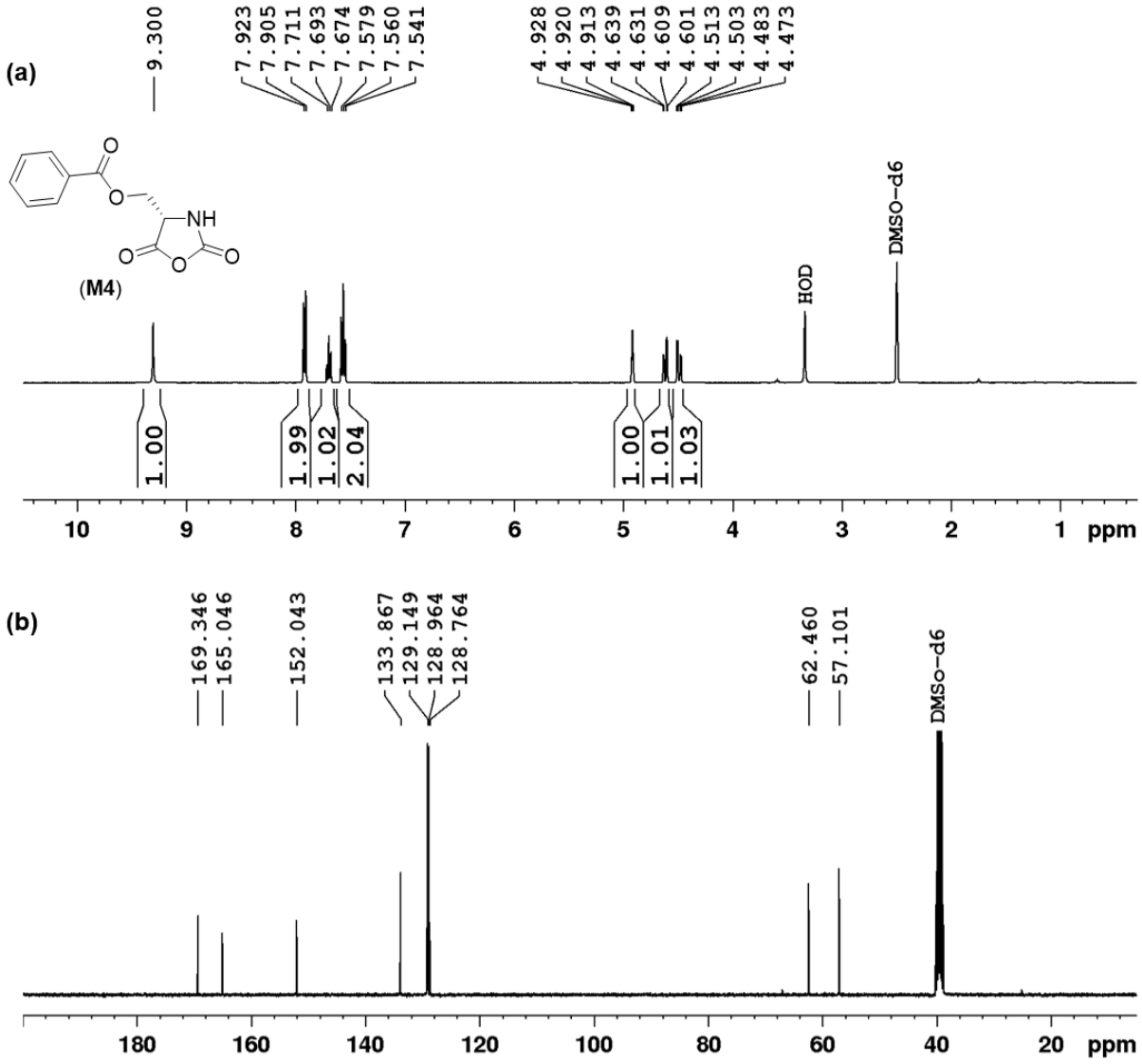

Appendix Figure 2.14: *(a) ^{1}H NMR of serine-ester NCA monomer-**M4** in DMSO-d_6, (b) ^{13}C NMR of serine-ester NCA monomer-**M4** in DMSO-d_6.*

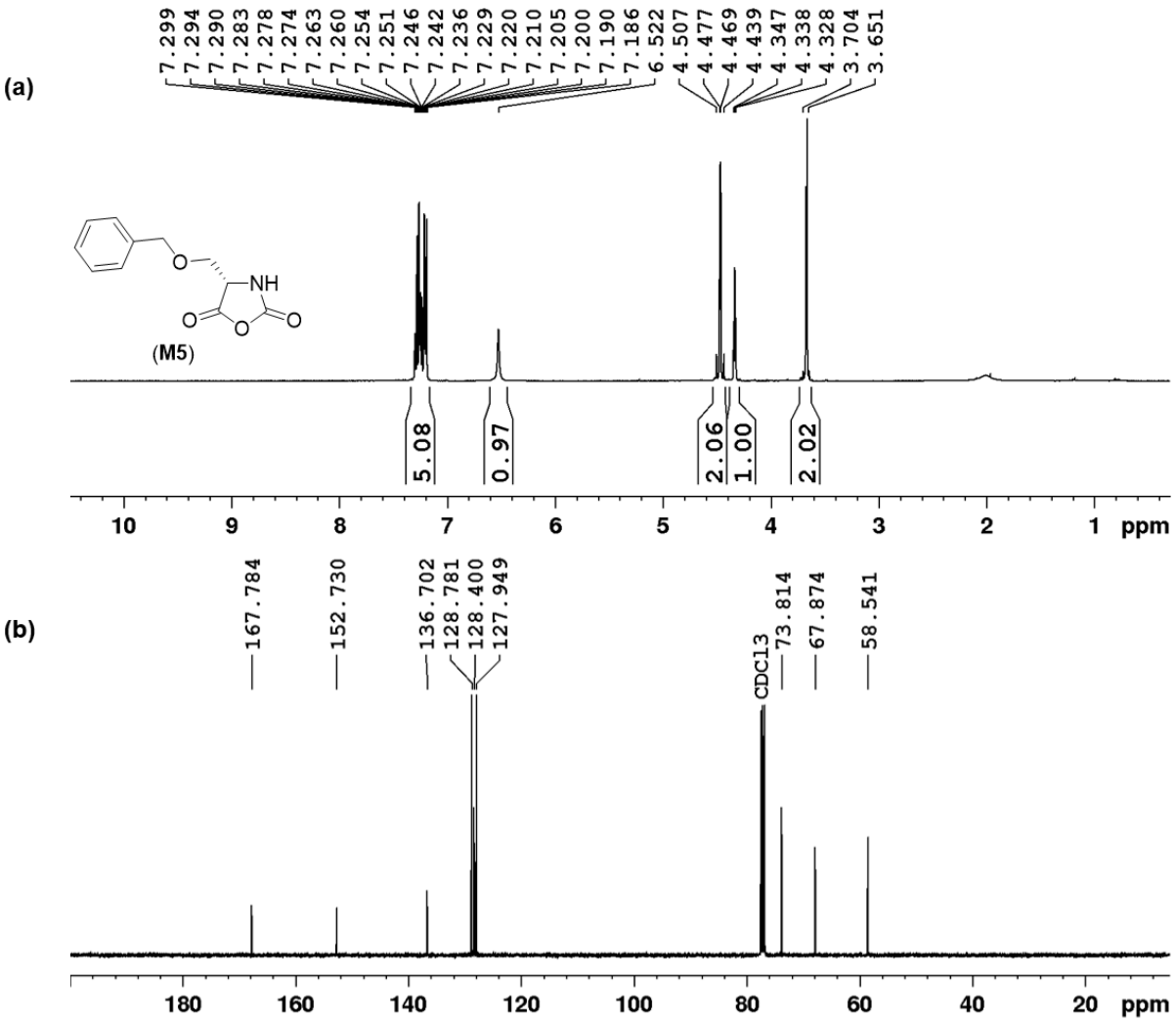

Appendix Figure 2.15: *(a) ^{1}H NMR of serine-ether NCA monomer-**M5** in $CDCl_3$, (b) ^{13}C NMR of serine-ether NCA monomer-**M5** in $CDCl_3$.*

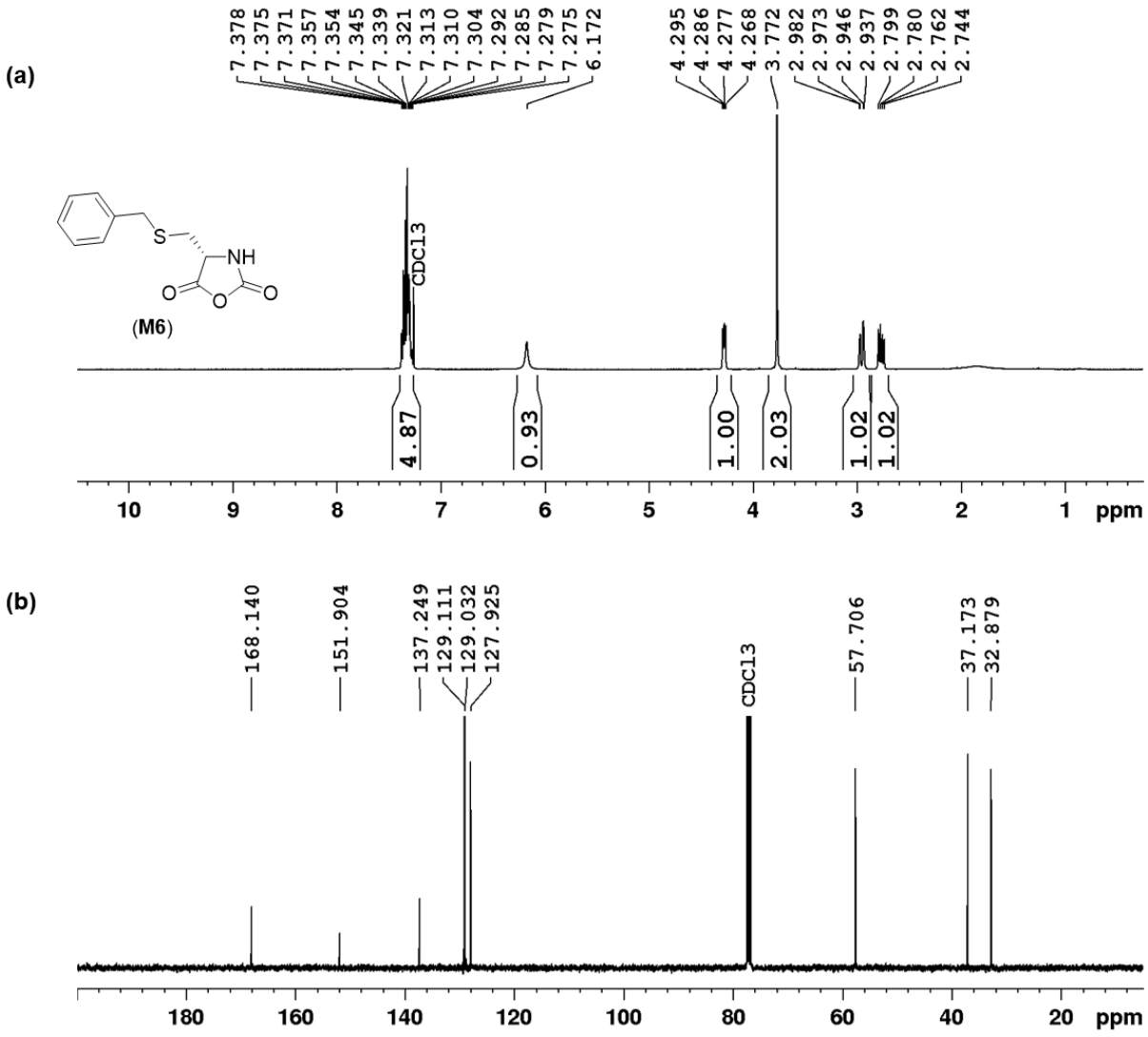

Appendix Figure 2.16: *(a) ^{1}H NMR of cysteine NCA monomer-**M6** in $CDCl_3$, (b) ^{13}C NMR of cysteine NCA monomer-**M6** in $CDCl_3$*

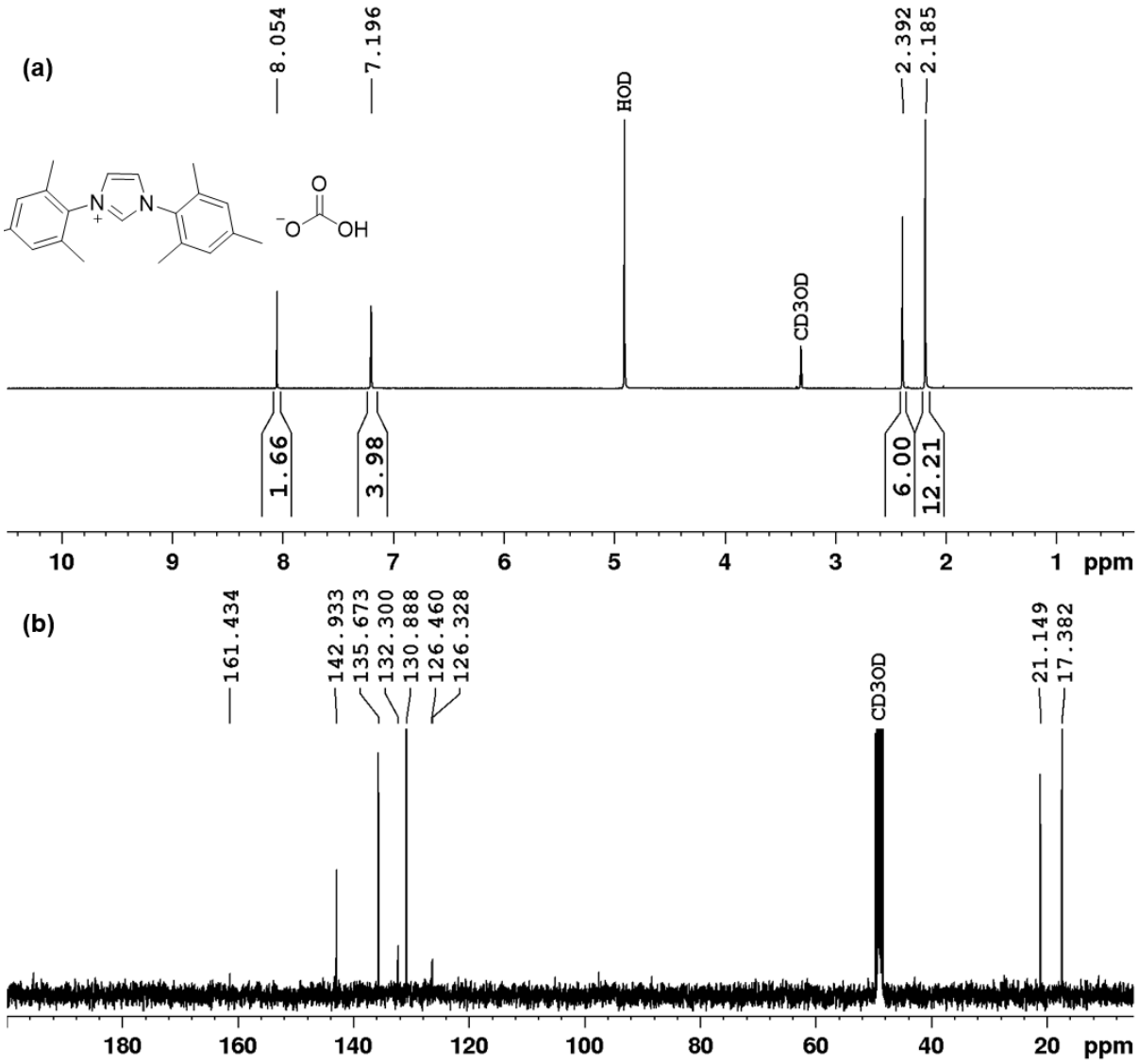

Appendix Figure 2.17: *(a) ^{1}H NMR of compound IMes NHC bicarbonate salt in CD_3OD (b) ^{13}C NMR of compound IMes NHC bicarbonate salt in CD_3OD*

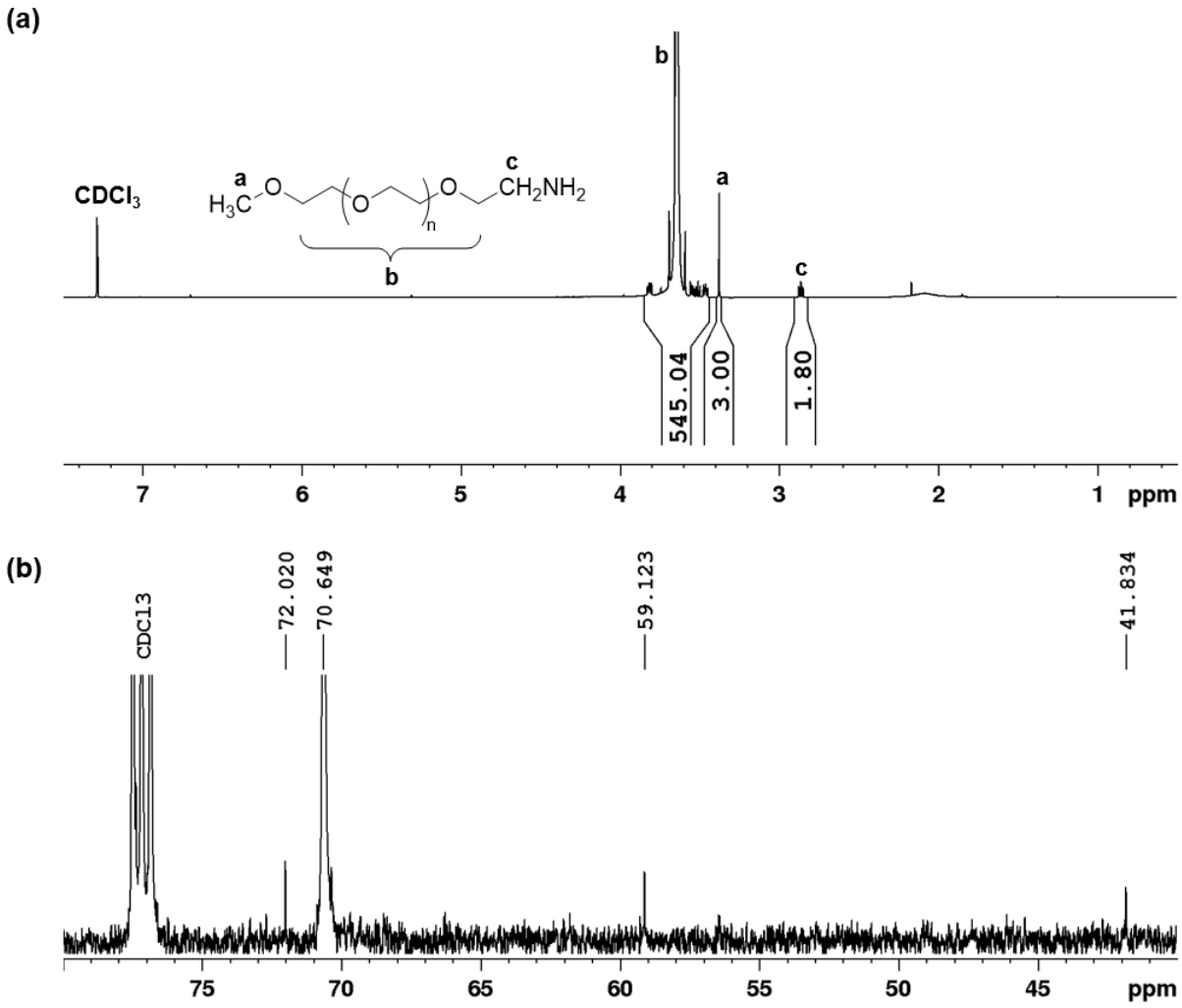

Appendix Figure 2.18: *(a) ^{1}H NMR of compound MeO-PEG$_{5000}$-NH$_2$ in CDCl$_3$ (b) ^{13}C NMR of compound MeO-PEG$_{5000}$-NH$_2$ in CDCl$_3$*

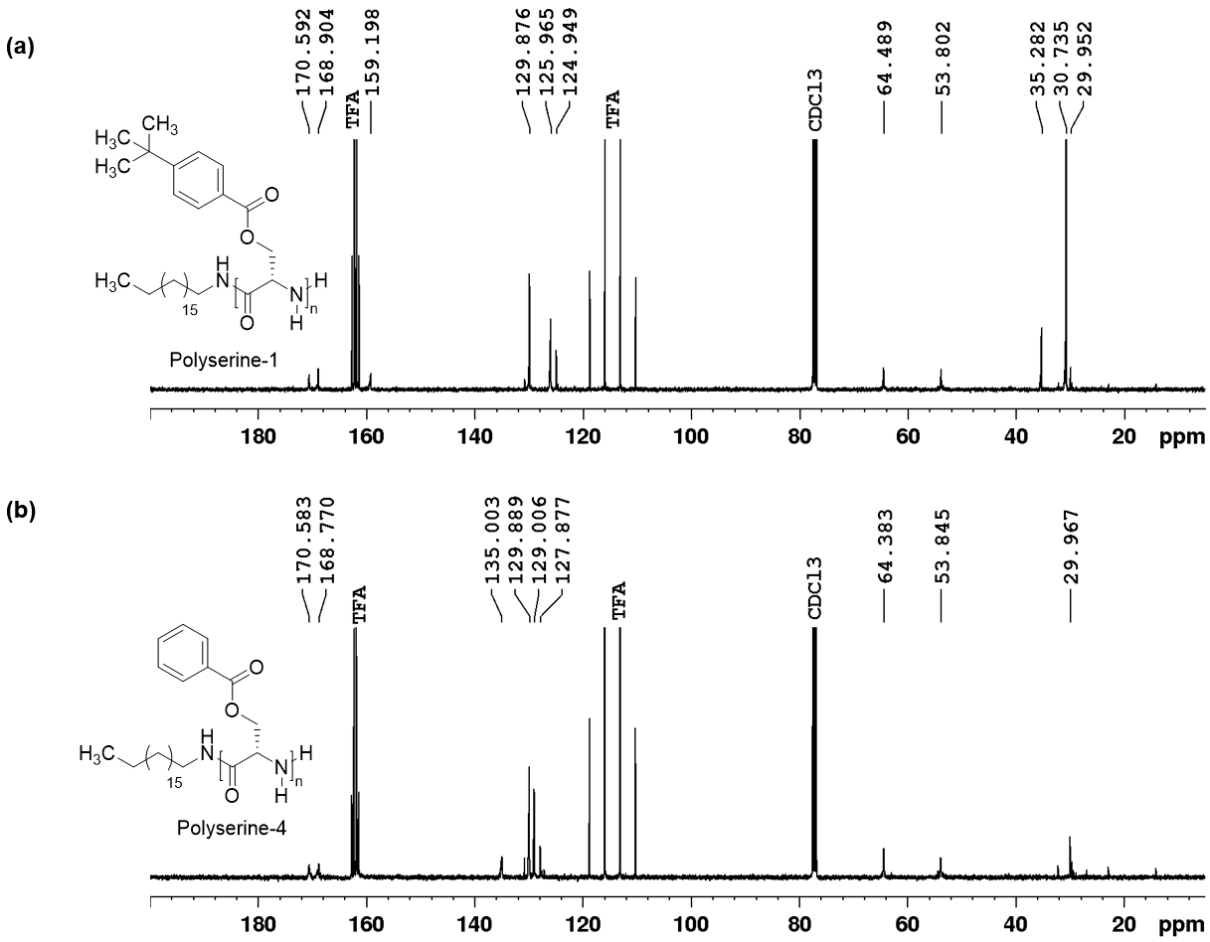

Appendix Figure 2.19: *(a) ^{13}C NMR of polyserine-1 in $CDCl_3$+Trifluoroacetic acid (6:1, v/v) (b) ^{13}C NMR of polyserine-4 in $CDCl_3$+Trifluoroacetic acid (6:1, v/v)*

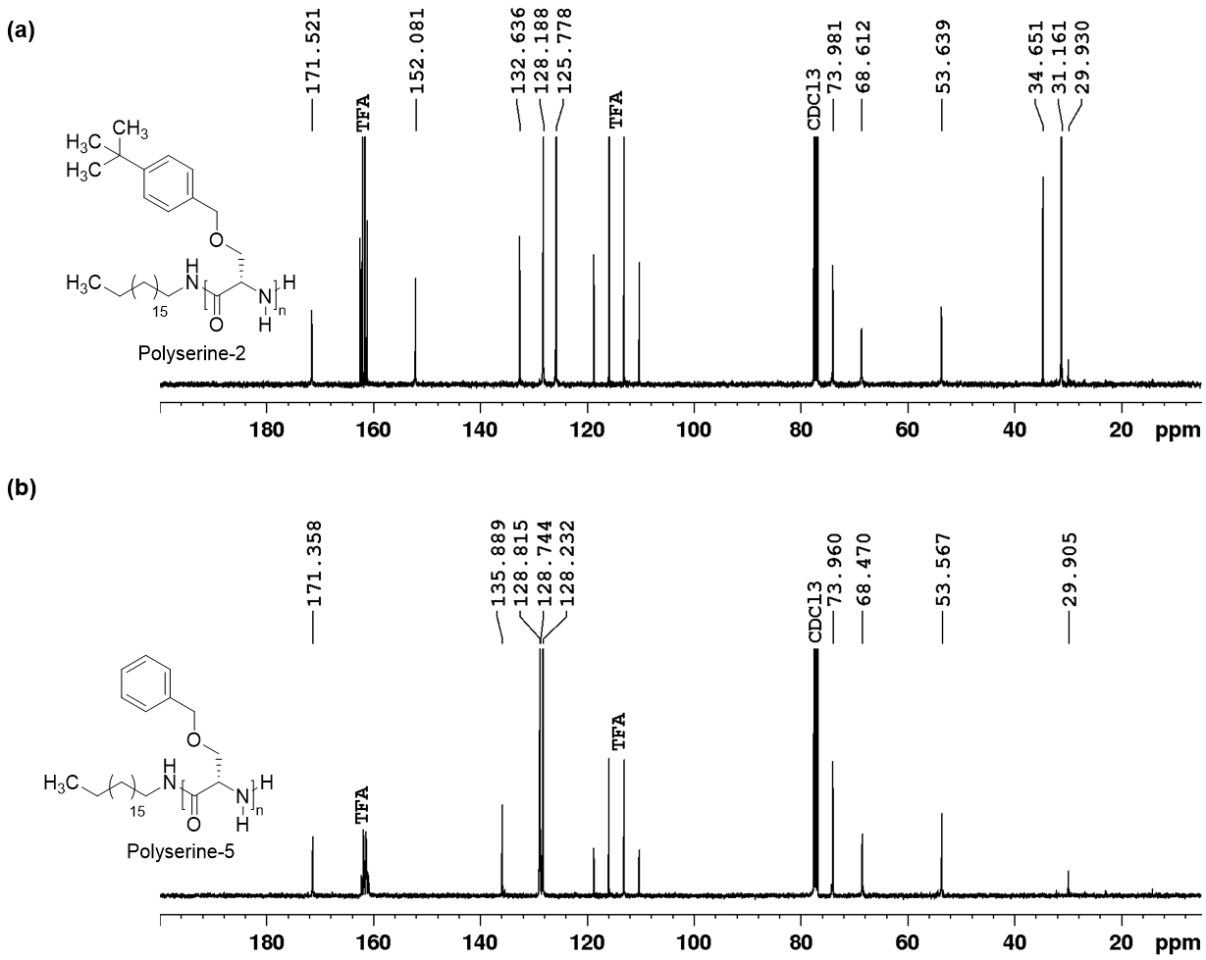

Appendix Figure 2.20: *(a) ^{13}C NMR of polyserine-2 in $CDCl_3$+Trifluoroacetic acid (6:1, v/v) (b) ^{13}C NMR of polyserine-5 in $CDCl_3$+Trifluoroacetic acid (6:1, v/v)*

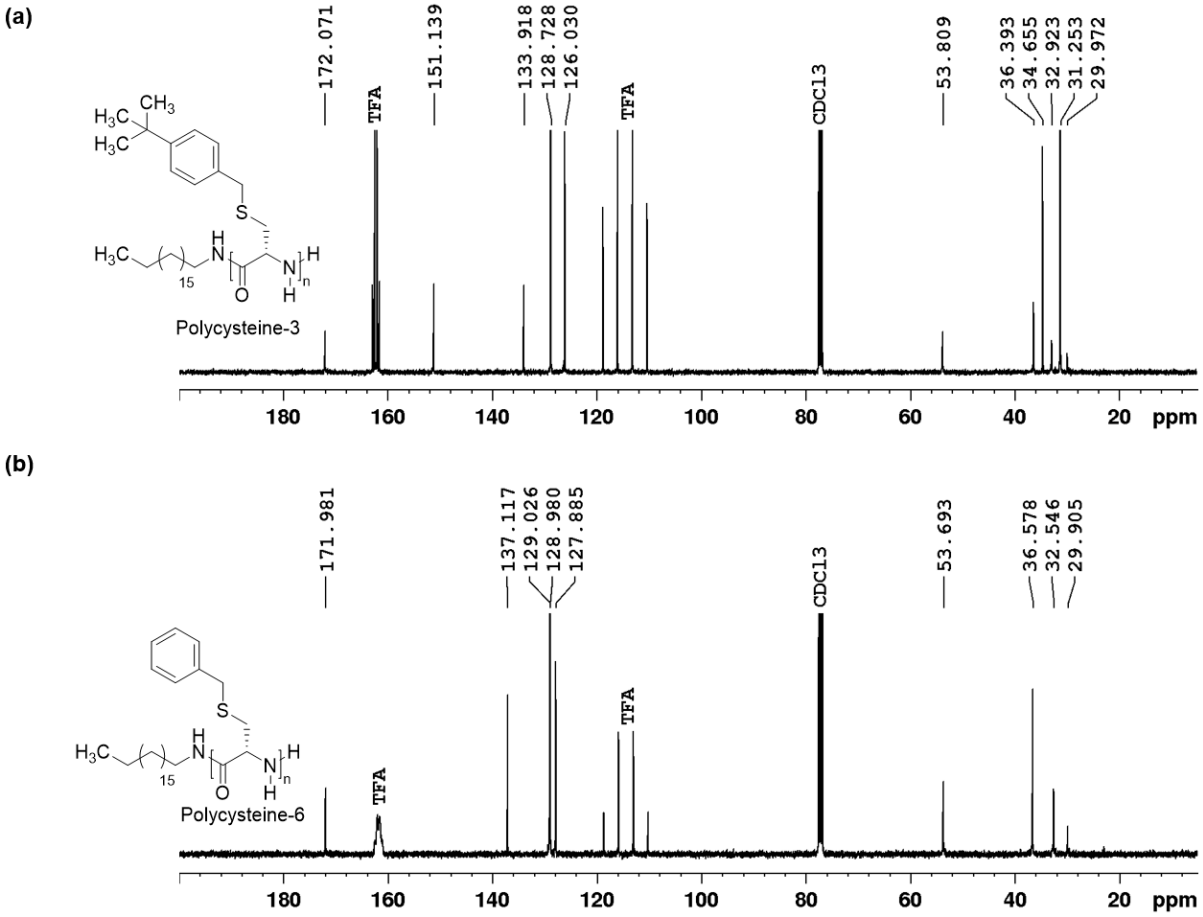

Appendix Figure 2.21: *(a) ^{13}C NMR of polycysteine-3 in $CDCl_3$+Trifluoroacetic acid (6:1, v/v) (b) ^{13}C NMR of polycysteine-6 in $CDCl_3$+Trifluoroacetic acid (6:1, v/v)*

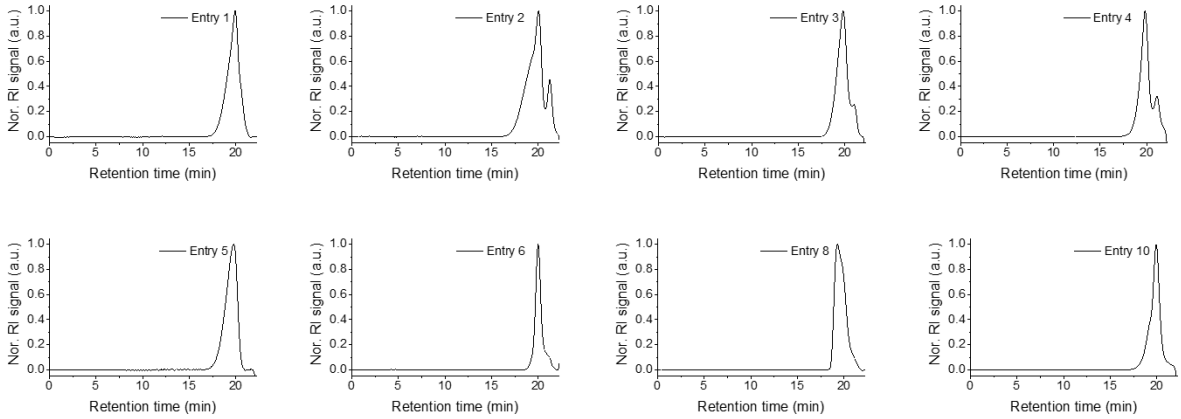

Appendix Figure 2.22: *Size exclusion chromatogram of the polyserine-1 corresponding to mentioned entries in Table 1 and ST3 using THF as eluent at 25℃.*

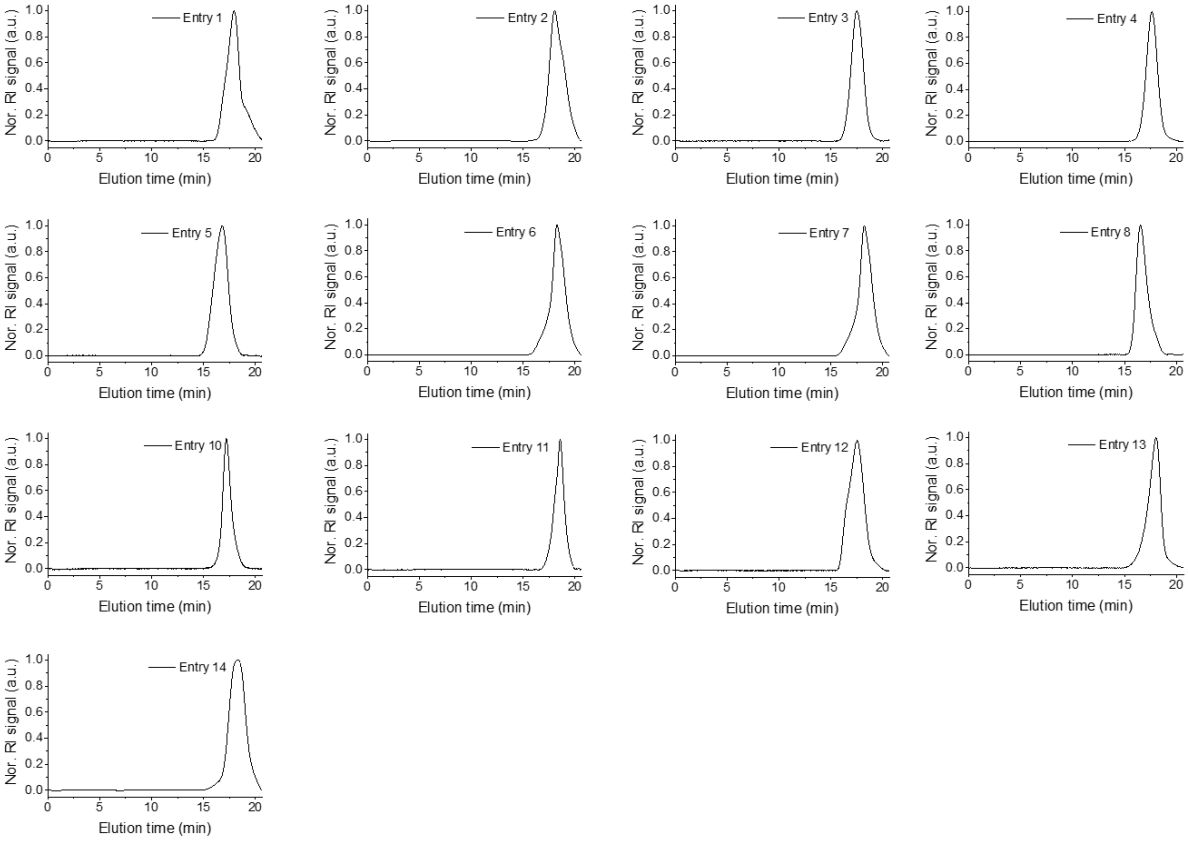

Appendix Figure 2.23: *Size exclusion chromatogram of the polyserine-1 corresponding to mentioned entries in Table 1 and ST3 using $CHCl_3$ as eluent at 25℃.*

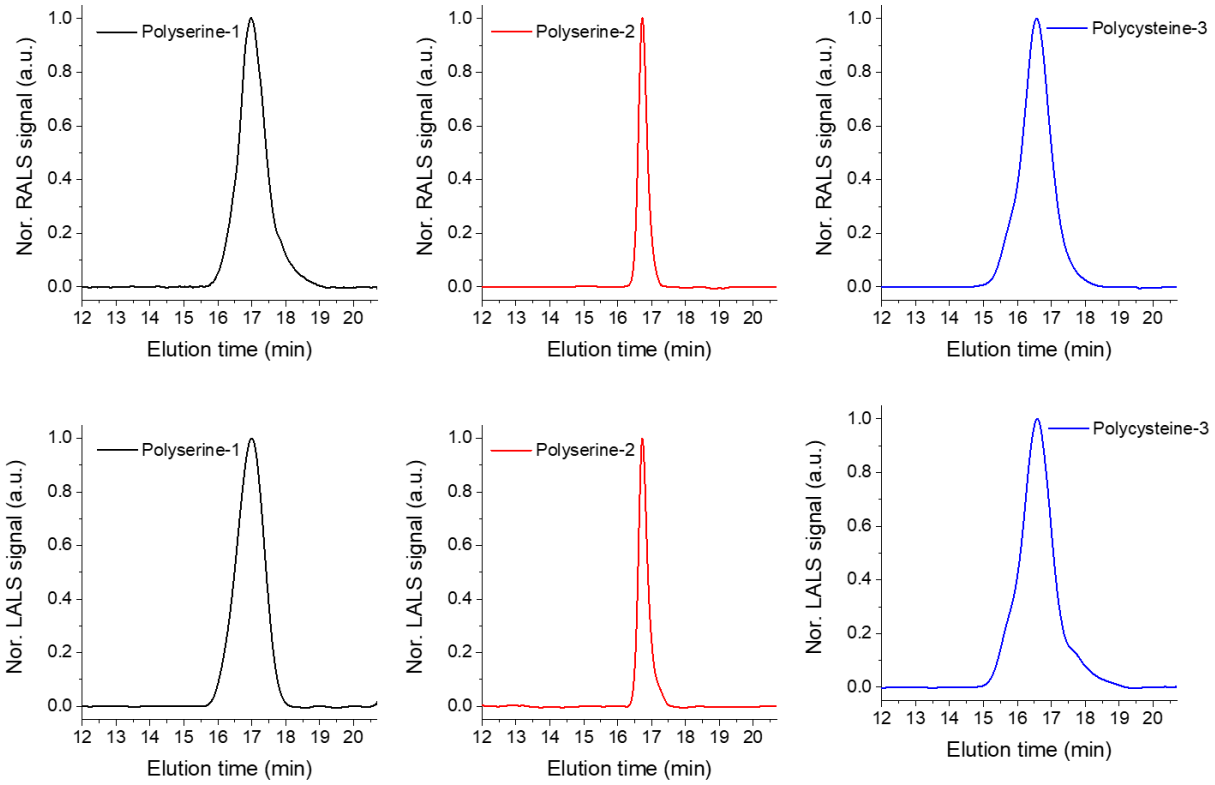

Appendix Figure 2.24: *Representative Size exclusion chromatogram of the polyserine-1, polyserine-2 and polycysteine-3 using $CHCl_3$ as eluent at 25℃ and (a) RALS as detector and (b) LALS as detector.*

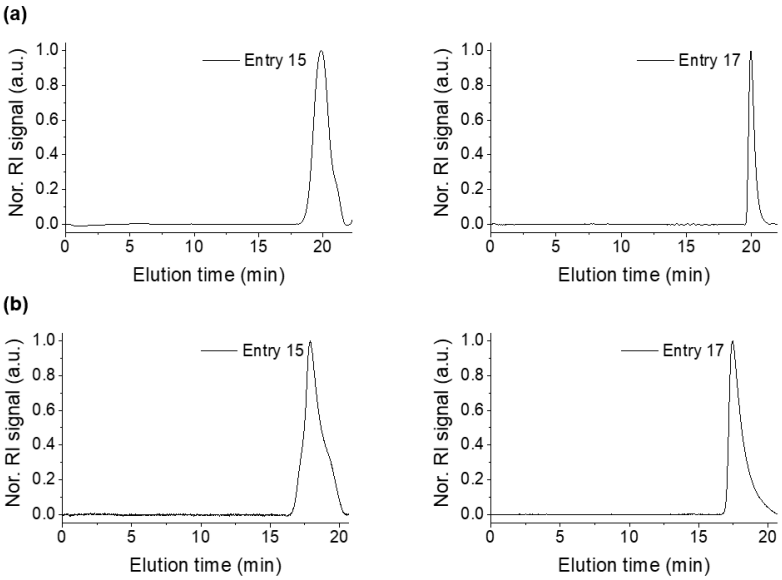

Appendix Figure 2.25*: Size exclusion chromatogram of the polyserine-2 corresponding to mentioned entries in Table 1 using (a) THF as eluent at 25 ℃ and (b) $CHCl_3$ as eluent at 25 ℃.*

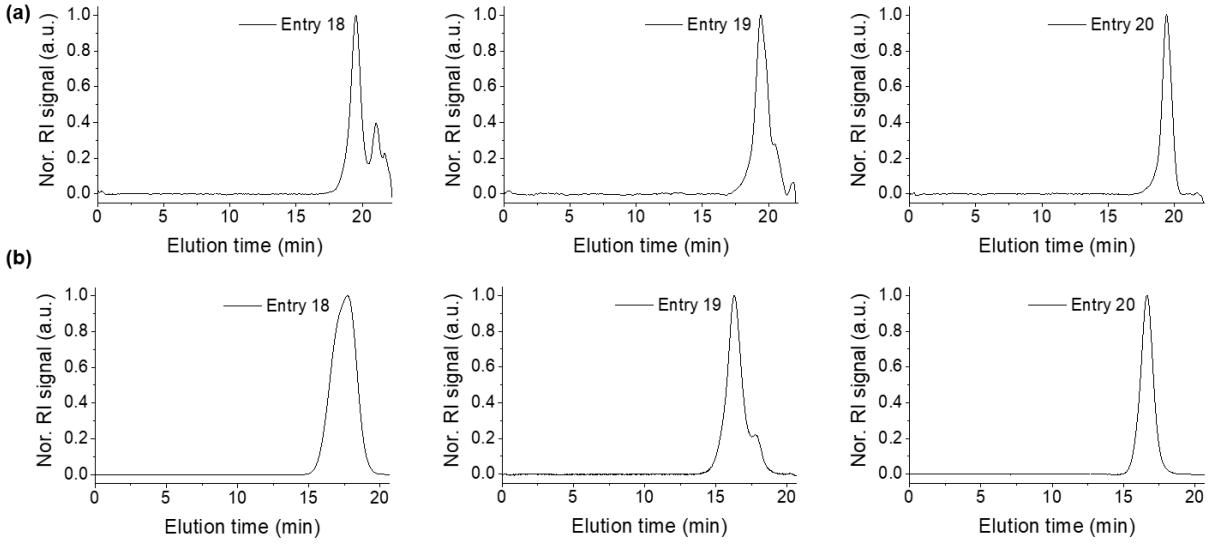

Appendix Figure 2.26: *Size exclusion chromatogram of the polycysteine-3 corresponding to mentioned entries in Table 1 using (a) THF as eluent at 25 ℃ and (b) $CHCl_3$ as eluent at 25 ℃.*

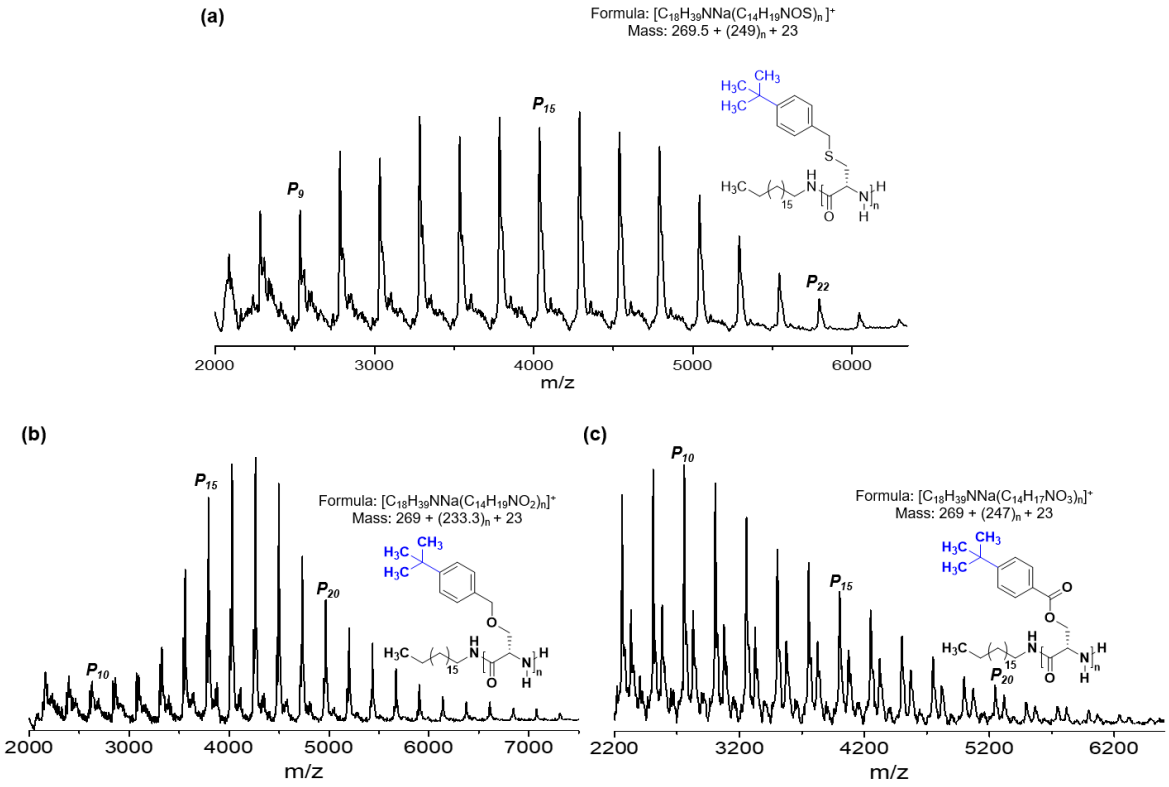

Appendix Figure 2.27: *MALDI-TOF spectrum of (a) Polycysteine-3, (b) Polyserine-2, (c) Polyserine-1.*

Chapter 3

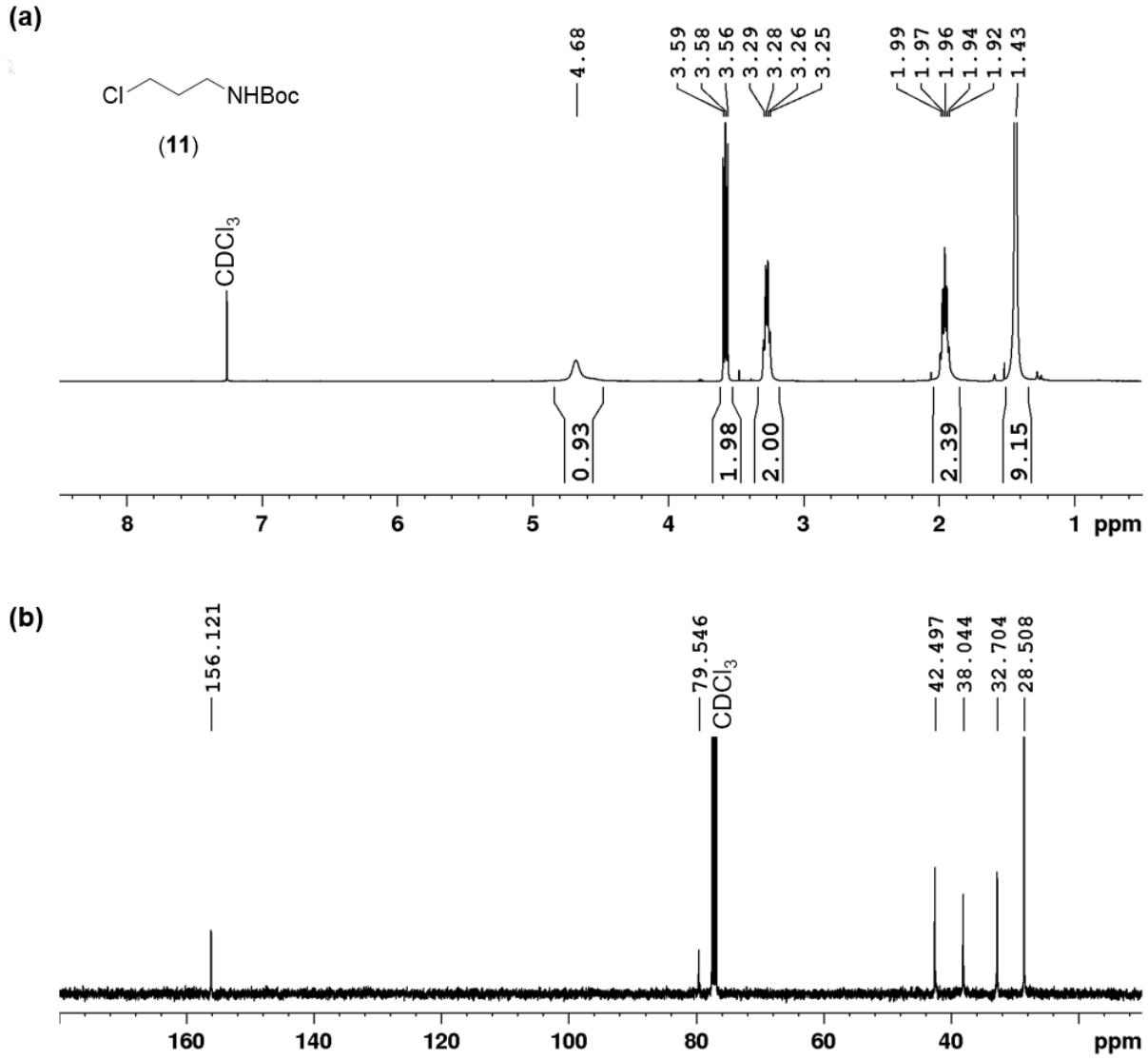

Appendix Figure 3.1: *(a) ^{1}H NMR of compound **11** in $CDCl_3$ (b) ^{13}C NMR of compound **11** in $CDCl_3$*

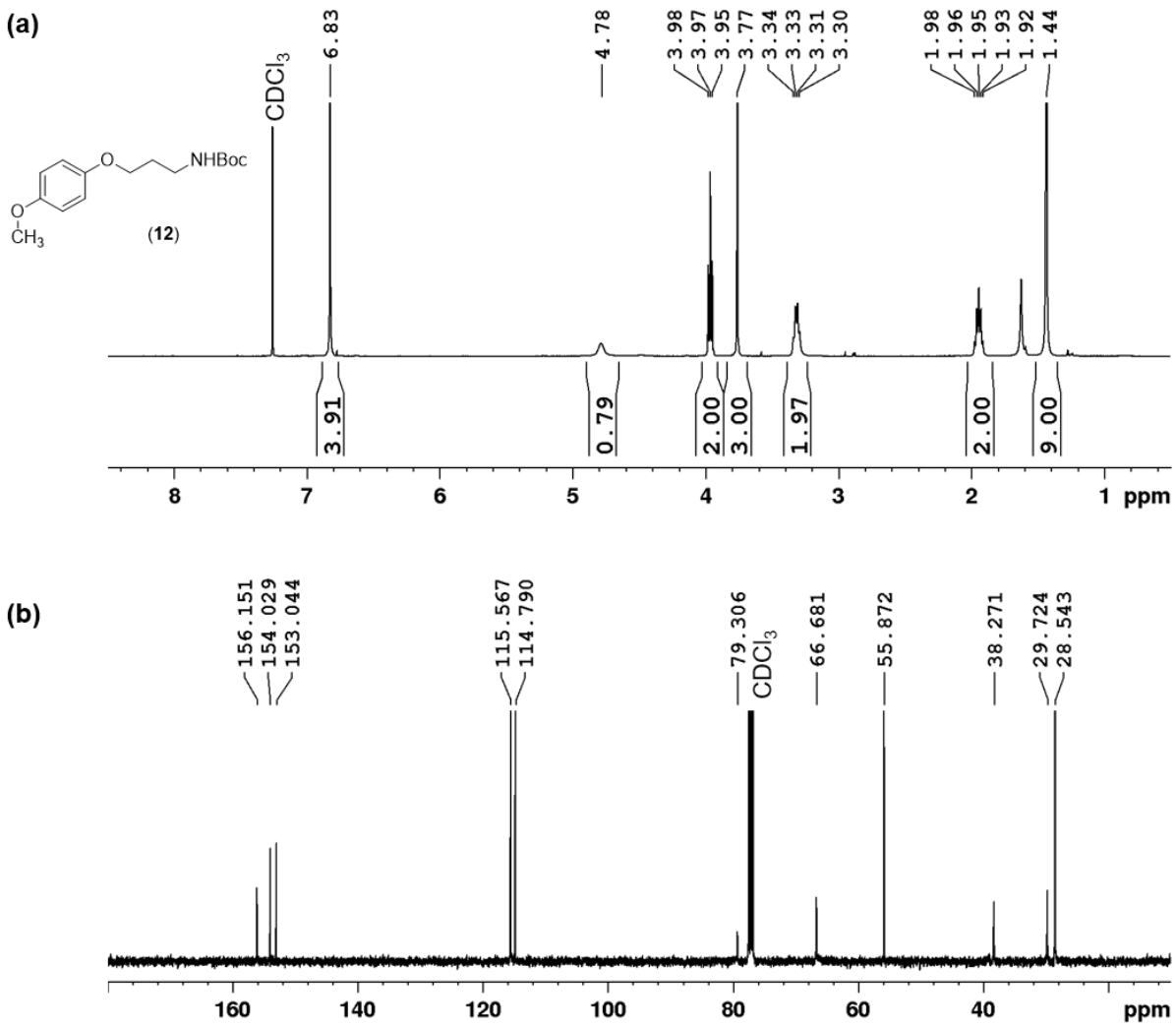

Appendix Figure 3.2: *(a) ^{1}H NMR of compound **13** in $CDCl_3$ (b) ^{13}C NMR of compound **13** in $CDCl_3$*

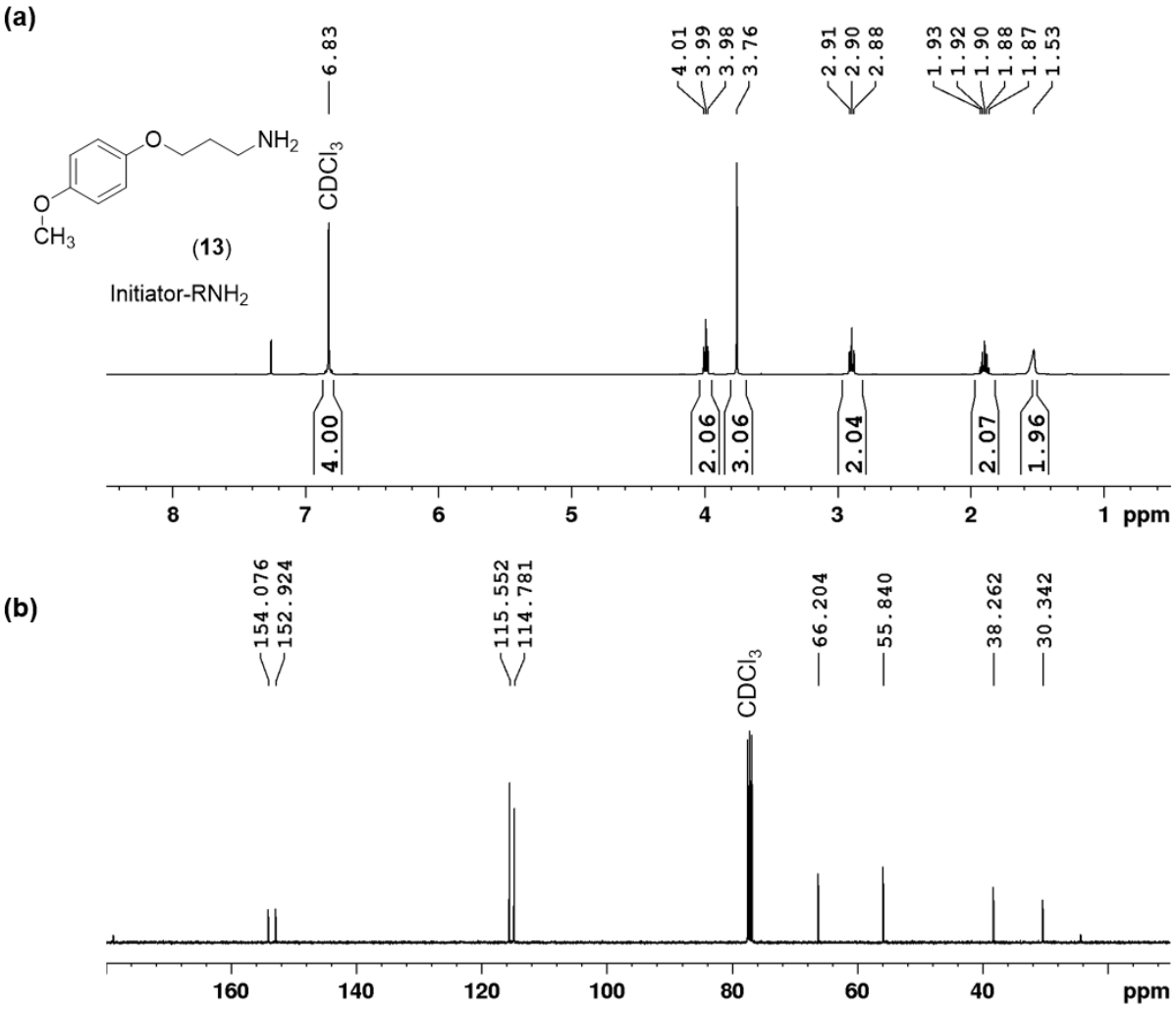

Appendix Figure 3.3: *(a) ^{1}H NMR of compound **14** in $CDCl_3$ (b) ^{13}C NMR of compound **14** in $CDCl_3$*

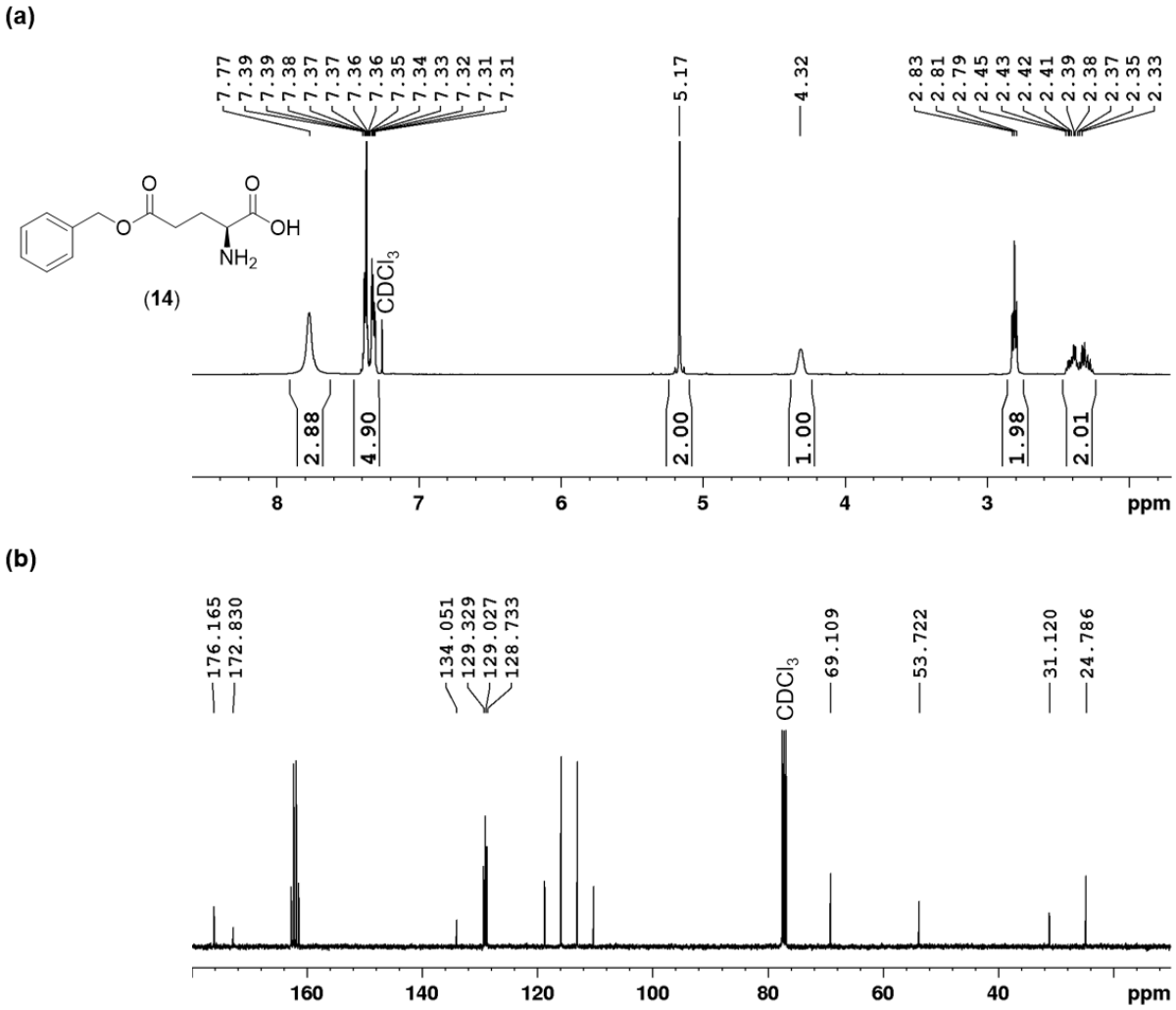

Appendix Figure 3.4: *(a) ^{1}H NMR of compound **14** in $CDCl_3$+Trifluoroacetic acid (6:1, v/v) (b) ^{13}C NMR of compound **14** in $CDCl_3$+Trifluoroacetic acid (6:1, v/v)*

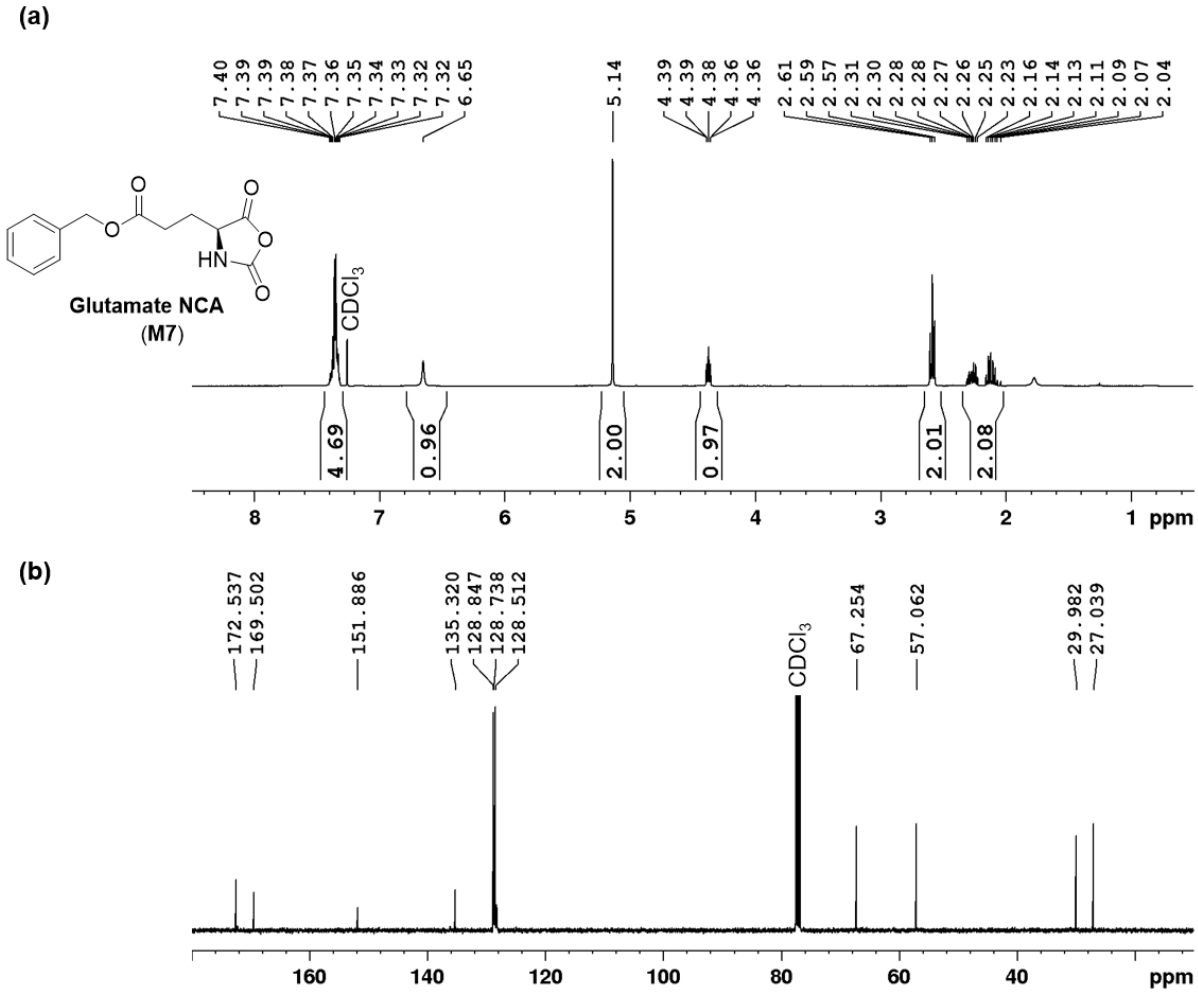

Appendix Figure 3.5: *(a) ^{1}H NMR of glutamate NCA monomer (**M7**) in $CDCl_3$ (b) ^{13}C NMR of glutamate NCA monomer (**M7**) in $CDCl_3$*

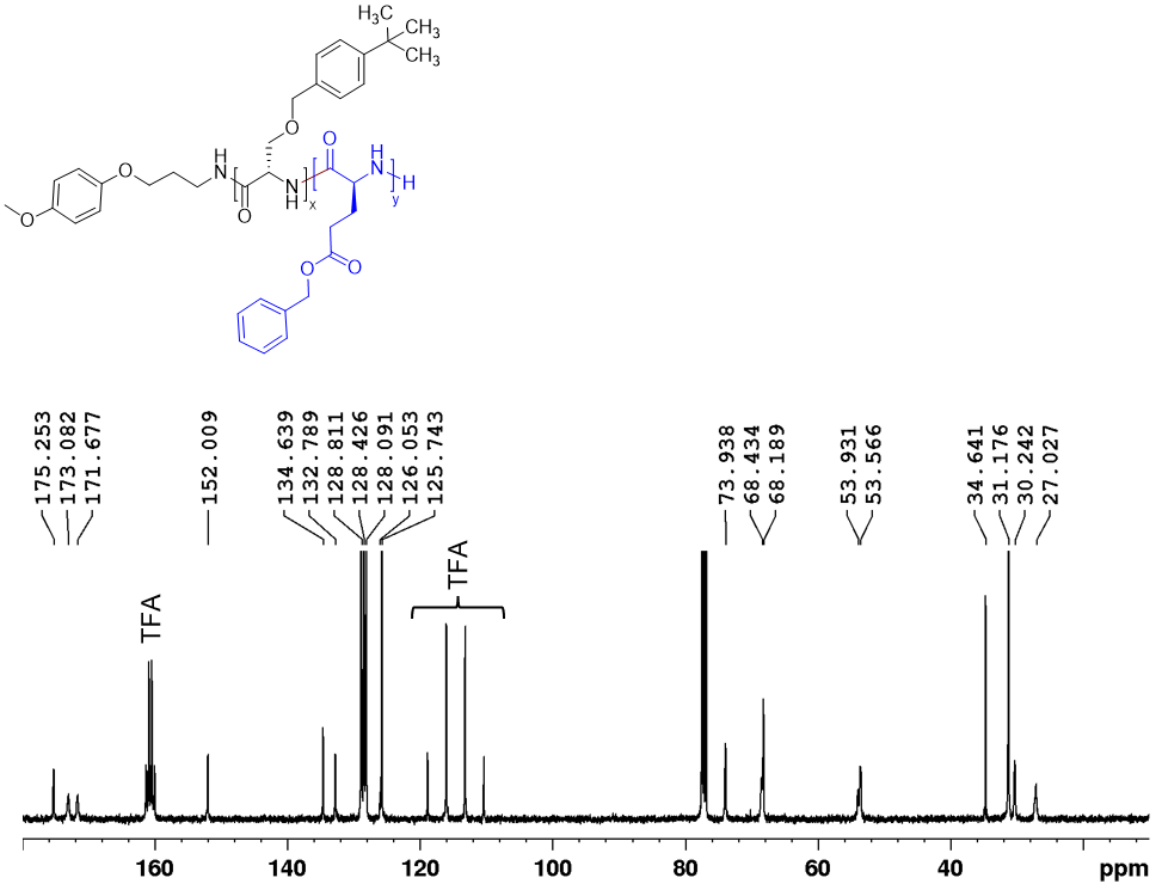

Appendix Figure 3.6: *^{13}C NMR of P(Bn-ser)-b-P(Bn-glu) in $CDCl_3$+Trifluoroacetic acid (6:1, v/v)*